IN-26
3826
P-254

NASA Technical Memorandum 106534

The Effect of Various Metallurgical Parameters on the Flow and Fracture Behavior of Polycrystalline NiAl Near the Brittle-To-Ductile Transition

Ronald D. Noebe
Lewis Research Center
Cleveland, Ohio

(NASA-TM-106534) THE EFFECT OF VARIOUS METALLURGICAL PARAMETERS ON THE FLOW AND FRACTURE BEHAVIOR OF POLYCRYSTALLINE NiAl NEAR THE BRITTLE-TO-DUCTILE TRANSITION (NASA. Lewis Research Center) 254 p
N94-29758
Unclas
G3/26 0003826

April 1994

National Aeronautics and
Space Administration

THE EFFECT OF VARIOUS METALLURGICAL PARAMETERS ON THE FLOW AND FRACTURE BEHAVIOR OF POLYCRYSTALLINE NiAl NEAR THE BRITTLE-TO-DUCTILE TRANSITION

by

Ronald D. Noebe

PREFACE

My primary assignment when I first arrived at NASA LeRC was and still is to find a way to increase the room temperature ductility and fracture resistance of NiAl. The original approach was to follow up on my M.S. thesis research on surface film effects by extending the concept to internal interfaces. However, very early on it became apparent that there were many inconsistencies concerning the flow and fracture behavior of NiAl and no accepted set of mechanisms describing deformation and fracture over low and intermediate temperatures. Consequently, I felt that the only reasonable approach in attempting a solution to the ductility issue was to first understand the intrinsic behavior of NiAl and the effect of minor alloying additions on properties. This meant defining the reason for the lack of ductility and then understanding the mechanism for the brittle-to-ductile transition at elevated temperatures to determine whether the BDTT could be shifted to below room temperature. This report is a summary for my initial findings.

There are many individuals who have contributed to this effort. I would especially like to thank R. Bowman, I. Locci and A. Garg for their assistance and collaboration with various aspects of the research involving TEM. Also, of great help were C. Culllers, M. Behbehani and Frank Ritzert who were undergraduate co-op students working at NASA LeRC and assisted with much of the mechanical testing described in this report. I would also like to thank R. Gibala, M. Nathal, J.D. Whittenberger and J. Cotton for their encouragement during this project and for the many useful and interesting discussions concerning the behavior of NiAl. Finally, I would like to thank A. Tenteris for proofreading and correcting the original manuscript.

PRECEDING PAGE BLANK NOT FILMED

TABLE OF CONTENTS

I. INTRODUCTION 1

II. BACKGROUND 5
  2.1 Physical Metallurgy of B2 Nickel Aluminides
  2.2 Plasticity and Operative Slip Systems
  2.3 Yield Behavior
  2.4 Ductility and Fracture
  2.5 High Temperature Deformation of NiAl

III. EFFECT OF INTERFACES ON THE MECHANICAL BEHAVIOR OF NiAl 27
  3.1 Introduction
    3.1.1 Low temperature mechanical behavior of NiAl
    3.1.2 Ductile phase toughening concepts
    3.1.3 Microstructure of two-phase NiAl alloys
    3.1.4 Transformation toughening
  3.2 Materials and Experimental Procedures
  3.3 Results and Discussion
    3.3.1 Necklace microstructures as compliant grain boundary layers
    3.3.2 Flow and fracture of a directionally solidified Ni-30Al alloy
  3.4 Caveats Pertaining to Ductile Phase Toughening Approaches
  3.5 Summary and Conclusions
  3.6 Redirection of Research Efforts

IV. ROOM TEMPERATURE FLOW AND FRACTURE BEHAVIOR OF POLYCRYSTALLINE NiAl 71
  4.1 Introduction
  4.2 Materials and Experimental Procedures
  4.3 Results and Discussion
    4.3.1 Tension versus compression yield behavior
    4.3.2 Observations and origins of fracture in binary near-stoichiometric NiAl
    4.3.3 Fracture initiation and origins in ternary NiAl alloys
    4.3.4 Effect of grain size on yield strength and ductility
  4.4 Summary and Conclusions

PRECEDING PAGE BLANK NOT FILMED

V. EFFECT OF TEMPERATURE ON THE BEHAVIOR OF NiAl AND NiAl(Zr) ALLOYS 116

- 5.1 Introduction
- 5.2 Materials and Experimental Procedures
- 5.3 Results and Discussion
    - 5.3.1 Microstructure of as-extruded alloys
    - 5.3.2 Effect of temperature on tensile properties of NiAl
    - 5.3.3 Brittle-to-ductile transition temperatures
    - 5.3.4 Flow and fracture behavior of NiAl near the BDTT
    - 5.3.5 Rate dependent deformation of NiAl
    - 5.3.6 Transmission electron microscopy observations
    - 5.3.7 Summary of deformation mechanisms in polycrystalline binary NiAl and the mechanism responsible for the BDTT
    - 5.3.8 Effect of Zr on the BDTT of NiAl
- 5.4 Summary and Conclusions

VI. EFFECT OF STRAIN RATE ON THE TENSILE PROPERTIES AND BRITTLE-TO-DUCTILE TRANSITION TEMPERATURE OF NiAl 152

- 6.1 Introduction
- 6.2 Materials and Experimental Procedures
- 6.3 Results
- 6.4 Discussion
    - 6.4.1 Rate dependent deformation behavior of NiAl
    - 6.4.2 Activation energy for deformation at the BDTT
- 6.5 Summary and Conclusions

VII. EFFECTS OF DILUTE TERNARY ALLOYING ADDITIONS AND SUBSTITUTION SCHEMES ON THE TENSILE PROPERTIES AND BDTT OF POLYCRYSTALLINE NiAl 169

- 7.1 Introduction
- 7.2 Materials and Experimental Procedures
- 7.3 Results and Discussion
    - 7.3.1 Effect of microalloying additions on room temperature properties
    - 7.3.2 Effect of microalloying additions on the BDTT
    - 7.3.3 Effect of substitution scheme on tensile properties of dilute ternary NiAl alloys
- 7.4 Summary and Conclusions

VIII. EFFECT OF INTERSTITIAL ELEMENTS ON THE MECHANICAL BEHAVIOR OF NiAl 186

- 8.1 Introduction
- 8.2 Materials and Experimental Procedures
- 8.3 Results
    - 8.3.1 Microstructural characterization
    - 8.3.2 Tensile properties
- 8.4 Discussion
- 8.5 Summary and Conclusions

IX. PROSPECTS FOR FUTURE ALLOY DEVELOPMENT 200
  9.1 Flow and Fracture Behavior of Polycrystalline NiAl
  9.2 Potential Alloying Schemes
    9.2.1 Possible macroalloying and microalloying additions
    9.2.2 Alloying to impart a change in slip character
    9.2.3 Ductile phase reinforced and multi-phase alloys
  9.3 Concluding Remarks

REFERENCES 214

APPENDICES 236
  A. Detailed Description of Materials Studied
  B. Room Temperature Tensile Properties and Fracture Behavior of NiAl Alloys

ABSTRACT

The Effect of Various Metallurgical Parameters on the Flow and Fracture Behavior of Polycrystalline NiAl Near the Brittle-to-Ductile Transition

by

Ronald D. Noebe

This report summarizes an investigation of the effect of various metallurgical parameters such as interfaces, alloying additions, test temperature and strain rate on the flow and fracture behavior of polycrystalline NiAl. From this study a more complete understanding of the deformation and fracture behavior of polycrystalline NiAl near the brittle-to-ductile transition temperature has been developed. A mechanism for the BDTT is proposed that is based on the operation of localized dislocation climb processes that operate within the vicinity of the grain boundaries and provide the additional deformation mechanisms necessary for grain-to-grain compatibility during plastic deformation. Finally, methods for improving the low temperature mechanical behavior of NiAl were considered and reviewed within the context of the present knowledge of NiAl-based materials and the operative deformation and fracture mechanisms determined in this study. Special emphasis was placed on the use of second phases for improving low temperature properties.

PRECEDING PAGE BLANK NOT FILMED

CHAPTER I
INTRODUCTION

As with many ordered intermetallic alloys, NiAl was originally designated for study as a potential structural material because of its high melting temperature, hardness and chemical stability. Early investigations were exploratory in nature, designed to determine whether NiAl held promise as a high temperature refractory compound (Wachtell 1952; Grala 1957). These were followed by studies during the first half of the 1960's that concentrated on the effects of processing and other metallurgical variables on mechanical behavior (Wood et al. 1960-1966). By the mid 1960's NiAl was identified as a possible candidate material for use as the leading edge of a superalloy turbine vane (Singleton, Wallace and Miller 1966). However, no solution was found for the low temperature brittleness of this compound and by the end of the 1960's government and industrial interest in NiAl faded. At this point, research shifted primarily to universities and between 1970 and the mid 1980's there was a very small but steady effort in the investigation of oxidation behavior, mechanical properties and deformation mechanisms.

Then suddenly in the mid to late 1980's research effort and the number of available publications on NiAl increased at a very significant rate. The physics/surface science community became intrigued with the surface properties and catalytic behavior of NiAl. This work was motivated by the fact that NiAl is one of the few intermetallic systems known to have a stable, well defined surface structure on an atomic level (Franchy, Wuttig and Ibach 1987; Castro et al. 1991). Because of the high melting point, excellent thermal stability, and serendipitous lattice match with GaAs compounds, the electronics industry began to take a serious look at the application of NiAl as a buried interconnect in electronic components (Sands 1988; Chambers and Loebs 1990; Joo et al. 1992). But the majority of effort is again centered on its possible use as a high temperature structural material. The renewed driving forces for this type of application have been generic government aeropropulsion programs (Stephens 1988; Doychak 1992) and industrial development of NiAl as a turbine engine material (Darolia 1991; Darolia et al. 1992). Thus, the research cycle for NiAl has come full circle.

As a high temperature structural material, NiAl offers a number of distinct advantages over conventional superalloys such as a significantly higher melting point, a density that is about 2/3 that of typical superalloys, a four to eight fold advantage in thermal conductivity, and cyclic oxidation resistance that is superior to any existing high temperature alloy (Darolia 1991). Through these differences in properties, the following benefits would be gained by using NiAl in engine applications: reduced cooling requirements, reduced weight, and higher operating temperatures. These, in turn, would lead to increased engine thermodynamic efficiency and increased thrust-to-weight ratio. The weight savings alone would be significant. For example, design studies have shown that the replacement of superalloy turbine blades with NiAl could lead to a 40% reduction in the weight of the rotor system (blades plus disk) (Darolia 1991). Less glamorous applications for NiAl have also been targeted. These range from automotive supercharger rotors to furnace and incinerator components to glass making molds.

Yet, the problems hindering widespread acceptance of NiAl as a structural material are the same as those originally identified in the early 1960's, namely poor creep resistance and inadequate low temperature toughness and ductility. However, recent advances in single crystal alloy development (Darolia 1993), eutectic solidification processing (Johnson et al. 1993), and particulate (Whittenberger, Arzt and Luton 1990a,b) and continuous fiber (Bowman 1992) composite fabrication hold promise for significantly improving the creep strength of NiAl. Through these technologies, NiAl alloys have been developed that are close to or have surpassed the creep strength of Ni-based superalloys.

The other technologically limiting problem, poor low temperature ductility, has been an issue that I have been working on over the years. I was first introduced to NiAl by R. Gibala during my M.S. thesis research, which was an investigation of the effect of surface films on the mechanical behavior of single crystal NiAl (Noebe 1987). Research then continued at NASA LeRC where the laboratory's staff and additional resources enabled me to investigate the deformation and fracture mechanisms in NiAl with the goal of improving low temperature properties. Initially, research focused on the effect of interfaces and second phases on the mechanical behavior of NiAl. This work was a natural extension of the surface film softening research that I was first involved in and is described in Chapter III.

While this work was progressing it became clear that the underlying reason for the low ductility in NiAl was not well understood. Furthermore, the lack of understanding concerning the flow and fracture behavior of NiAl seemed to result in a proliferation of unsound proposals for improving the mechanical properties of NiAl. Consequently, it was felt that improvements in room temperature toughness and ductility could best be achieved by first understanding the deformation and fracture mechanisms responsible for the mechanical behavior of this intermetallic over a broad temperature range that included the region surrounding the brittle-to-ductile transition temperature (BDTT). Specifically, the origins of low temperature fracture in NiAl and the mechanism responsible for the change from brittle-to-ductile behavior with increasing temperature needed to be identified and understood. These issues are addressed in Chapters IV-VI. Insight concerning the low and intermediate temperature behaviors of binary NiAl can also be gained by understanding the manner in which alloying additions alter mechanical properties. Consequently, in Chapters V, VII and VIII the behavior of binary and ternary NiAl alloys are compared and contrasted. Finally, a working knowledge of the deformation and fracture behavior of NiAl and the mechanisms responsible for BDTT, which are developed in this report, should provide more accurate guidance in developing improved NiAl-based alloys. This final topic is addressed briefly in Chapter IX where results of concurrent alloying programs are reviewed and their future prospects are analyzed. Directions for future research programs on NiAl-based alloys are also suggested.

CHAPTER II
BACKGROUND

2.1 Physical Metallurgy of B2 Nickel Aluminides

NiAl is an ordered intermetallic compound that crystallizes in a primitive cubic CsCl structure and exists over the composition range of 45 to almost 60 atomic percent Ni. While the phase diagram indicates that stoichiometric Ni-50Al melts congruently at 1911 K (Singleton, Murray and Nash 1986), more recent determinations place the melting temperature, T_m, of binary stoichiometric NiAl closer to 1955 K (Walston and Darolia 1993). The originally lower value of T_m, reported by Singleton et al., could be attributed to the steep drop-off in melting temperature with deviations from stoichiometry and/or unintentional additions of ternary elements (Cotton, Noebe and Kaufman 1993c,d). NiAl not only has the highest melting temperature of any compound in the Ni-Al system but is also the most thermodynamically stable. NiAl has the largest negative heat of formation, -72 kJ/mol at the stoichiometric composition, of any compound in the Ni-Al system (Henig and Lukas 1975). This high degree of thermodynamic stability and the existence of a wide phase field makes NiAl relatively easy to fabricate in a range of forms from fine homogeneous powders to single crystals.

Properties such as lattice parameter and density have been thoroughly studied as a method to infer the type of defect structure that occurs in the NiAl lattice. Consequently, significant data have been generated for these properties, Fig. 2.1. Since Ni is a smaller but heavier atom than Al, increasing the Ni content by substitution of Ni on Al sites should cause the lattice parameter to decrease and the density to increase, consistent with the data shown in Fig. 2.1 for alloys containing greater than 50% Ni. However, the behavior for

Al-rich alloys does not continue to follow these trends in lattice parameter and density. Instead, for Al-rich alloys, the lattice spacing decreases and the decrease in density is more rapid than would be expected by the replacement of Ni atoms by aluminum. Consequently, the deviation in stoichiometry of Al-rich alloys is accommodated by the creation of vacancies on the Ni-lattice sites instead of by substitutional defects as in Ni-rich alloys. This can result in the presence of an extremely large number of constitutional vacancies. For example, a Ni-55Al intermetallic would contain a constitutional vacancy concentration of almost 10%.

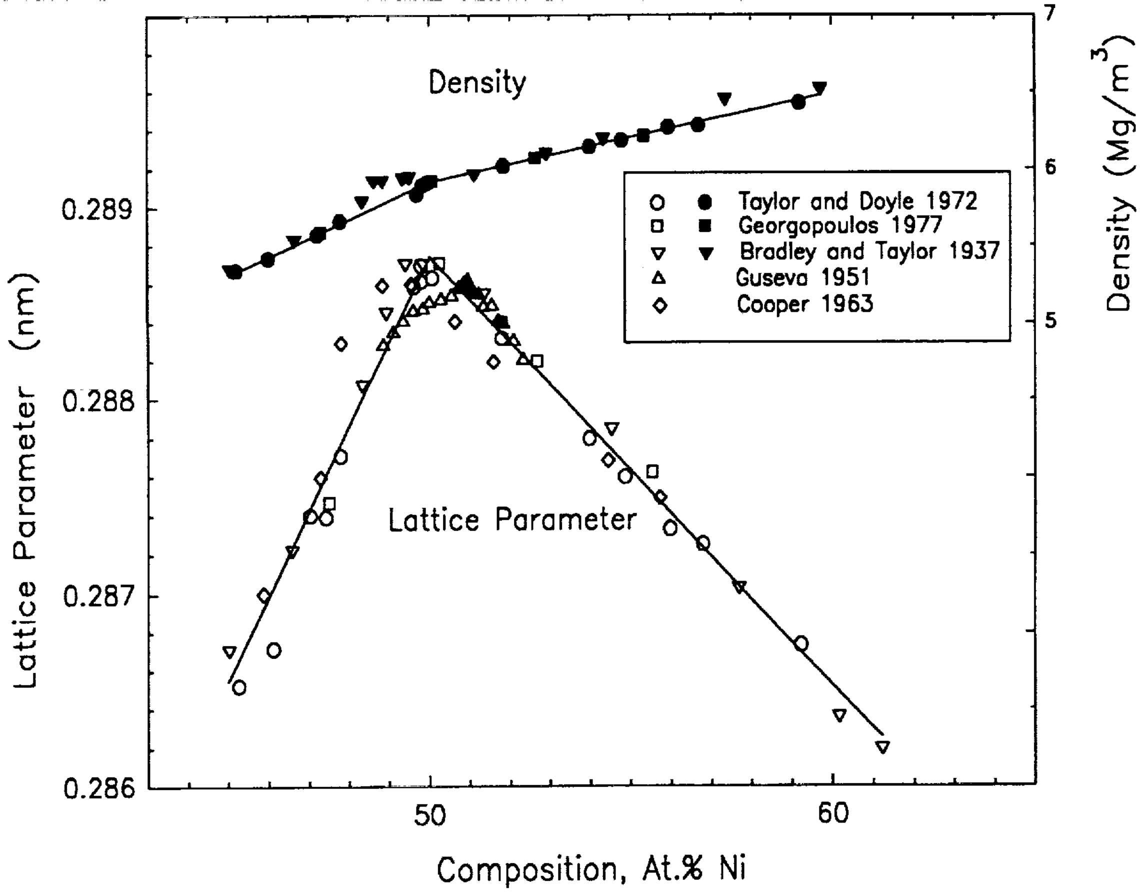

Fig. 2.1. Room temperature lattice parameter and density for NiAl as a function of stoichiometry.

Another property that has been extensively studied is elastic behavior. The single crystal elastic constants for binary NiAl have been determined as a function of temperature, cooling rate (thermal vacancy concentration), and stoichiometry. This data has been conveniently summarized by Rusovic and Warlimont (1977). The elastic properties of NiAl are anisotropic, $A = 3.28$ at room temperature (Wasilewski 1966), and the degree of anisotropy depends mildly on temperature and strongly on stoichiometry. The dynamic Young's modulus, E, for near-stoichiometric NiAl as a function of orientation is depicted in Fig. 2.2a, demonstrating the mild but linear dependence of temperature on modulus and slightly decreasing anisotropy with increasing temperature. Good agreement exists between the temperature dependence of modulus for <100> crystals determined by Wasilewski in 1966 and more recently by Walston and Darolia (1993). Minor alloying additions have been found to have relatively little effect on the dynamic Young's modulus of <001> single crystals (Walston and Darolia 1993).

The elastic properties of polycrystalline NiAl have also been determined in some detail. Young's modulus has been found to be very dependent on processing technique and temperature but relatively insensitive to stoichiometry (Rusovic and Warlimont 1979; Harmouche and Wolfenden 1987; Moose 1991) or minor alloying additions (Wolfenden, Raj and Kondlapudi 1993). The effect of processing route on the temperature dependence of the Young's modulus for near-stoichiometric NiAl is shown in Fig. 2.2b. It is apparent from this figure that extrusion produces a material with a higher modulus and slightly different temperature dependence than for hot pressed prealloyed powders or cast and homogenized ingots. By comparison with the single crystal data, the effect of processing technique on Young's modulus of polycrystalline NiAl can be rationalized in terms of crystallographic texture. The extruded materials probably had a preferred <111> orientation as demonstrated for similarly processed NiAl alloys (Bieler et al. 1992; K. Bowman et al. 1993). The NiAl material produced by casting or hot pressing would not be expected to have a strong preferred orientation and would therefore, have a lower

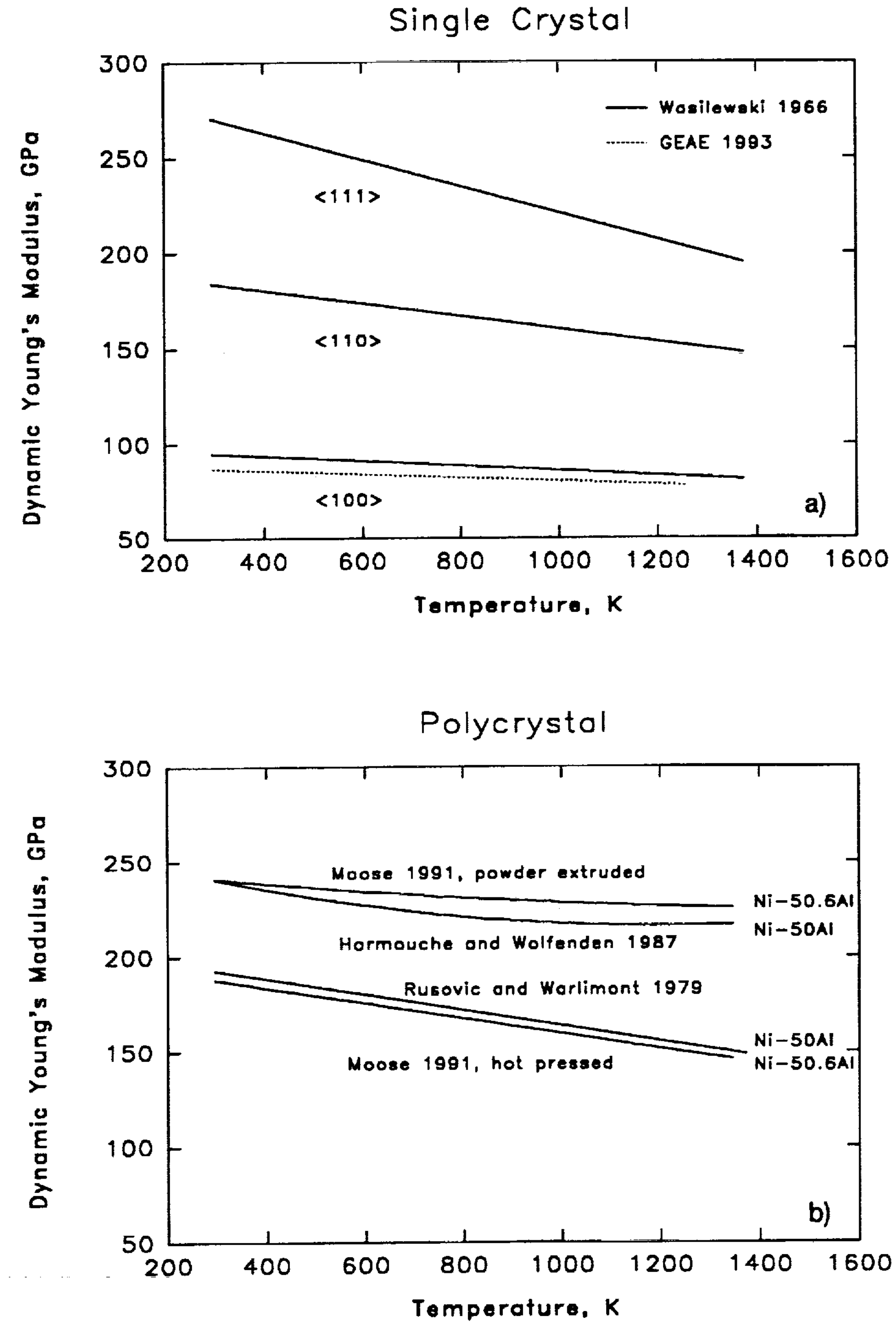

Fig. 2.2. Dynamic Young's modulus: a) for single crystal NiAl as a function of orientation and temperature and b) as a function of processing and temperature for polycrystalline NiAl.

modulus. Finally it is useful to note that the NiAl alloy studied by Moose (1991) in both the hot pressed and extruded forms was material supplied from alloy heat P541, an alloy extensively studied during this investigation. The mechanical properties of this alloy are described in detail in Chapters IV and V.

Most other physical properties have not been characterized to the same degree as the lattice parameter, density or elastic modulus. The current awareness of a high thermal conductivity has only recently prompted investigators to determine the effects of alloying additions on thermal and other physical properties of NiAl (Walston and Darolia 1993; Darolia 1993). These and other properties have been recently reviewed (Noebe, Bowman and Nathal 1993; Miracle 1993).

2.2 Plasticity and Operative Slip Systems

The operative slip systems in NiAl single crystals and polycrystalline material have been rigorously studied by numerous investigators and also critically reviewed in previous articles (Noebe, Misra and Gibala 1991; Noebe, Bowman and Nathal 1993). In general, NiAl single crystals exhibit two significantly different types of slip behavior depending on orientation. The dominant slip vector for "soft" single crystal orientations and polycrystalline material is <001>. But if the loading direction is along [001], known as the "hard" single crystal orientation, the operative slip vector is <111> at low and intermediate temperatures and a combination of <110> and <100> at elevated temperatures. Soft orientations include all non-<001> loading directions where <100> slip dominates; test orientations close to <001> are the hard orientations because <001> Burgers vectors have a zero or near-zero resolved shear stress.

By all indications, NiAl obeys Schmid's law and deforms by a <001> slip vector on either {100} or {110} planes for all but near [001] crystal orientations (Lahrman, Field and Darolia 1993a). Ball and Smallman (1966a and 1966b) were the first to make a complete slip system determination for NiAl with the identification of a <001> slip vector and {110} slip plane in all soft orientations and at all temperatures investigated (300-1273 K). They also observed cross slip or pencil glide on orthogonal {110} planes. In addition to viewing <001>{110} slip, Wasilewski, Butler and Hanlon (1967) observed duplex cube slip, <010>{100}, in [110] oriented single crystals, as have Field, Lahrman and Darolia (1991a). Cube slip has also been seen by Loretto and Wasilewski (1971) in [112] crystals deformed between 77 and 1053 K. Operation of dislocations with only <001> slip vectors in soft orientation single crystals is due to the non-dissociated, compact nature of the <001> dislocation core structure making it much more mobile compared to other slip vectors (Mills and Miracle 1993).

Consistent with deformation studies on soft orientation single crystals, investigators generally report the operation of a <001> slip vector in polycrystalline NiAl gliding on either {110} or {100} planes (Bowman et al. 1992; Nagpal and Baker 1992; Cotton, Noebe and Kaufman 1993b). Isolated dislocation segments with Burgers vectors other than <001>, usually of the type <011>, have been identified in as-extruded NiAl (Lloyd and Loretto 1970; Dollar et al. 1992). However, the presence of non-<001> dislocations in these polycrystalline studies do not constitute an alternative deformation mechanism at low and intermediate temperatures. Furthermore, non-<001> dislocations are not observed in cast materials either in the as-cast condition or after room temperature deformation (Cotton, Noebe and Kaufman 1993b). However, it is now believed that <111> slip does contribute to the deformation behavior of NiAl during high temperature extrusion, though not during monotonic deformation at low and intermediate temperatures (Bieler, Noebe and Hebsur 1994; Cotton and Margevicius 1994).

The operation of a <100> slip vector on planes other than {001} and {011} has been observed but only under special conditions of localized constraint. A (210) slip plane was observed by Miracle (1991) in just one of the many deformed bicrystals he analyzed. Wunderlich, Machon and Sauthoff (1992) have observed the operation of <100>{310} slip in NiAl within the plastic zone produced by an arrested crack that was initiated in the

NiAlNb phase after high temperature deformation of a NiAl/NiAlNb alloy. While observations of atypical slip systems are ardently reported, these results need to be tempered by the realization that the operation of a higher order slip plane was not the dominant slip plane observed in these studies.

In terms of operative slip systems, single crystals oriented along [001] are a special case since the resolved shear stress for <100> slip approaches zero. As a result, deformation occurs by non-<001> dislocation processes. These non-<001> deformation processes result in high flow stresses at low temperatures (Wasilewski, Butler and Hanlon 1967) and enhanced creep strength at elevated temperatures (Forbes et al. 1993) for [001] crystals compared to other orientations. As a result, significant effort has been spent on analyzing and understanding the operative deformation mechanisms in hard crystals through experimental means.

From 77 to approximately 600 K the primary slip vector in hard crystals is <111> with the most likely slip plane being {112} (Pascoe and Newey 1968a; Kim and Gibala 1991; Veyssiere and Noebe 1992). Previous reports of deformation by <001> dislocations in [001] crystals over this same temperature range (Fraser, Loretto and Smallman 1973) have been attributed to an unstable sample geometry that invariably leads to kinking (Bowman, Noebe and Darolia 1989). At higher temperatures (>600 K), which is above the brittle-to-ductile transition temperature (BDTT) for [001] crystals, the operative slip vector changes and deformation occurs by non-conservative motion of <001> and <011> type dislocations (Kim 1990; Kim and Gibala 1991; Field, Lahrman and Darolia 1991b).

While the previous discussion dwells significantly on the exceptions to general slip behavior in NiAl it should be re-emphasized at this point that the basic deformation mechanisms operative in NiAl at low and intermediate temperatures are either glide and/or climb of <001> dislocations. The exceptions mentioned above get significant coverage in the literature because they are exactly that, exceptions or special cases. They were mentioned above to acknowledge their existence and point out the special circumstances under which they occur.

2.3 Yield Behavior

Although yield stress is highly sensitive to many metallurgical variables, all studies on single crystal and polycrystalline material concur that with increasing temperature, yield strength decreases or remains essentially constant over certain temperature regimes, Figs. 2.3a and 2.3b. In general, the flow stress of NiAl is similar to that of bcc metals, exhibiting a strong temperature dependence at low absolute temperatures that is attributed to a large Peierls stress (Kitano and Pollock 1993). At intermediate temperatures there is a plateau where yield stress is only mildly dependent on temperature followed by a further drop in strength at elevated temperatures.

Due to the very strong dependence of yield strength on single crystal orientation it is also necessary to discuss the temperature dependence of yield strength with respect to specific crystallographic orientations. In Fig. 2.3a, yield stress as a function of temperature is shown for several different crystal orientations. Single crystals with soft orientations exhibit a yield strength versus temperature relationship that is distinct from the [001] material but very similar to low yield strength polycrystalline NiAl. At low temperatures, single crystals of NiAl loaded along [001] directions exhibit yield stresses several times higher than that for other orientations and are less dependent on temperature than soft orientations. At temperatures above 600 K the yield strength of [001] crystals becomes very sensitive to temperature with a significant reduction in yield stress occurring over a relatively narrow temperature range. It is within this temperature regime that the slip vector in hard crystals begins to change from <111> to <001> plus <110> (Kim and Gibala 1991). Above 1000 K, where bulk diffusional processes begin to dominate, hard single crystals have yield strengths similar to soft single crystals and polycrystalline NiAl.

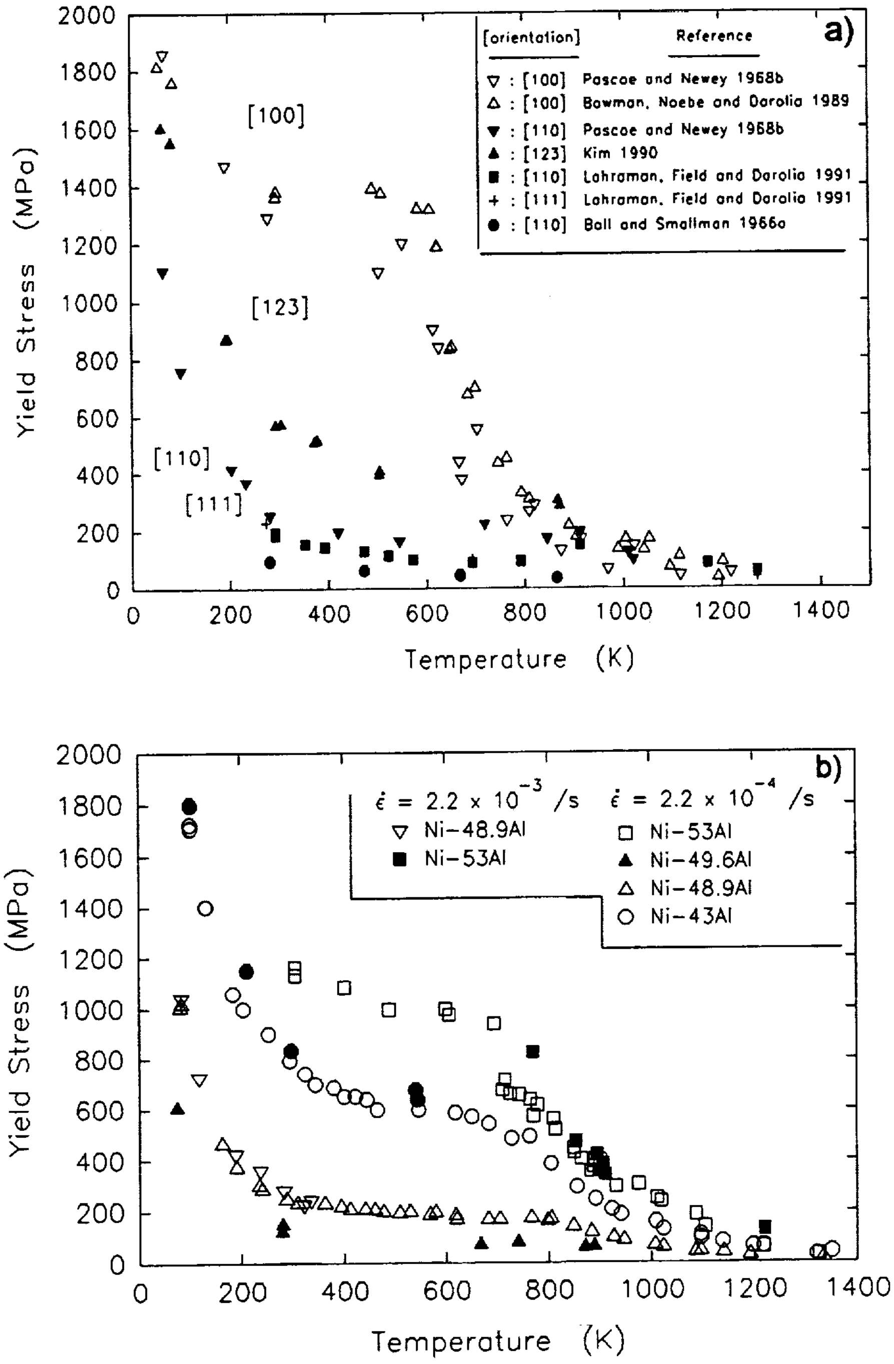

Fig. 2.3. Yield stress as a function of temperature for: a) single crystal NiAl of different orientations and b) polycrystalline NiAl as a function of strain rate, stoichiometry and temperature (Part b after Pascoe and Newey 1968).

In Fig. 2.3b, typical polycrystalline NiAl yield stress values as a function of temperature, stoichiometry and strain rate are shown. Although the values of the yield stress and the shape of the yield stress versus temperature curves depend on composition and strain rate, in all cases the yield stress basically decreases with increasing temperature. The behavior of near-stoichiometric polycrystalline NiAl resembles that of soft orientation single crystal material. With significant deviations from stoichiometry, polycrystalline material has considerably higher strength, comparable to that of stoichiometric [001] single crystals, even though slip is expected to occur by <001> dislocations in all polycrystalline NiAl alloys.

Not only is there an anisotropy in yield strength for NiAl single crystals but there is also an anisotropic behavior in strain rate sensitivity. Cube oriented crystals display a greater sensitivity to strain rate than soft orientations at intermediate temperatures (500 - 1000 K) (Pascoe and Newey 1968b; Lahrman, Field and Darolia 1991). This is due to the decomposed core structure of <110> dislocations, which have no possibility for conservative glide in hard crystals but must rely on thermal activation to assist their motion (Mills et al. 1993). On the other hand, deformation of soft single crystals is controlled by <001> dislocations which have a compact core structure. Consequently, the yield stress of soft orientation single crystals is relatively insensitive to strain rate below the BDTT. Also, the actual brittle-ductile-transition temperature is only mildly dependent on strain rate for soft orientation single crystals (Lahrman, Field and Darolia 1991). Since little has been discussed in the literature on the effects of strain rate and temperature on properties of polycrystalline NiAl below 1000 K, this was a major topic covered during the present investigation.

Significant deviations from the stoichiometric composition of NiAl are possible without altering the basic crystal structure of the material. This, in turn, has a significant effect on mechanical behavior, which has been reviewed previously by Vedula and Khadkikar (1990). Although an increase in yield stress is observed for both Ni and Al rich alloys, at lower temperatures the magnitude of the strengthening effect is not equivalent. From a previous compilation of low temperature data, the average hardening rate for Ni-rich alloys was found to be 120 MPa/at.% while that for Al-rich NiAl was approximately 350 MPa/at.% (Noebe, Bowman and Nathal 1993). Since there is a greater hardening rate for Al-rich alloys this would suggest that Ni vacancies provide a greater resistance to dislocation motion than that produced by anti-site atoms. Regardless of whether the material is Ni-rich or Al-rich the effect of non-stoichiometry on strength becomes negligible around 1000 K (Fig. 2.3b). At even higher temperatures a reversal in strength levels occurs such that the stoichiometric alloys become stronger than non-stoichiometric compositions (Ball and Smallman 1966a; Whittenberger et al. 1991).

The presence of vacancies significantly influences the flow properties of NiAl as evident from the high hardening rates in Al-rich alloys where constitutional vacancies are formed on the Ni sub-lattice. Another type of vacancy defect which can exist in NiAl is a thermal vacancy, introduced by rapid quenching from elevated temperatures. Therefore, cooling rate becomes another important variable to be considered when processing and testing NiAl, though it has not been considered extensively. In polycrystals, a 50-fold increase in cooling rate from temperatures above 1000 K can result in an almost 30% increase in compressive yield stress for near-stoichiometric binary NiAl. However, when the material is doped with minor alloying additions such as 500 ppm Zr, there is no dependence of cooling rate on strength, though the solute addition itself has a significant effect (Bowman et al. 1992). Similarly, deviations from stoichiometry reduce the sensitivity of binary NiAl to cooling rate effects (Nagpal and Baker 1990a). The dependence of cooling rate on flow properties of single crystal NiAl is similar to that of polycrystalline material. A significant reduction in yield strength occurs in samples that were slow cooled from intermediate temperatures compared to samples quenched from higher temperatures (Weaver, Kaufman and Noebe 1993).

Substitutional and interstitial elements also significantly impact the strength of NiAl. However, published single crystal data are relatively scarce and much of the available information is for hard orientations. Additions of Cr (Field, Lahrman and Darolia 1991c), V (Darolia et al. 1989), and Zr (Noebe et al. 1989) do not have any demonstrated hardening effect on [001] single crystals at low temperatures but do strengthen NiAl at temperatures above 600-700 K, where a change in slip mode is known to occur. Systematic study of the influence of Mo, Ga and Fe on the yield strength of <110> oriented single crystal NiAl has revealed a range of strengthening behaviors at room temperature (Darolia, Lahrman and Field 1992). Molybdenum was a potent solid solution hardening agent but with very limited solubility in NiAl. Gallium had a mild strengthening effect while Fe, at levels of less than 1%, resulted in a slight decrease in yield stress. Preliminary testing of high purity single crystals also indicates that interstitial levels can have a significant influence on flow stress (Weaver, Kaufman and Noebe 1993). The critical resolved shear stress reported for high purity/low interstitial NiAl is only 57 MPa compared to 79 MPa for commercial purity material that received an identical thermal treatment.

Solid solution alloying data for polycrystalline NiAl is more abundant than for single crystal material. Ternary additions to polycrystalline NiAl have included beryllium, boron, carbon, chromium, copper, yttrium, molybdenum, and lanthanum (George and Liu 1990; Cotton, Noebe and Kaufman 1993a,d; Graham 1984). Additionally, the effects of zirconium, rhenium, iron, gallium, and nitrogen will be discussed in the following chapters.

No acceptable theory of solid solution strengthening can explain all aspects of intermetallic behavior, even for the relatively simple B2 compounds (Fleischer 1993). For example, substituting a particular ternary addition such as Cu for Ni in NiAl will result in significantly different hardening characteristics than if the element were substituted for Al (Cotton, Noebe and Kaufman 1993d). A further complication occurs if the alloying addition causes a change in the overall stoichiometry of the intermetallic or is added to a nonstoichiometric base. For example, chromium has a moderate strengthening effect on near-stoichiometric NiAl up to its solubility limit of about 2% but even more significant hardening is observed on either side of stoichiometry due to constitutional defects (Cotton, Noebe and Kaufman 1993a). Consequently, defect structures in ternary alloys need to be characterized so that addition and cancellation rules for the various defect hardening mechanisms can be defined. The potential for defect pairing or clustering also has to be accounted for if solid solution models are to be effective (Cotton, Noebe and Kaufman 1993d).

Finally, grain size also influences the room temperature yield strength of NiAl but not in a straightforward manner. Grain size effects are complicated by the additional variables of alloy stoichiometry and third element additions (Nagpal et al. 1991; Zeller, Noebe and Locci 1990). The relationship between alloy stoichiometry and Hall-Petch parameter indicates that the influence of grain size on yield stress is more significant with increasing deviation from stoichiometry (Nagpal et al. 1991). Consequently, yield stress is essentially independent of grain size for Ni-50Al, whereas the yield stress of even slightly non-stoichiometric alloys is strongly influenced by grain size. This will be discussed in additional detail in Chapter IV.

2.4 Ductility and Fracture

Cube oriented, Ni-50Al single crystals exhibit essentially zero plastic strain to failure at room temperature but undergo a sharp brittle-to-ductile transition at temperatures just above 600 K, (Bowman, Noebe and Darolia 1989; Darolia et al 1992; Takasugi, Watanabe and Hanada 1992). This corresponds to the same temperature that [001] crystals begin to undergo a steep decrease in yield strength with increasing temperature (Fig. 2.3a) due to a change in deformation mechanism from <111> slip to deformation by a combination of <100> and <110> dislocations. Ni-rich Ni-40Al cube oriented crystals undergo a similar brittle-to-ductile transition but at a much higher temperature, approximately 1000 K (Noebe, Misra and Gibala 1991).

It was believed that soft orientation single crystal NiAl also possessed very limited room temperature tensile ductility, however, the intrinsic ductility and toughness of NiAl may be much greater than once suspected (Brzeski et al. 1993). Originally, soft orientation single crystals of near-stoichiometric composition were routinely reported to exhibit room temperature elongations on the order of 1% (Lahrman, Field and Darolia 1993b; Takasugi, Kishino and Hanada 1993). Now depending on the post-test heat treatment, room temperature tensile ductilities on the order of 5 - 7% have been observed (Brzeski et al. 1993; Field, Lahrman and Darolia 1993). Single crystals of soft orientations undergo a fairly abrupt brittle-to-ductile transition at intermediate temperatures. Depending on the specific orientations the BDTT occurs between 475 - 525 K (Lahrman, Field and Darolia 1991; Takasugi, Kishino and Hanada 1993). Just above the BDTT anomalously large tensile elongations of greater than 120% were observed for soft single crystals before decreasing to values on the order of 50% at higher temperatures due to the onset of necking. The anomalously large elongations at intermediate temperatures have been attributed to a balance between work hardening due to glide and relaxation processes due to climb, resulting in a high necking resistance (Takasugi, Kishino and Hanada 1993).

An intriguing effect of microalloying additions on the tensile properties of soft orientation single crystal nickel aluminides has been observed by Darolia, Lahrman and Field (1992). When near-stoichiometric [110] single crystals were doped with approximately 1000 ppm of Fe, Mo or Ga the room temperature tensile elongation increased from approximately 1% to upwards of 6%. The peak in ductility occurs at very small alloying additions and as the level of dopant exceeds 0.5 at.% the benefits to ductility become lost. This ductilizing effect is possibly due to "gettering" of interstitial contaminants, which would be consistent with the recent observations of up to 5% tensile ductility for high purity low interstitial NiAl single crystals (Johnson et al. 1993).

Originally, the room temperature fracture toughness of single crystal NiAl bend samples was reported between 7 - 12 MPa $m^{1/2}$ when the notch is cut perpendicular to <100> and 4 - 6 MPa $m^{1/2}$ when the notch is cut perpendicular to <110> (Chang, Darolia and Lipsitt 1992; Vehoff 1993). The fracture toughness of the soft orientation single crystals is in perfect agreement with fracture toughness values for binary, single phase polycrystalline NiAl, which have been measured between 4 and 7 MPa $m^{1/2}$. Furthermore, the fracture toughness of polycrystalline NiAl is essentially independent of grain size, stoichiometry or processing technique (Reuss and Vehoff 1990a; Rigney and Lewandowski 1992a; Kumar, Mannan and Viswanadham 1992).

However, it has been recently discovered that the fracture toughness of commercial purity, single crystal NiAl is extremely sensitive to heat treatment and cooling rate, as determined from double cantilever beam specimens with a notch plane perpendicular to <110>. For example, single crystal samples rapidly air cooled to room temperature from 1573 K had a fracture toughness of almost 16 MPa $m^{1/2}$; but when they were reannealed at 473 K and then slowly cooled to room temperature, the fracture toughness dropped to about 3 MPa $m^{1/2}$ (Hack, Brzeski and Darolia 1992). Comparable heat treatments had no affect on the toughness of zone refined, low interstitial single crystal NiAl when tested in four-point bending with the crack plane normal to the <100> direction (Johnson et al. 1993). The fracture toughness of the high purity NiAl was 10-12 MPa $m^{1/2}$ independent of heat treatment. Furthermore, experiments in biaxial bending and tension indicate that zone-refined, low interstitial NiAl single crystals have a much greater room temperature ductility and fracture strength than commercial purity material (Johnson et al. 1993; DeMarco and Ardell 1993). These observations are consistent with a strain aging phenomenon in NiAl. This behavior would be similar to that observed in mild steels where carbon and nitrogen are responsible for pinning the mobile dislocation density, causing brittle fracture. Thus, the inherent ductility and fracture toughness of single crystal NiAl may be much greater than originally assumed. However, additional work is still necessary to understand this phenomenon and pinpoint the particular interstitial element(s) responsible for affecting properties. A first attempt at identifying the interstitial elements responsible for the strain aging behaviors observed in NiAl is presented in Chapter VIII.

Fracture in polycrystalline alloys is complicated by an additional factor, the presence of grain boundaries. Because NiAl deforms by a <001> slip vector, there are only three independent slip systems available for deformation with no extra independent systems provided by cross slip (Ball and Smallman 1966b). Since this is less than the five independent deformation modes considered necessary for extensive, uniform, crack free deformation of a polycrystalline aggregate, NiAl in polycrystalline form should have no potential for exhibiting significant room temperature ductility. However, this is not a universally accepted assumption (Hahn and Vedula 1989; Schulson 1981,1985). The relationship between deformation mechanisms and fracture behavior of polycrystalline NiAl and the potential for this intermetallic alloy to exhibit significant room temperature tensile ductility will be discussed in detail in Chapter IV.

Even though limited tensile ductility can be achieved in low yield strength NiAl alloys at room temperature (Hahn and Vedula 1989; Pascoe and Newey 1968b), this does not constitute the brittle-to-ductile transition temperature. Instead, a dramatic increase in tensile ductility corresponding to the BDTT is observed at elevated temperatures. A detailed characterization of the BDTT in polycrystalline NiAl was a major aim of this investigation. For polycrystalline material, the changes in mechanical behavior with increasing temperature, leading to the BDTT have been attributed to the onset of bulk dislocation climb processes that occur at temperatures above a 1000 K (Ball and Smallman 1966a,b). However, the BDTT for polycrystalline NiAl can occur as low as

550 K. Consequently, a modified mechanism for the brittle-to-ductile transition in NiAl is developed in Chapter V.

2.5 High Temperature Deformation of NiAl

The majority of investigations concerning the mechanical behavior of NiAl have been performed either at room temperature as briefly discussed above, or in the creep regime at temperatures above 1000 K. One of the many objectives of this work was to rectify this situation by focusing on the mechanical behavior of NiAl at intermediate temperatures, i.e., in the vicinity of the BDTT. But before this issue will be addressed it is appropriate to review the deformation behavior of NiAl at elevated temperatures.

High temperature deformation behavior in B2 aluminides including NiAl is analogous to that for metals and alloys and can be analyzed accordingly. The second stage or steady-state creep rate, $\dot{\varepsilon}$, is usually expressed as a form of the Dorn equation:

$$\dot{\varepsilon} = A\,(\sigma/E)^n \exp^{(-Q/RT)}$$

where σ is the applied stress, E is Young's modulus, n is the stress exponent, Q is the activation energy for creep, R is the gas constant, T is the absolute temperature, and A is a constant which takes into account such variables as microstructure and stacking fault or anti-phase boundary energy. The values for n and Q are dependent on the operative deformation mechanisms within a given temperature and stress regime and are thus useful indicators of deformation mode. Creep is most commonly found to be diffusion controlled, hence the value of Q for creep deformation is often similar to that for diffusion, Q_D. Therefore, knowledge of diffusion behavior is also desirable as an aid to understanding creep processes.

Diffusion data for NiAl have been compiled and discussed previously (Noebe, Bowman and Nathal 1993; Miracle 1993). Unfortunately, this is one area in which no new experimental data have been generated for a number of years. Additional work is required to determine the activation energy and mechanisms of diffusion at lower temperatures, since almost no data exist for diffusion in NiAl below 1200 K. This problem is similar to the limited availability of mechanical property data for NiAl below 1000 K. From previous studies (Hancock and McDonnell 1971; Lutze-Birk and Jacobi 1975; Berkowitz, Jaumot and Nix 1954), it appears that the activation energy for diffusion is a maximum at Ni-50Al, which is consistent with the diffusion coefficient minima at the same composition.

Although there is considerable scatter among the various diffusion studies, critical analysis of the available data for NiAl indicates that the most likely range for Q_D is on the order of 250-300 kJ/mol. The average reported value for the activation energy of creep in NiAl is approximately 315 kJ/mol and when this value is corrected for the temperature dependence of the elastic modulus, Q would be on the order of 285 kJ/mol (Noebe, Bowman and Nathal 1993). Therefore, the activation energy for creep of binary NiAl falls within the range of data reported for bulk diffusion, as would be expected for a diffusion controlled process.

Dislocation creep in single phase metals and alloys can usually be classified as one of two main types: Class M, or pure metal creep, and Class A, or alloy type behavior (Mohamed and Langdon 1974). Class M creep is characterized by glide being much faster than climb, and thus, creep becomes controlled by the rate of dislocation climb past substructural obstacles. Class A creep is often called viscous glide controlled creep since the glide of dislocations is restricted by solute atoms or perhaps by a high lattice friction stress due to long range order. This reduced glide mobility is the limiting creep process, while climb can occur readily. These two types of behavior can be distinguished by several criteria including the stress exponent, the shape of the primary creep curve, the formation of a dislocation substructure, and the response of the material to stress or strain rate transients.

Figure 2.4 is a summary of measured and interpolated creep data for binary NiAl at 1175 K. Most of the data fall within reasonable agreement, with no more than a factor of

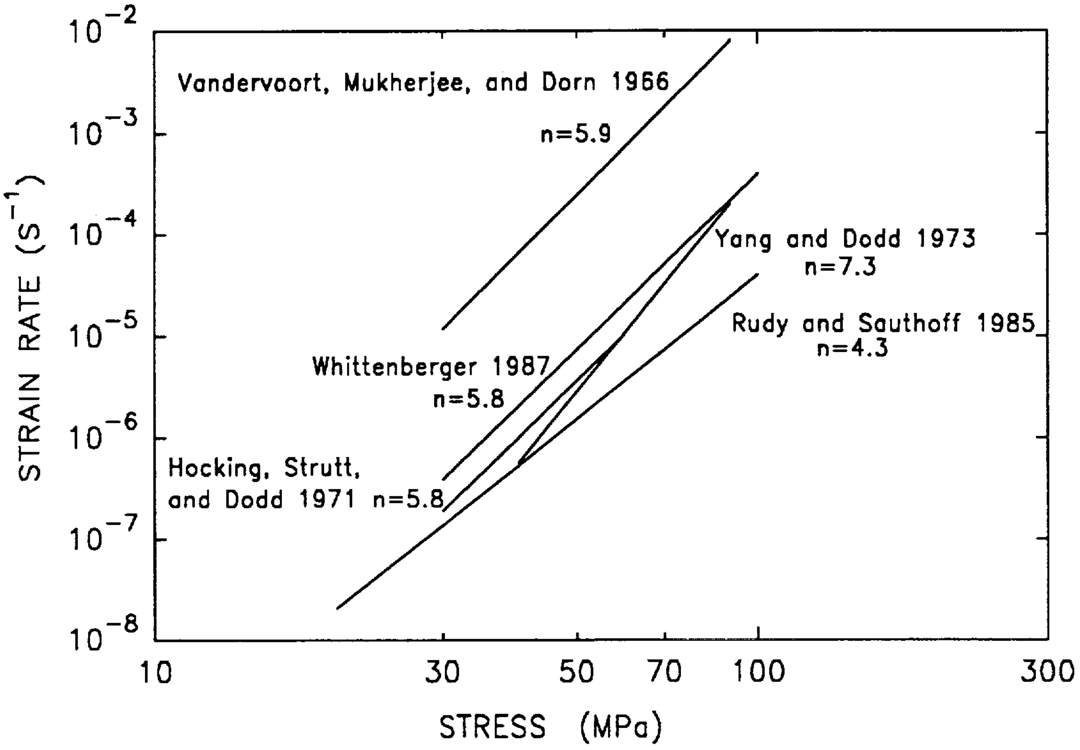

Fig. 2.4. Measured or interpolated creep behavior of near stoichiometric NiAl at 1175 K.

5 difference in creep rate at a given stress level, except for the strengths reported by Vandervoort, Mukherjee and Dorn (1966), which are abnormally weak. The alloys in Fig. 2.4 also have similar stress exponents, on the order of 4.5 to 6, except for a transition to a lower stress exponent at the lowest stress levels. Examination of the stress exponents for materials having a wide variety of grain sizes, including single crystals, reveals that between 1100 - 1400 K, the values for n cluster between 5 and 7 (Nathal 1992). Class A materials are usually characterized by a stress exponent of three while Class M behavior is typically characterized by a stress exponent of five. Although a stress exponent of 7 is higher than characteristic for class M behavior, such high values have been observed in

several Class M materials (Ashby 1972). Observations of subgrain formation after high temperature deformation (Kanne, Strutt and Dodd 1969; Yang and Dodd 1973), the operation of normal primary creep behavior, under both constant load and constant crosshead speed conditions (Strutt, Dodd and Rowe 1970; Whittenberger 1987 and 1988), strain rate transient test results (Yaney and Nix 1988; Forbes et al. 1993) and strengthening via a reduction in grain size (Whittenberger 1988) are all consistent with Class M behavior. Consequently, high temperature creep in binary NiAl is apparently climb controlled over most stresses and temperatures investigated.

Forbes et al. (1993) have argued that creep deformation in single crystal NiAl is a mixture of both Class A and M behavior, with the relative proportions of each type dependent on crystal orientation and the stress/temperature regime. Both Forbes et al. (1993) and Vandervoort, Mukherjee and Dorn (1966) show a gradual decrease in stress exponent, approaching 3 at high temperatures (1400-1500 K), which is consistent with this idea. However, it remains to be determined whether the viscous glide contribution is significant in cases other than very high temperature creep of soft orientation single crystals, where subgrain formation is suppressed due to the limited availability of slip systems.

Time dependent deformation can also occur by stress assisted vacancy flow at stresses that are too low for dislocation processes to be significant. Creep by these diffusional mechanisms such as Nabarro-Herring or Coble creep is attributed solely to the movement of vacancies from sources to sinks, which are usually grain boundaries of different orientations with respect to the applied stress. These mechanisms are characterized by a stress exponent of $n = 1$ and a clear dependence of creep strength on grain size, with large-grained materials being more creep resistant.

Evidence for the operation of diffusional creep mechanisms in B2 alloys was reported by Rudy and Sauthoff (1985) who observed $n = 1$ behavior during experiments on a Ni-20Fe-50Al alloy. Some recent data for binary NiAl at very low stress levels and temperatures above 1300 K indicated that the stress exponent was between 1.6 - 2.1 (Raj and Farmer 1993), which is also indicative of the operation of a grain boundary assisted deformation mechanism. It should be noted that the study by Raj and Farmer (1993) was performed on NiAl samples consolidated from powder heat P541. Thus, when their data is combined with the data from this report (Chapter V), the temperature range over which a single alloy composition has been studied in detail is extended from 300 to 1400 K and includes four different deformation regimes. There is additional evidence for diffusional creep processes in binary NiAl at temperatures above 1300 K and at low strain rates, where grain growth during creep testing resulted in coarser grained material having higher strengths (Whittenberger 1987). Therefore, the limited data generated to date indicates that diffusional creep may occur in polycrystalline NiAl at $T > 1200$ K and at very low stresses.

One final point about the creep behavior of binary NiAl is worth noting. Unlike most properties for NiAl, there is a broad range in composition between about 45 and 51 at.% Al, where the creep rate is roughly independent of stoichiometry (Yang and Dodd 1973; Whittenberger 1987; Whittenberger, Kumar and Mannan 1991). The largest difference in creep rates within this range of compositions is about a factor of 5. Only at very low and high Al contents were nonstoichiometric alloys noticeably weaker (Whittenberger et al. 1991; Whittenberger, Kumar and Mannan 1991). This loss in strength is most easily explained by the lower melting points of these compositions, which in turn implies a higher diffusivity. The diffusivity data for NiAl (Hancock and McDonnell 1971; Lutze-Birk and Jacobi 1975; Berkowitz, Jaumot and Nix 1954) actually suggests a more significant effect on properties than is observed. Nevertheless, these trends in strength as a function of stoichiometry are reversed from those observed at lower temperatures, where defect hardening predominates (Pascoe and Newey 1968b).

The design of creep resistant NiAl alloys has been discussed in detail by Nathal (1992) and additional properties not germane to this thesis such as fatigue behavior, oxidation resistance and processing have been previously reviewed (Noebe, Bowman and Nathal 1994). Our knowledge of the behavior of NiAl has come a long way since the first exploratory studies of the late 1950's and early 1960's. However, many areas concerning the flow and fracture behavior of polycrystalline NiAl in the vicinity of the BDTT are still poorly understood. This inadequate understanding of the flow and fracture mechanisms in the region of the BDTT for NiAl was the main driving force behind the experimental program described in the following chapters.

CHAPTER III
EFFECT OF INTERFACES ON THE MECHANICAL BEHAVIOR OF NiAl

3.1. Introduction

The demand for new structural materials to be employed in advanced jet engines and other high performance aerospace applications has been the driving force behind the development of intermetallic, ceramic and composite materials. Investigation of these "alternative" materials has been necessitated primarily by the need for greater engine operating efficiencies, which can only be met by materials that are capable of withstanding substantially higher operating temperatures and/or possess lower densities than currently available superalloys. Furthermore, these new structural materials must exhibit some semblance of ductility and toughness at both ambient and operating temperatures as well as possess adequate oxidation and hot corrosion resistance. The balance of these properties in advanced single-crystal nickel-based superalloys is difficult to surpass. However, a serious limitation to Ni-based superalloys is the low melting point of Ni_3Al (1638 K), which is the principal strengthening phase of these materials.

To meet the demands of ever greater engine efficiencies, alloys based on intermetallic systems including NiAl (Grala 1957; Darolia 1993) have been targeted for research over the years. NiAl offers a number of distinct advantages over conventional superalloys, which have already been discussed in Chapter I. Unfortunately, the mechanical properties of NiAl fall short of superalloys in several critical areas. NiAl is considered unsuitable as a structural material due to its limited low temperature ductility and toughness and poor elevated temperature strength. However, recent advances in single crystal alloy development (Walston et al. 1993), AlN particulate reinforced alloys

(Whittenberger 1993), continuous fiber composite technologies (Bowman 1992), and eutectic alloy development (Johnson et al. 1993) hold promise for significantly improving the creep strength of NiAl. Creep strengths comparable to first generation single crystal Ni-based superalloys have already been achieved. Unfortunately, no similar progress has been made relative to the improvement of low temperature properties of near stoichiometric NiAl. Consequently, poor low temperature fracture toughness and ductility remain the last stumbling blocks to the development of a structural NiAl-based alloy.

Ductile phase reinforcement has become a common response for improving the toughness and ductility of brittle materials including NiAl. Therefore, both the low temperature behavior of binary NiAl and recent attempts at improving properties through the incorporation of a second ductile phase will be discussed. Emphasis will be placed on the mechanisms involved in ductile phase reinforcement, as determined from several model two-phase NiAl-based alloys produced and studied specifically for this purpose. Finally, both the advantages and disadvantages associated with ductile phase reinforcement will be addressed.

3.1.1. Low temperature mechanical behavior of NiAl

The low temperature deformation processes active in NiAl have been reviewed in the previous chapter. However, it cannot be emphasized enough that for all non-[001] single crystal orientations and polycrystalline materials, only <100> slip on {011} and occasionally {001} type planes is observed after monotonic deformation (also see review by Noebe, Bowman and Nathal 1993). As a consequence of this preferred deformation mode, only three independent slip systems are available for polycrystalline deformation by <100> slip regardless of the operative slip planes (Ball and Smallman 1966b). Because this is less than the five independent deformation modes considered necessary for extensive, uniform, crack free deformation of a polycrystalline aggregate (Groves and Kelly 1969), NiAl is considered to have little potential for exhibiting substantial room temperature tensile ductility.

Experimental evidence supports this view. The room temperature tensile ductility of polycrystalline NiAl is minimal with reported values ranging from zero to a maximum of about 4% (Rozner and Wasilewski 1966; Hahn and Vedula 1989; George and Liu 1990). However, NiAl is also brittle in single crystal form. Generally, only 0.5 to 2.5% tensile ductility is observed below about 475 K in non-[001] oriented crystals (Lahrman, Field and Darolia 1991) and zero ductility up to approximately 600 K in stoichiometric NiAl of near [001] orientation (Bowman, Noebe and Darolia 1989). While grain boundaries are obviously not a consideration in the deformation of single crystals, a limited number of potential slip systems can affect the ductility of an alloy such as NiAl even in single crystal form. Dislocation glide on a limited number of slip systems is not sufficient to accommodate the complex stress states that can develop near surface notches or internal defects such as inclusions, pores or shrinkage cavities. Therefore, without the means of relaxing the stress concentrations that develop at grain boundaries in polycrystalline materials or at defects in single crystals, low ductility, brittle fracture can be expected in NiAl. This problem is enhanced by the poor, low-temperature fracture toughness of the intermetallic.

The plane strain fracture toughness for single phase B2 NiAl polycrystalline alloys is usually measured between 4 and 7 MPa $m^{1/2}$ (Reuss and Vehoff 1990a,b; Rigney and Lewandowski 1992a). These values are about the same as those obtained from polycrystalline ceramics, e.g. 5-6 MPa $m^{1/2}$ for polycrystalline Al_2O_3 and about 7 MPa $m^{1/2}$ for polycrystalline Al_2O_3-ZrO_2 of eutectic composition (Kazmin, Mileiko and Tvardovsky 1990). The fracture toughness of single crystal NiAl is comparable, varying between 4 and 10 MPa $m^{1/2}$ depending on crystallographic orientation (Chang, Darolia and Lipsitt, 1992; Vehoff 1993).

While low fracture toughness tends to have a detrimental impact on tensile ductility, it is likely that both the poor ductility and fracture toughness of NiAl at low temperatures are a result of the operative deformation processes, i.e. <100> slip.

Consequently, the underlying cause of the poor low temperature properties of NiAl can be traced to the fact that it is a slip system limited material. Two possibilities for overcoming this deficiency become immediately obvious. One approach would be to alloy NiAl to lower the ordering energy in hopes of initiating alternate or additional slip systems. This approach will be discussed in Chapter IX. Another possibility is to add a ductile second phase to NiAl to increase the ductility and toughness through extrinsic or even intrinsic toughening mechanisms. This latter approach will be the focus of the remainder of this chapter.

3.1.2. Ductile phase toughening concepts

A. Macrostructural Toughening

Macrostructural toughening involves the incorporation of a ductile second phase in a brittle matrix. The purpose of the ductile phase is to interact or interfere with the progression of cracks through the matrix phase. The ductile second phase can take the form of isolated particles, interpenetrating networks or continuous phases such as lamellae or fibers. While the degree of toughening is generally dependent on the volume fraction and morphology of the second phase, the actual characteristics of the ductile phase that will generate optimum toughness have not yet been adequately established or modeled. However, much information has been acquired through semi-empirical studies of ductile phase toughened systems such as glass/Al (Krstic, Nicholson and Hoagland 1981), WC/Co (Sigl and Exner 1987), Al_2O_3/Al (Flinn, Ruhle and Evans 1989), Al_2O_3/Mo (Kazmin, Mileiko and Tvardovsky 1990), MgO/Ni, Fe or Co (Hing and Groves 1972) and TiAl/Nb (Odette et al. 1989). From these and other studies it was determined that toughening can occur by several different mechanisms that are generally categorized as crack bridging, crack blunting or crack deflection. These three mechanisms are schematically illustrated in Fig. 3.1.

During crack bridging (Fig. 1a), moderate to strongly bonded ductile particles are intercepted by a crack, which causes the particles to undergo extensive plastic stretching in the crack wake. This contributes to the toughness of the material by inhibiting or making further crack opening very difficult. Empirical observations indicate that toughening by this mechanism is enhanced by increasing the volume fraction of the ductile particles, increasing the size of the individual particles, and increasing the work of rupture of the ductile second phase (Sigl et al. 1988; Evans 1990). In addition, toughness can be improved by a ductile phase that exhibits high strength, a large strain hardening exponent, and a high necking resistance (Odette et al. 1989). Crack bridging is further optimized when the ductile phase is continuous in nature since the only ductile regions which experience extensive plastic strain are those segments that stretch between the crack surfaces in the bridging zone just behind the crack tip (Evans 1990). If the crack can easily circumvent the ductile second phase it will obviously have much less of an impact than if the crack has to intersect the ductile phase. Overall, energy dissipation due to plastic deformation in the bridged region can be quite large and provide a major increase in toughness as well as shield the crack from the external load.

Toughening may be enhanced further by designing a ductile phase with an interface capable of undergoing limited debonding (Odette et al. 1989; Nardone and Strife 1991). This was demonstrated in one study where it was observed that energy absorption in a continuous ductile phase reinforced material increased as the length of the debond area along the bridged crack increased (Nardone and Strife 1991). However, extensive debonding does not result in a significant increase in steady state toughness and generally results in a decrease in the tearing modulus (Odette et al. 1989). Therefore, while some debonding along the interface may be required for optimizing energy absorption there are limits to the amount of debonding that is preferred.

A second type of bridging mechanism, which is sometimes included in discussions of crack deflection mechanisms, is the bridging of a crack by brittle fibers or whiskers. During this type of bridging process, the bridging material has the same level of toughness as the matrix and is usually incapable of undergoing plastic deformation. By combining two brittle components into a composite, limited toughening is achieved through interfacial debonding with crack deflection along the interface accompanied by frictional sliding along the debonded area (Evans and Marshall 1989). However, the degree of toughening achieved through this process is significantly less than can be realized when the bridging phase can also undergo plastic deformation.

Crack blunting (Fig. 1b) occurs when the propagation of a crack tip is impeded as it intersects a ductile particle. Extensive localized plastic deformation of the second phase causes the stresses at the crack tip to relax sufficiently to blunt the crack and in the ideal case will prevent the crack from propagating further. Again, the crack tip is shielded from the external load. A second phase material with a low yield strength will tend to maximize this effect (Sigl et al. 1988).

Any second phase that is weakly bonded to the matrix has the potential to increase the toughness of the system through crack deflection processes. As illustrated in Fig. 1c, the crack is redirected during the deflection process in such a way that the stress intensity at the crack tip becomes diminished (Evans 1990; Evans, He and Hutchinson 1989). However, because the particle is weakly bonded to the matrix the crack will have a chance to renucleate on the other side of the second phase component. Therefore, crack deflection due to interfacial debonding contributes much less to the toughening of a component than the two previous mechanisms. In spite of this shortcoming, crack deflection is one of the easiest and most common mechanisms used to toughen ceramics (Evans and Marshall 1989).

Recently, ductile phase toughening has been attempted in a number of intermetallic systems with varying degrees of success. These systems have included Cr_3Si reinforced with Cr (Newkirk and Sago 1990), $MoSi_2$ reinforced with Nb (Xiao, Kim and Abbaschian 1990), $NbAl_3$ reinforced with Nb (Lu et al. 1990), Nb_5Si_3 reinforced with Nb (Lewandowski et al. 1988), TiAl reinforced with Nb or titanium alloys (Elliot et al. 1988), and of course, NiAl reinforced with various refractory metal compounds such as Cr, Mo and V (Johnson et al. 1992,1993; Heredia and Valencia 1992). The presence of the ductile second phase in these alloy systems resulted in an increase in toughness ranging from 1 to 5 times that of the monolithic intermetallic. Without serious critical analysis, the major toughening mechanism in all of these ductile phase reinforced systems has been attributed to crack bridging. Secondary contributions to the toughness of some of these materials has also been attributed to crack deflection and crack blunting mechanisms (Elliot et al. 1988).

The examples of ductile phase toughening summarized in the previous paragraph with the possible exception of the *in-situ* eutectic alloys, are primarily laboratory-based model systems. A successful example of the practical application of ductile phase toughening concepts is the development of $\alpha_2 + \beta$ titanium aluminide alloys (Nishiyama et al. 1990; Chan 1990a). In this system Nb is added to Ti_3Al (α_2) to stabilize the formation of the more ductile high temperature β-phase. The β-phase in most cases is a disordered Nb-rich bcc phase and while it constitutes only about 10% of the microstructure, it exists as a continuous ductile phase (Lukasak and Koss 1990). Alloys with a composition of Ti-24Al-11Nb (at.%) exhibit room temperature plane strain fracture toughness values of 20-23 MPa $m^{1/2}$ (Chan 1990a; Aswath and Suresh 1989), while similar alloys containing Mo and slightly higher levels of Nb can exhibit K_{IC} values of up to 30 MPa $m^{1/2}$ (Blackburn and Smith 1989). Tensile ductility for this family of alloys varies from about 2% to greater than 10% elongation at room temperature, depending on the exact composition and heat treatment (Chan 1990a, Blackburn and Smith 1989).

The toughness of these alloys, as in most ductile phase toughened systems, is attributed to crack bridging by the ductile β-ligaments (Chan 1990). In addition, the β-phase acts like a crack blunting component and can also deflect propagating microcracks (Chan 1990). Hence, all the mechanisms described in Fig. 1 contribute to the toughness of $\alpha_2 + \beta$ Ti-aluminides, although the exact contribution of each component to the toughness of these materials has not been determined quantitatively. Nevertheless, good low temperature toughness and ductility have been achieved even though Ti_3Al, like NiAl, is a slip system limited material (Sastry and Lipsitt 1977). Consequently, the toughening mechanisms presented in Fig. 1 and the type of microstructure developed in the $\alpha_2 + \beta$ Ti-aluminides should serve as qualitative guidelines for the design of NiAl-based alloys.

B. Microstructural Toughening

The constrained deformation of the ductile phase may also lead to dislocation generation at the interphase interface of a two-phase material and thus, promote plastic deformation in the brittle matrix. This process is known as strain transfer and can be facilitated by the presence of specific orientation relationships between the two phases and a strong interphase interface. Through this mechanism additional mobile dislocations would be available to contribute to the plastic deformation of the brittle intermetallic phase and thus, postpone the initiation and/or propagation of fracture. This is not a traditional toughening mechanism nor is it widely recognized in the literature. However, certain intermetallic systems seem to benefit greatly from this process and the reader is referred to the dissertation by Misra (1994) and related articles (Misra, Noebe and Gibala 1992, 1993) for specific examples.

Theoretically, the transfer of strain from the ductile second phase to the brittle matrix can be understood by analyzing the similar case of strain transfer across a grain boundary. Slip transfer across grain boundaries in single phase materials has been described in a model proposed by Shen, Wagoner and Clark (1988) and later modified by Lee et al. (1990a,b). During this process, lattice dislocations in the first grain (or phase) approach a grain boundary (or interface) followed by subsequent initiation of slip into a second grain (or phase). Lee et al. (1990b) have proposed three criteria that can be used to determine the slip system that will be activated in grain 2 by a stress concentration at the boundary due to the constrained deformation of grain 1. The slip system initiated in the second grain will be the one for which: i) the angle between the lines of intersection at the boundary of the incoming and outgoing slip planes will be minimized, ii) the resolved shear stress acting on the outgoing slip system from the piled-up dislocations will be maximized, and iii) the magnitude of the Burgers vector of the residual boundary dislocations generated during the slip transfer process will be minimized.

Similarly, if grain 1 is a ductile phase and grain 2 is the brittle intermetallic phase, then a pile-up of dislocations in phase 1 may result in slip occurring in the adjacent brittle phase. The process of deformation transfer between phases can occur by at least two mechanisms (Lee et al. 1989), either by the direct transmission of dislocations from one grain to another or by nucleation of dislocations in a neighboring grain or phase. Both processes are aided by stress concentrations at the boundaries due to the pile-up of dislocations. However, direct transmission of dislocations across a boundary generally requires a dislocation reaction such that one product dislocation is transferred to the neighboring grain while a residual dislocation remains in the boundary to insure interface compatibility. While this process has been observed in single phase metals and ordered alloys (Shen, Wagoner and Clark 1988; Bond, Robertson and Birnbaum 1987) it would seem improbable in two-phase systems. Therefore, strain transfer between two dissimilar phases would most likely occur by nucleation of dislocations in the brittle phase as opposed to direct transfer of dislocations across the boundary.

Similar to the case of single phase materials, strain transfer will be facilitated by an orientation relationship between the two phases that minimizes the angle between the lines of intersection at the boundary of the incoming and outgoing slip planes. Dislocation nucleation will occur when the resolved shear stress on the outgoing slip system from the pile-up of dislocations in the ductile phase exceeds the critical value for the onset of slip in the brittle phase. The dislocations generated at the interface will then contribute to the plastic deformation of the brittle phase, imparting additional ductility and possibly toughness to the material. However, if the interface is weak, the stress concentration due to the constrained deformation of the ductile phase may nucleate cracks at the interface and thus, inhibit operation of such a mechanism. Similarly, fracture of either phase would tend to inhibit the strain transfer process.

3.1.3. Microstructure of two-phase NiAl alloys

Some qualitative guidelines for choosing a ductile second phase and for the subsequent development of ductile phase toughened NiAl alloys have been discussed in the previous section. The first place to look for an appropriate ductile phase for reinforcing NiAl is in the binary Ni-Al or a ternary Ni-Al-X system. A binary phase diagram for Ni-Al is shown in Fig. 3.2. This is essentially the same phase diagram developed by Singleton, Murray and Nash (1986) with the following modifications. The melting point of stoichiometric NiAl, while still assumed to be congruent, is approximately 44 K greater than previously reported (Walston and Darolia 1993). This higher solidus temperature also has been confirmed by my own DTA measurements on both single crystal and prealloyed powder NiAl materials. The peritectoid reaction, resulting in the formation of Ni_5Al_3, is approximately 25 K higher in temperature (Dulmaine 1989) and the boundary for the Al-rich side of the Ni_5Al_3 phase has been modified based on more recent information (Khadkikar et al 1993). The most significant changes in this version of the phase diagram, however, concern the Ni_3Al region. The peritectic and eutectic lines are approximately 20 K lower in temperature than previously reported and the position of the eutectic and peritectic reactions are reversed. The changes to the Ni_3Al portion of the phase diagram are based on significant experimental work by Bremmer et al. (1988) and are in agreement with previous work by Schramm (1941).

It is evident from Fig. 3.2 that the only potentially ductile phase in equilibrium with NiAl (β) in the binary Ni-Al system is Ni_3Al (γ') which is an ordered fcc phase. Ni_3Al has potential as a ductile second phase for reinforcing NiAl because it has inherent tensile ductility in single crystal form, exhibiting over 98% elongation at room temperature for [001] oriented crystals (Copley and Kear 1967). Though Ni_3Al is generally brittle in polycrystalline form it is now realized that this is due to environmental attack (George, Liu and Pope 1992,1993). However, this problem can be alleviated through microalloying additions of boron (Aoki and Izumi 1979). In addition, the fracture toughness of polycrystalline Ni_3Al increases from about 20 MPa $m^{1/2}$ in the undoped condition to greater than 28 MPa $m^{1/2}$ for B-doped material (Lewandowski et al. 1990). Even without B additions, polycrystalline Ni_3Al has superior toughness to NiAl. The important point is that in contrast to NiAl, Ni_3Al is inherently ductile at room temperature as demonstrated by single crystal behavior. Furthermore, because low temperature deformation occurs by <110>{111} slip (Pope 1990), Ni_3Al has enough independent slip systems to accommodate plastic deformation in polycrystalline form. This makes γ' a possible candidate for ductile phase toughening of NiAl since two-phase systems can be easily formed in-situ from the melt or by proper heat treatment of certain alloys.

A slight complication to this approach is that a number of other stable and metastable phases can occur in the compositional region between NiAl and Ni_3Al. These include the metastable phase Ni_2Al (Reynaud 1976; Khadkikar et al. 1993) and the equilibrium phase Ni_5Al_3 (Robertson and Wayman 1984; Dulmaine 1989; Khadkikar et al. 1993). Fortunately, the peritectoid reaction resulting in Ni_5Al_3 is extremely sluggish, requiring days or weeks to reach completion even when the aging treatment occurs within 40 K of the peritectoid temperature (Khadkikar et al. 1993). Consequently, this phase was not even identified until very recently (Robertson and Wayman 1984). The same is true for Ni_2Al (Reynaud 1976), which is not observed except as a metastable phase during heat treatments to form Ni_5Al_3 (Khadkikar et al. 1993). Limited evidence suggests that Ni_5Al_3 is much more brittle than NiAl (Khadkikar, Vedula and Shabel 1987), making it useless as a toughening agent and an undesirable phase. Therefore, it is fortunate that this phase does not occur readily in practice unless a very deliberate, intermediate temperature aging treatment is performed. Furthermore, Ni_5Al_3 has not been observed in some ternary alloys, i.e., NiAlCo alloys (Pank, Nathal and Koss 1990) so it may be possible to eliminate this phase by alloying. However, this phase has been observed in ternary NiAlFe alloys

(Yang and Wayman 1993). Therefore, each alloy system will have to be evaluated independently for the presence of a Ni_5Al_3 type phase.

The only other phase to commonly appear in the two-phase NiAl-Ni_3Al regime during normal processing and short term aging treatments is $L1_0$ NiAl-martensite. This martensitic reaction is a thermoelastic, reversible transformation which occurs when NiAl of appropriate composition is quenched below its martensitic start, M_s, temperature (Smialek and Hehemann 1973: Chakravorty and Wayman 1976). The M_s temperature is very sensitive to chemistry and follows a very steep linear dependence on composition. Noebe, Misra and Gibala (1991) have combined the data of 10 different investigators to determine the relation between composition and M_s temperature. The best linear fit of the data is described by the following equation:

$$M_s = 122.8(\text{at.\% Ni}) - 7363.6$$

where the M_s temperature is in degrees Kelvin and the composition of the binary alloy is entered in atomic percent Ni. From the above relation it is apparent that a very slight change in chemistry results in a very dramatic change in M_s temperature. This steep temperature dependence is best illustrated by superimposing the M_s relationship given above onto the phase diagram in Fig. 3.2.

3.1.4. Transformation toughening

As in TRIP steels (Antolovich and Fahr 1972) and transformation toughened ceramics (McMeeking and Evans 1982; Lange 1982a,b), the martensitic reaction has been proposed as a mechanism for increasing the toughness of NiAl. The strongest proponents for transformation toughening of NiAl-based materials are Russell, Law and Blackburn (1989), who have investigated the toughness of Ni-Al and Ni-Co-Al alloys. Some of their results are worth noting in greater detail. Ordered Ni-Co-Al alloys were found to have a fracture toughness of approximately 10 MPa $m^{1/2}$ (Russell et al. 1989). By slightly modifying the composition of these Ni-Co-Al alloys it was possible to generate two-phase microstructures containing 5 to 35 vol.% γ'. These two-phase alloys exhibited toughness values in the range of 15 - 25 MPa $m^{1/2}$. Russell and Law (1990) attributed this increase in toughness to martensitic transformation toughening mechanisms. However, this increase in fracture toughness over the single phase alloys is probably due to the operation of ductile phase toughening mechanisms.

The martensitic reaction would offer little benefit in the way of classical transformation toughening in the NiAl intermetallic system. In its simplest terms, transformation toughening is a process that is controlled by the volume increase of a second phase particle due to a phase transformation (Evans 1990; McMeeking and Evans 1982). The martensitic reaction which occurs in TRIP steels and in $Zr0_2$ toughened ceramics results in a volume change (ΔV) or volume dilatation of 3 - 5% (Antolovich and Fahr 1972; Lange 1982a). Martensite formation in NiAl results in a volume change of only 0.4% (Chakravorty and Wayman 1976). The increase in toughness due to transformation toughening (ΔK) is directly proportional to the volume dilatation associated with the transformation (McMeeking and Evans 1982). For ceramic systems, a ΔV of 3 - 5% results in a ΔK on the order of 5 MPa $m^{1/2}$ (McMeeking and Evans 1982; Lange 1982b). Because the volume increase for the martensitic transformation in NiAl is an order of magnitude less than in these ceramic systems, the increase in toughness, to a first approximation, would be an order of magnitude less. Therefore, transformation toughening in the NiAl system would only result in a ΔK of about a 0.5 MPa $m^{1/2}$, which would barely be noticed above experimental scatter in the test results. In agreement with this argument, all the single phase alloys studied by Russell et al (1989), whether fully B2, fully martensitic or a mixture of the two phases had similar fracture toughness values of approximately 10 MPa $m^{1/2}$ (Russell et al. 1989). Therefore, deformation of the B2 alloy resulting in stress induced martensite during fracture does not appear to result in any increase in toughness over the already fully martensitic material or fully B2 alloys. Consequently, transformation toughening in NiAl-based alloys does not result in a significant increase in toughness and is therefore not a suitable approach for toughening these materials. Conversely, the data of Russell et al. (1989) indicate that ductile phase toughening would appear to be a viable approach to increasing the fracture resistance of NiAl-based materials.

3.2. Materials and Experimental Procedures

In order to produce model material systems to study the effect of microstructure on the mechanical behavior of ductile phase reinforced NiAl, two-phase alloys were processed by several different techniques. First, a series of Ni-Al arc melted buttons was used to identify potential alloy compositions/microstructures that would warrant further study. Promising alloys were then processed by directional solidification or extrusion of prealloyed metal powders for the purpose of mechanical testing.

One material chosen for study in greater detail, because the microstructure resembles that of the $\alpha_2 + \beta$ Ti-aluminides, was a Ni-36(at.%)Al alloy. This alloy composition lies within the two component, $\beta + \gamma'$, Ni-Al phase field. Prealloyed powder (Heat P895) was loaded into plain carbon steel extrusion cans and extruded at 1200 K and an area reduction ratio of 16:1. A full chemical analysis of this alloy appears in Appendix A. After extrusion, half of the material was subsequently annealed at 1000 K for 10 hours to increase the amount of γ' present.

Also, a composite-like material was produced through directional solidification of a Ni-30(at.%)Al alloy at withdrawal rates ranging from 0.5 to 55 cm/hr. This material was used to investigate the various toughening concepts in further detail. Properties of this material are compared to a single phase, single crystal of composition Ni-40(at.%)Al. Both the Ni-30Al and Ni-40Al alloys were produced by directional solidification in a modified Bridgman type furnace at NASA LeRC.

Mechanical testing was performed on cylindrical button head tensile specimens with typical gauge diameters of 3.2 mm and lengths of 30 mm. Each specimen was electropolished in a 10-percent perchloric acid-90 percent methanol solution prior to testing. Tensile tests were performed to failure in a universal testing machine under displacement control at temperatures between 300 and 1200 K at an initial strain rate of 1.4×10^{-4} s^{-1}. A three-zone, resistance-heated furnace was used for the mechanical tests, which were performed in air. The temperature gradient along the gauge section of the tensile samples was within ± 2K at all temperatures. Compression tests were also performed at various temperatures and strain rates to determine the yield behavior of these alloys. Optical microscopy and scanning electron microscopy (SEM) were used to characterize the microstructure of both as-processed and fractured samples.

3.3 Results and Discussion

3.3.1. Necklace microstructures as compliant grain boundary layers

From examination of the phase diagram in Fig. 3.2, it is obvious that a ductile phase reinforced intermetallic can be formed by annealing Ni-Al alloys in the two-phase $\beta + \gamma'$ region at temperatures above 1000 K. The precipitation processes leading to the formation of Ni_3Al in NiAl have been studied previously (Russell and Edington 1972; Moskovic 1977). An example of the microstructure that results from aging a Ni-36Al alloy for ten hours at 1000 K is shown in Fig. 3.3b. The microstructure is similar in appearance to that of $\alpha_2 + \beta$ Ti-aluminides. In the case of the Ni-aluminide sample, however, γ' preferentially nucleates at the grain boundaries forming a continuous film around the β grains, a microstructure that is now commonly referred to as a necklace microstructure (Pank, Nathal and Koss 1990).

The mechanical properties of NiAl, Ni_3Al, and alloys across the two-phase compositional field are briefly summarized in Fig. 3.4. Figure 3.4a is a plot of hardness versus composition for arc-melted single and two-phase Ni-aluminides, heat treated to maximize the γ' content in the two-phase alloys. This plot gives an indication of the flow behavior of these materials. From the figure it is evident that the hardness of single phase B2-NiAl alloys increases with increasing deviation from stoichiometry for Ni-rich compositions. An increase in hardness with increasing Ni content has been observed previously by Westbrook (1956). The hardness data also follow the same trend as yield strength versus composition for single phase binary NiAl alloys, as summarized by Vedula and Khadkikar (1990). This increase in hardness or yield strength has been attributed to defect hardening. In the off-stoichiometric alloys, excess Ni atoms will occupy Al-sublattice sites acting like "substitutional" solute atoms, which result in solute strengthening. Once the two-phase field is reached, hardness begins to decrease rapidly as the volume fraction of the softer Ni_3Al phase increases, reaching a minimum at stoichiometric γ'.

Fracture toughness values for Ni-Al alloys, from several references are plotted in Fig. 3.4b. From this data, it is evident that the fracture toughness for single phase NiAl is essentially independent of composition in the single phase field but begins to increase substantially in the two-phase field. The increase in toughness of the two-phase alloys is proportional to the volume fraction of Ni_3Al and is a result of ductile phase toughening mechanisms.

The beneficial effect of a two-phase necklace microstructure on the tensile properties of a binary Ni-36Al alloy is demonstrated in Fig. 3.5. Fig. 3.5 is a series of stress-strain curves as a function of temperature for the powder extruded Ni-36Al alloy in both the as-extruded condition containing only 4% γ' (Fig. 3.4a) and after annealing at 1000 K for 10 hours in order to form a necklace microstructure of γ' (Fig. 3.4b). The BDTT for the two-phase alloy composed of the necklace type microstructure occurs at a significantly lower temperature, by least 200 K, than the as-extruded material containing only 4% Ni_3Al. While tensile ductility is still minimal in the two-phase alloy containing 32% γ', the room temperature fracture strength has been increased by a factor of 2.5 over that of the alloy containing 4% γ'. Failure of the alloy in the two-phase condition occurred primarily along γ'/β phase boundaries.

Since the materials represented in Figs. 3.4 and 3.5 were processed identically except for the post extrusion annealing treatment, it can be assumed that the critical flaw size in these samples would be similar. Furthermore, since the test geometry was also the same for both sets of samples the 2.5 fold increase in fracture strength would, as a first approximation, correspond to a 2.5 fold increase in fracture toughness due to the presence of the ductile second phase. This is the same percentage increase in toughness that would be expected in Fig. 3.4b for a two-phase alloy containing 64 at.% Ni compared to single phase β-alloys. Therefore, while ductility was not significantly affected by the presence of the ductile second phase, the fracture resistance of the Ni-36Al alloy was improved.

Significant increases in tensile ductility have been achieved in two-phase B2-based alloys when the ductile phase consisted of a disordered fcc γ-phase (Ishida et al. 1991) rather than γ'. In the work by Ishida et al. (1991), a film of disordered γ-phase was formed by alloying Ni-rich NiAl with either Fe, Co, Cr or Cu. The greatest room temperature ductility, nearly 10%, was achieved in a ternary Ni-26Al-50Co alloy that contained 30 vol.% intergranular γ-phase. For all the two-phase alloys studied by Ishida et al. (1991), improvements in hot workability and room temperature ductility over single phase NiAl was attributed to the presence of the intergranular γ-phase. Unfortunately, these alloys would be expected to have very poor high temperature strength.

The existence of a ductile necklace microstructure in an intermetallic such as NiAl, which does not have enough slip systems to satisfy grain boundary compatibility, could be beneficial because the continuous film of γ or γ' with multiple independent <110>{111} slip systems may enable grain-to-grain compatibility to be restored. The continuous, ductile grain boundary film would thus act as a compliant layer between grains. Unfortunately, the very limited tensile ductilities of alloys which exhibit γ' necklace microstructures are due in part to a weak interface between the β and γ' phases with fracture occurring readily along the β/γ' interface. However, as demonstrated in Fig. 3.4b, toughness can still be enhanced through this type of microstructure and better tensile ductility may be achieved if the interface can be strengthened. So far, significantly greater tensile ductilities have been observed with necklace structures composed of a γ-phase (Ishida 1991). This is possibly a consequence of the stronger interface and the suggestion that the γ films are inherently more ductile than γ' (Ishida 1991).

Due to the weak β/γ' interface, toughening of β-alloys with a necklace microstructure composed of γ' is apparently the result of a crack deflection mechanism which redirects the crack along γ'/β interfaces. There was insufficient information from the literature to conclusively determine the mechanism involved in the toughening of the γ reinforced alloys, though it is probably a combination of crack bridging and some inherent toughening process such as slip transfer and/or maintenance of slip compatibility through the compliant layer concept. Consequently, alloys with very similar microstructures can have very different toughening responses due to such factors as interfacial strength.

3.3.2. Flow and fracture of a directionally solidified Ni-30Al alloy

To further examine the effect of microstructure (other than a necklace structure) on the mechanical properties of two-phase NiAl-based alloys, directional solidification was used to alter the second phase morphology of a Ni-30Al alloy by varying the solidification rate. The microstructure, flow behavior, and fracture resistance of this alloy was determined as a function of directional solidification rate and subsequently the second phase morphology. The intent of these experiments was to characterize toughening mechanisms in greater detail and to determine the optimum second phase morphology for fracture resistance of two-phase nickel aluminides. Again, the system studied was a β + γ' alloy, which would be expected to have similar interfacial characteristics and interfacial strength as the Ni-36Al alloy studied in the previous section. The major difference between the two systems is that the γ' content is greater in the Ni-30Al alloy and the γ' morphology has been modified by directional solidification.

A. Microstructure

Conventional solidification of a Ni-30Al alloy produces a microstructure consisting of β-NiAl dendrites surrounded by interdendritic γ'. On cooling, the β-dendrites transform through solid state precipitation to β + γ'. An example of the resulting microstructure is shown in Fig. 3.6a. Slow directional solidification of the melt at 0.5 cm/hr resulted in an aligned rod-like γ' microstructure in a single crystal NiAl matrix. The liquid solidifies as a single crystal of Ni-rich NiAl followed by solid state nucleation and directional growth of γ' within the single crystal parent β-phase (Fig. 3.6b). Directional solidification at faster rates, 5 - 15 cm/hr, also resulted in an aligned rod-like morphology of γ' in a NiAl matrix. Except at this faster rate the Ni_3Al rods were discontinuous and aligned at a 40 - 50 degree angle to the growth direction as shown in Fig. 3.6c. Directional solidification at much faster solidification rates (55 cm/hr) results in an aligned dendritic microstructure as shown in Fig. 3.6d.

The bulk orientation relationship between the two phases, determined by x-ray diffraction, is the Kurdjumov-Sachs relationship that was first identified by Moskovic (1977) for fine Ni_3Al precipitates in NiAl:

$$\langle 111\rangle_{NiAl} \,//\, \langle 101\rangle_{Ni_3Al}$$

$$\{011\}_{NiAl} \,//\, \{111\}_{Ni_3Al}$$

The growth direction of the parent NiAl phase was <001> and the loading axis for all mechanical testing was parallel to the growth direction of the crystals.

The most important difference between these directionally solidified microstructures is the morphology of the ductile γ'-phase. For example, at solidification rates of 4.5 and 15 cm/hr, the γ'-phase forms as discontinuous rods while at the slowest rate of 0.5 cm/hr the aligned γ' rods are continuous. At much faster solidification rates, i.e. 55 cm/hr, the γ' exists as a continuous interdendritic phase along the entire length of the crystal. In all cases, the alloy contains approximately 40% β-phase and 60% γ'. The composition and properties of the individual phases in the two-phase alloy are shown in Table 3.1. The β-phase of the two-phase Ni-30Al alloy is very similar to single phase B2 Ni-40Al, Table 3.1, and therefore was used as a baseline material for mechanical property comparisons.

Table 3.1
Comparison of the phases present in a Ni-30Al alloy with a Ni-40Al alloy.

Alloy	Volume Percent of Each Phase Present	Composition (at.%)		Hardness $H_{V_{100}}$	Lattice Parameter (nm)
		Ni	Al		
Ni-30Al	B2 (40%)	62.1	37.9	387 ± 7	0.288 ± 0.001
	$L1_2$ (60%)	73.4	26.6	310 ± 10	0.3572 ± 0.0003
Ni-40Al	B2 (100%)	60.0	40.0	386 ± 10	0.2868 ± 0.0004

B. Flow Behavior

The particular morphology of the γ'-phase (continuous or discontinuous) did not significantly affect the flow strength of the two-phase alloy at the 0.2% and 3% strain levels. This is demonstrated in Fig. 3.7, which shows the compressive flow strength of the Ni-30Al alloy as a function of temperature for material produced at four different solidification rates and tested at a strain rate of 1.4×10^{-3} sec^{-1}. While there was some scatter in the data, no particular microstructure was consistently stronger than any other. For all solidification rates, the yield strength of the Ni-30Al alloy initially increased with temperature, consistent with materials containing high volume fractions of γ', reaching a peak near 850 K. By comparison of Figs. 3.7a and 3.7b it is apparent that significant strain hardening occurs in the two-phase alloy at temperatures below the peak temperature. No work hardening was observed at temperatures greater than 1200 K, with work hardening and relaxation processes balancing each other at elevated temperatures.

Fig. 3.8 contains the compression yield strength of the single phase constituents that make up the two-phase Ni-30Al alloy and data for the Ni-30Al directionally solidified at 4.5 cm/hr all tested at a strain rate of approximately 1×10^{-4} sec^{-1}. The yield strength of the two-phase ($\beta + \gamma'$) alloy increases with increasing temperature until a peak in strength is reached at approximately 800 K. While the strength of the two-phase alloy is greater than single crystal γ' (Heredia and Pope 1988), it is significantly less than [001] Ni-40Al single crystals at temperatures below 800 K. The extremely low yield stress for the two-phase alloy can be attributed to the difference in operative slip systems within the β-phases of the single and two-phase alloys. [001]-oriented NiAl, including the [001] Ni-40Al single crystals, deform by slip of <111> type dislocations at low temperatures unless the sample is mechanically unstable, in which case kinking occurs (Pascoe and Newey 1968a; Field, Lahrman and Darolia 1991b; Bowman, Noebe and Darolia 1989). In contrast, only <100> dislocations were observed in the β-phase of the two-phase Ni-30Al alloy even though the samples were mechanically loaded parallel to the [001] growth direction of the NiAl phase. Slip by <100> dislocations in the β-phase of the two-phase alloy occurred at stresses below which macro-kinking or <111> slip can occur because of the extensive operation of interfacial dislocation sources (Noebe et al. 1990), operating in a manner similar to the micro-kinking model proposed by Kim, Noebe and Gibala (1991) to explain the deformation of oxide film softened single crystal NiAl. Near room temperature, this process leads to a significantly reduced flow stress for the directionally solidified Ni-30Al alloy compared to a rule of mixtures analysis based on the strengths of the individual components.

C. Fracture Behavior

In contrast to the flow behavior, tensile ductility of the two-phase Ni-30Al alloy is dependent on the morphology of the γ'-phase as demonstrated in Figs. 3.9 and 3.10. When the ductile phase is continuous, as in the Ni-30Al alloy directionally solidified at a rate of 0.5 cm/hr or 55 cm/hr, the tensile ductility for the material is about 10% at room temperature and is independent of temperature up to 1000 K. When the γ'-phase is discontinuous, as shown in Fig. 3.6c, the tensile ductility of the two-phase alloy is on the order of 4% for temperatures between 300 and 1000 K. This is still a considerable improvement over the single phase β-alloy which has zero tensile ductility up to 950 K. The upturn in ductility at temperatures greater than 1000 K for the directionally solidified Ni-30Al alloy corresponds to the BDTT of the β-phase and the onset of extensive plasticity in Ni-40Al single crystals, Fig. 3.9.

The advantage of a continuous ductile phase over a discontinuous reinforcement becomes apparent after examining the fracture behavior of the Ni-30Al alloy as a function of second phase morphology. Directional solidification at 4.5 cm/hr results in discontinuous lengths of γ' oriented approximately 45 degrees to the tensile axis (Fig. 3.6c). The tensile ductility of this alloy at room temperature is on the order of 4% compared to zero tensile ductility for single crystal Ni-40Al (Fig. .3.10). The fracture morphology of the 4.5 cm/hr directionally solidified alloy is shown in Fig. 3.11. It is apparent from Fig. 3.11a that secondary cracking of the β-phase does not occur away from the main crack plane. This is actually quite exciting since it indicates that the β-phase has exhibited inherent ductility, which can be attributed to a very active slip transfer process (Misra, Noebe and Gibala 1992). It is also evident from Fig. 3.11 that the crack did not propagate straight through the sample perpendicular to the loading direction but took a very tortuous path along β/γ' interfaces. This is especially evident from the scalloped fracture surface shown in Fig. 3.11b. Therefore, two mechanisms are responsible for the tensile ductility of the two-phase alloy containing the discontinuous reinforcement. The most important is slip transfer, leading to intrinsic ductility of the β-phase. Because of the induced plasticity of the β-phase, crack initiation and subsequently tensile fracture is significantly delayed in the material. However, once the crack has initiated and begun to propagate some additional increment in toughness is achieved through a very active crack deflection process.

When the ductile phase is continuous (Fig. 3.12), the crack no longer travels along the interface but is blunted or bridged by the γ'-phase resulting in a tensile ductility of about 9-10% (Fig. 3.10). While the inherent ductility of the β-phase has been exceeded, as evident from the extensive secondary cracking that is observed along the entire gage length of the sample (Fig. 3.12a), the alloy was still capable of exhibiting significant tensile elongation and load carrying capability (Fig. 3.10). If the behavior of this material is similar to the material directionally solidified at 4.5 cm/hr, then it can be expected that the first 3 -4% strain was accommodated by slip transfer processes that delayed the onset of microcracking in the material. Tensile ductility beyond the 4% strain level was accomplished by extrinsic ductile phase toughening processes, namely crack bridging and crack blunting. Limited debonding along γ'/β interfaces is also evident in Fig. 3.12. This behavior occurred primarily along the main fracture plane and also contributed to the enhanced toughness of this material. Consequently, for the same volume fraction of reinforcement, ductility and toughness are dependent on the morphology of the second phase, with continuous microstructures providing the largest benefits.

The results of the Ni-30Al alloy also indicate that slip transfer can be an extremely important mechanism for enhancing the fracture resistance of β-alloys by delaying the onset of fracture. Since the Ni-36Al alloy did not display significant macroscopic room temperature plasticity, slip transfer apparently did not occur. This probably can be attributed to two factors. First, the γ'-phase was extremely thin so that dislocation pileups at the interface would have been very small. Since the stress concentration at the interface would be proportional to the pileup length, the resolved shear stress on the outgoing slip system from the pile-up of dislocations in the γ'-phase probably did not exceed the critical value for the onset of slip in the β-phase. Second, the general slip system in the β-phase is <001>{110} while slip in the γ'-phase was <110>{111} type. Since the orientation relation between the two phases in the directionally solidified material is a Kurdjumov-Sachs relationship there is perfect alignment of the slip planes across the boundary that provides the ideal geometric condition for strain transfer. This would not be the case in the Ni-36Al alloy where the γ'-phase occurs along the grain boundaries and thus would have a random orientation relationship with the β-phase. Therefore, without an efficient mechanism for transferring strain between the two phases in the Ni-36Al alloy, fracture occurred along the weak interface before strain transfer processes could take place.

By providing favorable conditions for slip transfer processes, as in the directionally solidified material, significant ductility can be generated by increasing the inherent ductility of the NiAl phase. However, the final ductility of the material can be further enhanced by optimizing the morphology of the second phase and taking advantage of certain extrinsic toughening mechanisms. A continuous reinforcement that cannot be circumvented by a crack is superior to other reinforcement morphologies, especially for materials that exhibit a weak interface.

D. Creep Strength

As stated in the introduction of this paper, binary NiAl suffers from very poor elevated temperature creep strength, which is several orders of magnitude less than a first generation single crystal Ni-base superalloy. Moreover, reinforcing NiAl with a soft, low temperature ductile phase will probably not be of much benefit, though the creep behavior of two phase intermetallics has not been studied extensively. Therefore, while the low temperature properties of the Ni-30Al alloy were of primary interest during this study, the creep behavior of this alloy was also evaluated. The strain rate - steady state creep stress behavior of the Ni-30Al alloy at 1000 - 1200 K is shown in Fig. 3.13. At stresses less than about 500 MPa, the Ni-30Al alloy displays a well behaved power law creep behavior. At stresses greater than about 500 MPa the alloy exhibits power law breakdown. In the power law creep regime, the deformation behavior of the alloy can be described by the following power law relation:

$$\dot{\varepsilon} = 743\ \sigma^{3.6}\ \exp^{(-320/RT)}$$

The stress exponent of n = 3.6 is not typical of NiAl alloys, which usually has a stress exponent of 5 - 7. The activation energy for creep of this alloy was 320 kJ/mol, which is very similar to the activation energy for diffusion in both NiAl and Ni_3Al.

The creep behaviors of the Ni-30Al alloy and its constituent single phase components at 1200 K are shown in Fig. 3.14. From this plot it is evident that the creep strength of the two-phase alloy is very similar to that of the Ni-40Al β-phase. However, the stress exponent of the Ni-30Al alloy is similar to that of Ni_3Al indicating that deformation of the γ'-phase in the two-phase alloy is rate controlling.

The creep strength of a number of nickel-aluminide materials are also presented in Fig. 3.15, including the polycrystalline Ni-36Al alloy with a necklace γ' microstructure and the directionally solidified Ni-30Al alloy. The creep strengths of the two-phase alloys are significantly lower than binary Ni-50Al in either single crystal or polycrystalline form. In fact, the Ni-36Al alloy is even slightly weaker than the single phase Ni-40Al alloy. Also, all the nickel aluminides including the Ni_3Al alloy are many orders of magnitude weaker than a first generation single crystal superalloy. Consequently, some type of high temperature reinforcing phase will also have to be incorporated into these ductile phase toughened systems or a more judicious choice of reinforcing phase will have to be made.

3.4. Caveats Pertaining to Ductile Phase Toughening Approaches

Thus far, a mostly favorable view of ductile phase toughening has been presented. Unfortunately, all NiAl-based systems described in this chapter as examples of various toughening concepts suffer from new problems that severely compromise their prospects for use in high temperature structural applications. The admirable properties of NiAl were described in some detail in Chapter I (e.g. high melting point, environmental resistance, low density, high thermal conductivity, etc.). These advantages must not be lost in a ductile-phase toughened NiAl component or else the driving force for its use disappears. For example, the use of γ or γ' as a reinforcing agent depresses the melting point of the

NiAl-based material to that of typical superalloys or worse, eliminating the original temperature advantage and reducing the density advantage of NiAl. Creep strength is also significantly compromised as discussed in the previous section.

In addition, the cyclic oxidation resistance of NiAl-based materials would almost certainly be degraded in ductile phase toughened systems. NiAl has outstanding cyclic oxidation resistance when doped with rare earth elements because of the tenacity of the Al_2O_3 scale which forms during oxidation and its resistance to spalling (Barrett 1988). This behavior, however, is extremely sensitive to the Al content of the alloy (Doychak, Barrett and Smialek 1989). When the composition of single phase NiAl varies by as little as 5 at.% Ni from the equiatomic composition, the long term cyclic oxidation resistance of the alloy begins to severely degrade due to the formation of non-Al_2O_3 oxides. This problem is aggravated in the two-phase ($\beta + \gamma'$) composition regime, which is the region of interest for ductile phase toughened alloys. A simple solution to this problem would be the application of an oxidation resistant coating to the toughened alloy. Coating compatibility and integrity then become additional issues that need to be addressed during component development. Finally, a significant loss in thermal diffusivity, by as much as a factor 4, occurs for Ni-rich β-NiAl alloys and two-phase $\beta + \gamma'$ compositions (Lowell 1993). Therefore, the thermal conductivity advantage is also reduced in these alloys.

Therefore, while tremendous advances have been made in the development of ductile and/or tough two-phase NiAl-based alloys, to date, none of these materials would qualify as a high temperature structural material. Clearly, future efforts will have to concentrate on not only improving the low temperature properties of NiAl but on developing a well rounded structural alloy. In the long run, this may prove more difficult than first envisioned.

3.5. Summary and Conclusions

1. At low temperatures, NiAl suffers from poor fracture toughness and inherently low ductility due to an insufficient number of independent slip systems to accommodate grain boundary compatibility. In two-phase alloys a continuous ductile phase surrounding NiAl grains may act as a compliant layer and restore some mechanical compatibility to the material. This mechanism has been successful in increasing the toughness of Ni-36Al alloys though increases in ductility seem to be dependent on the type of grain boundary film present.

2. The largest improvements in low temperature behavior seem to result from the presence of a continuous, ductile phase in either fiber or lamellar form. Toughening is attributed to crack bridging with additional contributions by crack blunting and crack deflection mechanisms.

3. When special orientation relationships exist between the NiAl matrix phase and the ductile phase, toughening also appears to be the result of strain transfer into the NiAl due to plastic deformation of the ductile phase. The amount of toughening attributed to this mechanism has not determined quantitatively. However, it is apparent that slip transfer significantly contributes to the enhanced plasticity of the β-phase in Ni-30Al alloys for the first several percent plastic strain. This two-phase alloy exhibits enhanced ductility and fracture resistance by inhibiting the onset of crack nucleation.

4. It was demonstrated that the ductility and toughness of NiAl-based materials can be improved by the incorporation of a ductile second phase. Presently, this has been accomplished at the expense of other properties. In particular, the creep resistance of the two-phase alloys that were studied were inferior to even unalloyed Ni-50Al. Degradation of other properties such as oxidation resistance, melting point, thermal conductivity and density are also concerns.

3.6. Redirection of Research Efforts

While strides have been made in improving the room temperature ductility and toughness of two-phase NiAl-based materials and in understanding the mechanisms responsible for this progress, these advances have been at the expense of the original properties that have made NiAl a high temperature material candidate. Consequently, it became apparent that no obvious two-phase NiAl-based system existed that met all the requirements of a competitive high temperature structural alloy. Therefore, an alternative direction was taken. Instead of developing two-phase alloys methods to improve the inherent ductility and toughness of NiAl were investigated. But before alternative approaches could be examined it was necessary to fully understand the flow and fracture behavior of the binary intermetallic. Several years ago very little was actually known about the deformation and fracture behavior of NiAl at low and intermediate temperatures and there was no accepted mechanism for the brittle-to-ductile transition. Even today many investigators still do not understand the basic behavior of NiAl (Cotton and Noebe 1994).

Therefore, my research interests shifted from two-phase alloys to an investigation of the deformation and fracture behavior of binary NiAl. The purpose of this research was to understand and then hopefully, overcome the ductility and toughness problem in NiAl through a logical approach. The ensuing chapters describe this effort.

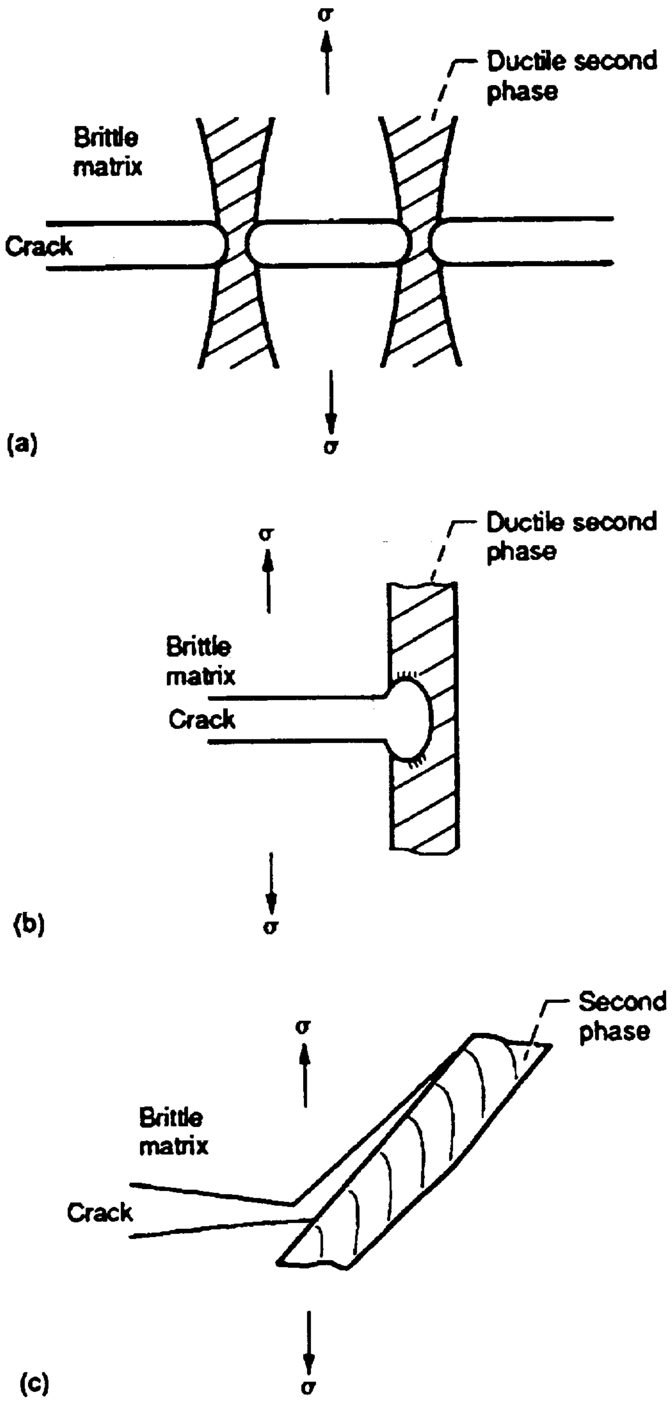
σ
Ductile second phase
Brittle matrix
Crack
(a)
σ
σ
Ductile second phase
Brittle matrix
Crack
(b)
σ
Second phase
σ
Brittle matrix
Crack
(c)
σ

Fig. 3.1. Schematic illustration of the possible mechanisms for enhancing the toughness of brittle materials through the addition of a ductile second phase: a) crack bridging, b) crack blunting, and c) crack deflection. (After Chan 1990b)

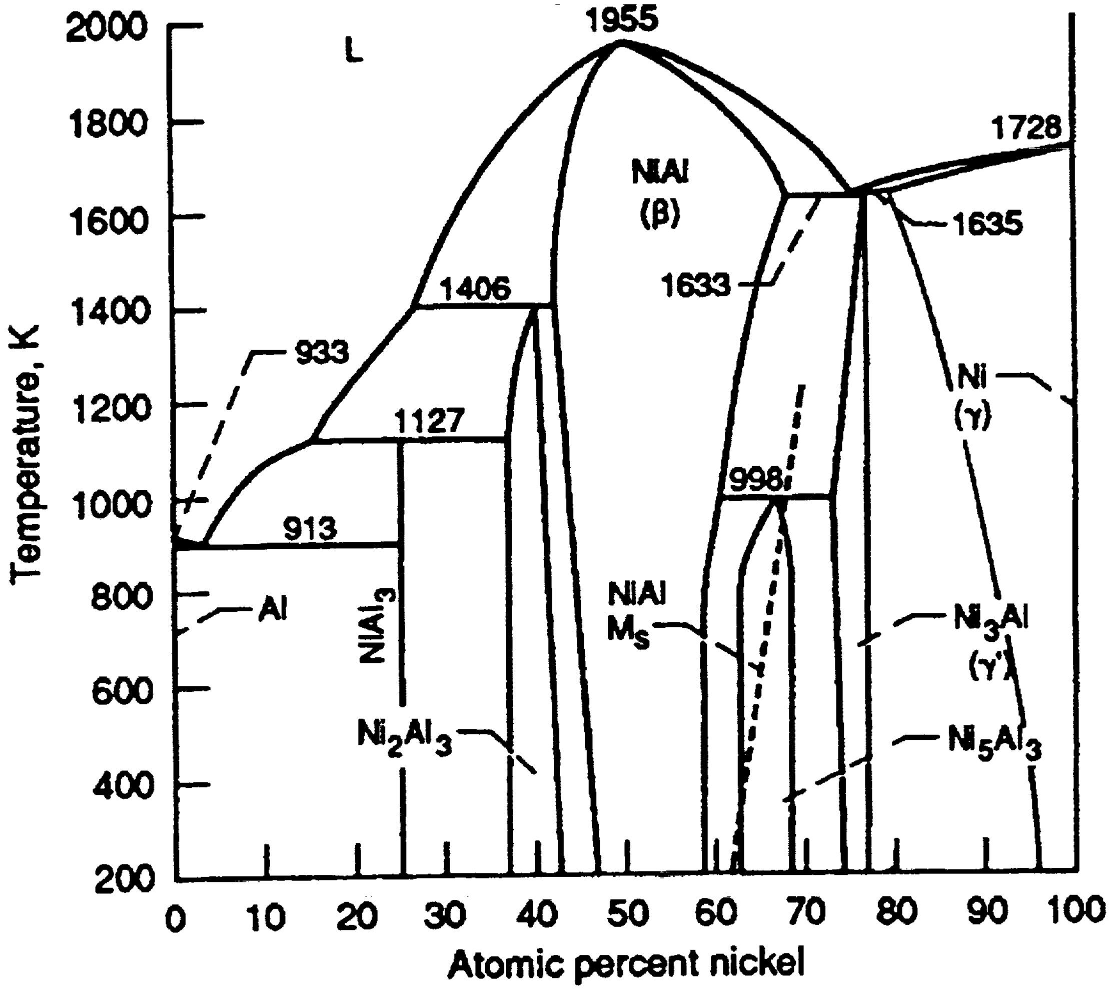

Fig. 3.2. Ni-Al phase diagram similar to that of Singleton, Murray and Nash (1986) but with several modifications that are discussed in the text. The NiAl martensite start temperature (M_S) determined from the compilation of data by Noebe, Misra and Gibala (1991) is also superimposed on the plot.

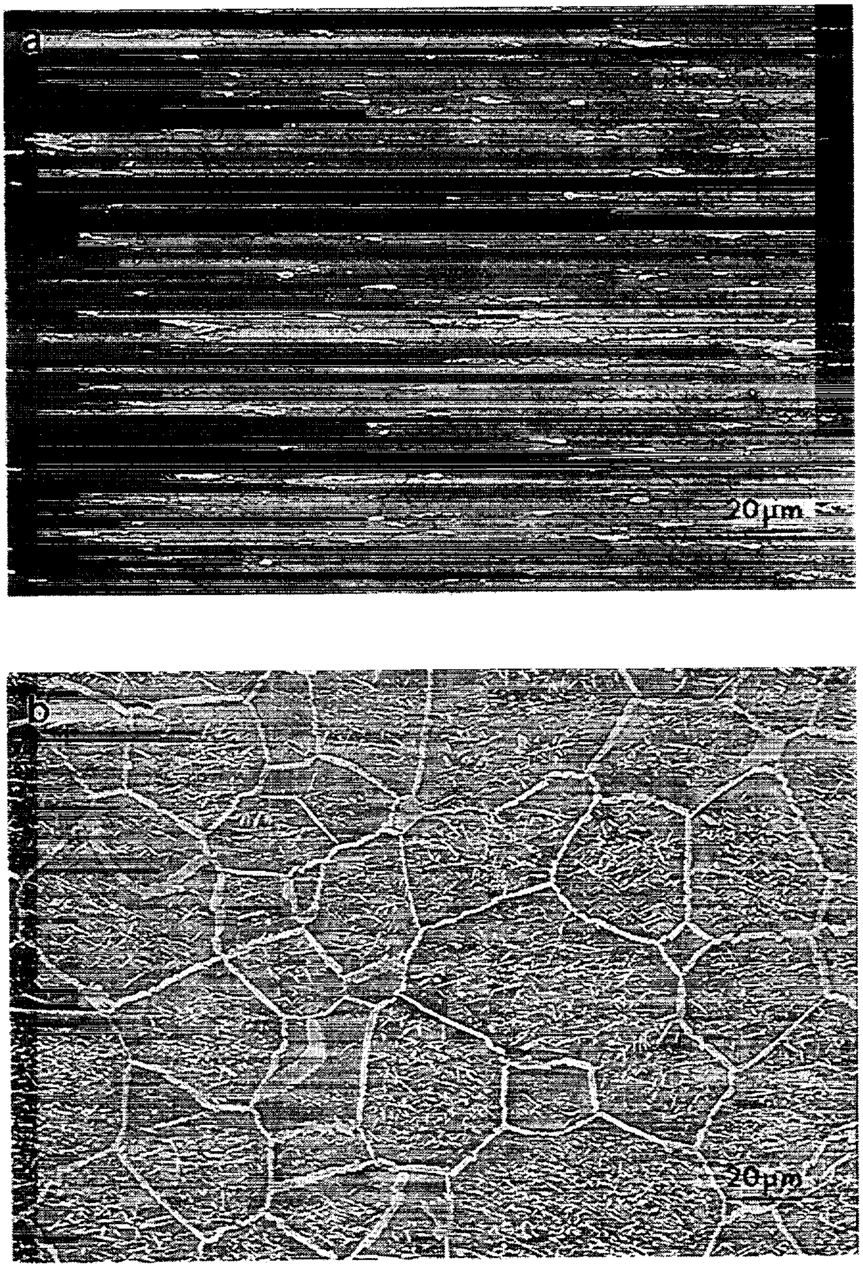

Fig. 3.3. Microstructure of a Ni-36Al alloy: a) backscatter SEM micrograph of the as-extruded alloy containing approximately 4% γ' and b) backscatter SEM micrograph of an extruded alloy annealed at 1000 K for 10 hours resulting in a necklace microstructure of γ'. The bright phase is Ni_3Al and the matrix phase is Ni-rich NiAl.

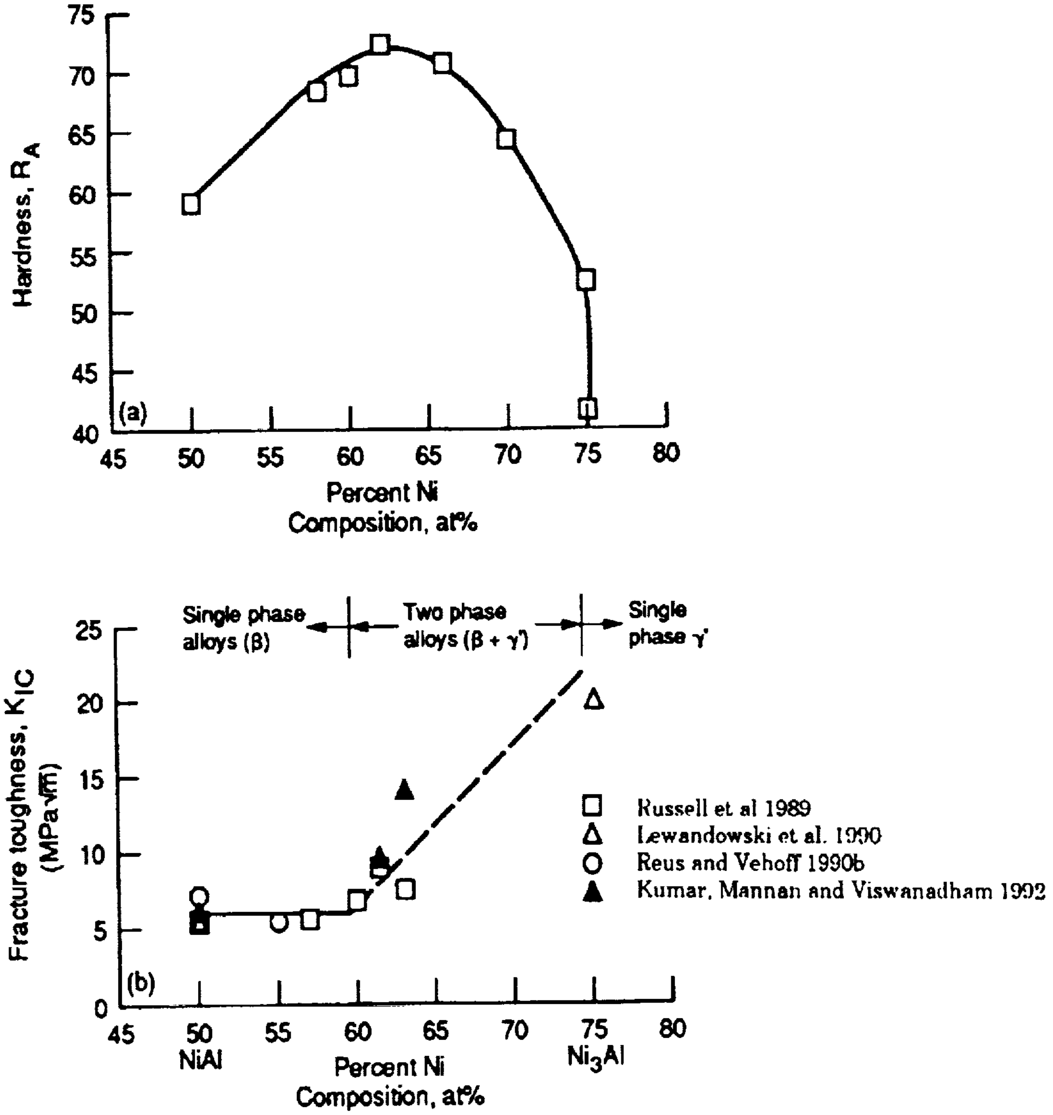

Fig. 3.4. The mechanical behavior of single and two-phase binary Ni-Al alloys: a) Rockwell A hardness and b) fracture toughness.

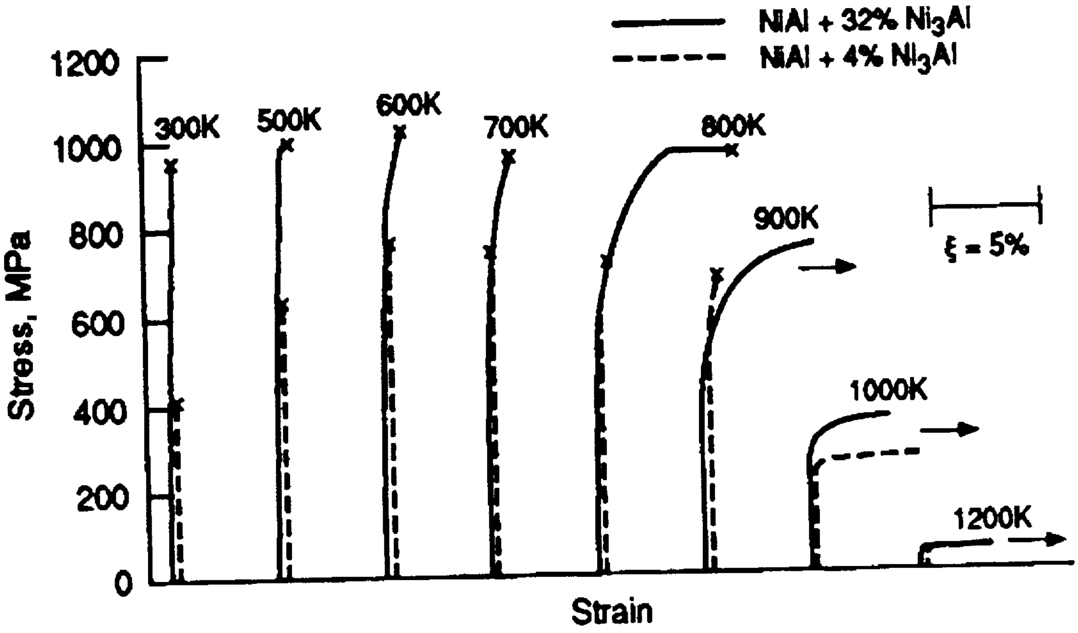

Fig. 3.5. Tensile stress-strain curves as a function of temperature for a Ni-36Al alloy containing 4 and 32 vol.% Ni_3Al.

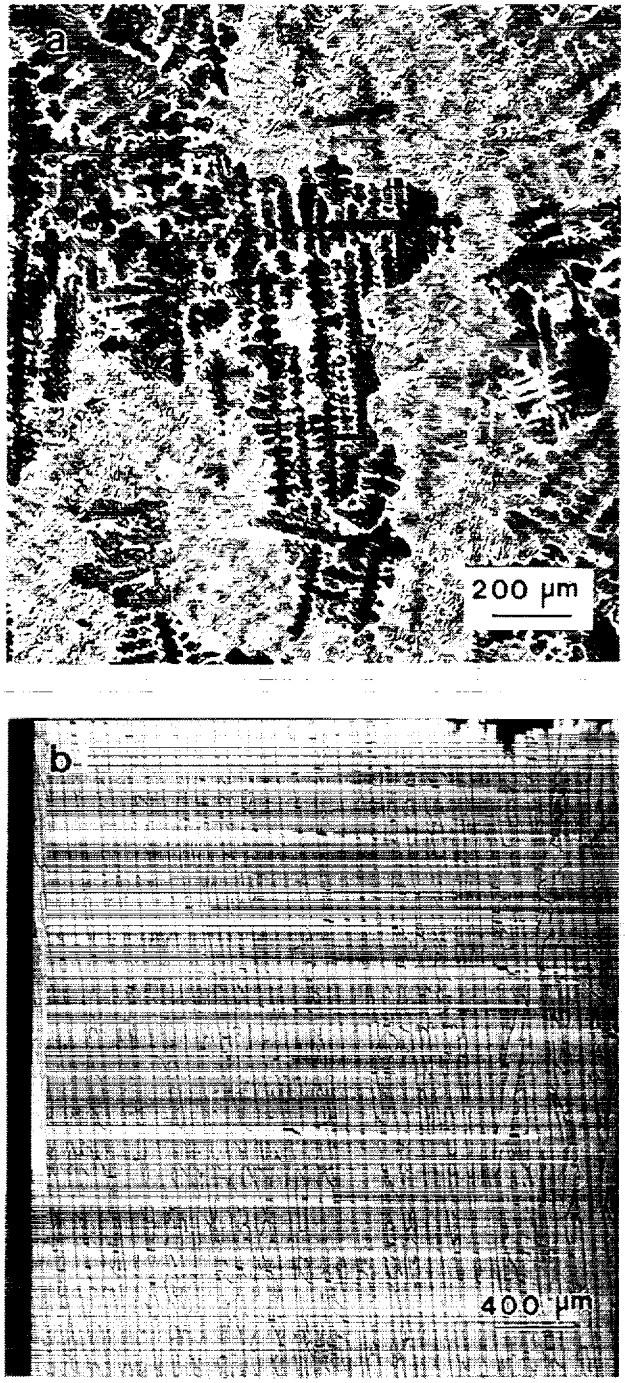

Fig. 3.6. Effect of processing condition on the microstructure of a Ni-30Al alloy: a) arc melted and chill cast alloy and longitudinal sections of material directionally solidified at b) 0.5 cm/hr (after tensile testing), c) 4.5 cm/hr and d) 55 cm/hr. The growth direction for Figs. b - d is vertical, which is also parallel to the loading direction for the mechanical test specimens.

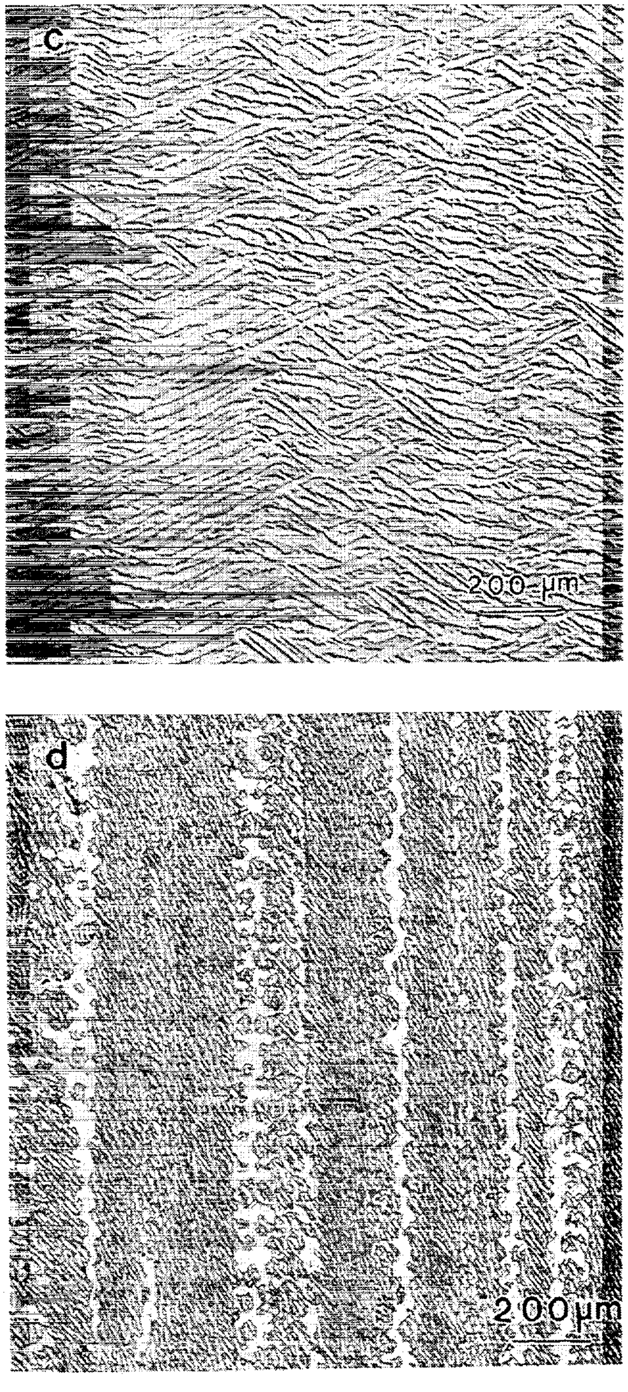

Fig. 3.6. cont. Effect of processing condition on the microstructure of a Ni-30Al alloy: a) arc melted and chill cast material and longitudinal sections of material directionally solidified at b) 0.5 cm/hr (after tensile testing), c) 4.5 cm/hr and d) 55 cm/hr. The growth direction for Figs. b - d is vertical, which is also parallel to the loading direction for the mechanical test specimens.

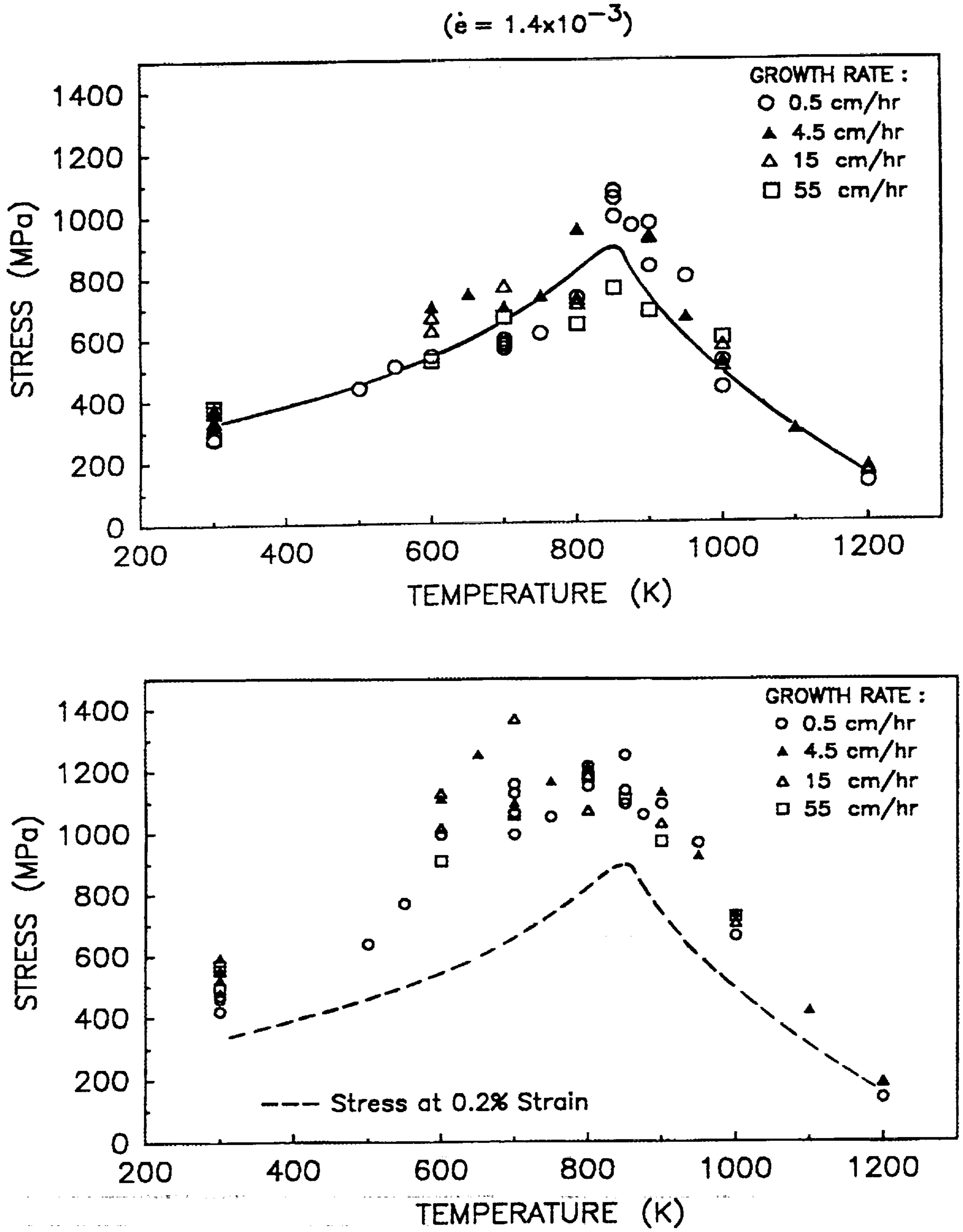

Fig. 3.7. Compression flow stress as a function of temperature and solidification rate for Ni-30Al alloys: a) at the 0.2% strain level and b) at the 3% strain level indicating a significant level of work hardening over most of the temperature range investigated.

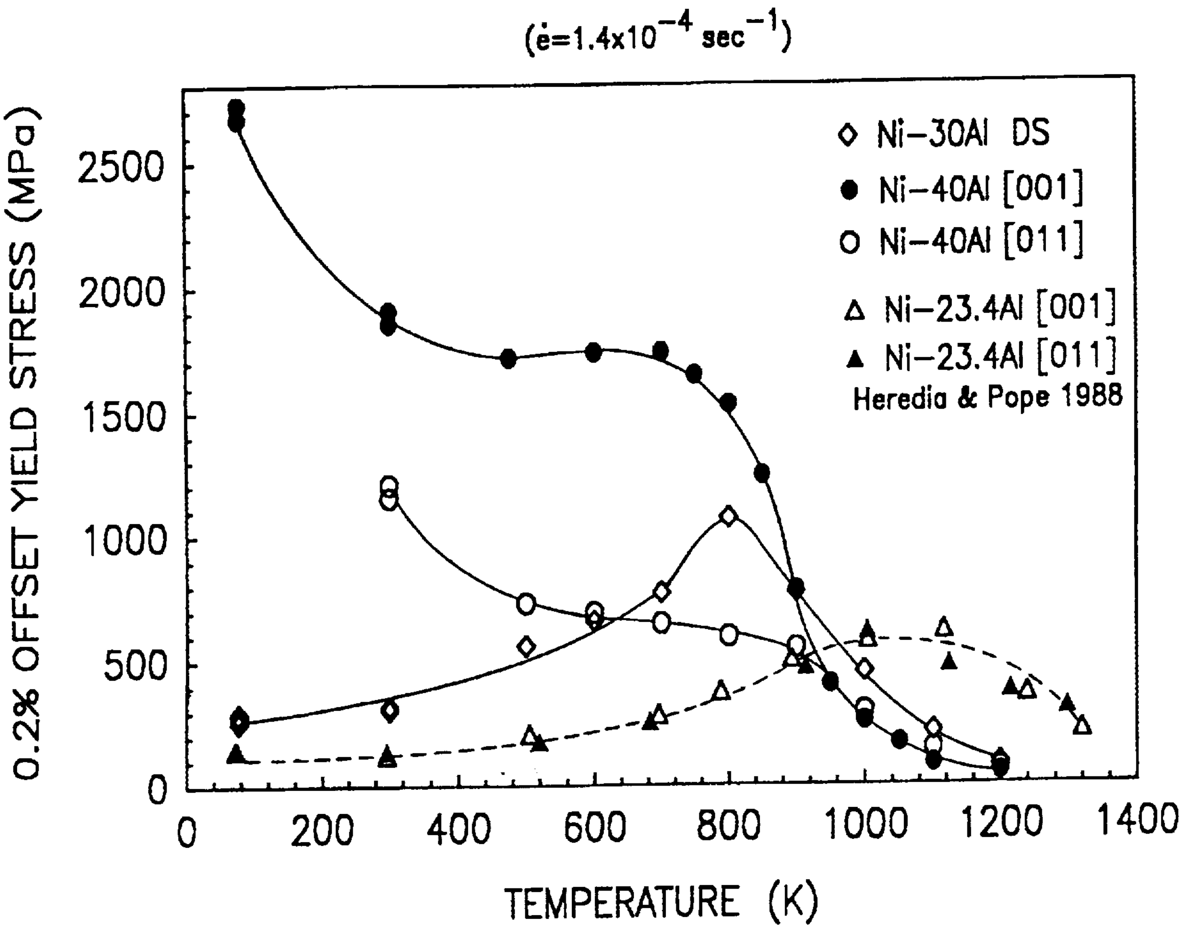

Fig. 3.8. Compression flow stress of the two-phase Ni-30Al alloy as a function of temperature compared to the strength of the individual component phases. Data for the Ni-23.4Al alloy from Heredia and Pope (1988).

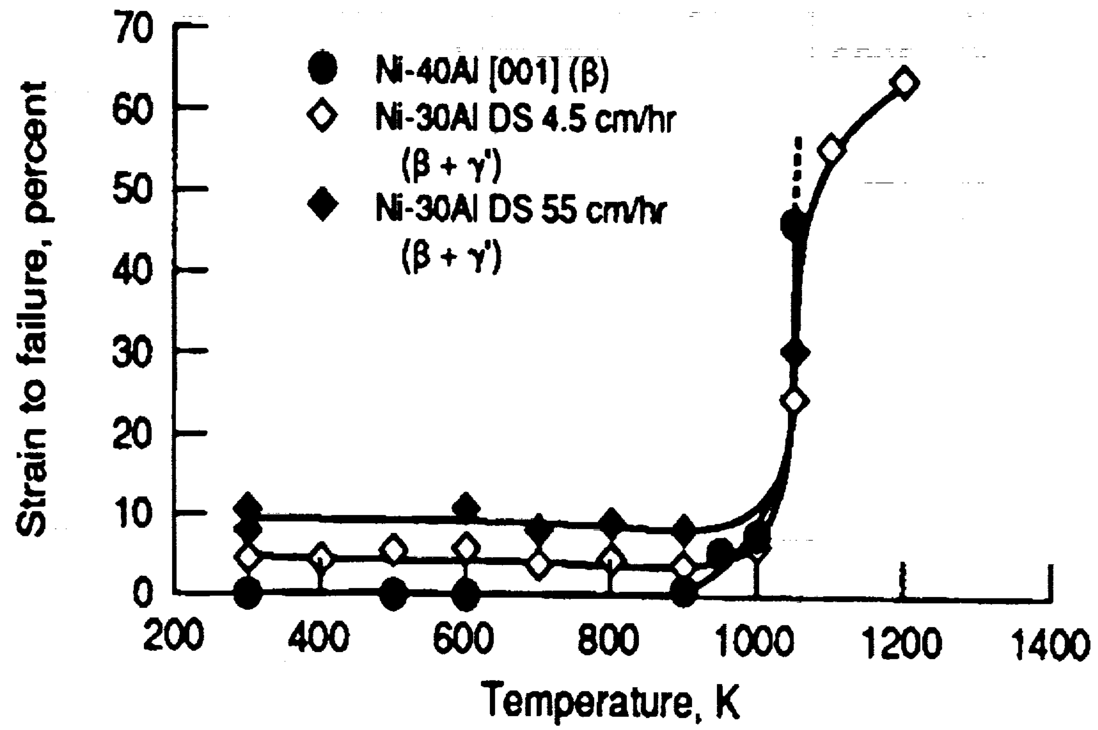

Fig. 3.9. Tensile ductility of the Ni-30Al alloy directionally solidified at 4.5 and 55 cm/hr compared to the tensile ductility of the Ni-40Al matrix phase.

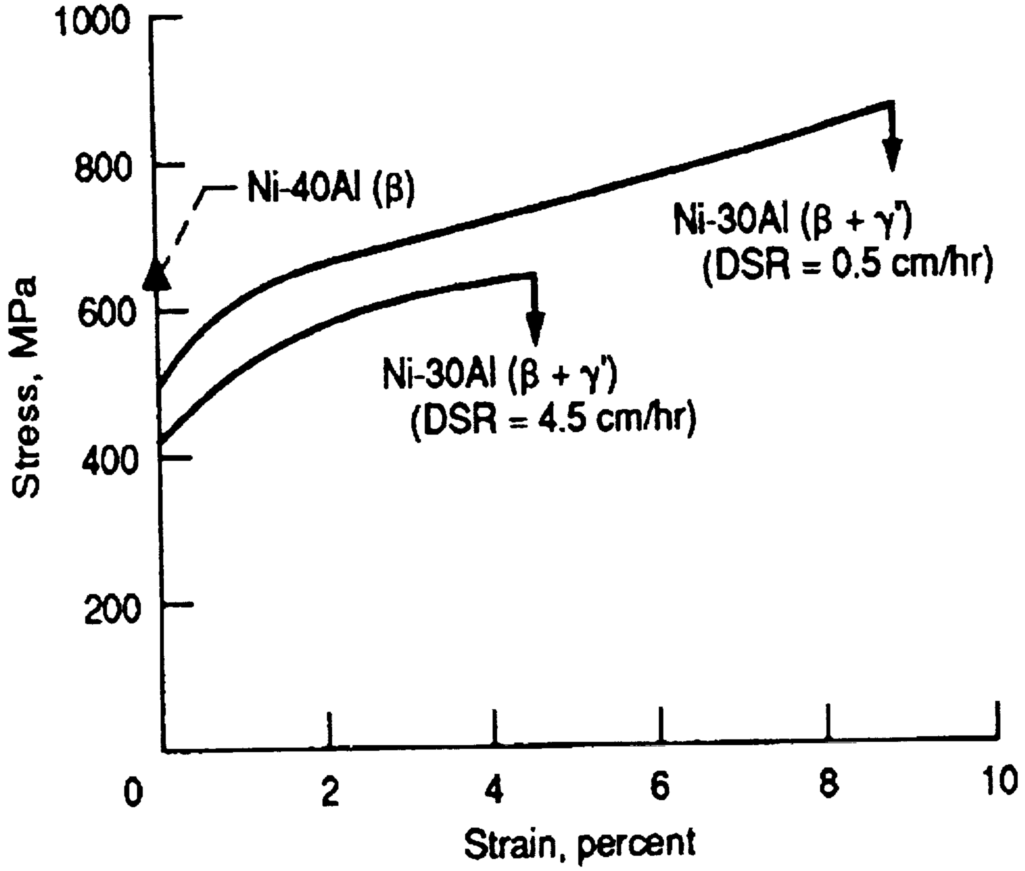

Fig. 3.10. Room temperature tensile stress-strain response of the two-phase Ni-30Al alloy directionally solidified at 0.5 and 4.5 cm/hr compared to single phase Ni-40Al.

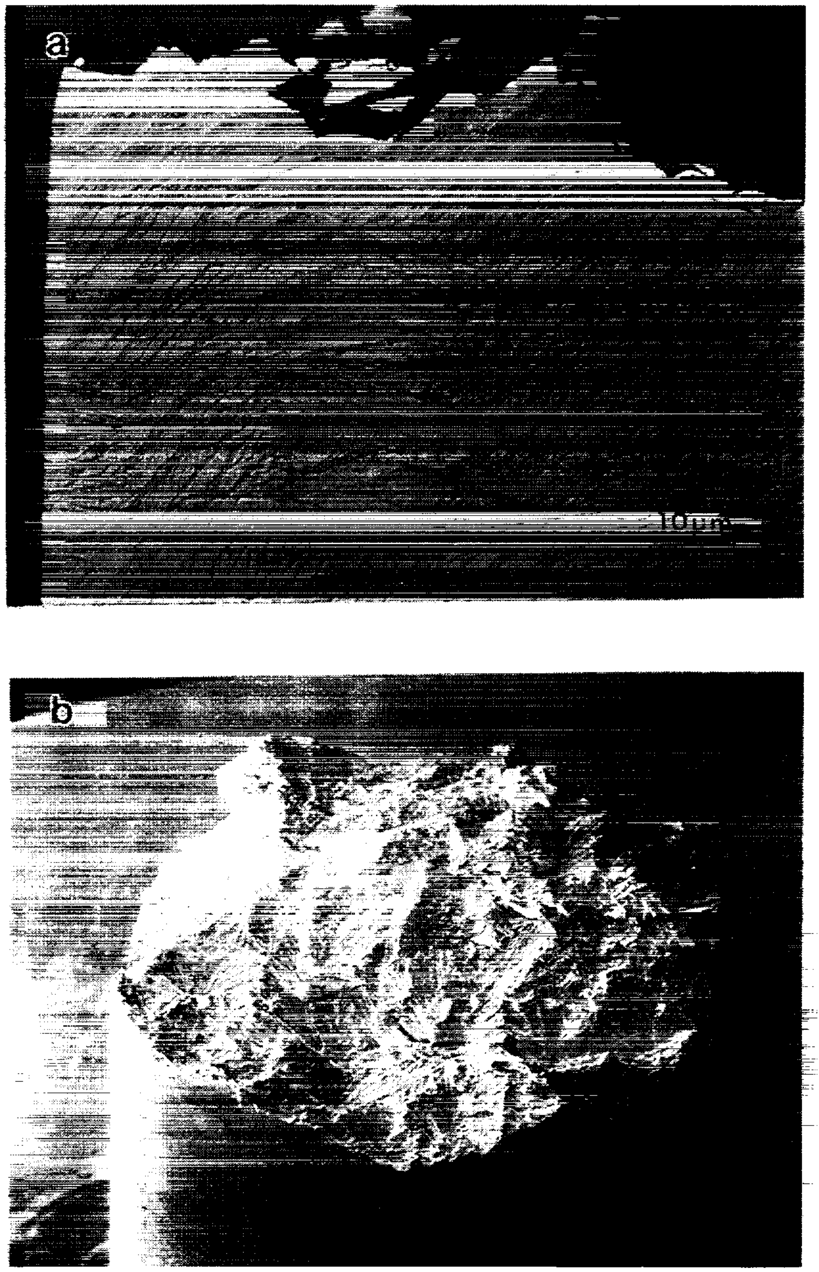

Fig. 3.11. Room temperature fracture behavior of a Ni-30Al alloy directionally solidified at a rate of 4.5 cm/hr: a) polished cross-section of a fractured tensile sample and b) fracture surface morphology. Evidence suggests that slip transfer and crack deflection are the operative toughening mechanisms.

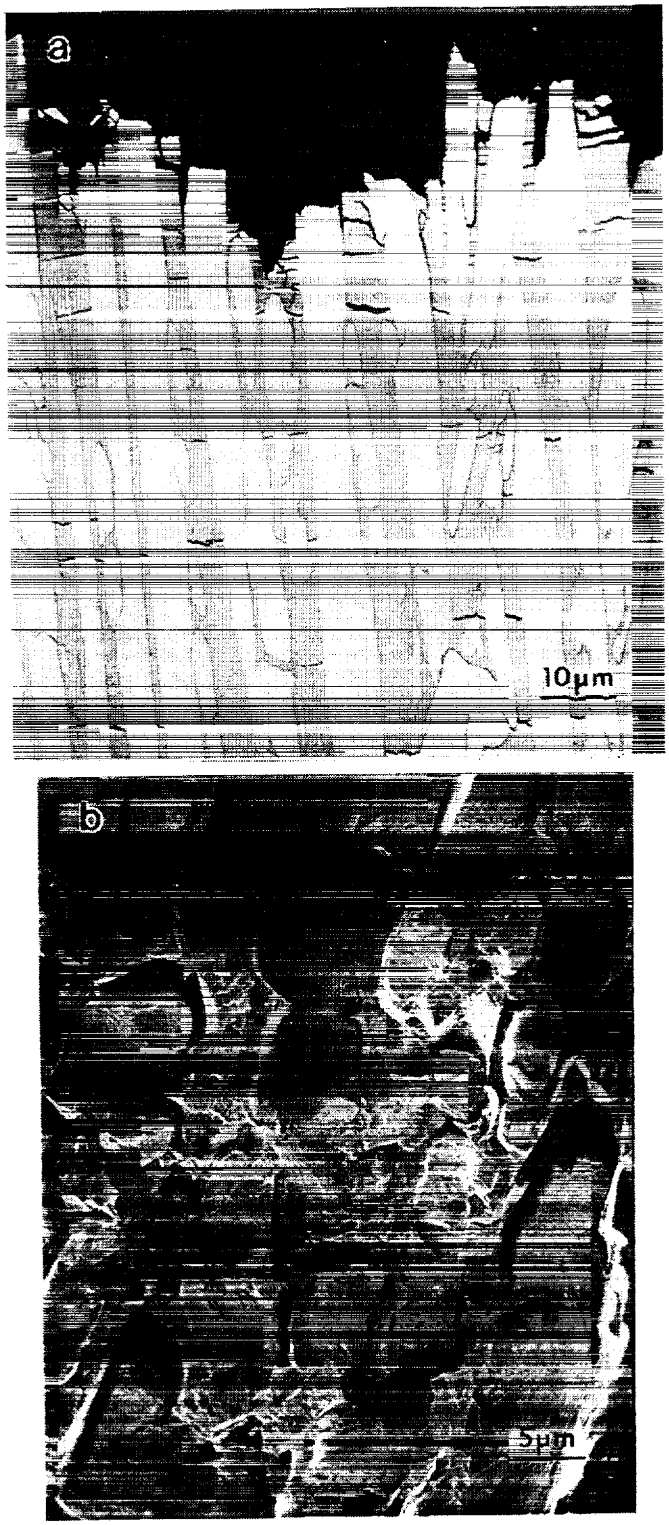

Fig. 3.12. Room temperature fracture behavior of a Ni-30Al alloy directionally solidified at a rate of 0.5 cm/hr: a) polished cross-section of a fractured tensile sample and b) fracture surface morphology. Evidence suggests that crack bridging and crack blunting are the operative toughening mechanisms.

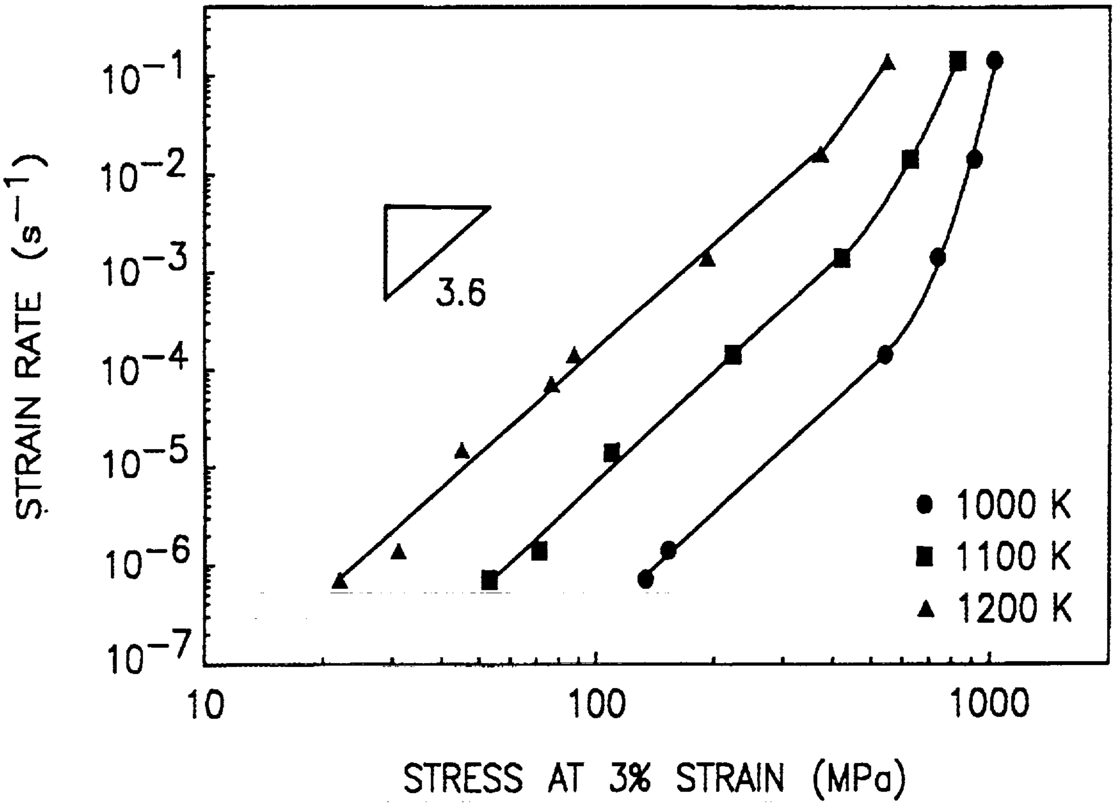

Fig. 3.13. The 1000 - 1200 K compressive creep behavior of the Ni-30Al alloy directionally solidified at 4.5 cm/hr.

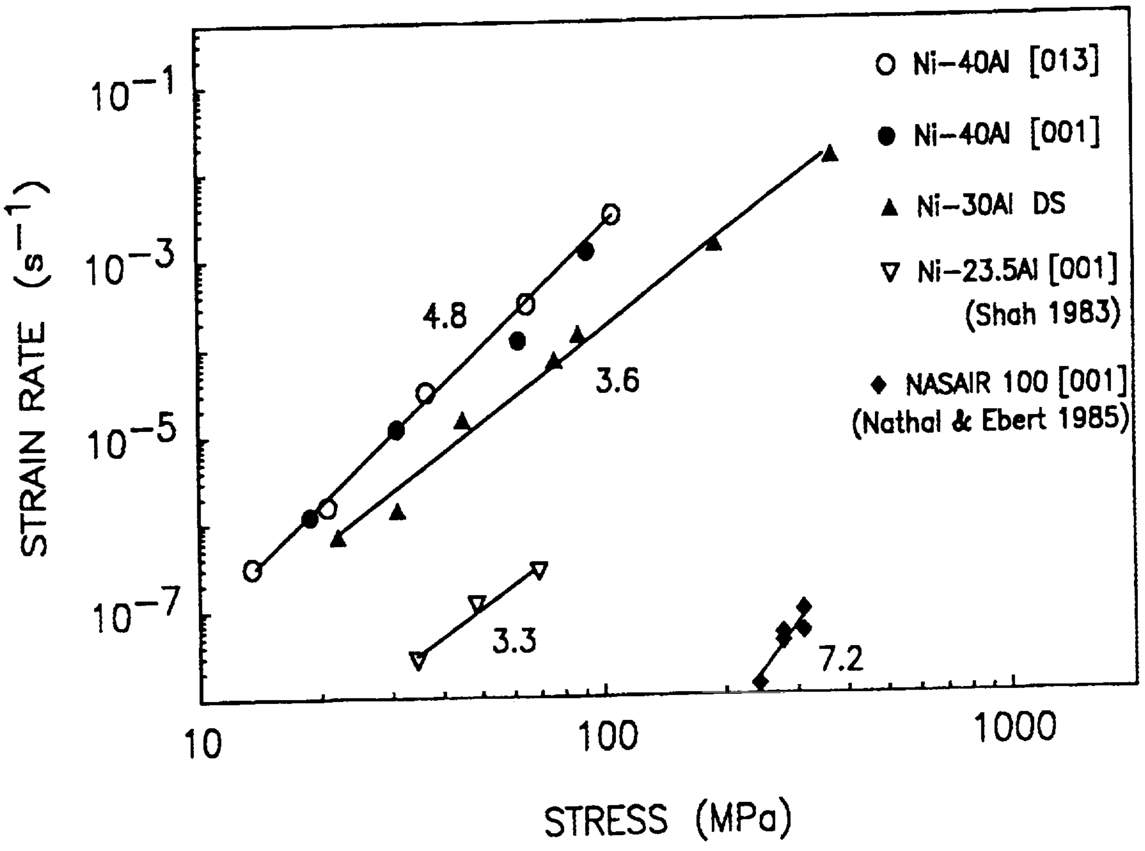

Fig. 3.14. Comparison of the 1200 K creep strength of Ni-30Al and its constituent phases compared to a single crystal Ni-based superalloy. Creep data for Ni-23.5Al from Shah (1983) and for NASAIR100 from Nathal and Ebert (1985).

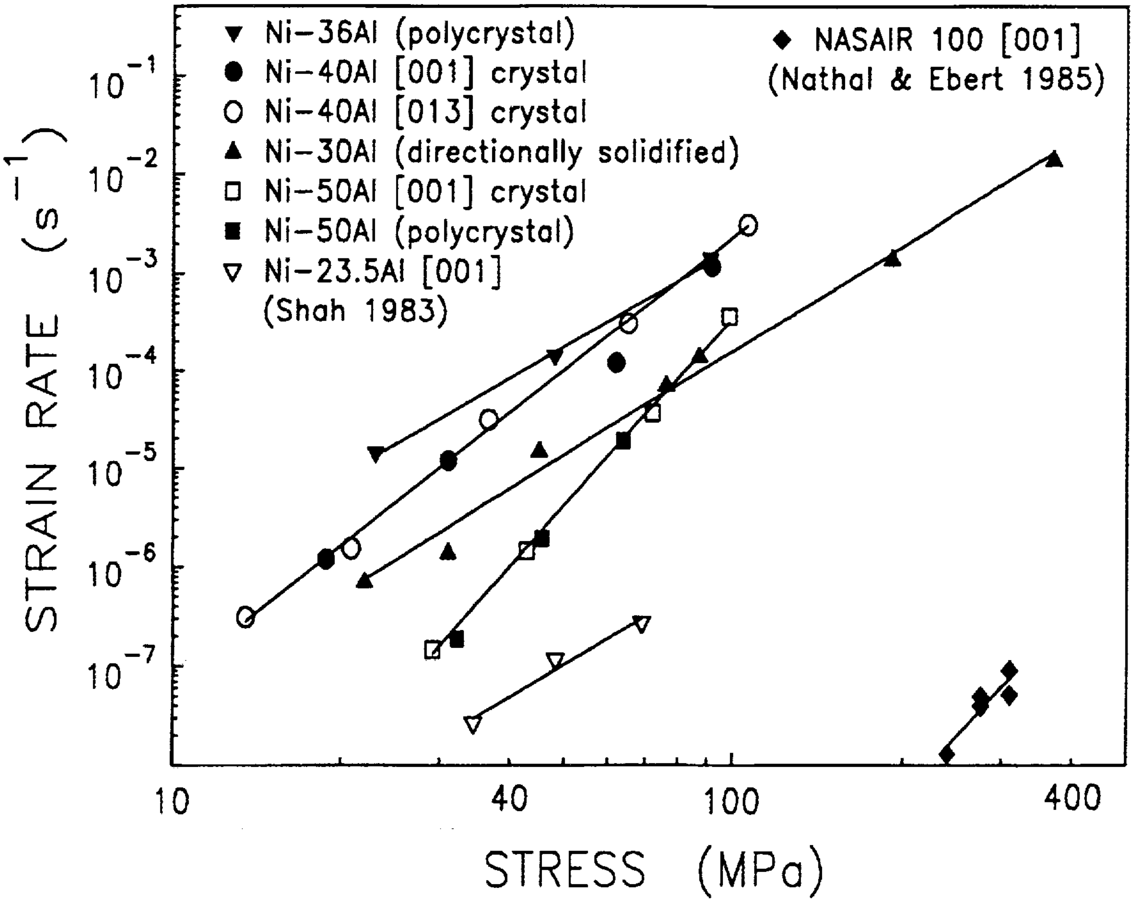

Fig. 3.15. The 1200 K creep strength of various single and two-phase nickel aluminides compared to a first generation single crystal superalloy. Creep data for Ni-23.5Al from Shah (1983) and for NASAIR100 from Nathal and Ebert (1985).

CHAPTER IV
ROOM TEMPERATURE FLOW AND FRACTURE BEHAVIOR OF POLYCRYSTALLINE NiAl

4.1 Introduction

NiAl has a B2 crystal structure, but unlike most B2 compounds that deform by <111> slip (Baker and Nagpal 1990), polycrystalline NiAl and single crystals, except for [001] orientations, deform almost exclusively by <100> type dislocations (Noebe, Bowman and Nathal 1993). Consequently, only three independent slip systems are available for polycrystalline plasticity (Ball and Smallman 1966b; Groves and Kelly 1963), which is less than the five independent deformation modes considered necessary for the uniform plastic deformation of a polycrystalline aggregate (Von Mises 1928). Therefore, polycrystalline NiAl should have little or no capacity for exhibiting significant room temperature tensile ductility.

A report by Fleischer (1987), however, had given superficial hope to the idea that binary NiAl may not be bound by the Von Mises criterion. Fleischer observed that fewer than five independent slip systems operated in approximately 40% of the grains in polycrystalline brass. Although the conclusions of this study have been seriously challenged (Jayaram 1988), Fleischer and Taub (1989) have continued to insist that the Von Mises criterion may not strictly apply to many intermetallic systems. Fleischer's comments in conjunction with additional observations concerning the behavior of NiAl, had helped rejuvenate interest in this intermetallic. Other encouraging results included those of Rozner and Wasilewski (1966), who originally reported 2 to 4% room temperature, tensile ductility in wrought NiAl. This result has been reproduced more recently by Vedula, Hahn and Boulgne (1989), George and Liu (1990) and Nagpal and

Baker (1990b,1991) for cast and extruded NiAl. These limited room temperature tensile ductilities have been attributed to everything from texture to the presence of extrinsic grain boundary dislocations (Vedula, Hahn and Boulgne 1989; Hahn and Vedula 1989; Dollar et al. 1993), implying the potential for even greater tensile ductilities assuming the responsible property could be optimized. Furthermore, the work of Pascoe and Newey (1968b) and Ball and Smallman (1966a) had demonstrated substantial compressive ductilities in NiAl.

Another point that has fueled hope in the development of ductile nickel aluminides is the suggestion by Schulson that grain refinement can be used to increase the ductility of brittle intermetallics such as NiAl (Schulson 1981). Tensile tests were performed on NiAl as a function of grain size and temperature and the results were used to support this view (Schulson and Barker 1983; Schulson 1985). However, grain size only had a critical effect on the ductility of NiAl at temperatures above 550 K. Even though no tensile ductility was achieved at room temperature in these studies the results are often quoted in support of a critical grain size for room temperature ductility of NiAl and have propelled research in rapid solidification processing of intermetallics.

Unfortunately, these observations alone, without an understanding of the underlying flow and fracture mechanisms, may have blinded recent investigators to the inherent problem with NiAl -- too few independent slip systems. Consequently, one of the motivating factors for this work was to determine the potential room temperature tensile ductility that can be expected from NiAl based on the operative deformation and fracture mechanisms in this material. This will be accomplished in this chapter by presenting a series of experimental results exploring the room temperature behavior of NiAl. Overall, the results describe the room temperature deformation and fracture behavior of NiAl and clarifies the potential for NiAl to actually exhibit significant room temperature tensile ductility. The results also serve as a typical example of the behavior of NiAl below the BDTT.

4.2 Materials And Experimental Procedures

Because several different materials were utilized during the course of this study a detailed description of each alloy can be found in Appendix A. For the investigation of room temperature properties, the majority of testing was performed on a prealloyed powder nickel aluminide (Heat P541) produced by the vacuum, soluble gas, atomization process and supplied by Homogeneous Metals, Inc. of Clayville, New York. A schematic illustration of the vacuum atomization process is shown in Fig. 4.1 and a description of the process can be found elsewhere (Wentzell 1974). The powder was sieved to several size ranges but a -100/+325 mesh cut was used for almost all subsequent extrusion runs. The powders were spherical in morphology (Fig. 4.2a) and had an average grain size of 15 μm (Fig. 4.2b). The advantage of having one large lot of powder is that numerous extrusion runs could be made with assurance that the chemical composition between billets would be identical.

The powders were packed in mild steel extrusion cans that were 50.8 mm in diameter with a 6.35 mm wall thickness. The cans were evacuated, sealed air tight and extruded at NASA Lewis Research Center using a vertical Loewy Hydropress. To obtain a variety of grain sizes, extrusions were performed at various temperatures between 1150 and 1500 K using a 16:1 reduction ratio. After extrusion, all canning material was removed by pickling in dilute nitric acid and the blanks machined into tensile or compression samples. All extruded samples exhibited a fully recrystallized, equiaxed grain structure (Fig. 4.3) except for the material extruded at 1150 K, which exhibited an elongated grain structure parallel to the extrusion direction with a grain aspect ratio of about 3:1. Grain sizes for these and all other materials investigated were determined by an average linear intercept method. The relationship between grain size and extrusion temperature for powder Heat P541 is shown in Fig. 4.4 and follows the linear relationship:

$$GS(\mu m) = 0.093T - 100.7$$

where GS is the grain size in microns and T is the extrusion temperature in Kelvin. To produce larger grain sizes than those that could be obtained from extrusion, post-extrusion annealing was performed on extruded P541 samples. Specimens of various initial grain size were wrapped in Ta foil to prevent oxidation and annealed at 1725 K for 100 hours and furnace cooled. Data for a ternary NiAl(0.05 Zr) alloy, P896, is also shown in Fig. 4.4 but will not be discussed until Chapter V.

The composition of the binary powder extruded material is given in Appendix A under the heading "Powder Extruded NiAl (Heat P541)". The Ni and Al levels were determined by wet chemical analysis and the reported value of Ni-50.6 Al was obtained from an average of three samples. The absolute errors in the Ni and Al levels are approximately ±0.2 atomic percent. Therefore, while this alloy was initially tested under the assumption that it was stoichiometric, it was actually slightly Al-rich in composition.

A number of other binary and ternary alloys were produced to determine the effect of alloy composition on the room temperature fracture behavior of NiAl. A description of these alloys is presented in Appendix B. These alloys were not studied in the same detail as P541 but are included primarily to make a point about the effect of alloy composition on fracture initiation mechanisms. These alloys were produced by extrusion of NiAl prealloyed precursors including cast billets, atomized powder and melt spun ribbon.

Button-head tensile specimens were ground from the extruded rods. Typical gauge lengths were 30.5 mm parallel to the extrusion axis, and gauge diameters were 3 mm. A schematic diagram of the tensile sample design is shown in Fig. 4.5. Prior to testing, each specimen was electropolished in a 10% perchloric acid - 90% methanol solution at -208 K and 20-25 volts and 1 amp. Tensile tests were performed to failure in a screw driven Instron machine under displacement control at room temperature. During testing, the samples were gripped within the upper part of the radius by split grip keepers machined to fit within the radius of the samples. Samples almost always failed within the gauge section but when they did not, the results were not used and the tests were repeated if additional material was available. Yield stress was determined using the 0.2% offset method and true fracture stress was calculated based on the final diameter of the sample. To measure yield stress under conditions where there was no tensile ductility, compression tests were performed on specimens centerless ground from the extruded NiAl rods. Samples were 3-5 mm in diameter and 6-10 mm in length. Since no difference in strength was observed as a function of sample size, the smaller samples were used when there was a chance that TEM was going to be performed or when material was limited, otherwise, the larger samples were used. Most tests were performed under constant crosshead speed conditions resulting in an initial strain rate of 1.4×10^{-4} /sec. Tests at any other strain rates are specifically noted. All stress and plastic strain values are reported as true stress and true strain by appropriately converting the load-time curves obtained during testing.

Fracture surfaces of selected tensile samples were examined using a Cambridge 200 scanning electron microscope (SEM). Quantitative fractography was performed to determine the percentage of intergranular fracture for most alloys. This was done by taking at least five random micrographs of appropriate magnification relative to the grain size from each test sample and using a point counting technique. These results are summarized in Appendix B. Additionally, polished cross-sections of compression samples deformed to various strain levels were observed by both optical and SEM techniques to determine fracture initiation sites.

Transmission electron microscope (TEM) specimens were cut from assorted as-received and deformed samples and jet-electropolished in a solution of 70% ethanol, 14% distilled water, 10% butylcellosolve, and 6% perchloric acid. Electropolishing was performed at 273 K at 30 V and 0.18 mA, and was most successful when an "old" solution of electrolyte was used. TEM examinations were conducted in a Phillips 400 T electron microscope at an accelerating voltage of 120 kV.

4.3 Results And Discussion

4.3.1. Tension versus compression yield behavior

An anisotropy in yield properties is only expected when deformation occurs by dislocations with complex core configurations, permitting slip to occur much easier in one direction than in another. For NiAl, slip occurs by <001> dislocations. In a model B2 lattice, <001> screw dislocations (Yamaguchi and Umakoshi 1975) and edge dislocations (Benhaddane and Beauchamp 1986) are expected to have narrow, planar core configurations with no complex core transformations necessary before dislocation motion can initiate. More recent modeling of the core structure of dislocations, specifically in NiAl (Farkas and Vailhe 1993; Parthasarathy et al. 1993) is consistent with these earlier and more general results by Yamaguchi and Umakoshi (1975) and Benhaddane and Beauchamp (1986). These computer modeled results of the dislocation core structure of <001> dislocations in NiAl have recently been validated with actual high resolution TEM observations of a compact and essentially planar dislocation core structure (Mills and Miracle 1993; Crimp et al. 1993). Therefore, from a dislocation dynamics viewpoint, no tension versus compression anisotropy would be expected in NiAl alloys that deform by <001> slip.

However, because both tension and compression flow properties are used extensively throughout this report in interchangeable combinations, it was necessary to confidently determine whether these properties are equivalent. This would also rule out the possibility of a Bauschinger effect in extruded NiAl that may occur as a consequence of processing. Consequently, 5 tension and 5 compression cast plus extruded NiAl samples (L2692) were tested at room temperature. To assure that all the samples were identically prepared, the compression samples were cut from the gauge section of machined and electropolished tensile samples and all samples were tested at a strain rate of 1.4×10^{-4} s^{-1}. The yield stress of the cast plus extruded NiAl in compression was 189 ± 6 MPa versus 183 ± 8 MPa in tension. These values are statistically indistinguishable.

The absence of any tension/compression anisotropy is consistent with numerous low cycle fatigue studies performed on various NiAl-based alloys over a range of temperatures. Room temperature low cycle fatigue results of cast plus extruded NiAl (Noebe and Lerch 1992) and powder extruded NiAl and NiAl(N) (Lerch and Noebe 1994) indicate that tension and compression flow properties were identical over most of the sample's life. The cyclic work hardening characteristics of the alloys in tension and compression were also similar. Likewise, low cycle fatigue of powder extruded NiAl near the brittle-to-ductile transition temperature (Cullers1993) and HIP'ed powder or cast plus extruded NiAl at 1000 K (Lerch and Noebe 1993) also indicated that tension and compression flow properties were identical.

Consequently, there is nothing to suggest that an anisotropy in yield behavior is prominent in NiAl alloys produced by any number of techniques. Therefore, tension and compression flow properties are used interchangeably in this report when it was necessary to extract yield values from brittle materials that did not exhibit tensile ductility. None of the findings during the course of this investigation lead me to believe that this was an incorrect assumption.

4.3.2. Observations and origins of fracture in binary near-stoichiometric NiAl

NiAl tensile samples prepared from powder Heat P541 by extrusion at 1200 K or higher temperatures exhibited little measurable plastic elongation with only an occasional sample (1 out of every 5) displaying several tenths of one percent ductility prior to fracture. The fracture morphology for all samples was mixed mode but with a higher proportion of intergranular fracture than transgranular cleavage (Fig. 4.6). No obvious fracture initiation sites were observed anywhere on the fracture surfaces including near the tensile gauge surfaces where machining defects would be apparent if present.

Consequently, a set of powder extruded tensile samples were systematically evaluated in order to identify fracture origins or at least rule out possible fracture initiation sources such as surface disparities. All the tensile samples were from the same extrusion rod and had an average grain size of 11 μm. Each tensile sample in this group had successively greater amounts of material removed from the surface by electropolishing prior to testing. All samples failed at the very onset of yielding except for two specimens which exhibited less than one percent strain prior to failure.

The fracture stresses for these samples were independent of the amount of surface material removed prior to testing (Fig. 4.7) and were essentially the same in all cases. This similarity in fracture stress independent of the amount of surface material removed would tend to rule out fracture initiation from surface defects. Fractographic analysis supports this suggestion. Representative SEM micrographs of the tensile fracture surfaces from the samples with the least and most amount of surface material electrochemically removed are shown in Fig. 4.8. Fractography did not yield an obvious initiation source in any of the samples. The fracture mode in all cases was mixed with a slightly higher percentage of intergranular fracture.

Because the tensile samples failed at relatively the same fracture stress (416 ± 21 MPa), this would indicate that failure originated from defects of nearly the same size in all samples. Thus, fracture must be initiating at some microstructural aspect, characteristic of all the samples. Since these are fully dense, single phase materials the only microstructural feature that could act as fracture initiation sites are grain boundaries.

Compression samples were used to further investigate room temperature fracture processes in polycrystalline NiAl. The advantage of using compression specimens is that the material could be subjected to significantly greater strain levels than tensile samples since crack propagation processes are retarded. Consequently, crack initiation sources would be much easier to identify. Fig. 4.9 shows a series of optical micrographs of polished longitudinal cross-sections of NiAl compression samples (Heat P541) deformed from zero to about 14% strain. None of these samples failed in the macroscopic sense, since no load drop was observed during testing nor were any macroscopic cracks visible to the eye. However, at higher magnification it was obvious that the grain boundaries began to fail throughout the entire cross-section of the plastically deformed samples. The grain boundaries have opened up, forming small cracks at the grain interfaces. These grain boundary microcracks increased in density and linked up forming larger defects as the plastic strain was increased. While these intergranular defects are readily apparent in the samples deformed at the higher strain levels it is important to note that the samples deformed to even 4 - 5% strain were literally full of these intergranular discontinuities and that they were observed even in samples deformed to approximately 1% plastic strain.

It is apparent from these observations that grain boundaries are a likely source of fracture initiation in binary, near-stoichiometric NiAl. It should be equally obvious that the reason for this behavior is the insufficient number of slip systems operating in NiAl, which leads to incompatible deformation at the grain boundaries as first proposed by Ball and Smallman (1966a,b). The consequence of this insufficient number of slip systems during plastic deformation is aptly demonstrated by the intergranular cracking exhibited in Fig. 4.9.

However, what should be a straight forward explanation for the lack of extensive tensile ductility in NiAl is not universally accepted. Recent investigations by George and Liu (1990) and George, Liu and Liao (1991) have shown that the addition of B changed the room temperature fracture behavior of NiAl from intergranular to transgranular. From this observation they concluded that the grain boundaries were inherently weaker than the cleavage strength of NiAl and that B increases the cohesive strength of the grain boundaries. Other investigators have also tried to explain the intergranular fracture of NiAl in terms of grain boundary chemistry suggesting that the grain boundaries in NiAl are weak or embrittled (Camus et al. 1988; Nagpal and Baker 1991). Still other investigators (Vedula and Khadkikar 1990) suggest that the Von Mises criterion does not apply to NiAl since it can exhibit limited tensile ductility and significant compressive ductilities. Therefore, it is necessary to explore all possible origins of intergranular fracture in NiAl in significantly more detail to ensure that intergranular fracture is not a consequence of some other factor. During this exercise, the above observations and ideas will also be reconciled.

One of the most common reasons for intergranular fracture in metals is impurity contamination of the grain boundaries and this was originally thought to be the case in NiAl. Westbrook and Wood (1962) and Seybolt and Westbrook (1964) investigated the effect of oxygen on the grain boundary hardness of NiAl. They concluded that because the grain boundaries were harder than the matrix material, oxygen embrittlement was responsible for the intergranular fracture of NiAl. Because grain boundary hardening occurred only after high temperature heat treatments followed by slow cooling or quenching and intermediate temperature annealing, this behavior was explained in terms of oxygen-vacancy interactions (Seybolt, Westbrook and Turnbull 1964). However, these same results can also be explained in terms of vacancy or point defect gradients near the grain boundaries without the necessity for the presence of oxygen since grain boundaries are very strong sources and sinks for vacancies. Furthermore, it was concluded from a recent in-situ Auger electron spectroscopy study of cast and extruded NiAl (George and Liu 1990) that the grain boundaries are clean and free from measurable impurity contamination including oxygen.

NiAl produced by consolidation of prealloyed powders might contain different impurity levels and a different distribution of interstitial elements than cast plus extruded material. Consequently, it was necessary to perform an Auger study on powder extruded NiAl using the powder (Heat P541) supplied by Homogeneous Metals. This Auger study was performed with the assistance of Mary Zeller of the NASA Lewis Research Center and was intended to compliment the experiments performed during the course of this investigation. Details of the experimental procedures and results of this Auger investigation on powder extruded NiAl alloys have been presented previously (Zeller, Noebe and Locci 1990). The conclusion of this study was that the grain boundaries in powder extruded NiAl in the as-extruded condition or after various heat treatments were free from any measurable impurity contamination including oxygen, carbon or sulfur. Therefore, these results and the work of George and Liu (1990) indicate that intergranular fracture in binary near-stoichiometric NiAl is not due to any form of impurity induced intergranular embrittlement since impurity segregation is not observed in NiAl.

Intergranular fracture could also arise because grain boundaries are intrinsically weak due to their structure, as was once thought to be the case for Ni_3Al (Kruisman, Vitek and DeHossan 1988, Vitek and Chen 1991; Chaki 1991). Because Ni_3Al is strongly ordered, the lattice on either side of the grain boundary is undisturbed right up to the boundary and therefore, due to the stoichiometry of the alloy, columnar cavities are formed at the boundary (Kruisman, Vitek and DeHossan 1988, Vitek and Chen 1991). It has been proposed (Chaki 1991) that the periodic formation of these cavities results in a "porous" grain boundary incapable of withstanding tensile stresses without the initiation and propagation of intergranular cracks. Now it is apparent that the situation in the Ni_3Al system is much more complicated than described above. Similar to Fe-Al based ordered alloys (Liu 1993), Ni_3Al is environmentally embrittled in air at room temperature (George, Liu and Pope 1992,1993). The embrittling species in both materials is thought to be hydrogen, though grain boundary structure may still play an important role in the loss of ductility.

In contrast to Ni_3Al, grain boundary structure simulations for NiAl indicate that there are no periodic structural defects present at the grain boundaries in near-stoichiometric NiAl which would cause the grain boundaries to be inherently weak (Vitek and Chen 1991, Chen et al. 1989; Petton and Farkas 1991). Consequently, there are no structural factors that could be responsible for intergranular fracture in near-stoichiometric NiAl. In addition, NiAl in single crystal (Lahrman, Field and Darolia 1993b) or polycrystalline form (Liu 1993a) does not suffer from environmental embrittlement. Comparable testing of NiAl in air, vacuum and various gas environments has demonstrated no repercussion of environment on tensile ductility.

Therefore, through actual measurement of grain boundary chemistries, computer simulations of grain boundary structure and environmental testing, all other conceivable causes of intergranular fracture in NiAl can be ruled out. This leaves only grain boundary incompatibility due to an insufficient number of independent slip systems as the primary reason for the poor tensile ductility and observed intergranular fracture of binary near-stoichiometric NiAl. The details of this type of fracture mechanism are described below.

The Von Mises criterion (Mises 1928), which is commonly used to determine whether a material has a sufficient number of slip systems to exhibit potential polycrystalline ductility, is based on the concept that there are six components to the generalized strain tensor. There are three primary strains, two of which are independent for plastic flow and three shear strains, for a total of five independent strains. The occurrence of each of these strains must be accommodated by an independent deformation mechanism in each grain of a polycrystalline material during plastic flow (Groves and Kelly 1963), at least in the vicinity of the grain boundaries. With the operation of less than five independent deformation mechanisms in a polycrystalline aggregate it is impossible for the grains to deform in a cooperative manner without generating grain boundary discontinuities. The so called Von Mises criterion does not address the extent of ductility that can occur in a material with fewer than five independent deformation mechanisms. It only says that when there are fewer than five mechanisms, grain boundary discontinuities will have to occur because of the basic mechanics involved. It is my contention that the presence of these grain boundary discontinuities or Griffith like defects in NiAl are responsible for limiting the tensile ductility of NiAl below the brittle-to-ductile transition temperature (BDTT) and not that the grain boundaries in NiAl are weak for some intrinsic reason.

Because NiAl deforms predominantly by <001>{110} type slip, there are only three independent slip systems (deformation modes) operating at low temperatures (Groves and Kelly 1963). Therefore, the formation of discontinuities (microcracks) at the grain boundaries will be an inevitable consequence of low temperature plastic deformation. This behavior is plainly demonstrated once again in Fig. 4.10. This figure demonstrates the abundant slip activity that can be induced in a large grained sample of arc melted NiAl by a Rockwell "C" hardness indentation. There was profuse plastic flow in the grain containing the indent, evident by the slip lines radiating from the indentation, as well as slip transfer into a neighboring grain due to the movement of material away from the indentation. Because neither grain was capable of deforming by more than three independent slip systems, separation of the grain boundary occurred in the region of concentrated plasticity (Fig. 4.10).

While Fig. 4.10 demonstrates the consequence of incompatible deformation between two grains, this behavior can be generalized to a polycrystalline aggregate of many grains as in Fig. 4.11. Part (a) of Fig. 4.11 schematically represents a polycrystalline material of arbitrary grain size while part (b) demonstrates what the polycrystalline aggregate would look like if all the grains deformed as though they were unconstrained single crystals. The consequence of the grains deforming independently would be the overlapping of some grains and the formation of voids between others. Grains cannot physically overlap since they cannot occupy the same space. However, with fewer than five independent deformation mechanisms operating in each grain to accommodate compatible deformation at the grain boundaries, voids or discontinuities will occur in NiAl as demonstrated in Fig. 4.10c.

In the absence of any external flaws larger than these grain boundary microcracks, these grain boundary cavities are obviously the source of failure in NiAl tensile samples deformed at room temperature. During compression testing these flaws are not able to propagate catastrophically but under tensile loading conditions it could take just one "critical" size defect to initiate failure. It is not unreasonable to assume that the high strain concentration along the grain boundaries due to incompatible deformation, especially if additional microcracks are physically present, would promote continued propagation of fracture in an intergranular fashion. Intergranular propagation of a crack would be especially easy in material with recrystallized, equiaxed grains of moderately fine size. In this case, there would be little resistance to cause the crack to deviate from its path. Consequently, fracture in polycrystalline NiAl initiates intergranularly and propagates in a mixed mode fashion resulting in a mostly intergranular to mixed mode fracture surface as shown in Figs. 4.6 and 4.8.

Therefore, while NiAl does exhibit significant macroscopic plasticity when tested in compression, and up to few percent ductility in tension, on a microscopic scale fracture is occurring at the grain boundaries because of the generation of incompatible strains. Consequently, the large apparent compressive ductilities observed in NiAl do not suggest that the Von Mises criterion is violated. The Von Mises criterion only implies that with fewer than five independent deformation mechanisms a polycrystalline aggregate cannot exhibit extensive ductility without the occurrence of discontinuities at the grain boundaries. As Figs. 4.9 to 4.11 demonstrate, these discontinuities do occur during the plastic deformation of NiAl. The limited tensile ductilities observed in NiAl are also not a contradiction to the Von Mises criterion. Limited tensile ductility would be expected if the yield strength of the material was lower than the stress necessary to immediately propagate a flaw that was comparable in size to the grain size of the alloy. This concept will be discussed further in the following section.

4.3.3. Fracture initiation and origins in ternary NiAl alloys

There are still several issues that need to be addressed concerning room temperature fracture of NiAl. What effect do ternary alloying additions have on the fracture behavior of NiAl and is there an alternative interpretation of George and Liu's (1990) observation concerning a change in fracture behavior due to B additions. These issues will now be addressed in terms of the fracture initiation mechanisms exhibited by binary and ternary NiAl alloys.

Figure 4.12 is a map summarizing the fracture behavior of NiAl and a number of different ternary alloys. Most of the alloys that are represented in the figure were those studied during the course of this investigation while some additional data were taken from the literature. A detailed description of each alloy represented in Fig. 4.12 is given in Appendix B. The idea for the plot is based loosely on the concept of a fracture mechanism map (Ashby, Gandhi and Taplin 1979; Gandhi and Ashby 1979). But instead of describing fracture mechanisms as a function of temperature for a single alloy composition and grain size this plot summarizes the fracture mechanisms for binary NiAl and a family of dilute ternary alloys as a function of the relationship between yield stress and tensile fracture stress at one temperature. The nomenclature used to define the fracture modes identified in the plot is the same as that described by Gandhi and Ashby (1979). Completely brittle fracture from a pre-existing flaw, below the yield strength of the material is referred to as cleavage type I or brittle intergranular fracture (BIF) type I depending on the fracture origin. Brittle failure from a defect that is nucleated by slip but fails at or just below the macroscopic yield strength of the alloy is cleavage type II or BIF type II. Cleavage or brittle grain boundary failure after general yielding with a small but measurable tensile elongation is considered cleavage type III or BIF type III. Three of these six brittle fracture mechanisms are represented in Fig. 3.12. Furthermore, it was observed that the resulting fracture initiation mechanisms had a definite relationship to the flow strength:fracture strength ratio of the various NiAl alloys.

All of the materials that exhibit BIF type III behavior are binary near-stoichiometric NiAl alloys, with the exception of the Be-doped, ternary alloy. However, Be seems to be the one element that has a negligible hardening affect on NiAl (George and Liu 1990). All materials in this region exhibited tensile yield strengths that were below approximately 250 MPa, possessed some tensile ductility (on the average of about 1%), and exhibited greater than 60% intergranular fracture. An example of the fracture morphology of an alloy from this group is shown in Fig. 4.13a. Failure in the BIF III region is a direct consequence of incompatible grain boundary deformation, but the yield strength is so low in these materials that limited tensile ductility is possible before fracture propagation and final failure. As deformation proceeds, the crack either grows and/or the stress increases due to work hardening causing the stress intensity to reach the critical value for fracture resulting in catastrophic failure of the sample after some finite tensile elongation. The important point to note is that the initiation mechanism in this case is intergranular in nature due to the strain incompatibility problem discussed in the previous section.

At higher yield strength levels, many of the alloys displayed no generalized tensile yielding or tensile ductility but failed at a stress very near the macroscopic yield strength of the material when determined in compression. This type of behavior was observed over a large yield stress range. These materials exhibited intergranular or mixed mode fracture surfaces and include the powder (Heat P541) extruded material discussed in the previous section. Examples of the intergranular to mixed mode type fracture surfaces typical of alloys in this group are shown in Figs. 4.6 and 4.8. This region represents BIF type II where crack initiation is dependent on slip or microscopic yielding. In this case, localized slip occurs in grains oriented for easy glide, but at applied stresses just below the bulk yield strength of the alloy. This localized yielding is capable of generating strain incompatibilities that can result in crack nucleation. Upon initiation of the first suitably oriented intergranular microcrack, the fracture propagation stress would already be exceeded and the material would fail before any significant tensile ductility could result. Therefore, Mode II BIF in NiAl is also a consequence of the Von Mises criterion since fracture initiation is the result of incompatible deformation between neighboring grains.

Ternary alloying additions to NiAl increase the yield strength of the alloy and in many cases alter the general fracture mode from BIF to cleavage (Fig. 4.13). For these alloys fracture almost always initiated and propagated in a transgranular manner as demonstrated in Fig. 4.14. For example, NiAl alloys containing Re, B, C, or Cr fractured in tension without any prior plasticity in a completely brittle manner. For these alloys, the yield stress was determined in compression and plotted versus the tensile fracture stress in Fig. 4.12. Consequently, these alloys would be classified as exhibiting cleavage type I since the fracture stress of the alloy is significantly below the bulk yield strength and even below the microyield strength of the material. Cleavage I fracture occurs at the nominal stress:

$$\sigma_f \sim K_c / (\pi c)^{1/2} \qquad (4.1)$$

where 2c is the pre-existing flaw length, and K_c is the fracture toughness. For completely brittle materials K_c is equivalent to $(2 Y E)^{1/2}$, where Y is the surface energy and E is Young's modulus. Fracture origins in these alloys were either inclusions as shown in Fig. 4.14, or fine surface flaws due to machining.

Nonstoichiometric binary NiAl alloys do not exhibit room temperature ductility, fail at stresses significantly below their respective yield stresses, and exhibit a transgranular fracture behavior (Vedula, Hahn and Boulogne 1989; Nagpal and Baker 1991). Therefore, similar to ternary alloys, non-stoichiometric binary NiAl alloys also exhibit cleavage type I behavior due to their high yield strengths.

The trend established in Fig. 4.12 is clear. When plasticity (macroscopic or microscopic) occurs, microcracks develop at the grain boundaries due to incompatible deformation causing intergranular fracture initiation. When the yield strength of the alloy is sufficiently high so that no plasticity occurs in the material, cleavage fracture initiates at extrinsic defects. Therefore, with the additional insight supplied by Fig. 4.12, George and Liu's results (1990) can be explained as follows. The large boron addition to NiAl solid solution strengthened the alloy such that fracture occurred well below the yield strength of the NiAl(B) alloy (labeled "s" in Fig. 4.12). Consequently, without plastic deformation intergranular fracture had no way of initiating and the material failed in a transgranular fashion, similar to the other solid solution strengthened ternary alloys. Based only on the observed change in fracture behavior for B-doped alloys, (George and Liu 1990; George, Liu and Liao 1991) there is insufficient evidence to conclude that B actually strengthens the grain boundaries in NiAl. But computer simulations by Chen et al. have (1989) indicated that B should have essentially no effect on the cohesive strength of grain boundaries in NiAl.

Finally, statements by George and Liu (1990) that the grain boundaries in NiAl are "intrinsically brittle" and need to be strengthened by alloying additions such as B are misleading. There is no evidence that the grain boundaries in NiAl are "brittle". It is true that because of an insufficient number of independent slip systems, incompatible deformation at the grain boundaries will cause the formation of grain boundary microcracks in NiAl. But in the absence of plastic deformation induced microcracks, the grain boundaries in NiAl are at least equal or possibly superior in strength to the cleavage strength of the intermetallic. This is evident by the conspicuous absence of a type I BIF field in Fig. 4.12. Consequently, when stresses are very high, NiAl fails by cleavage and not intergranular fracture. If the grain boundaries were brittle the opposite case would be true. While grain boundaries are not intrinsically weak in NiAl there may be reason for concern about the cleavage strength of the intermetallic.

4.3.4. Effect of grain size on yield strength and ductility

A final issue to be resolved is the effect of grain size on the tensile ductility of NiAl. Prospects for generally improving the mechanical properties of high temperature alloys by significantly reducing grain size have been a strong driving force propelling research in the area of rapid solidification during the 1980's, including the development of extensive rapid solidification facilities at NASA LeRC. The expectation of using rapid solidification (grain size refinement) to improve the properties of ordered intermetallics and to specifically solve the low temperature ductility problem in NiAl was further heightened by the work of Schulson (1981,1985).

In my opinion, however, the concept of trying to improve the strength and fracture resistance of high temperature alloys through grain refinement by rapid solidification is somewhat questionable. The initial fine grained or metastable structures produced by rapid solidification will not remain that way after prolonged high temperature exposure at high homologous temperatures. There is also the issue of a fine grain size adversely affecting creep properties. Even neglecting these issues, the idea of grain refinement as a cure-all for the limited tensile ductility of NiAl has serious limitations that are grounded in the fracture mechanisms discussed previously. The realistic prospects for improving the low temperature tensile ductility of NiAl by grain refinement will be discussed in the second part of this section. But first, a general description of the effect of grain size on yield strength will be presented for completeness.

Yield Strength

The effect of grain size on the compressive yield strength of powder (Heat P541) extruded NiAl is summarized in Fig. 4.15. The data are plotted as yield strength, σ_y, at room temperature and 700 K versus the reciprocal square root of the grain size, d. The data obeyed the conventional Hall-Petch relationship:

$$\sigma_y = \sigma_o + k_y\, d^{-0.5} \qquad (4.2)$$

where the constant σ_o is generally interpreted as the intrinsic lattice resistance to dislocation motion and k_y is a measure of the strengthening due to dislocation grain boundary interactions. The values of these constants were determined by linear regression. At room temperature the yield strength followed the relationship:

$$\sigma_y = 179\text{MPa} + 500\text{MPa}{*}\mu\text{m}^{0.5}\,(d^{-0.5}) \qquad (4.3)$$

and at 700 K the following relationship was observed:

$$\sigma_y = 86\text{MPa} + 229\text{MPa}{*}\mu\text{m}^{0.5}\,(d^{-0.5}) \qquad (4.4)$$

The value for σ_o represents the lattice resistance to dislocation motion and is determined by extrapolating the yield strength versus grain size data to infinite grain size (a single crystal). Therefore, it should be possible to relate σ_o to the critical resolved shear stress (τ_{CRSS}) of single crystals by the following relationship:

$$\tau_{CRSS} = \sigma_o / M \qquad (4.5)$$

where M is the Taylor orientation factor (Taylor 1938), which is dependent on the crystal structure and active slip plane. For bcc metals, which deform by slip on {110} planes, M was estimated to be 2.75 (Hutchinson 1964). Consequently, using equation 4.5 with M = 2.75, the equivalent room temperature τ_{CRSS} for the material in this study was 64 MPa. This value is in agreement with the τ_{CRSS} reported for NiAl assuming <001>{110} slip, which ranges from 34 to 158 MPa with an average reported value of 93 MPa (see Table V in Noebe, Bowman and Nathal 1993).

The relationships observed in this study indicate a significant dependence of yield strength on grain size, which was confirmed by the data of Barker (1982). The value for k_y determined by Barker (1982) for a Ni-49Al alloy at room temperature a was 670 MPa*$\mu m^{0.5}$ and at 673 K a k_y of 156 MPa*$\mu m^{0.5}$ was observed. However, my data and that of Barker can be very misleading. Since the time these tests were performed, additional investigators have determined the effect of grain size on yield stress (Nagpal et al. 1991; George 1991) revealing some rather interesting results. All the available room temperature values for k_y are plotted in Fig. 4.16 as a function of stoichiometry. The data clearly indicate that the influence of grain boundaries on resisting dislocation motion increases with increasing deviation from stoichiometry. Consequently, yield stress is relatively independent of grain size for NiAl alloys very close to stoichiometry, whereas the yield stress of non-stoichiometric alloys is strongly influenced by grain size, even for very minor deviations from stoichiometry such as Barker's (1982) Ni-49Al alloy or the powder from Heat P541, which has a composition of Ni-50.6Al.

No satisfactory explanation has been offered to explain the dependence of k_y on composition. Since k_y is a measure of the grain boundary's resistance to slip transmittal, it can be postulated that in the non-stoichiometric alloys slip transferal across the boundaries is more difficult than in stoichiometric alloys. Recent computer modeling by Chen et al. (1989) has suggested that the grain boundary structure in NiAl is affected by compositional deviations from stoichiometry as is the bulk material. Specifically, their calculations show that unlike the bulk material, vacancies are the most stable defect at grain boundaries for both Ni- and Al-rich alloys. The presence of vacancies at the grain boundaries of non-stoichiometric alloys apparently hinder slip transmittal across the boundaries resulting in an increase in the Hall-Petch slope. However, further work is obviously needed in this area to fully understand the mechanism by which the grain boundaries are strengthened by point defects and the relationship between grain boundary structure and slip transferal.

Tensile Ductility

The prediction by Schulson (1981) of a brittle-to-ductile transition based on grain size for intermetallics was one of several factors that had reinvigorated interest in the development of ordered alloys for high temperature applications (Committee on Application Potential for Ductile Ordered Alloys 1984). Schulson's model was of the form:

$$d_c = \{(K_{IC} - k_y) / \sigma_o\}^2 \qquad (4.6)$$

where d_c is the critical grain size below which the intermetallic is ductile, K_{IC} is the fracture toughness of the material and k_y and σ_o are the Hall-Petch parameters described previously. This model is similar to the criterion for brittle fracture in steels and other materials proposed by Cottrell (1958) where K_{IC} in equation 4.6 is replaced by an expression for surface energy. Mechanistically the model assumes that a dislocation pileup at a grain boundary or other feature is responsible for nucleating a critical microcrack. The grain diameter limits the number of dislocations that comprise the pileup and therefore, controls the length of the microcrack that subsequently nucleates. The critical grain diameter, d_c, is then the diameter that leads to a critical crack that propagates rapidly under the applied tensile stress based on the fracture toughness of the material. The fracture toughness for polycrystalline NiAl is 5 - 7 MPa $m^{1/2}$ and is essentially independent of grain size or stoichiometry (see Table X in Noebe, Bowman and Nathal 1993). If the room temperature Hall-Petch parameters for NiAl alloy P541 and the fracture toughness limits of 5 and 7 MPa $m^{1/2}$ are inserted into equation 4.6, the critical grain size for extensive ductility in this alloy should be between 647 and 1354 μm. However, alloy P541 has little tensile ductility above a grain size of 20 μm. In fact, the model fails in predicting the critical grain size for ductility in any NiAl alloy.

The reason Schuslon's model does not have predictive capabilities in the case of NiAl is because the fracture initiation mechanism assumed in the model is not the same as that which occurs in NiAl. As already discussed in significant detail, the mechanism for fracture in NiAl is the formation of Griffith type defects at the grain boundaries due to slip incompatibility because of an insufficient number of independent slip systems. For NiAl and other slip limited materials, defects will form during the onset of plastic deformation. The initial defect size in NiAl will be on the order of the grain size while in non-slip limited materials it is on the order of the dislocation pileup width, which is only a small fraction of the grain size. Finally, any further deformation will exacerbate the problem in slip limited materials by causing the intergranular microcracks to link up creating continuously larger defects. Consequently, a Cottrell type grain size criterion for ductility does not apply to slip limited materials.

This last point was even acknowledged in Schulson's original paper (Schulson 1981) and yet, Schulson used NiAl as the prototypical intermetallic to justify his model. Tensile ductility was determined for NiAl as a function of grain size, temperature, and strain rate (Schulson and Barker 1983; Schulson 1985). For convenience the results are reproduced in Fig. 4.17. These results are often referenced in support of a critical grain size for room temperature ductility even though it is clear from the data that no ductility was achieved at room temperature at any grain size. In actuality, grain size only had a significant effect on the ductility of NiAl above 550 K or above the BDTT. While this is getting slightly ahead of the story, the deformation behaviors above and below the BDTT are not the same in NiAl. Therefore, the high temperature results cannot be extrapolated to room temperature.

Thus, contrary to popular belief: 1) Schulson's model does not predict a critical grain size for room temperature ductility of NiAl because the model is not applicable to NiAl. 2) The experimental data generated by Schulson does not demonstrate a critical grain size for room temperature ductility of NiAl. On the contrary it shows that tensile ductility is independent of grain size at room temperature, Fig. 4.17. Similarly, Nagpal and Baker (1990b) have recently concluded that room temperature ductility of cast plus extruded NiAl was independent of grain size. Similar findings were observed during this study for powder extruded NiAl and will be discussed below. 3) The ductility dependence on grain size for NiAl at elevated temperatures should not be extrapolated to room temperature because these are two different deformation regimes. This final point will be demonstrated in the following two chapters.

While Schulson's model is not applicable to NiAl there is a quantitative model developed by Chan (1990a) using a critical J-integral approach that predicts the dependence of tensile ductility on grain size for semi-brittle materials and is based on assumptions more pertinent to NiAl. The model assumes that the critical flaw size is on the order of the grain size and the geometry of the problem has been set up to simulate an internal circular crack in a round tensile bar. The general expression is of the form:

$$J = J_e (1 + J_z/J_e + J_p/J_e) \tag{4.7}$$

where J_e is the J-integral for elastic loading, J_z is the contribution to the J-integral due to Irwin's plastic zone term, and J_p is the J-integral due to plastic loading. For elastic-plastic materials exhibiting power-law hardening:

$$J_e = \frac{0.405(1-\nu^2)\sigma_a^{\,2}\pi a}{E}$$

$$J_z/J_e = \frac{0.0675[(n-1)/(n+1)](\sigma_a/\sigma_y)^2}{\{1+(\sigma_a/\sigma_y)^2\}}$$

$$J_p/J_e = \frac{3(\varepsilon_p)}{2(\varepsilon_e)(1-\nu^2)\sqrt{1+3/n}}$$

where E is Young's modulus, ν is Poisson's ratio, n is the inverse of the strain hardening exponent, σ_y is the yield stress, σ_a is the applied or remote stress, ε_e is the elastic strain and ε_p is the plastic strain. It is assumed that the half length of the internal crack is on the order of the grain size, d, (i.e. a = d in the above equations). For axisymmetric loading such as a tensile test, the J-integral is related to the stress intensity factor, K, through the relationship:

$$J = \frac{K^2(1-\nu^2)}{E} \tag{4.8}$$

By assuming that unstable fracture occurs at a critical value of the J-integral or stress intensity factor, K_{IC}, the strain at the onset of fracture or tensile ductility, ε_p, can be calculated using equations 4.7 and 4.8. A short basic program was written to calculate ε_p as a function of grain size at 300 and 700 K using the above relationships and the mechanical properties determined for powder extruded NiAl (Heat P541). The input parameters for the model are given in Table 4.1.

Actual tensile ductilities and the results using Chan's model for NiAl alloy P541 are shown in Fig. 4.18. There is very good agreement between the experimental data and the results of the model at both 300 and 700 K. There is a strong dependence of tensile ductility on grain size at 700 K, when the grain size is less than about 20 µm. In contrast, there is very little grain size dependence on ductility at 300 K for grain sizes greater than 1 µm. Although ductility is predicted by Chan's model to increase with decreasing grain size below 1 µm, only about 5 percent tensile ductility is expected at grain sizes of approximately 0.1 µm. Consequently, tensile ductility is relatively insensitive to grain size at room temperature.

Table 4.1. Input Parameters Used in Chan's Model for Predicting Tensile Ductility of Alloy P541 as a Function of Grain Size.

Parameter	300 K	700 K	Comments
Yield strength, σ_y, (MPa)	$179 + 500 (d^{-1/2})$	$86 + 229 (d^{-1/2})$	Given as a function of grain size, d, in μm
Strain hardening exponent, m	0.361	0.178	1/m; used in Chan's model
Fracture toughness, K_{IC}, (MPa $m^{1/2}$)	6	22	From Reuss and Vehoff (1990a)
Young's Modulus, E, (GPa)	241	232	From Moose (1991)
Poisson's ratio, ν	0.313	0.322	From Moose (1991)

Then there is the question of whether it is practical or even possible to produce a material with a uniform grain size on the order of 0.1 μm. Furthermore, it would be extremely difficult to stabilize such a fine grain size, because of grain growth during processing and service exposure. Finally, there is an implicit assumption in the model that the critical defect in the material is always the size of the grains. However, extrinsic defects, such as the inclusion shown in Fig. 14b, that are greater in size than the grain size will become the critical defect for fracture initiation. In other words, if it was possible to produce a material with a uniform grain size of less than 0.1 μm but the alloy had an inclusion that was larger 0.1 μm, then it would fail at the inclusion at a much lower tensile ductility than expected based on the grain size.

Consequently, grain size refinement alone is not a practical method for achieving significant improvements in the ductility of NiAl at room temperature. A more pragmatic approach would be to increase the number of independent slip systems without substantially altering the yield strength of the alloy and/or increase the fracture toughness of the material. The implicit relationship between fracture toughness and ductility is apparent when examining Fig. 4.18 and Table 4.1. The higher ductility of NiAl at 700 K, in comparison to room temperature, is due to the higher fracture toughness exhibited by NiAl at elevated temperatures. Finally, it is clear that deformation and fracture at room temperature is very different from that at intermediate temperatures. These differences will be described and analyzed in detail in the following chapters.

4.4 Summary and Conclusions

1. Intergranular fracture in binary, near-stoichiometric NiAl is a consequence of incompatible deformation at the grain boundaries due to the operation of only three independent slip systems. Intergranular fracture is not due to the existence of "inherently weak" grain boundaries as sometimes proposed and in fact the grain boundary strength of NiAl is probably superior to the cleavage strength of the bulk material. In the absence of plastic deformation, e.g. many ternary NiAl alloys, fracture occurs by cleavage, originating at internal or surface defects.
2. NiAl can exhibit significant macroscopic plasticity when tested in compression, and up to a few percent ductility in tension, however, on a microscopic scale fracture is occurring at the grain boundaries due to the generation of incompatible strains. Therefore, the large macroscopic compressive ductilities observed in NiAl do not suggest that the Von Mises criterion is violated. The fact that limited tensile ductility is possible in NiAl is also not a contradiction of the Von Mises criterion. Limited tensile ductility is expected when the yield strength of the material is below the stress needed to propagate a flaw that is on the order of the grain size. Because NiAl is bound by the Von Mises criterion it does not have the potential for exhibiting significant tensile ductility at room temperature.
3. Grain size refinement by itself is not a practical approach for achieving significant room temperature tensile ductility in NiAl because the process does not address the root cause of the ductility problem, which is an insufficient number of independent deformation mechanisms.

4. By assuming that the critical defect in NiAl is the grain boundaries, as proposed throughout this chapter, it is possible to accurately model the tensile ductility of NiAl as a function of grain size when the mechanical properties of the alloy are well defined.

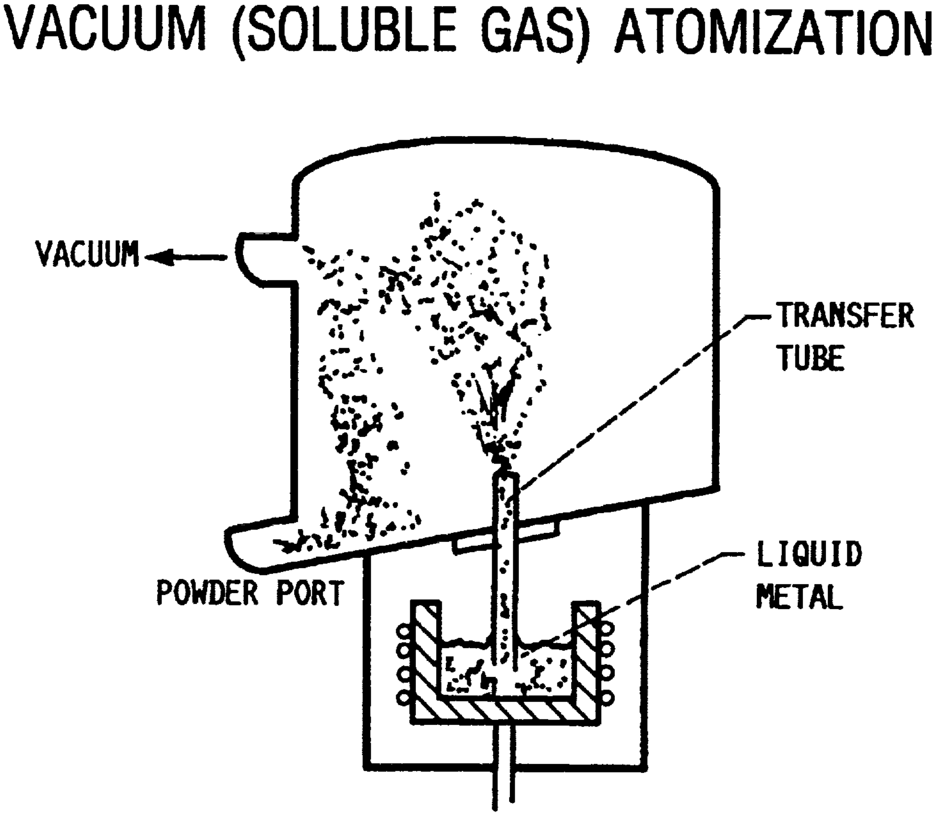
VACUUM (SOLUBLE GAS) ATOMIZATION
VACUUM
TRANSFER TUBE
POWDER PORT
LIQUID METAL

Fig. 4.1. Schematic illustration of the vacuum, soluble gas, atomization process used to produce all prealloyed powders used in this investigation.

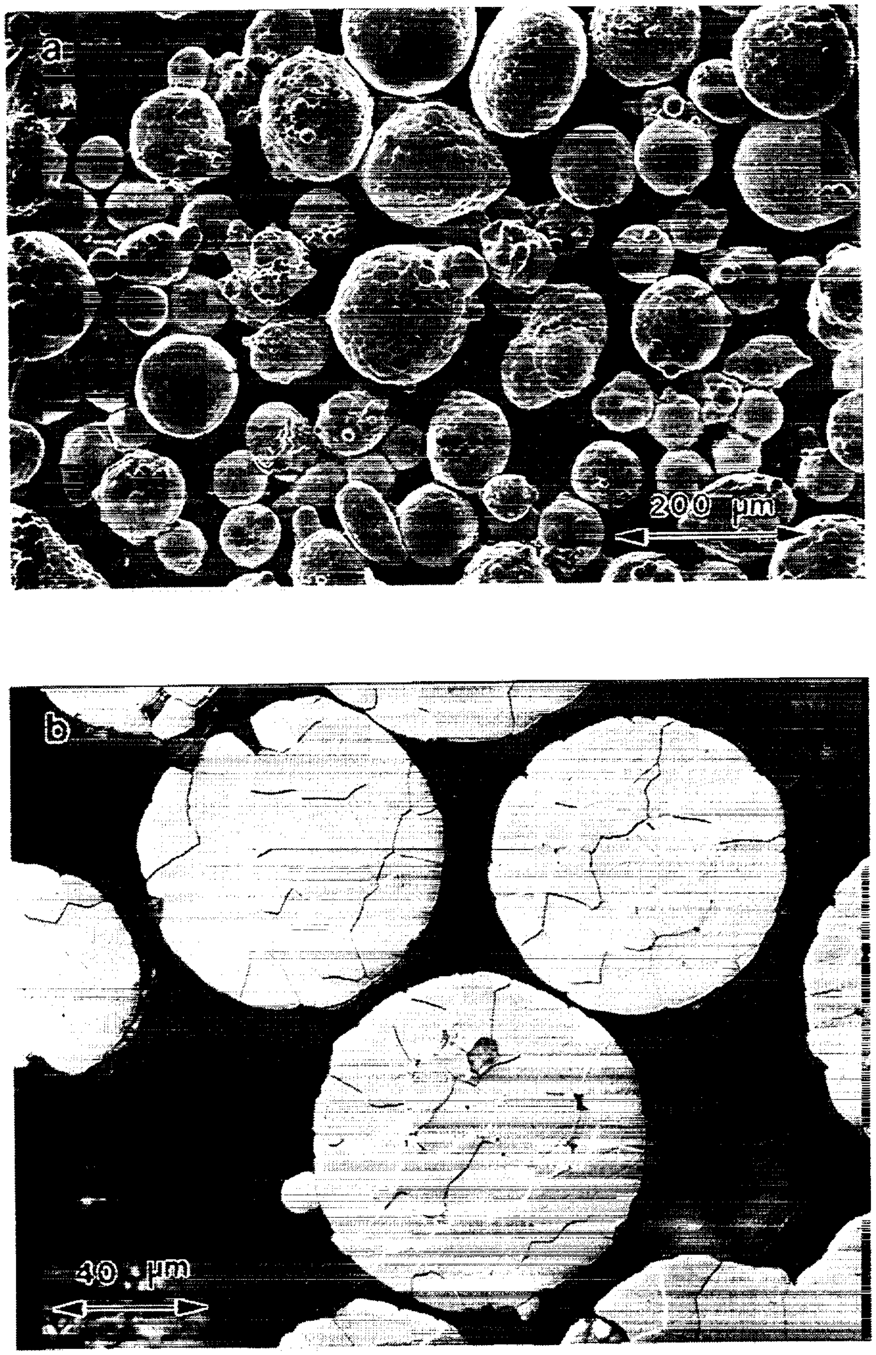

Fig. 4.2. As-received prealloyed powders from Heat P541: a) spherical morphology of the powders as revealed by SEM and b) grain structure of the powders as revealed by optical microscopy.

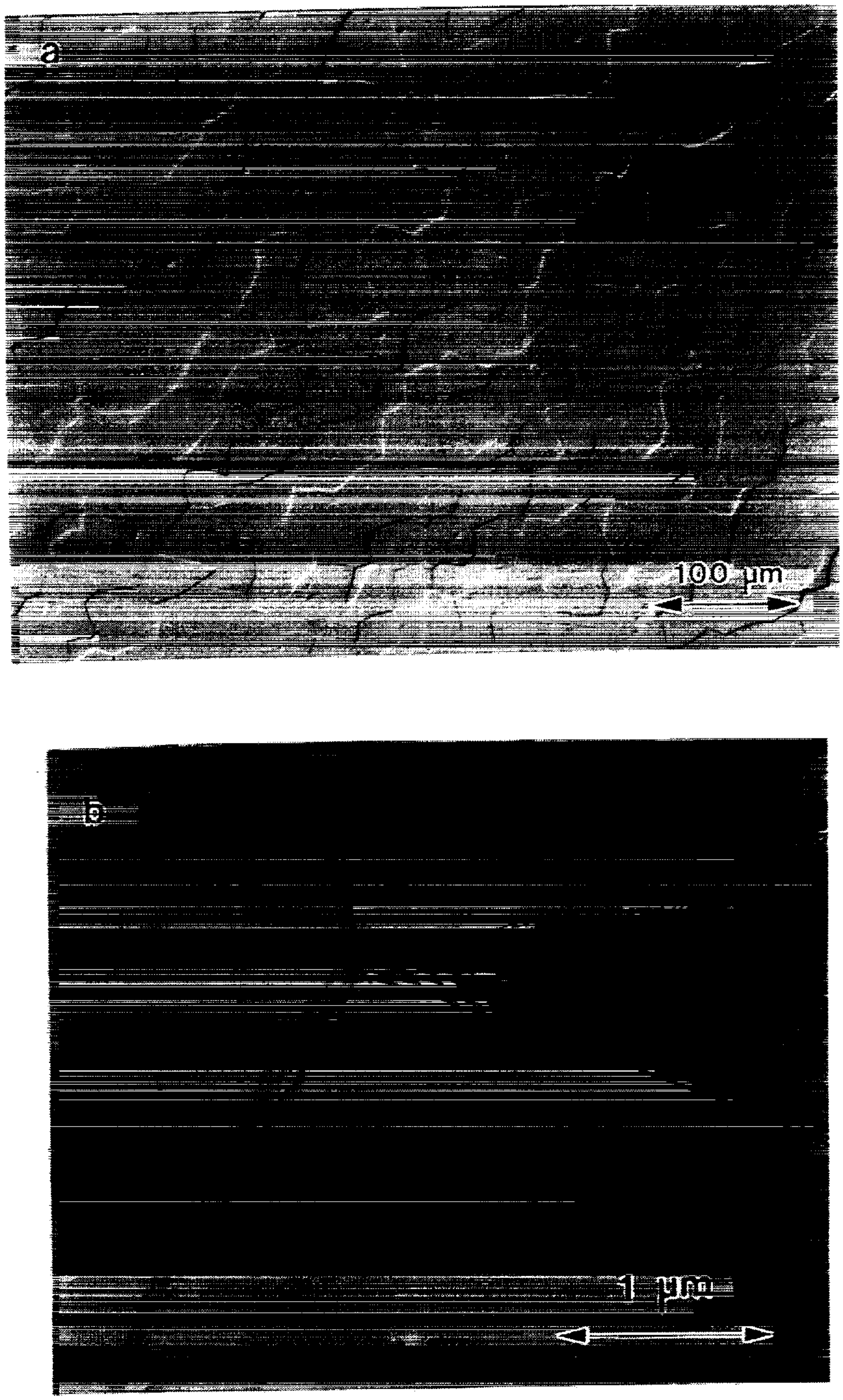

Fig. 4.3. Microstructure of as-extruded NiAl: a) optical micrograph of NiAl extruded at 1400 K showing an equiaxed grain structure and b) TEM micrograph showing a low dislocation density, indicative of a fully recrystallized material. Numerous extrinsic grain boundary dislocations (EGBD's) were observed.

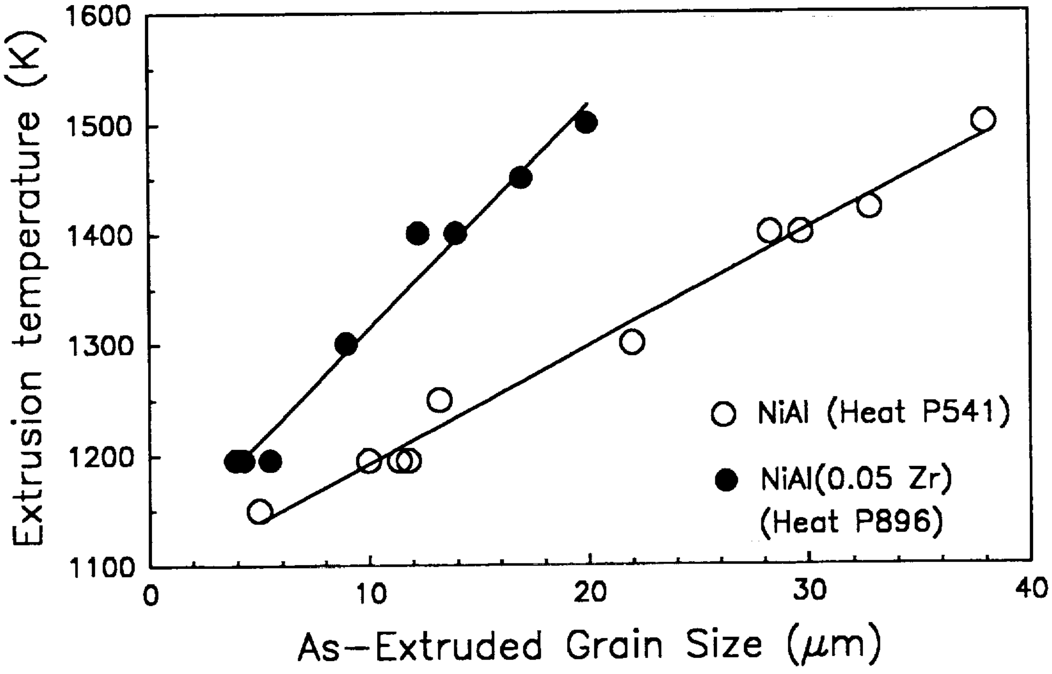

Fig. 4.4. Effect of extrusion temperature on the grain size of NiAl (Heat P541) and NiAl(0.05Zr) (Heat P896) extruded at a reduction ratio of 16:1.

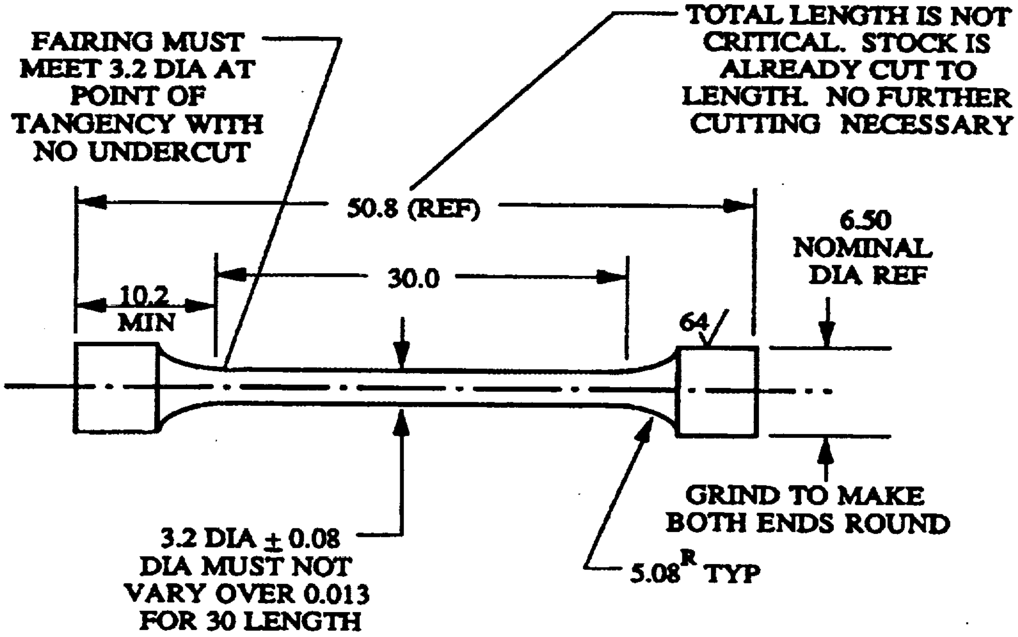
FAIRING MUST MEET 3.2 DIA AT POINT OF TANGENCY WITH NO UNDERCUT
TOTAL LENGTH IS NOT CRITICAL. STOCK IS ALREADY CUT TO LENGTH. NO FURTHER CUTTING NECESSARY
50.8 (REF)
6.50 NOMINAL DIA REF
30.0
10.2 MIN
64
GRIND TO MAKE BOTH ENDS ROUND
3.2 DIA ± 0.08 DIA MUST NOT VARY OVER 0.013 FOR 30 LENGTH
5.08R TYP

Fig. 4.5. Tensile specimen design for testing extruded NiAl alloys. All dimensions are in millimeters.

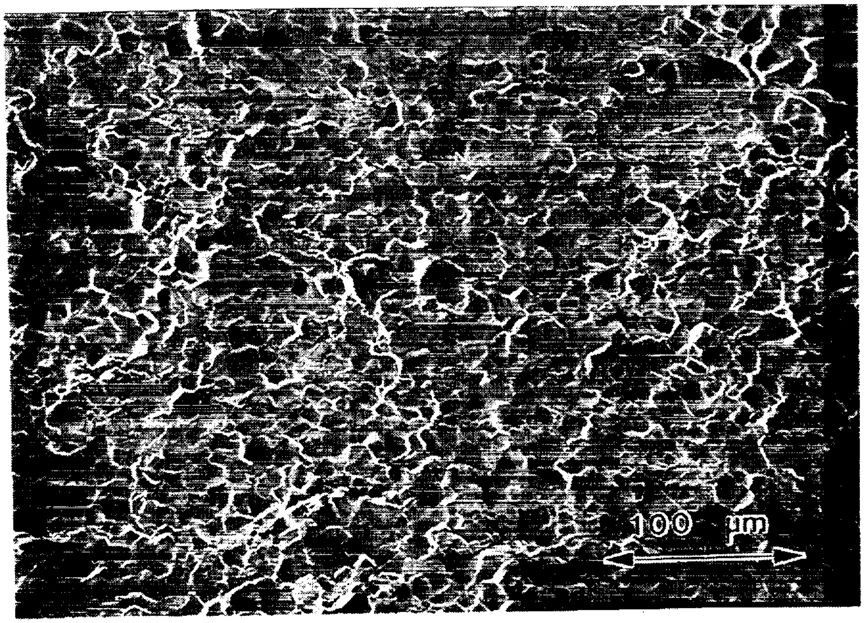

Fig. 4.6. Fracture surface of a powder (Heat P541) extruded NiAl tensile sample tested at room temperature.

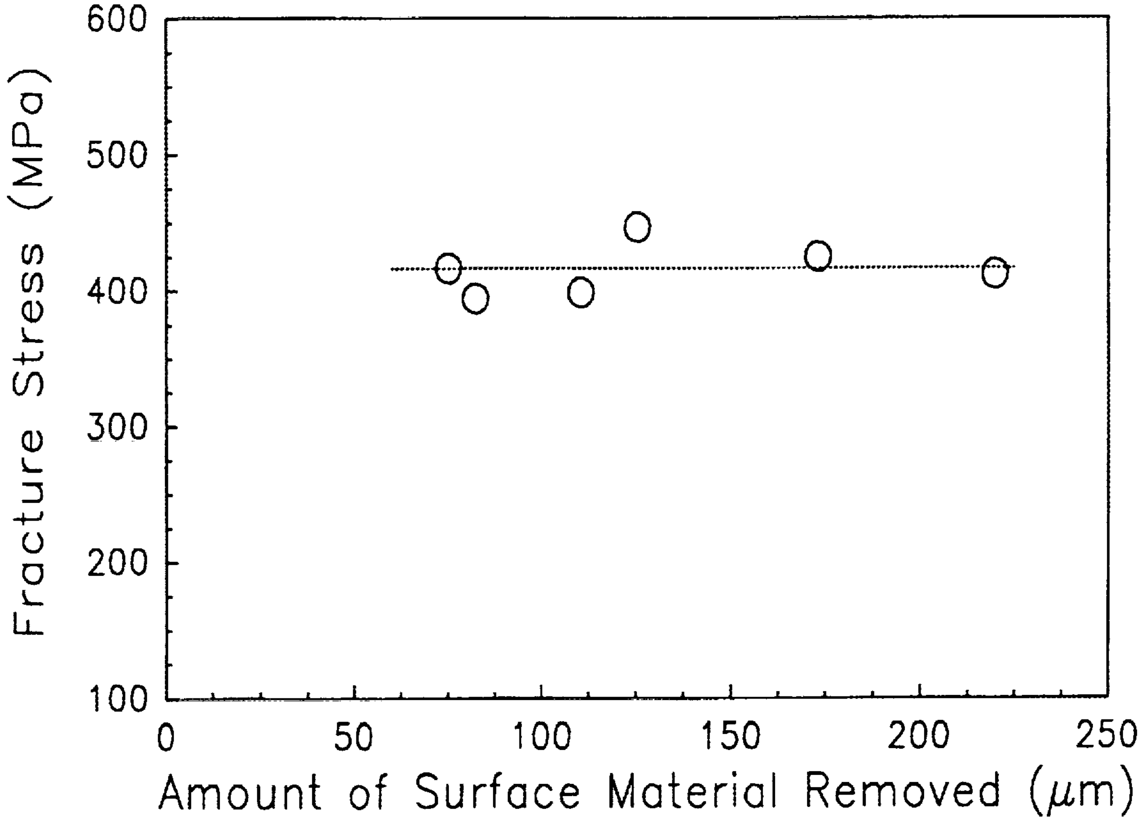

Fig. 4.7. Effect of surface removal by electropolishing on the room temperature tensile fracture strength of powder (Heat P541) extruded NiAl. Grain size was 11 μm.

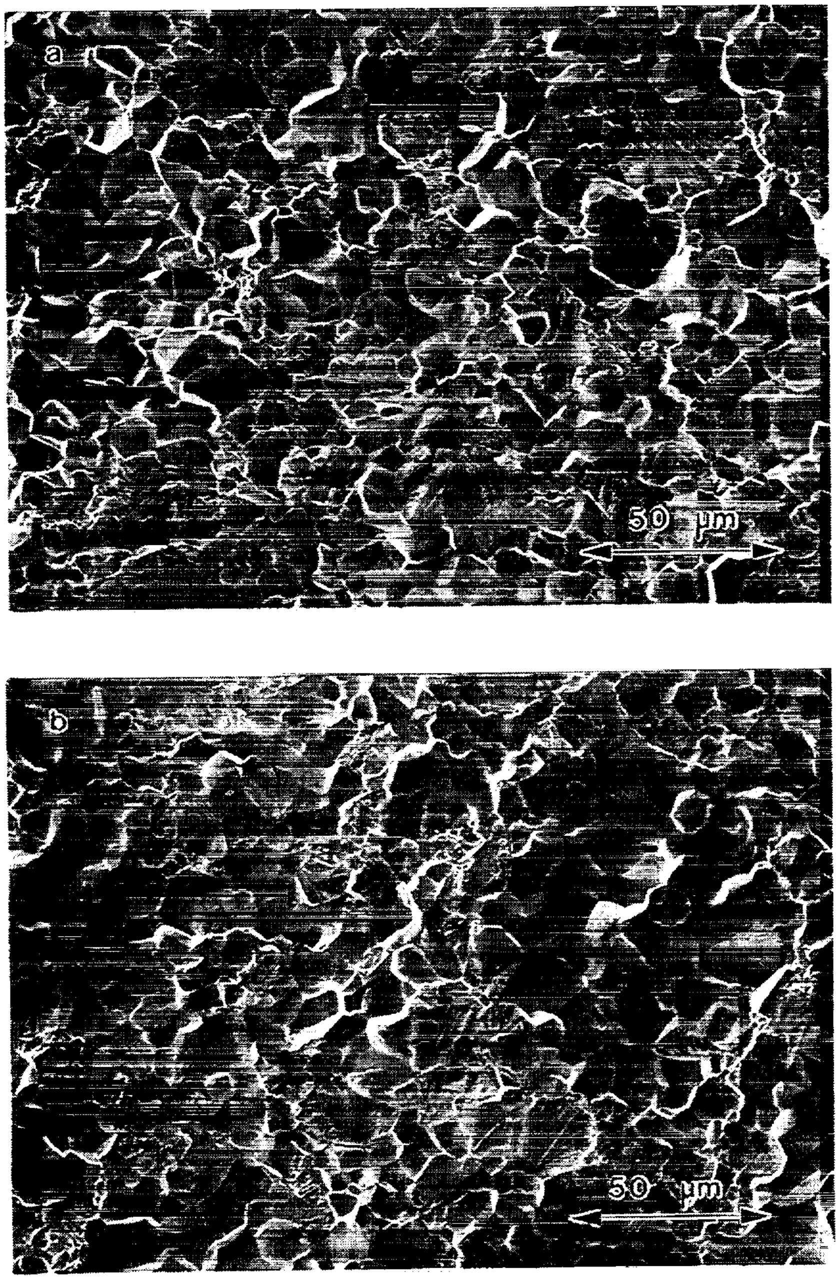

Fig. 4.8. Fracture surfaces of powder extruded tensile samples tested after electrochemically removing: a) 75 µm of surface material from the gauge and b) 220 µm of material from the gauge surface.

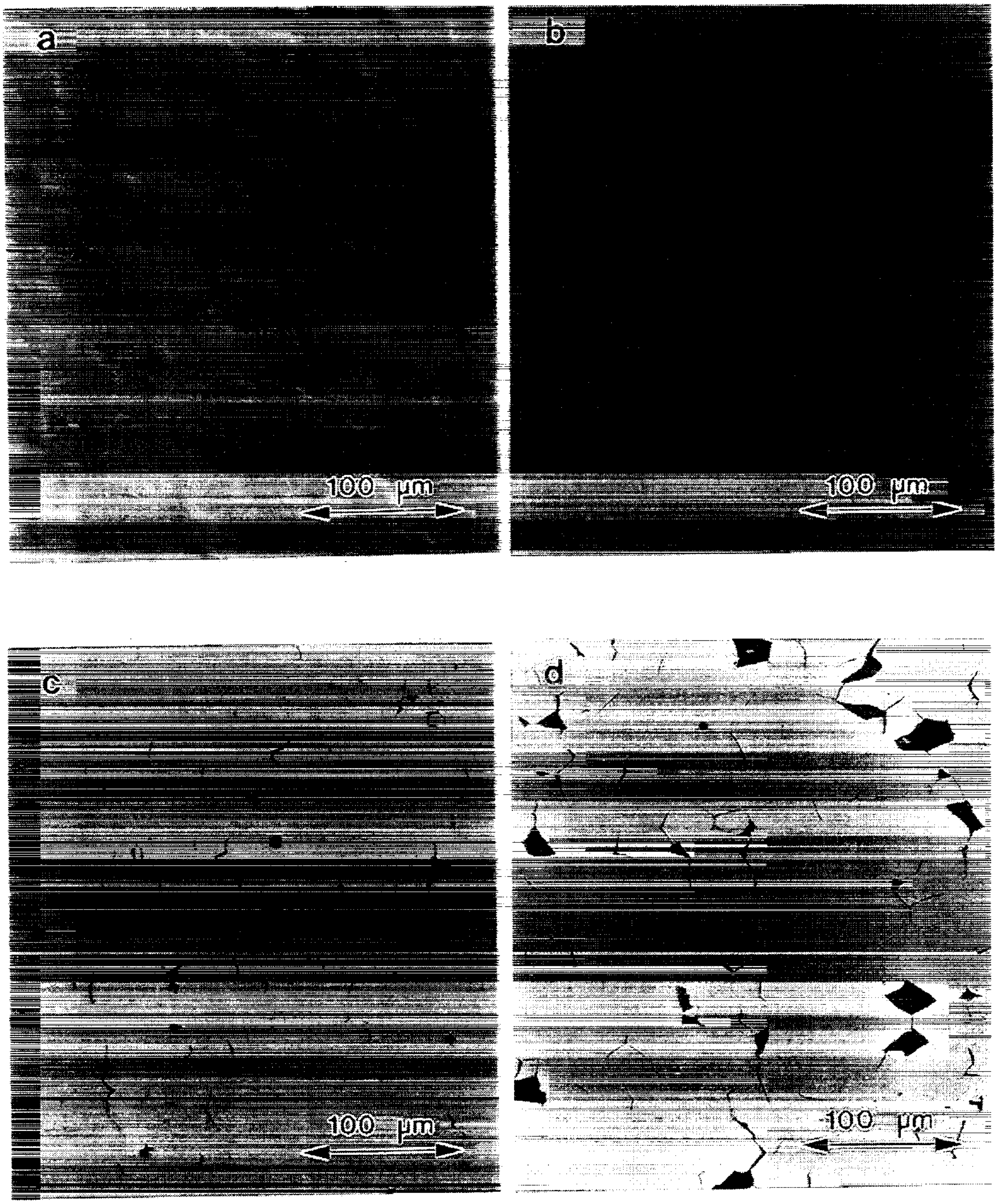
a
b
c
d
100 μm
100 μm
100 μm
100 μm

Fig. 4.9. Longitudinal cross-sections of polycrystalline NiAl samples deformed in compression at 300 K to various levels of plastic strain: a) as-extruded material, b) after 5% strain, c) after 11.7% strain and d) after 14.2% strain.

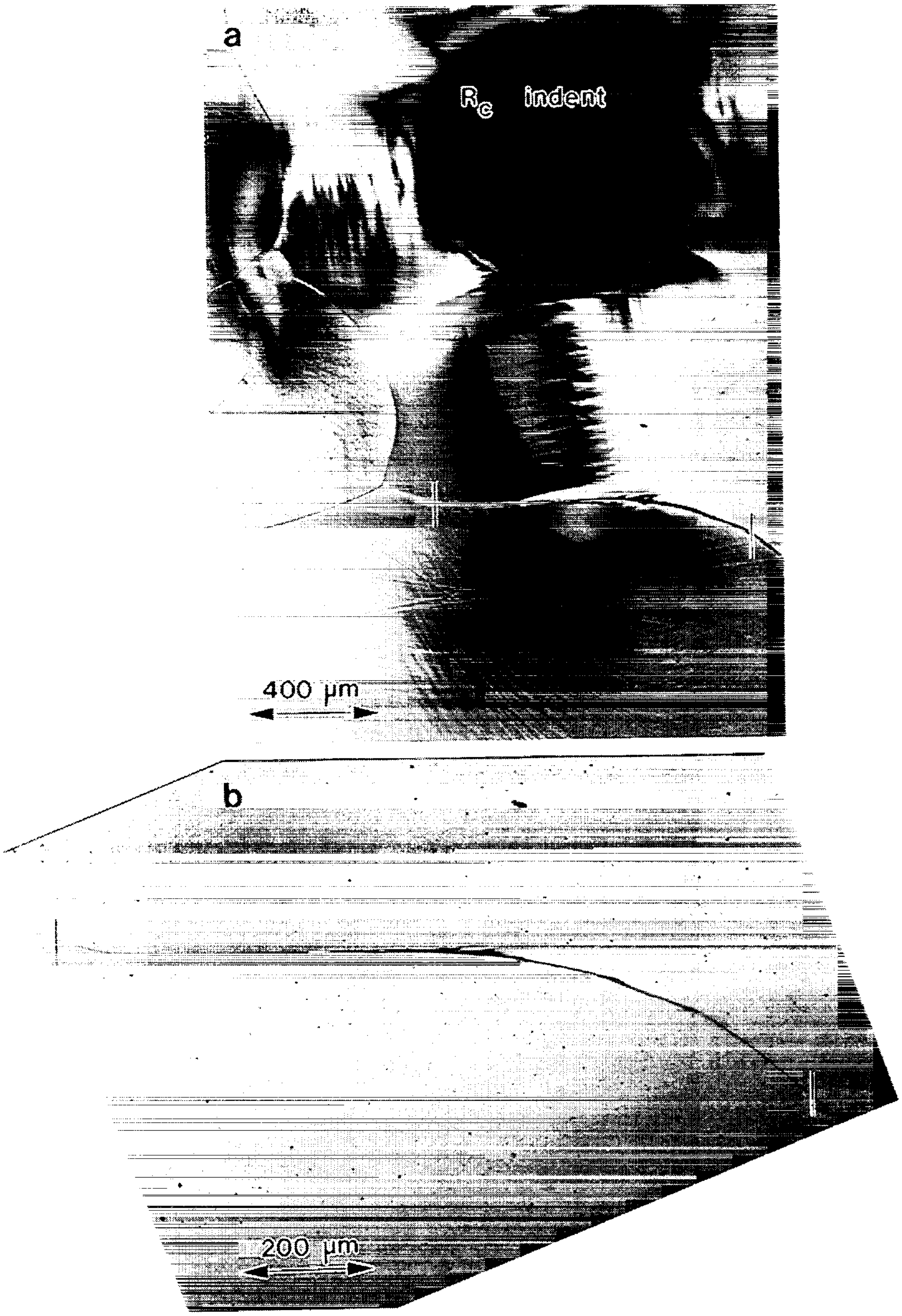

Fig. 4.10. a) Optical micrograph of the extensive plastic deformation surrounding an Rc indent in arc melted NiAl. b) Higher magnification of the area showing a grain boundary microcrack due to incompatible deformation across the boundary.

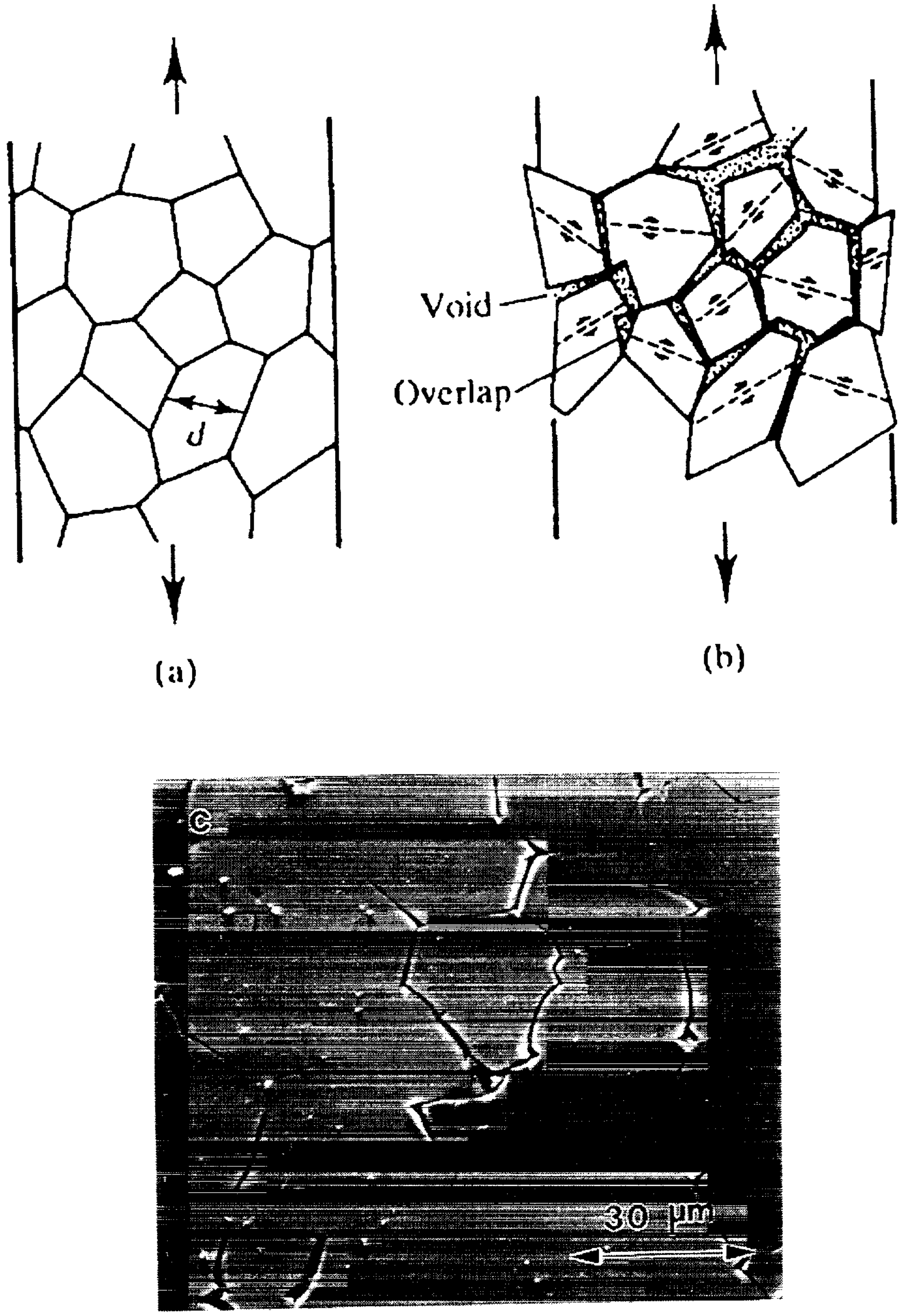

Fig. 4.11. a) Schematic illustration of plastic deformation of a polycrystalline solid with grain size , "d", b) appearance of the material if the grains deformed as if they were unconstrained single crystals and c) the actual appearance of polycrystalline NiAl deformed to approximately 8% strain in compression at room temperature. (Parts a & b after Ashby 1970.)

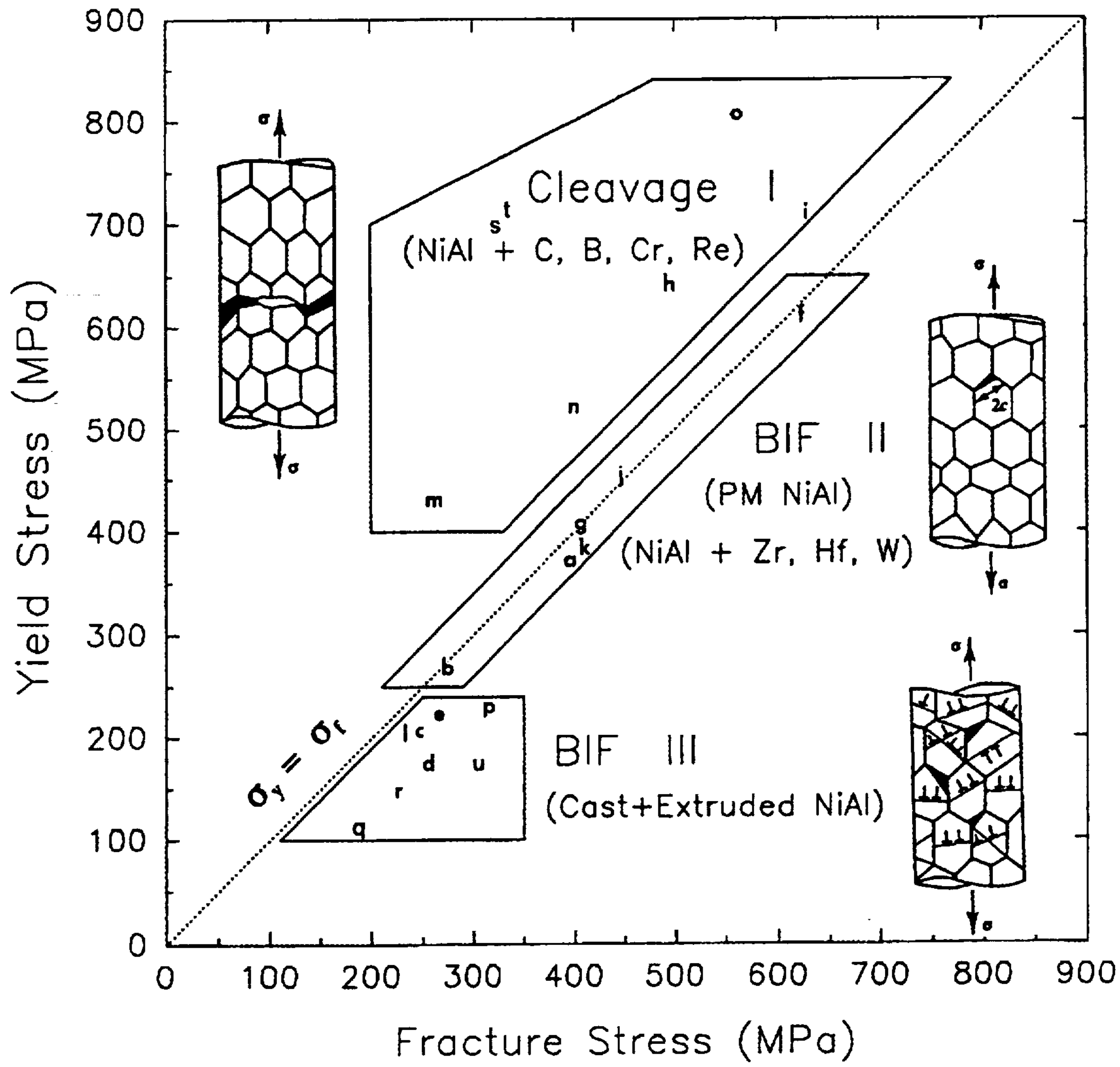

Fig. 4.12. The relationship between alloying additions, room temperature tensile properties and fracture initiation mechanisms in NiAl alloys. Compression tests were used to determine the room temperature yield strength when samples failed in tension before yielding. A description of all alloys represented in this plot is included in Appendix B.

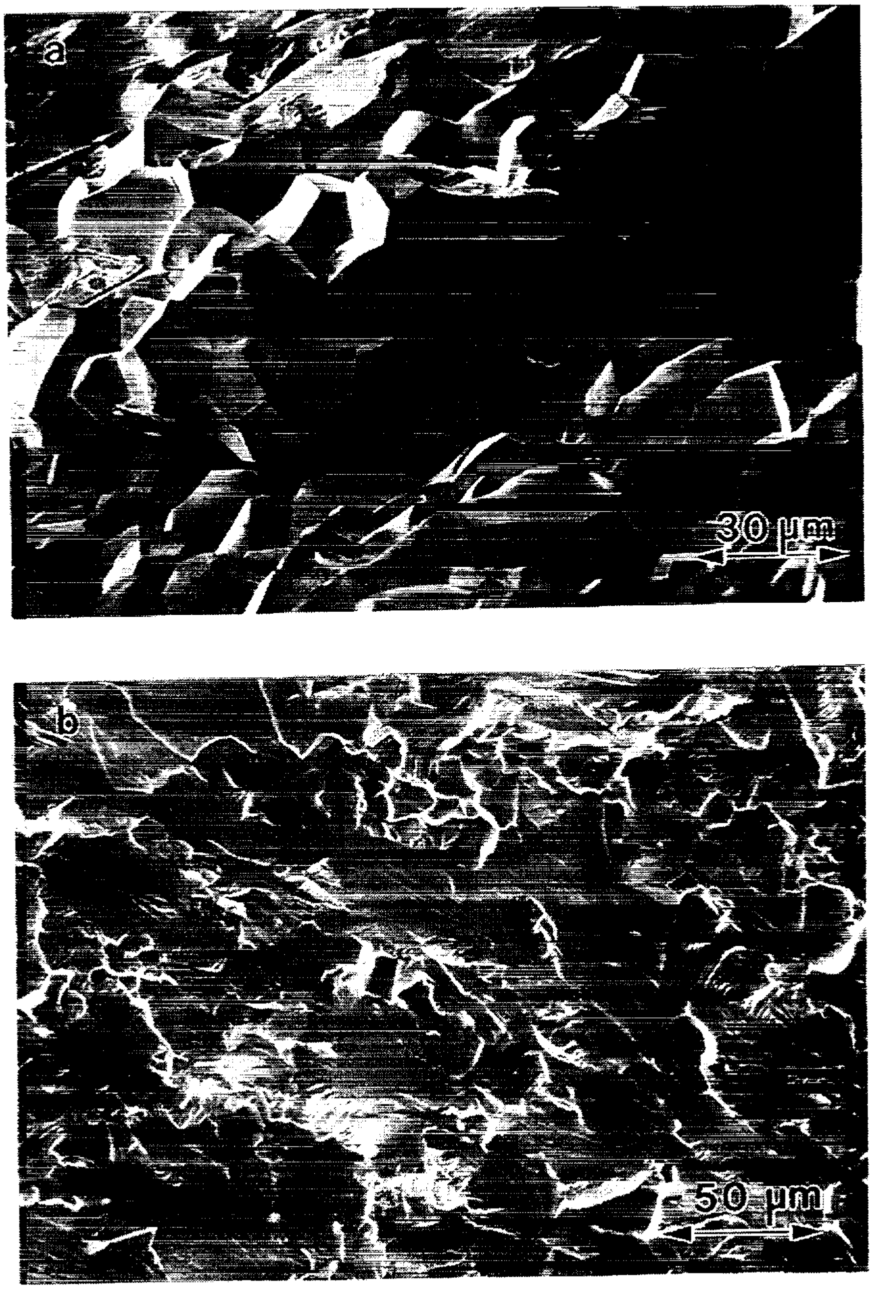

Fig. 4.13. Typical range of tensile fracture morphologies that are observed in NiAl alloys: a) fracture surface of alloy "c", a ductile cast plus extruded binary NiAl alloy representative of materials displaying BIF II behavior and b) fracture surface of alloy "m", a cast plus extruded NiAl-1Cr alloy representative of materials displaying cleavage I type behavior.

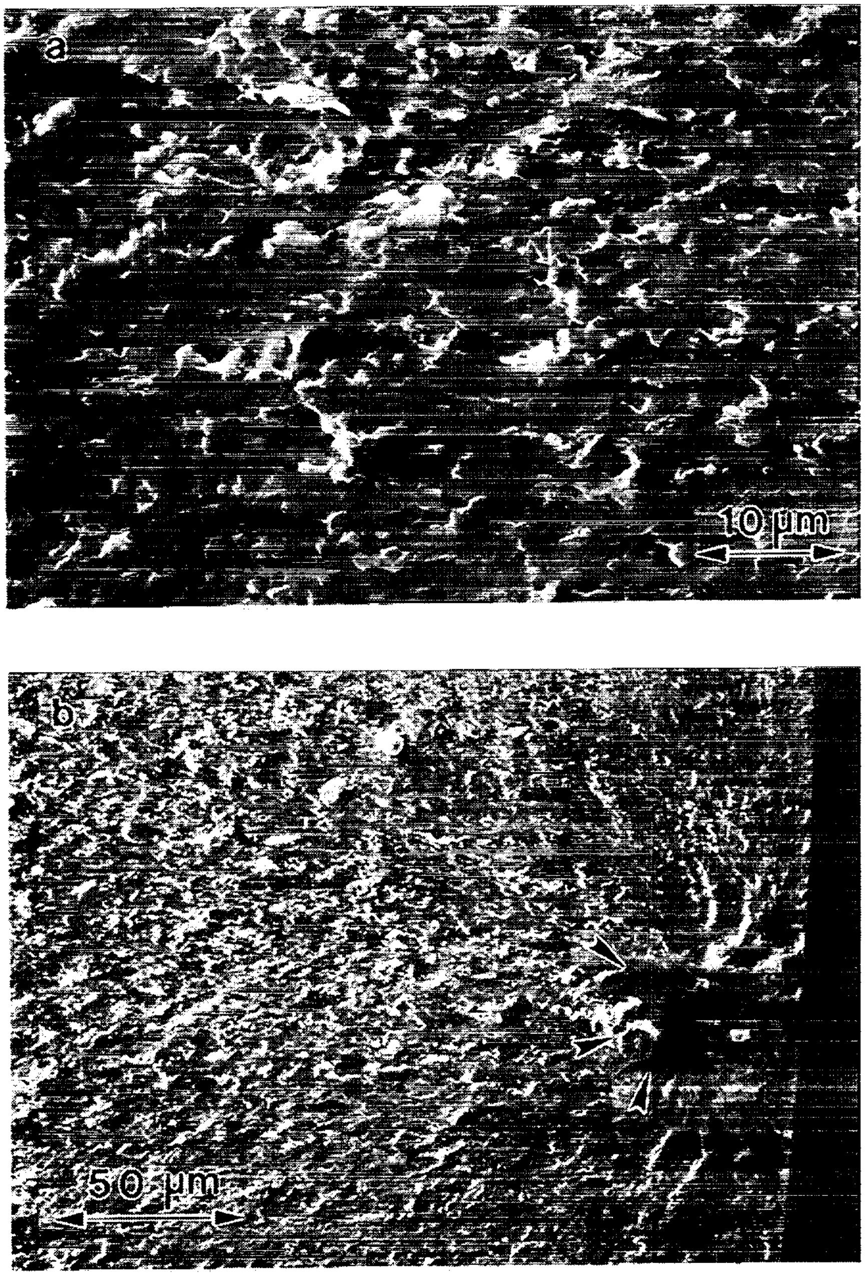

Fig. 4.14. a) A high strength NiAl-3Re (alloy "h") displaying cleavage I type behavior with b) fracture initiation at an Fe-rich inclusion.

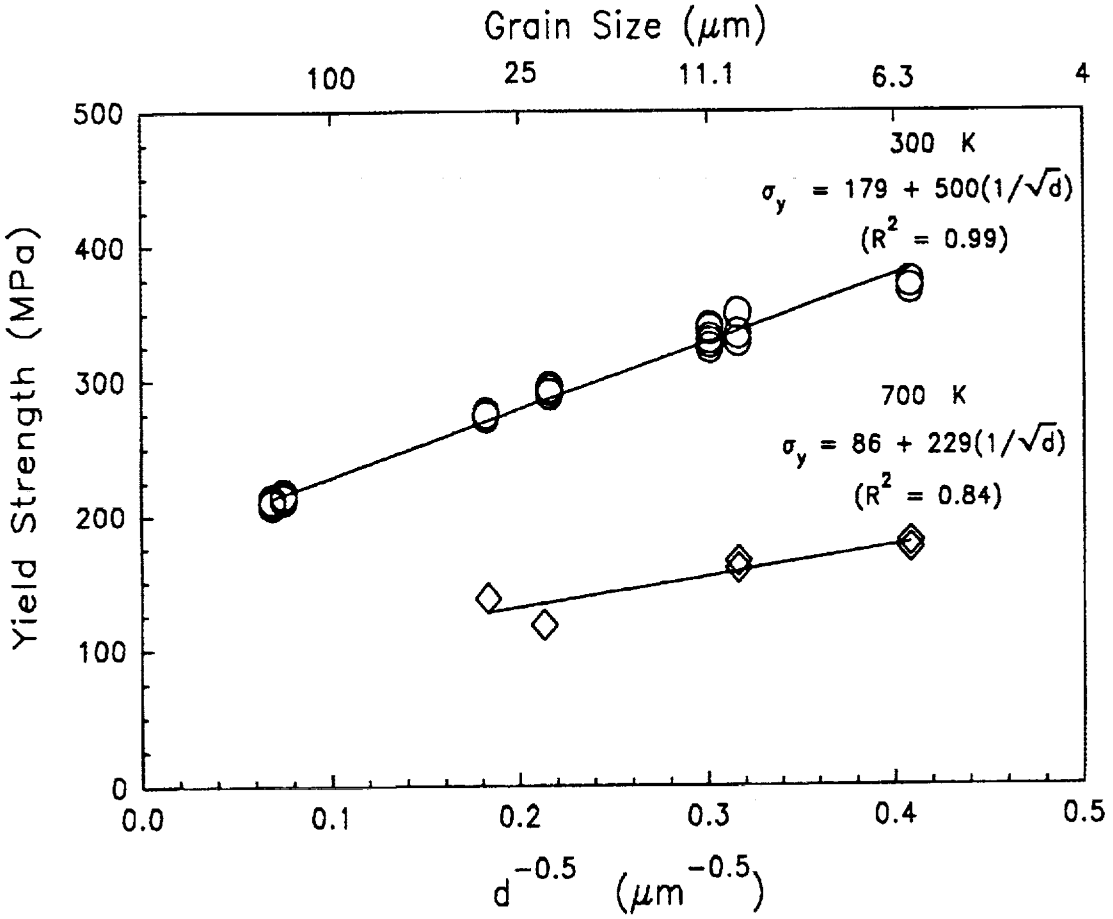

Fig. 4.15. Dependence of yield strength on grain size for powder extruded (Heat P541) NiAl deformed in compression at a strain rate of 1.4x10^{-4} s^{-1}.

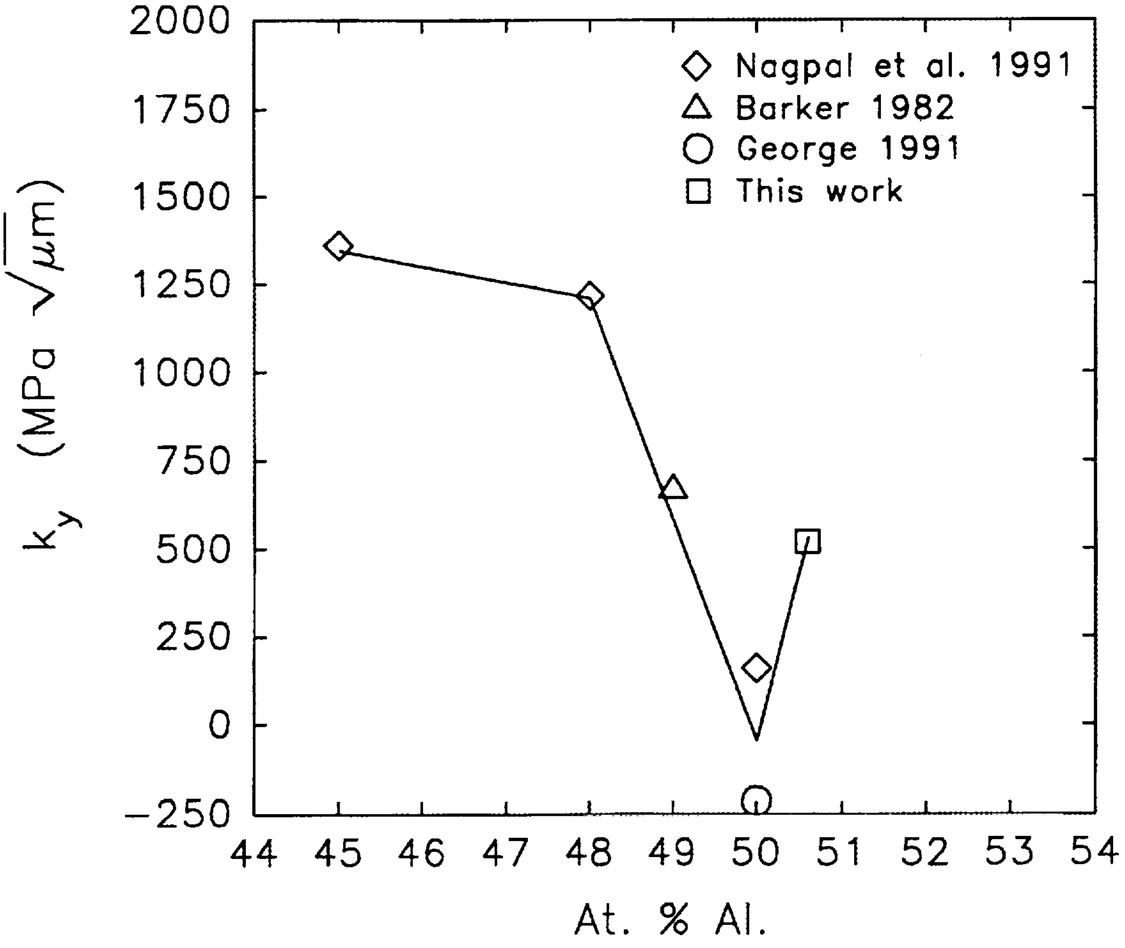

Fig. 4.16. The Hall-Petch slope for NiAl as a function of stoichiometry at room temperature.

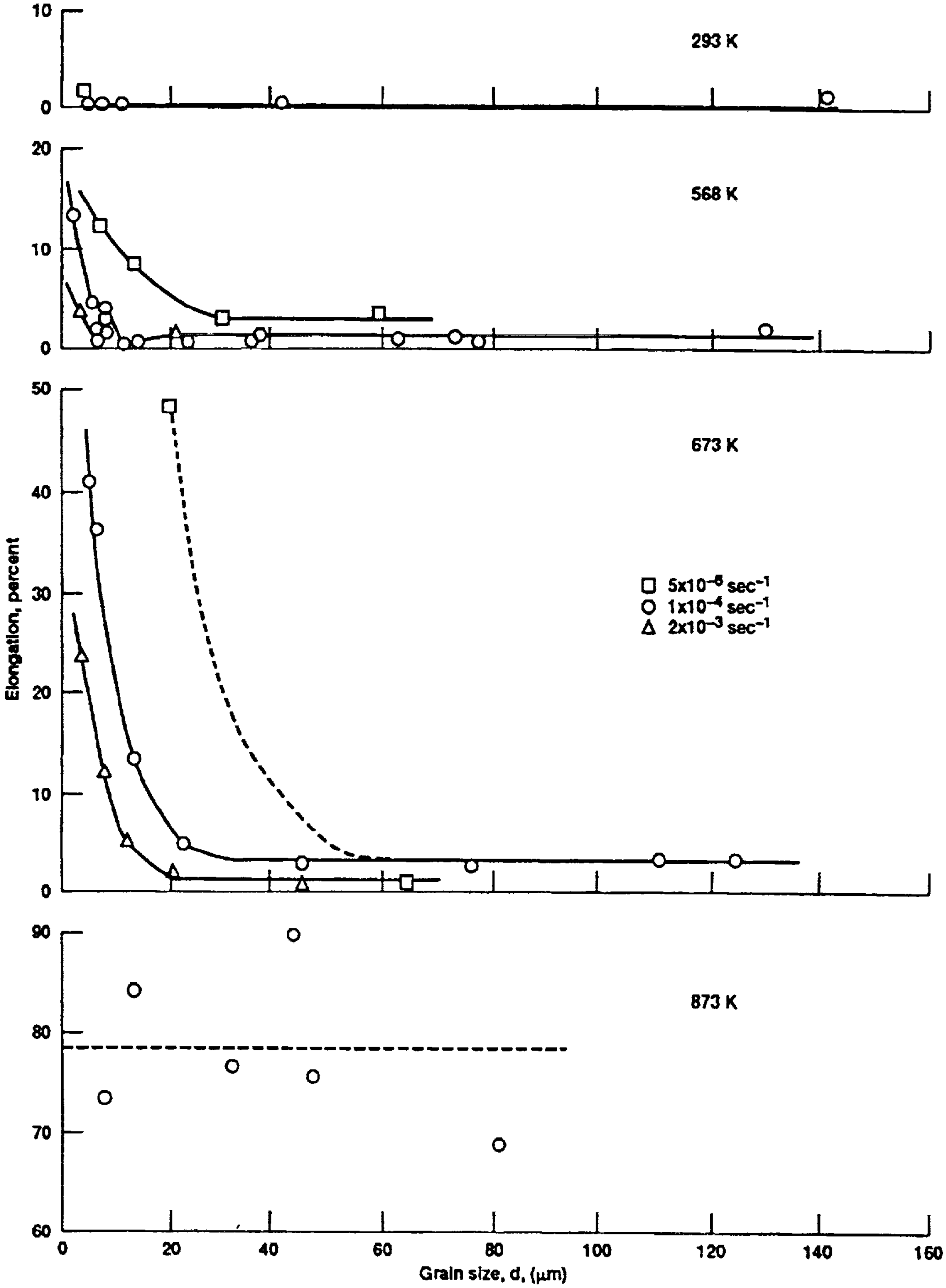

Fig. 4.17. Tensile elongation versus grain size for Ni-49Al at temperatures from 293 K to 873 K from Schulson (1985).

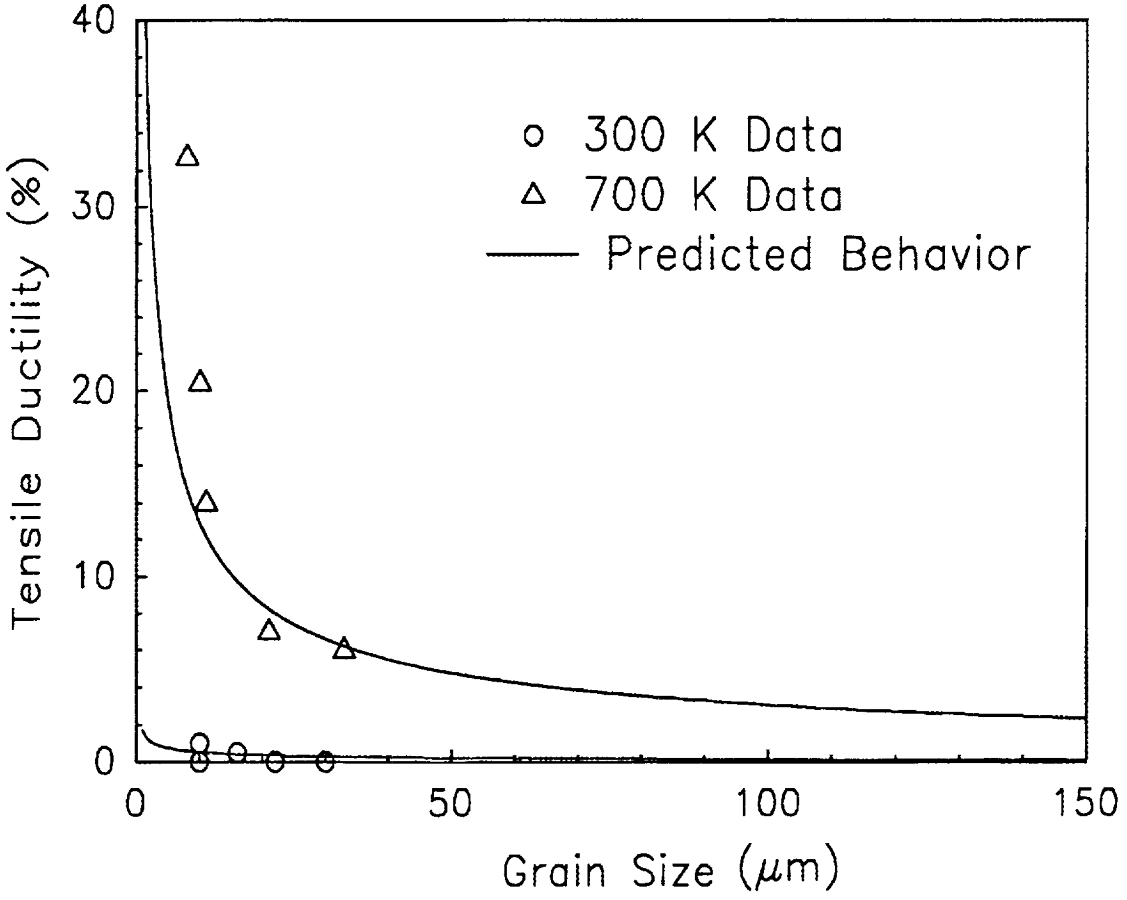

Fig. 4.18. Calculated and measured tensile ductilities for NiAl P541 as a function of grain size at 300 and 700 K.

CHAPTER V
EFFECT OF TEMPERATURE ON THE DEFORMATION BEHAVIOR OF NiAl AND NiAl(Zr) ALLOYS

5.1. Introduction

The poor room temperature tensile ductility of polycrystalline NiAl has been attributed to a number of different factors, but as demonstrated in the previous chapter, it is an insufficient number of independent slip systems or deformation modes that is responsible for this behavior. In contrast to room temperature properties, polycrystalline NiAl undergoes a dramatic change in mechanical behavior becoming remarkably ductile in tension at elevated temperatures (Grala 1960; Rozner and Wasilewski 1966; Hahn and Vedula 1989). Unfortunately, in these few studies (Grala 1960; Rozner and Wasilewski 1966; Hahn and Vedula 1989) the BDTT has been reported to occur at temperatures between 550 to greater than 1000 K. Therefore, while it is recognized that NiAl exhibits a BDTT, this is not a well characterized phenomenon. Furthermore, while the poor tensile ductility below the BDTT is due to a lack of independent deformation mechanisms, apparently something is occurring above the BDTT, whatever that temperature may be, to overcome this deficiency. A few investigators have suggested that the BDTT in NiAl is the result of a change in slip behavior (Lloyd and Loretto 1970; Miracle 1991). However, TEM observations do not support such a mechanism. It has also been suggested that the BDTT is due to the activation of bulk diffusion processes that have been observed to operate above 900 K (Ball and Smallman 1966b). Unfortunately, bulk diffusion processes are not expected to be active at temperatures as low as 550 K.

Consequently, the purpose of this chapter is to explore the deformation and fracture behavior of NiAl in the range of the BDTT to better characterize this transition and to understand the mechanism responsible for the changes in mechanical behavior at elevated temperatures. As in the previous chapter the alloy studied was the binary NiAl alloy P541. In addition, a ternary alloy doped with Zr (P896) was also investigated. Zirconium was chosen as a ternary addition since it is the most commonly used alloying element due to the improvement in oxidation behavior of Zr-doped NiAl compared to unalloyed material (Barrett 1988; Nesbitt and Barrett 1993). Also, preliminary testing of the ternary alloy P896 (Noebe et al. 1989) indicated a very dramatic difference in the BDTT of this material compared to binary NiAl. Consequently, any proposed mechanism for the BDTT in NiAl would also have to account for the effect of microalloying additions on the brittle-to-ductile transition.

5.2. Materials and Experimental Procedures

Vacuum atomized -100/+325 mesh pre-alloyed powders of near stoichiometric NiAl (P541) and NiAl + 0.05 at.% Zr (P896) were obtained from Homogeneous Metals, Inc. The compositions of both alloys are described in detail in Appendix A. The powders were packed in mild steel extrusion cans, which were then evacuated and sealed. The alloys were extruded at temperatures between 1150 and 1400 K with a 16:1 area reduction ratio to produce different grain sizes. The relationship between extrusion condition and grain size is shown in Fig. 4.4. After extrusion, the canning material was removed by pickling in dilute nitric acid. The extruded microstructures consisted of recrystallized and equiaxed grains with average linear intercept grain sizes ranging from 4-33 μm.

Button-head tensile specimens with typical gauge lengths of 30.5 mm parallel to the extrusion axis and gauge diameters of about 3.2 mm were ground from the extruded rods, Fig. 4.5. Each specimen was electropolished in a 10% perchloric acid - 90% methanol solution prior to testing. Tensile tests were performed to failure in an Instron screw driven load frame with a constant cross-head velocity corresponding to an initial strain rate of 1.4×10^{-4} s^{-1}. Tests were conducted between 300 and 1300 K in air using a resistance heated furnace. Stress-strain data were obtained from the load-time plots and yield stress was determined using the 0.2% offset method. At low temperatures, no significant tensile plasticity was observed in most cases. Therefore, to measure yield stress over the entire temperature range, compression tests were performed on specimens machined from the extruded bars and centerless ground to 3-5 mm in diameter and 6-10 mm in length. Testing was conducted to various strain levels in a screw driven load frame at a constant cross-head velocity resulting in an initial strain rate of 1.4×10^{-4} s^{-1}. Temperature gradients along the gauge section of both tensile and compression samples was ± 1 K at all temperatures.

Additional testing was performed in both tension and compression as a function of temperature and strain rate using either constant crosshead load frames or constant load creep machines. Constant load creep tests were used primarily to determine deformation behavior at very low strain rates (low loads). Sample dimensions were the same as those described above for both tension and compression tests regardless of the test technique. Details of how the constant load tests were performed can be found in the paper by Nathal and Ebert (1985). It was determined that constant load tension and compression testing gave identical creep results as tests performed under a constant crosshead speed. This similarity in creep test results independent of test technique is implied from the Dorn equation for steady state creep rates (Nix and Ilschner 1980).

Transmission electron microscope (TEM) specimens were cut from the gauge section of the tested specimens and jet-electropolished in a solution of 70% ethanol, 14% distilled water, 10% butylcellosolve, and 6% perchloric acid. Electropolishing was performed at 273 K at 30 V and 0.18 mA. TEM examination of slip systems was conducted in a JEOL 100C microscope operating at an accelerating voltage of 120 kV by Randy Bowman. Initial TEM examination of the compression samples demonstrated that the dislocation density was sufficiently low for detailed analysis, such as Burger's vector and slip plane determination of single dislocations, only in the specimens plastically strained to less than approximately 1%.

Dislocation mobility as a function of temperature was investigated *in-situ* using a single tilt Gatan hot-stage specimen holder in a Phillips 400T microscope. The purpose of the observations was to determine the stability of extrinsic grain boundary dislocations (EGBD's) and lattice dislocations in deformed NiAl and NiAl(Zr) alloys. This technique has been used previously to characterize grain boundary diffusion in other alloy systems (Swiatnicki and Grabski 1986,1989; Swiatnicki, Lojkowski and Grabski 1986). Specimens for the *in-situ* annealing study were pre-strained in compression at room temperature to about 0.5% plastic strain. The deformation resulted in the extensive formation of EGBD's within all grain boundaries in both alloys. Electron transparent thin foils were then prepared in the same manner as described in the previous paragraph. At least 15 boundaries from each foil were characterized prior to *in-situ* annealing. These same boundaries were compared after annealing and the difference in EGBD density was determined. The thin films were rapidly heated (1.7 K/s) *in-situ* to temperatures just above and below the BDTT of each alloy. Once stabilized, the temperature was kept constant with an accuracy of ± 2 K for 120 seconds before cooling to room temperature in approximately 120 seconds. Additional samples were held just below the BDTT for times up to 1 hour.

5.3. Results and Discussion

5.3.1. Microstructure of as-extruded alloys

Other than differences in grain size, Fig. 4.4, the microstructures of the NiAl and NiAl(Zr) alloys were similar. The extruded microstructures were fully dense and consisted of recrystallized and equiaxed grains. An example of the as-extruded structure of these alloys is shown in Fig. 4.3. The only difference in microstructure between the two alloy systems was that the grain sizes of the NiAl(Zr) alloy were smaller than the binary NiAl material for nominally identical extrusion temperatures.

TEM of the as-extruded NiAl and NiAl(Zr) alloys indicated that the overall dislocation density was low, consistent with a recrystallized microstructure. The majority of the grains were nearly dislocation free, while approximately 10% of the grains contained a moderately higher dislocation density. Most dislocations analyzed in the as-extruded alloys were found to be <001>{110} (Bowman et al. 1992), though <110> type dislocation segments have been observed in other studies of as-extruded NiAl materials (Lloyd and Loretto 1970; Cotton, Noebe and Kaufman 1993b).

By determining the orientation of individual grains, a distinct texture was observed in the alloys even though the grains were recrystallized (Bowman et al. 1992). At least 80% of the grains analyzed were found to have a <111> direction within five degrees of the extrusion direction (tensile axis). The remaining grains had orientations lying between the <011> and <111> directions. These results are consistent with previous studies that have confirmed the presence of a <111> recrystallization texture in extruded NiAl alloys (Khadkikar, Michal and Vedula 1990; Bieler et al. 1992,1994).

In the ternary alloy, the majority of Zr was in solution since no precipitates were observed except for an occasional ZrO_2 particle. Zr, however, was effective in retarding grain growth since the grain sizes of the NiAl(Zr) alloy were always finer than those of the binary NiAl alloy extruded at the same temperatures. This would imply segregation of Zr to the grain boundaries. Segregation of Zr to the grain boundaries was confirmed in a companion study by Zeller, Noebe and Locci (1990). In this study, auger electron spectroscopy was performed on both alloys studied in this investigation. No measurable segregation of any impurities was observed at the grain boundaries in the binary NiAl alloy. In the Zr-doped alloy, segregation of Zr was observed at the grain boundaries but no other elements beside Ni, Al and Zr were detected. While the alloy was doped with only 0.05 at.% Zr, between 2 - 4 at.% Zr was measured on each surface of the analyzed grain boundaries. This meant that the total Zr content at the grain boundaries, 4 - 8 at.%, was about two orders of magnitude greater than present in the bulk alloy.

5.3.2. Effect of temperature on tensile properties of NiAl

The effect of temperature on the mechanical behavior of NiAl is summarized in Fig. 5.1. This figure shows the temperature dependence of the tensile properties (0.2% offset yield stress, fracture stress and tensile elongation) for the binary NiAl alloy of 5 μm grain size. The yield strength decreases gradually with temperature, as expected from the discussion in Chapter 2. However, the fracture strength, σ_f, remains essentially constant or decreases slightly before increasing very dramatically at temperatures just above 500 K. Recent work by Reus and Vehoff (1990a,b), reproduced for convenience in Fig. 5.2, demonstrates that the fracture toughness for binary NiAl alloys also increases in a manner similar to the fracture strength shown in Fig. 5.1, increasing significantly between 500 and 600 K. The similarity in behavior between fracture strength and fracture toughness would be expected based on the direct correspondence between K_{IC} and σ_f for a constant flaw size. Finally, it is evident that the transition from brittle to ductile tensile behavior, as defined by a sudden and significant increase in tensile ductility, occurs because of the concomitant increase in fracture strength (or fracture toughness) over the same temperature range.

By examining Figs. 5.1 and 5.2, several conclusions about the mechanical behavior of NiAl can be made. First, there is a relatively sharp BDTT in NiAl occurring over a relatively narrow temperature range. However, this transition in mechanical behavior can be defined by more than just a sudden and dramatic increase in tensile elongation. It also corresponds to a change in fracture strength and fracture toughness. Therefore, the BDTT corresponds to a very significant change in the mechanical behavior of the intermetallic. Second, this change in behavior occurs at a very low temperature. In this case, the BDTT was near 550 K, consistent with the results of Rozner and Wasilewski (1966) and the fracture toughness data of Reus and Vehoff (1990a,b). This translates into a BDTT that can occur at temperatures as low as approximately 0.28 of the absolute melting point, T_m, of the alloy. Finally, it should be noted that the mechanical behavior manifested in Fig. 5.1 is typical of all NiAl alloys that have been studied during this investigation, though the absolute temperature at which the BDTT occurs can vary due to a number of factors that will be discussed shortly.

5.3.3. Brittle-to-ductile transition temperatures

The BDTT's for binary NiAl and the Zr-doped alloy as a function of grain size are shown in Fig. 5.3. Based on the data in Fig. 5.3 the BDTT for binary NiAl occurred between 550 and 650 K, consistent with the low transition temperature already reported for the fine grain size version of this alloy. Grain size as a variable had a relatively minor impact on the transition temperature. Within the BDTT range for binary NiAl shown in Fig. 5.3, material with a finer grain size tended to exhibit a greater tensile ductility at a given temperature. This behavior would be expected from the analysis in section 4.3.3 and shown in Fig. 4.18, demonstrating the effect of grain size on tensile ductility at intermediate temperatures.

In contrast to the low BDTT for binary NiAl, the NiAl(Zr) alloy had a BDTT on the order of 850 - 875 K. This is a significant increase in transition temperature due to a relatively minor (500 ppm) alloying addition of Zr. Also, the transition from brittle to ductile behavior occurred over a narrower temperature range for the Zr containing alloy than for the binary NiAl material.

5.3.4. Flow and fracture behavior of NiAl near the BDTT

It is readily apparent from the previous sections that a very dramatic change in mechanical behavior occurs near the brittle-to-ductile transition in NiAl. Therefore, it is worth taking a closer look at the flow and fracture behavior of NiAl in the temperature range surrounding the BDTT. The tensile fracture surfaces of binary NiAl at three different temperatures are shown in Fig. 5.4. Qualitatively, binary NiAl exhibits mixed mode to intergranular fracture at room temperature and below the BDTT. This changes to a predominantly transgranular fracture mode just above the BDTT. Then at temperatures far above the BDTT the fracture mode is ductile rupture, consistent with the large tensile ductilities that are obtained. From these observations alone (Fig. 5.4) it is not possible to determine whether a significant change in fracture behavior actually occurs at the BDTT.

A more conclusive investigation of fracture mechanisms was accomplished with compression samples, similar to the analysis performed in Chapter 4 and presented in Fig. 4.9. This time a series of compression samples were deformed to approximately 10% strain at different temperatures. The resulting microstructures for these samples are shown in Fig. 5.5. At temperatures of 500 K and below there was significant intergranular cracking in the samples with the density of cracks independent of temperature. However, at 600 K, approximately 50 K above the BDTT, there was no evidence of intergranular cracking in the material. Not a single microcrack was observed in the cross-section of the sample after 10% deformation at 600 K. This result indicates that at the BDTT some change in behavior occurred that satisfied the Von Mises criterion. In other words, there is some mechanism of accommodation for all the strains at or across the grain boundaries. This accommodation process is then responsible for the dramatic changes in mechanical behavior observed above the BDTT.

Thus far, it is apparent that at the BDTT for NiAl a change in fracture behavior occurs due to the elimination of grain boundary compatibility problems resulting in a significant improvement in tensile ductility, fracture strength and fracture toughness. However, this does not explain the mechanism for the BDTT. To begin to determine the actual mechanism responsible for the changes in fracture properties it is necessary to examine the deformation behavior of NiAl in more detail starting with the temperature dependence of the yield strength. The temperature dependencies of the compressive yield stresses for binary NiAl and the Zr-doped alloy at two different grain sizes are shown in Fig. 5.6. The yield stresses for both the coarse and fine grained NiAl and NiAl(Zr) alloys decreased with increasing temperature until reaching a plateau or discontinuity in the yield stress versus temperature dependence followed by mildly decreasing yield strengths at higher temperatures. As observed in Fig. 5.6, the temperature range over which this athermal behavior occurred was influenced significantly by composition and maybe to a lesser extent by grain size. For example, for the NiAl(Zr) alloy the athermal plateau occurred between 700 and 900 K. For the binary NiAl alloy the "plateau" existed over a very small temperature range around 550K and amounted to little more than a discontinuity in the σ_y versus T curve.

In both alloys the yield stress was greater for the fine grained materials, with the largest differences in strength occurring at low temperatures. This effect was especially pronounced in the Zr containing alloy (Fig. 5.6) and is discussed further in the paper by Zeller, Noebe and Locci (1990). The effect of grain size on the flow behavior of binary NiAl was discussed in the previous chapter. Yield stress data for both alloys converge as the temperature is increased although the Zr containing material remained stronger up to 1300 K (the highest temperature investigated).

While the Zr-doped material was stronger than the binary alloy the work hardening characteristics of the alloys were independent of alloying addition. The compressive flow stress, σ, could be described as a function of strain by the equation:

$$\sigma = A\, \varepsilon_p^{\,m}$$

where ε_p is the true strain, A is a constant and m is the strain hardening exponent. Although yield stress was markedly influenced by Zr additions, the strain hardening exponents determined from the compressive yield stress data of the binary NiAl and Zr-doped material were essentially identical over the entire temperature range investigated (Fig. 5.7). This result is consistent with data from Weaver, Kaufman and Noebe (1993) on NiAl single crystals where work hardening behavior was essentially independent of interstitial content or Mo additions. For both alloys studied here, the strain hardening exponent was approximately 0.35 at room temperature and steadily decreased with increasing temperature, approaching zero near 1300 K. From the work hardening behavior of the alloys depicted in Fig. 5.7 it is apparent that NiAl alloys begin to experience significant recovery during deformation at temperatures just above room temperature with the largest decrease in the work hardening exponent occurring between 500 and 600 K.

Often a brittle-to-ductile transition will correspond to a sudden decrease in yield strength with temperature or some other discontinuous change in the σ_y - T curve. This is essentially the case for NiAl and NiAl(Zr). The brittle-to-ductile transition for the NiAl and NiAl(Zr) alloys tends to correspond to the end of the athermal plateau or the discontinuity in the σ_y - T curves. However, it is very difficult to identify a definite change in deformation mechanism from the data plotted in Fig. 5.6. A more informative method of plotting the yield strength data would be an Arrhenius plot, of the form log. stress versus 1/T.

The binary NiAl data from Fig. 5.6 are replotted in Fig. 5.8 in an Arrhenius configuration. In this type of plot a change in slope is indicative of a change in deformation mechanism because the slope of the line is proportional to the activation energy for deformation. It is evident from Fig. 5.8 that the flow behavior for binary NiAl can be separated into three distinct deformation regimes based on temperature. Also plotted in Fig. 5.8 is the corresponding tensile ductility for binary NiAl as a function of inverse temperature. The transition from brittle to ductile behavior corresponds to the transition from the low temperature (Region I) to intermediate temperature (Region II) deformation regimes that occurs in the temperature range of 550 to 600 K. Therefore, the BDTT in NiAl can now be clearly associated with a definite change in deformation mechanism.

The low temperature deformation regime (Region I) in Fig. 5.8 is governed by dislocation glide. The mechanism responsible for controlling deformation in this temperature regime is the inherent resistance of the lattice to dislocation motion similar to the behavior observed in bcc metals (Pascoe and Newey 1971; Kitano and Pollock 1993).

The high temperature deformation regime (region III) that begins near 1000 K has also been characterized in significant detail (Whittenberger 1987,1988; Nathal 1992). In this regime, creep processes control deformation with dislocation climb the dominant or rate controlling factor. The existence of an intermediate temperature deformation regime represented by region II in Fig. 5.8 has not been previously reported. Past studies on NiAl have concentrated on either the room temperature deformation behavior or the creep response of the material, neglecting the deformation behavior near the BDTT.

This intermediate temperature deformation regime either represents a transition from glide dominated slip behavior to thermally activated deformation with varying components of both controlling plasticity or this regime could represent a new deformation mechanism. The case will be made in the following sections that Region II represents a new and distinct deformation regime. This region is governed by dislocation glide processes within the grain interiors with localized climb occurring in the vicinity of the grain boundaries permitting strain accommodation across the grain boundaries.

5.3.5. Rate dependent deformation of NiAl

The data in Fig. 5.8 represent the deformation behavior of NiAl at only one strain rate ($1.4\times10^{-4}\ \mathrm{s}^{-1}$). However, the presence of three distinct deformation regimes in NiAl is also demonstrated in Fig. 5.9. This figure is a plot of strain rate versus steady state flow stress covering seven orders of magnitude in strain rate over a 900 K temperature range.

Below the BDTT, at 500 K, there is little evidence of rate dependent deformation processes. The deformation behavior of NiAl is obviously rate dependent at high temperatures but deformation is also thermally activated above the BDTT at intermediate temperatures. Rate dependent deformation processes are usually described in terms of the Dorn equation:

$$\dot{\varepsilon} = A\, \sigma^{n} \exp^{(-Q/RT)}$$

where $\dot{\varepsilon}$ is the strain rate, σ is the steady state flow stress, Q is the activation energy for deformation, R is the universal gas constant, T is the temperature and A and n are constants. In the high temperature deformation regime, ≥ 0.45 T_m, which is considered the power law creep region for NiAl, the data (hollow symbols) fits the universal creep equation developed by Whittenberger (1987) to describe the deformation behavior of polycrystalline NiAl where:

$$\dot{\varepsilon} = 0.16\ \sigma^{5.75} \exp^{(-314.2/RT)}$$

The activation energy for deformation in the high temperature regime (314 kJ/mol) is similar to the activation energy for lattice diffusion in NiAl as expected for a diffusion controlled deformation process (Whittenberger 1987). The stress exponent of $n = 5\text{-}6$ is indicative of a dislocation climb controlled deformation process, typical of pure metals.

A best fit of all the data in the intermediate temperature regime (filled symbols) by multiple regression analysis gave an activation energy for deformation of $Q = 236$ kJ/mol and a stress exponent of $n = 16.2 \pm 1.3$. The very narrow standard deviation on the stress exponent is an indication that this is a separate, independent deformation regime and not just a transition region. If this intermediate temperature deformation regime represented a transition from glide dominated to climb dominated behavior then the stress exponents should gradually decrease with increasing temperature to a value of approximately 6. Instead, there is a constant stress exponent and activation energy extending throughout the entire intermediate temperature regime for stresses between 80 and 450 MPa.

Deformation in the intermediate temperature regime is thermally activated as the results above indicate. The lowest temperature that the BDTT occurs in NiAl is about 550 K or approximately 0.3 T_m and is still within the temperature regime for which thermally activated deformation mechanisms occur. However, instead of bulk diffusion processes controlling deformation at these lower temperatures, deformation mechanisms are dominated by short circuit diffusion processes (Brophy, Rose and Wulff 1967; Shewmon 1983). For example, climb could be restricted to grain boundary regions and yet be very influential in relieving compatibility stresses. Typical dislocation glide processes would still dominate the deformation behavior of the grain interiors until temperatures of approximately 0.5 T_m are reached. Deformation controlled by short circuit diffusion would explain the slightly lower activation energy calculated in the intermediate temperature regime while a combination of deformation mechanisms, glide within the grain interiors and climb in the vicinity of the grain boundaries, would explain the high value of the stress exponent. Evidence for the activation of localized climb processes near the grain boundaries was observed by *in-situ* TEM observations and are discussed in the following section.

5.3.6. Transmission electron microscopy observations

The most pronounced feature common to the microstructure of both alloys in this study was the presence of dislocations within the grain boundary regions as shown in Figs. 4.3 and 5.10. A high density of these trapped lattice dislocations is a common characteristic of NiAl alloys as previously noted by Hahn and Vedula (1989). These extrinsic grain boundary dislocations (EGBD's) were found to have <001> Burgers vectors although their character (edge, screw, or mixed) could not be firmly established (Bowman et al. 1992). The density of the EGBD's was directly related to the strain in the specimen but not to alloy composition. After 0.5% plastic deformation in compression at room temperature, all grain boundaries typically contained a high density of EGBD's. Similar behavior was observed at temperatures up to the BDTT. No difference in EGBD density was discernible between the binary NiAl and NiAl(Zr) alloys.

An example of these dislocations in a NiAl sample deformed at room temperature to just beyond the yield point is shown in Fig. 5.10. There are two groups of dislocations visible in the grain boundary region shown in this figure. Group "A" is oriented approximately horizontal, relative to the micrograph field of view and group "B" dislocations are oriented vertically in this figure. Using weak beam imaging techniques, it was determined that group "A" dislocations were crystallographically associated with grain #1 while group "B" dislocations were contained in grain #2.

The question arises whether the high density of dislocations within the vicinity of the grain boundaries were generated at the boundaries or were trapped in these regions. Hahn and Vedula (1989) proposed that these dislocations were generated at the grain boundaries in NiAl and were partly responsible for the room temperature ductility of NiAl. However, while these EGBD's were observed in both the NiAl and NiAl(Zr) alloys of all grain sizes, measurable tensile ductility was only observed in the finer grain size binary NiAl samples. Therefore, no correlation can be made between the presence of EGBD's and tensile ductility in NiAl alloys. Furthermore, a dislocation generated from a grain boundary is expected to appear as a loop with both ends connected to the grain boundary. This type of observation is very rare in polycrystalline NiAl alloys (Noebe et al. 1990). In contrast, a trapped dislocation will generally have one end arriving at the boundary while the remaining segment remains in the matrix until it is fully consumed by the grain surface. Continued motion of the dislocation will result in the eventual absorption of the entire dislocation line. TEM observations utilizing stereo-imaging clearly showed that these <001> dislocations were being absorbed into the boundaries with no evidence of dislocations looping from the boundaries (Bowman et al. 1992). In Fig. 5.10 a slip band intersecting a grain boundary region is observed. The dislocation spacing in the band decreased as the dislocations approached the boundary implying that they are gliding toward the grain boundary which acts as a barrier to further motion. These dislocations eventually enter the boundary and are trapped. Partially absorbed dislocations from the slip band in grain #1 assumed a horizontal orientation (group "A") upon entering the grain boundary region. This is consistent with the weak beam TEM results (Bowman et al. 1992), that showed that group "A" dislocations had an <001> Burgers vector and were associated with grain #1.

The EGBD's are not responsible for enhancing low temperature ductility of the material because they generally do not act as sources for further dislocation generation. Furthermore, these dislocations do not seem to undergo any type of slip transfer process from one grain to the neighboring grain. Instead, they just accumulate at the grain boundary region as deformation proceeds. However, these <001> EGBD's and all further dislocations trapped at the grain boundaries could be a dominant factor during the deformation of NiAl above the BDTT. At higher temperatures the EGBD's could move by non-conservative motion along the grain surfaces permitting a grain boundary sliding accommodation mechanism of strains in the material.

To further explore this hypothesis, *in-situ* TEM observations were made of the general mobility of the EGBD's versus typical lattice dislocations at various temperatures. It was observed that both alloys exhibited a very sharp transition in EGBD mobility as a function of temperature. After annealing the binary NiAl samples for 120 seconds at 500 K, only 50 K below the BDTT, no significant decrease in EGBD density or lattice dislocation density was observed, Fig. 5.11a, implying that diffusive mechanisms such as dislocation climb were not active at this temperature. In fact, samples were held at 500 K for over an hour without any measurable changes in dislocation density or structure. Conversely, annealing at 600 K, Fig. 5.11b, for 120 seconds resulted in the elimination of all EGBD's by climb out of the foil. At this temperature no evidence of dislocation motion (climb) was noted away from the grain boundary regions. In fact, no dislocation activity was observed in the grain interiors for temperatures below 1000 K. Above 1000 K, dislocation activity was observed in the grain interiors as dislocations quickly climbed out of the foils.

These results are consistent with the mechanical property data already described. For example, there is a sharp change in the mobility of EGBD's corresponding exactly to the BDTT in binary NiAl and the change in deformation from low to intermediate temperature behavior as observed in Figs. 5.8 and 5.9. Furthermore, the observation of bulk climb processes that become active in NiAl at temperatures near 1000 K also corresponds to the change from intermediate to high temperature behavior indicated in Figs. 5.8 and 5.9.

5.3.7. Summary of deformation mechanisms in polycrystalline binary NiAl and the mechanism responsible for the BDTT.

While limited tensile ductility is observed at room temperature this should not be construed as the BDTT for NiAl. Plastic flow at low temperatures, below the BDTT, occurs by glide of <001> dislocations and is accompanied by crack formation at the grain boundaries due to non-accommodation of the resulting shear and normal strains (and was discussed in detail in Chapter IV). Instead, the BDTT has been defined as the point where a large change in tensile ductility occurs over a small temperature range, which for binary NiAl is on the order of 550 - 600 K (Fig. 5.3). However, the BDTT represents much more than just an increase in tensile ductility. The BDTT corresponds to a concurrent increase in fracture strength (Fig. 5.1) and fracture toughness (Fig. 5.2). This is due to the activation of additional deformation mechanisms, permitting the accommodation of strains at the grain boundaries, thus, preventing the formation of grain boundary microcracks (Fig. 5.5). The accommodation of strains at the grain boundaries occurs at the BDTT due to a change in the overall deformation characteristics of the alloy, as demonstrated in both Figs. 5.8 and 5.9. Therefore, while the majority of the deformation may be carried by dislocation glide processes within the grain interiors, the data indicate that deformation behavior just above the BDTT is controlled by a thermally activated process resulting from short circuit diffusion. This is consistent with the activation of localized dislocation climb processes occurring in the vicinity of the grain boundaries at temperatures corresponding to the BDTT.

Therefore, the proposed mechanism for the BDTT in NiAl involves the onset of significant localized dislocation climb processes in the vicinity of the grain boundaries. The importance of dislocation climb occurring in NiAl has been demonstrated by Groves and Kelly (1969), who have determined that the combination of both glide and climb of dislocations with <001> Burgers vectors will result in five independent deformation mechanisms. This condition would then satisfy the Von Mises criterion for extensive plasticity in a polycrystalline material, congruous with the behavior of NiAl above the BDTT. Thus, at intermediate temperatures NiAl deforms by a combination of glide and localized climb processes, resulting in an intermediate temperature, rate limited deformation regime shown as region II in Fig. 5.8 and as the region between 550 and 1000 K in Fig. 5.9. It is the onset of this intermediate temperature deformation regime that is responsible for the BDTT in NiAl.

In a similar vain, Ball and Smallman (1966a) correlated the beginning of ductile behavior in NiAl with the annealing behavior of dislocation loops and concluded that the BDTT corresponded to the temperature that self diffusion became significant, i.e. temperatures greater than approximately 0.45 T_m or 900 K. This coincides with region III in Fig. 5.8 where deformation is controlled by bulk dislocation climb processes. Therefore, Ball and Smallman were right in concluding that the BDTT in NiAl was due to dislocation climb processes. However, they overestimated the BDTT, which for binary NiAl, is near 0.3 T_m. Instead, a well defined intermediate temperature deformation regime controlled by short circuit diffusion processes is responsible for a lower BDTT than predicted by Ball and Smallman (1966a,b).

In complete contrast, Lloyd and Loretto (1971), Miracle (1991), and Dollar et al. (1993) have proposed that operation of an alternate slip system is responsible for the BDTT in NiAl. Amazingly, all three groups propose that <110> slip is the alternate mechanism but provide no substantial evidence for their claims. Lloyd and Loretto (1971) and Dollar et al. (1993) observed occasional <110> dislocation segments in as-extruded NiAl. However, in neither case was <110> slip demonstrated to operate in monotonically deformed samples. In the final study by Miracle (1991), <110> slip was observed in [001] oriented halves of deformed bicrystals. But, in any bicrystal orientation other than [001], only <001> slip was observed (Miracle 1990,1991). These studies actually demonstrate that slip by anything other than <001> dislocations is extremely unlikely in NiAl, consistent with the myriad of other deformation studies performed over the years. Still, the operation of an alternate slip system should be considered further since it is still proposed at times as a possible mechanism for the BDTT in NiAl (Miracle 1993; Dollar et al. 1993).

It would seem to make more sense to propose <111> as the alternate slip system responsible for the ductile-to-brittle transition in NiAl. After all, this is a common slip vector in bcc metals and other B2 alloys and also provides 5 independent deformation mechanisms. But, this is not the case. Instead, <110> slip has been proposed as the alternate deformation mechanism responsible for the BDTT (Lloyd and Loretto 1971; Miracle 1991; Dollar et al. 1993). Yet, <011>{100} slip provides only three independent deformation mechanisms and these are not independent of <100> slip on either {110} or {100} (Cotton, Noebe and Kaufman 1991). For example, <011>{100} plus slip by <100>{110} would only provide three independent slip systems so that NiAl would still be slip system limited. <011>{110} slip provides only two independent slip systems but these are independent of <100>{011} slip. Therefore, in every grain both <011>{110} and <100>{110} slip would have to be active to provide for grain boundary compatibility. If this were the mechanism responsible for the BDTT then one would expect to see evidence of <110> slip in deformed samples. However, <110> slip or for that matter <111> slip have not been reported as dominant slip vectors in any previous polycrystalline studies. In a companion investigation to this work, exhaustive dislocation analysis of samples deformed between 300 - 900 K, often including every dislocation in a field of view, was performed (Bowman et al. 1992). This work revealed the presence of only <001>{110} dislocations. TEM observations cannot rule out the possibility that a small number of <111> or <110> dislocations were present. However, if activation of <110>{110} slip was responsible for the BDTT in NiAl it would have to occur in every grain and would be expected to appear in the post-deformed microstructure. Instead, only <001> dislocations are generally observed in uniaxially deformed samples.

Margevicius and Cotton (1994) also have confirmed a glide plus climb mechanism for the BDTT in NiAl through a texture evolution study that complements the work in this investigation. Their results indicated that axial compression of NiAl, irrespective of the initial texture and deformation temperature, produced no change in texture. Only glide and/or climb of <100> dislocations can produce deformation in NiAl without causing grain rotations that leads to a change in texture. Activation of any secondary slip systems would cause some textural evolution. Thus, they concluded that alternate slip systems do not contribute to the deformation of polycrystalline NiAl on a macroscopic scale. Consequently, after all the testing and analyses presented in this investigation with corroborating analyses by Bowman et al. (1992) and Margevicius and Cotton (1994), it is finally possible to state in indisputable terms that the BDTT in NiAl is due to the onset of <001> climb acting in conjunction with <001> slip and not the result of a change in the slip vector.

Finally, there is a distinct high temperature deformation regime in NiAl. This deformation regime occurs at temperatures above about 1000 K as demonstrated in Figs. 5.8 and 5.9. In this region, the activation energy for deformation is similar to the activation energy for bulk lattice diffusion in NiAl with deformation controlled by dislocation climb processes (Whittenberger 1987). The deformation characteristics of NiAl in this temperature regime have been thoroughly studied and reviewed (Whittenberger 1987,1988; Nathal 1992). It was not the intent of this study to investigate the high temperature deformation regime further other than to determine its significance to the BDTT in NiAl. The BDTT in NiAl occurs at temperatures significantly below the high temperature creep deformation regime, suggesting that the BDTT is not due to bulk climb processes but is due to localized climb behavior.

5.3.8. Effect of Zr on the BDTT of NiAl

Finally, the effect of microalloying additions on the BDTT of NiAl can be resolved. The BDTT for the NiAl(Zr) alloy is approximately 300 K higher in temperature than for binary NiAl, as indicated in Fig. 5.3. This is a rather dramatic effect considering that only

500 ppm Zr was added to NiAl. However, Zr segregates to the grain boundaries in this material at total levels of 4 - 8 at.% (Zeller, Noebe and Locci 1990). It will be demonstrated that this segregation of Zr to the grain boundaries is a critical factor controlling the BDTT in the Zr-doped alloy.

From Fig. 5.6 it is apparent that the NiAl(Zr) alloy has a higher yield strength than the undoped material. However, the real effect of Zr on flow behavior is apparent when the yield strength data is plotted in an Arrhenius form, as in Fig. 5.12. The presence of Zr at the grain boundaries causes the onset of region II deformation, that is responsible for the BDTT, to be shifted to higher temperatures. The onset of localized climb in the alloy indicated by the beginning of region II in Fig. 5.12, then corresponds to the BDTT in the alloy as defined by tensile ductility. Only, the BDTT is shifted to a much higher temperature than for binary NiAl.

Therefore, the presence of Zr at the grain boundaries must have a pinning effect on the EGBD's, preventing them from moving until much higher temperatures are reached. At a higher temperature there is then enough thermal activation to overcome the pinning effect of the Zr and these dislocations are free to climb away resulting in compatible deformation at the grain boundaries, heralding the advent of the BDTT. Further evidence for this scenario was again provided by the *in-situ* annealing experiments. For the Zr-doped material, the density of EGBD's remained unchanged after annealing at 700 K for up to an hour, Fig. 5.13. This is in contrast to binary NiAl where all EGBD's were annealed out of the foil in less than 120 sec. at 600 K. The EGBD's in the Zr-doped material were immobile until temperatures greater than 900 K were reached. This corresponds to the BDTT of 850 - 875 K for the NiAl(Zr) alloy.

I have observed a similar behavior in NiAl(Re) alloys. Similar to Zr, Re is a very large atom and would also be expected to segregate to the grain boundaries, though this has not been verified by Auger analysis. However, just as in the case of Zr, Re shifts the onset of region II deformation to much higher temperatures and correspondingly, the

BDTT is shifted to higher temperatures as demonstrated in Fig. 5.14.

Consequently, a short circuit diffusion assisted climb process is equally responsible for the BDTT in binary NiAl and ternary NiAl alloys. The only difference is that the BDTT can be shifted to increasingly higher temperatures due to the effect of minor alloying additions. This is especially true when the ternary alloying additions strongly segregate to the grain boundaries and are effective in preventing these localized climb processes. Consequently, the behavior of ternary NiAl alloys such as NiAl(Zr) and NiAl(Re) are compatible with the mechanism proposed in this report for the brittle-to-ductile transition in NiAl.

5.4. Summary and Conclusions

1. NiAl and NiAl(Zr) alloys have limited ductility below their BDTT due to an insufficient number of independent deformation mechanisms, resulting in the formation of grain boundary cracks during deformation.

2. With increasing temperature:

    - Yield stress decreases at a moderate rate.

    - Fracture stress (and toughness) remain essentially constant and then dramatically increase over a narrow temperature regime.

    - Tensile ductility remains low and then increases over the same temperature range as the fracture stress.

3. The temperature that the sudden increase in tensile ductility, fracture strength and fracture toughness occurs can be used to define the BDTT in NiAl alloys. For binary NiAl the BDTT is around 550 - 600 K. For NiAl(0.05Zr) the BDTT is approximately 850 - 875 K.

4. The transition from brittle to ductile behavior for each material was found to be associated with a change in deformation behavior. Therefore, the BDTT can also be defined by a change in deformation mode as manifested in an Arrhenius plot of yield

strength.

5. The brittle-to-ductile transition occurs at intermediate temperatures in NiAl due to the onset of localized <001> dislocation climb processes resulting in the availability of additional deformation modes, which in conjunction with <001> glide within the grain interiors allow the Von Mises criterion to be fulfilled.

6. Alloying additions that retard localized climb processes (e.g. Zr) will cause a significant increase in the BDTT for NiAl. These alloying additions do not have to be present in very large levels to have a significant effect on the BDTT if they have a strong tendency to segregate to the grain boundaries.

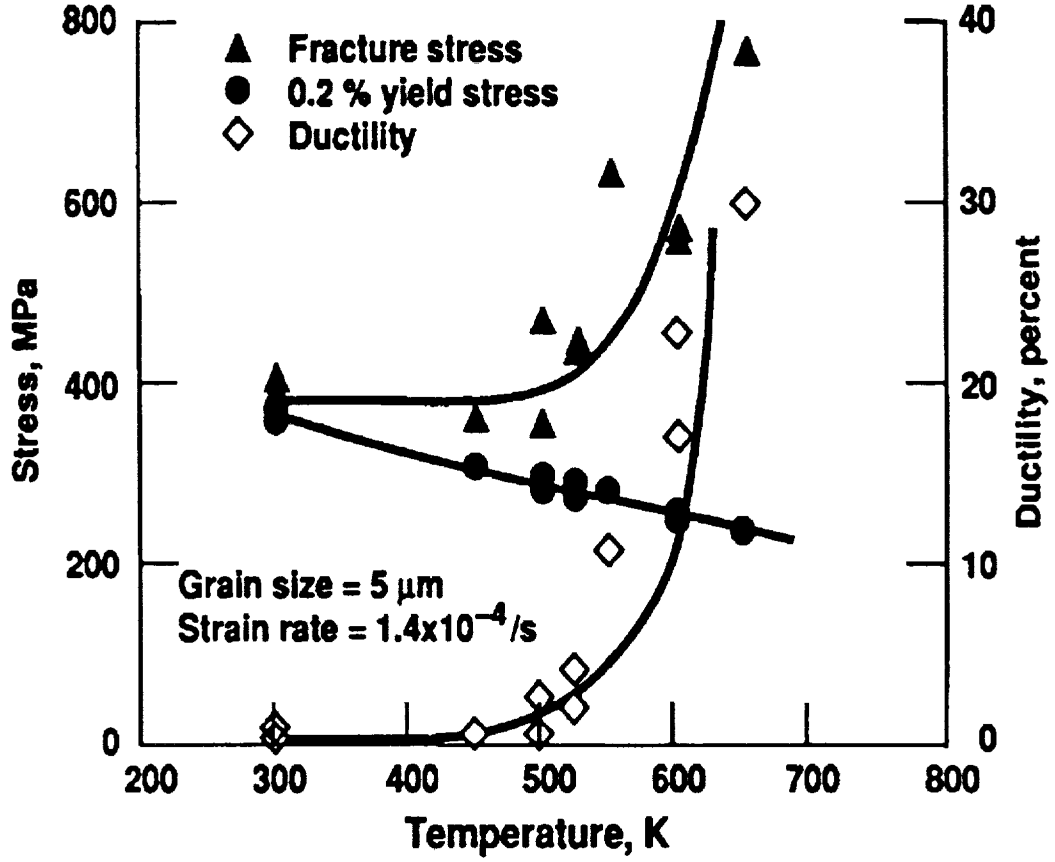

Fig. 5.1. The effect of temperature on the tensile properties (yield stress, fracture stress and tensile elongation) of powder (Heat P541) extruded NiAl. The BDTT is approximately 550 K.

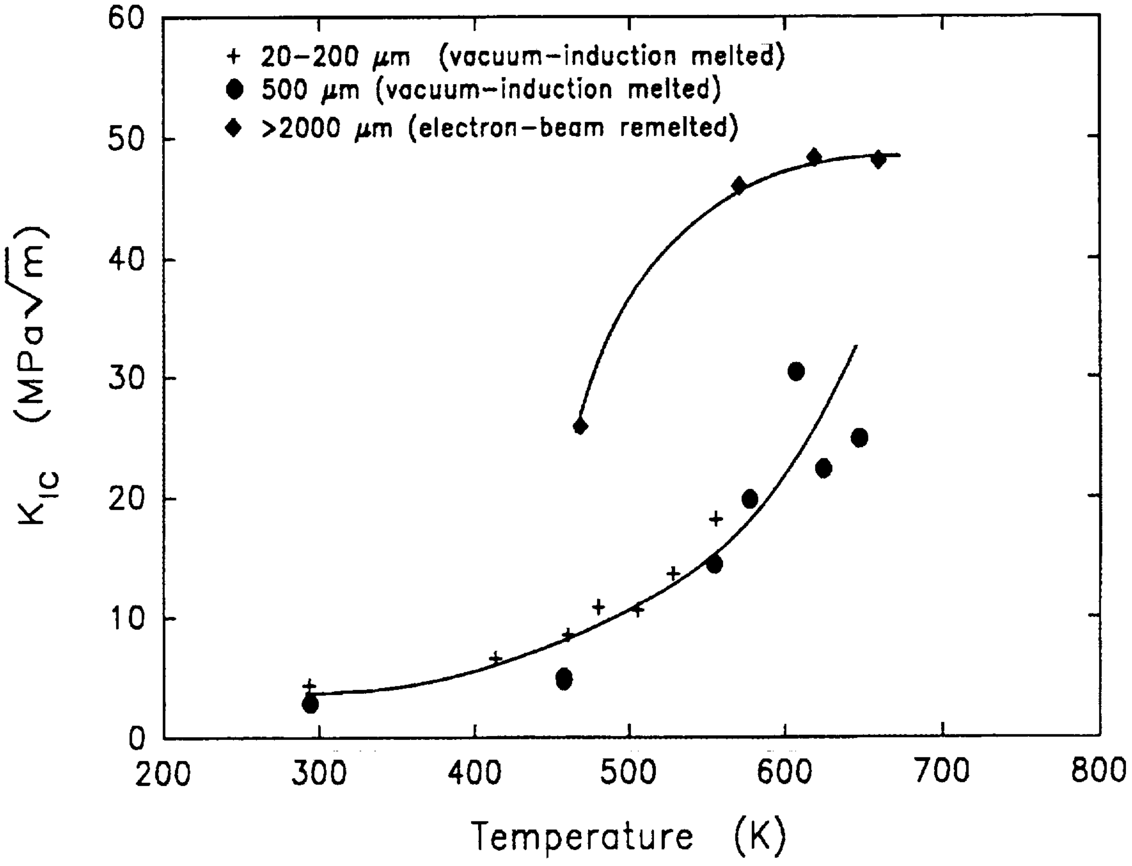

Fig. 5.2. Fracture toughness of binary near stoichiometric NiAl alloys as a function of temperature. Alloys were produced by several different techniques resulting in material with a range of grain sizes.
(Data from Reuss and Vehoff 1990.)

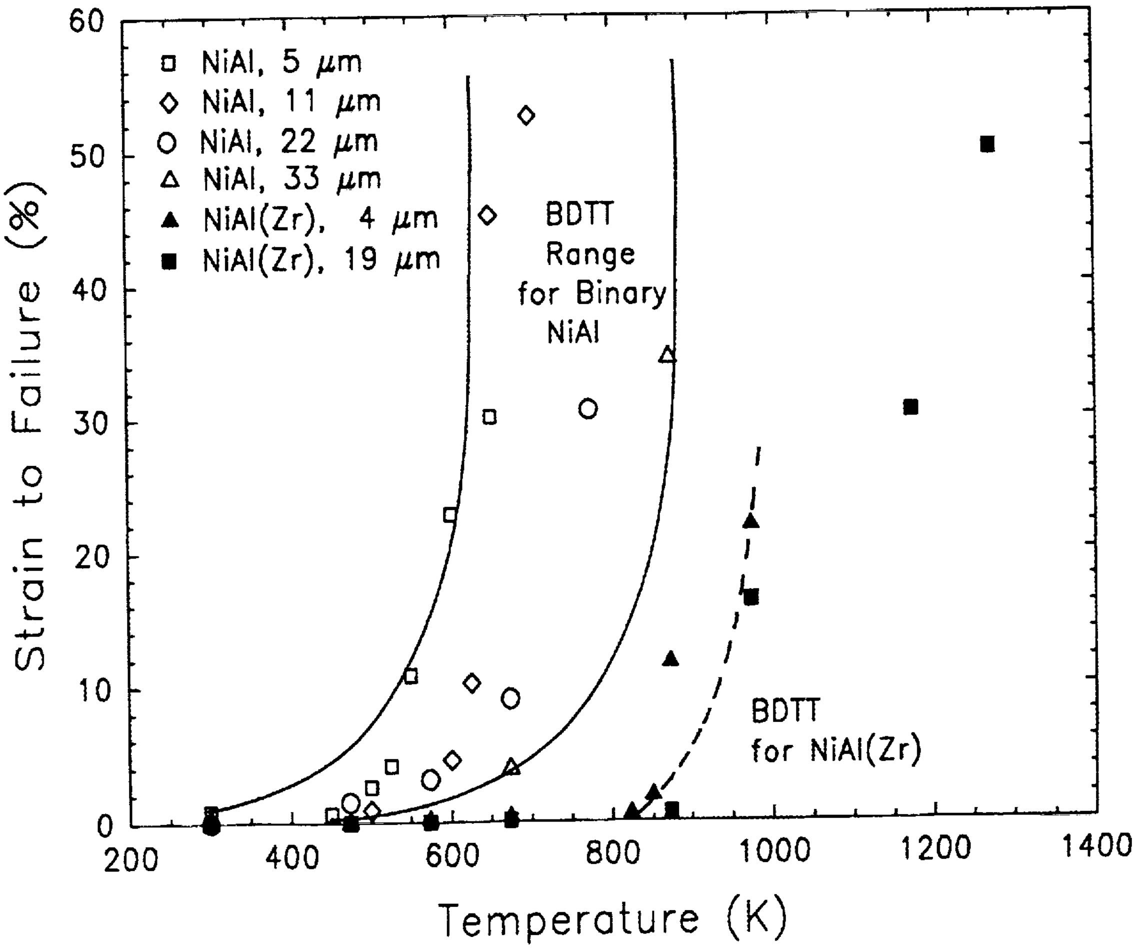

Fig. 5.3. Tensile strain to failure for powder extruded NiAl and NiAl(Zr) alloys of various grain sizes.

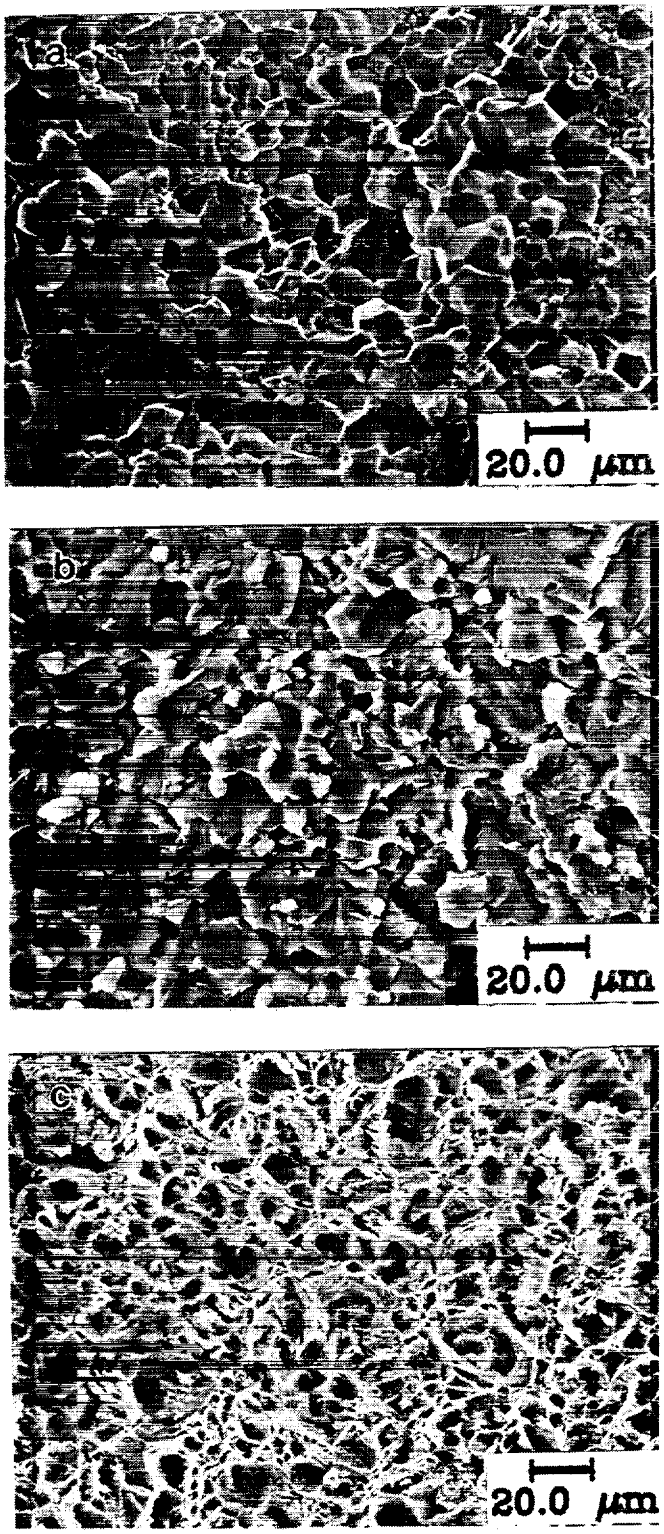
a
20.0 μm
b
20.0 μm
c
20.0 μm

Fig. 5.4. SEM micrographs of binary NiAl tensile fracture surfaces at temperatures above and below the BDTT (BDTT = 550-600 K). a) 300 K, $\varepsilon_f = 0.0\%$*, b) 673 K,* $\varepsilon_f = 9.0\%$*, and c) 873 K,* $\varepsilon_f = >30\%$*.*

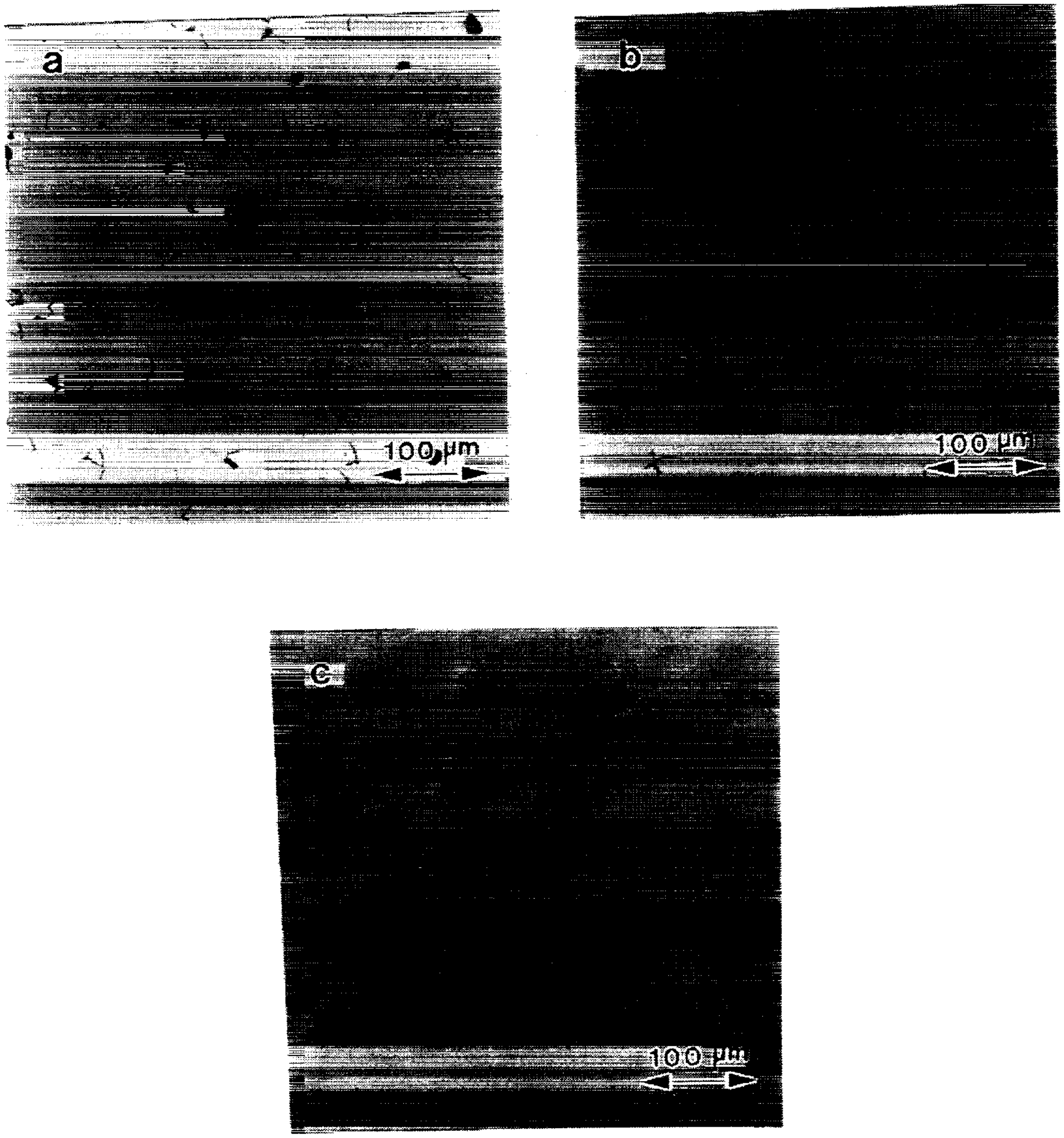
a
100 µm
b
100 µm
c
100 µm

Fig. 5.5. Longitudinal cross-sections of polycrystalline NiAl compression samples deformed to approximately 10% strain at temperatures of: a) 300 K, b) 500 K, and c) 600 K.

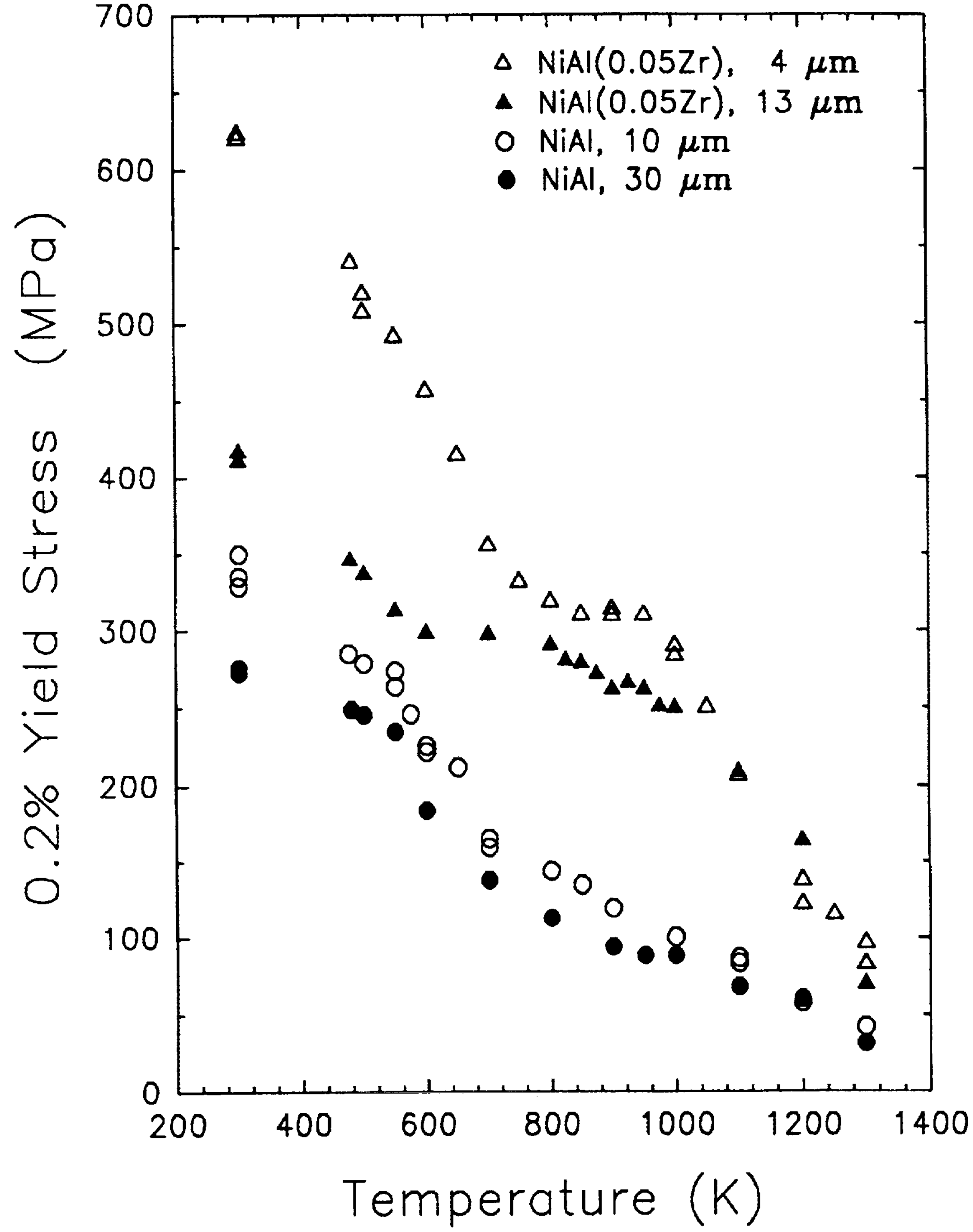

Fig. 5.6. The compressive 0.2% offset yield stress for binary NiAl and NiAl(Zr) as a function of temperature tested at a strain rate of 1.4x10^{-4} s^{-1}.

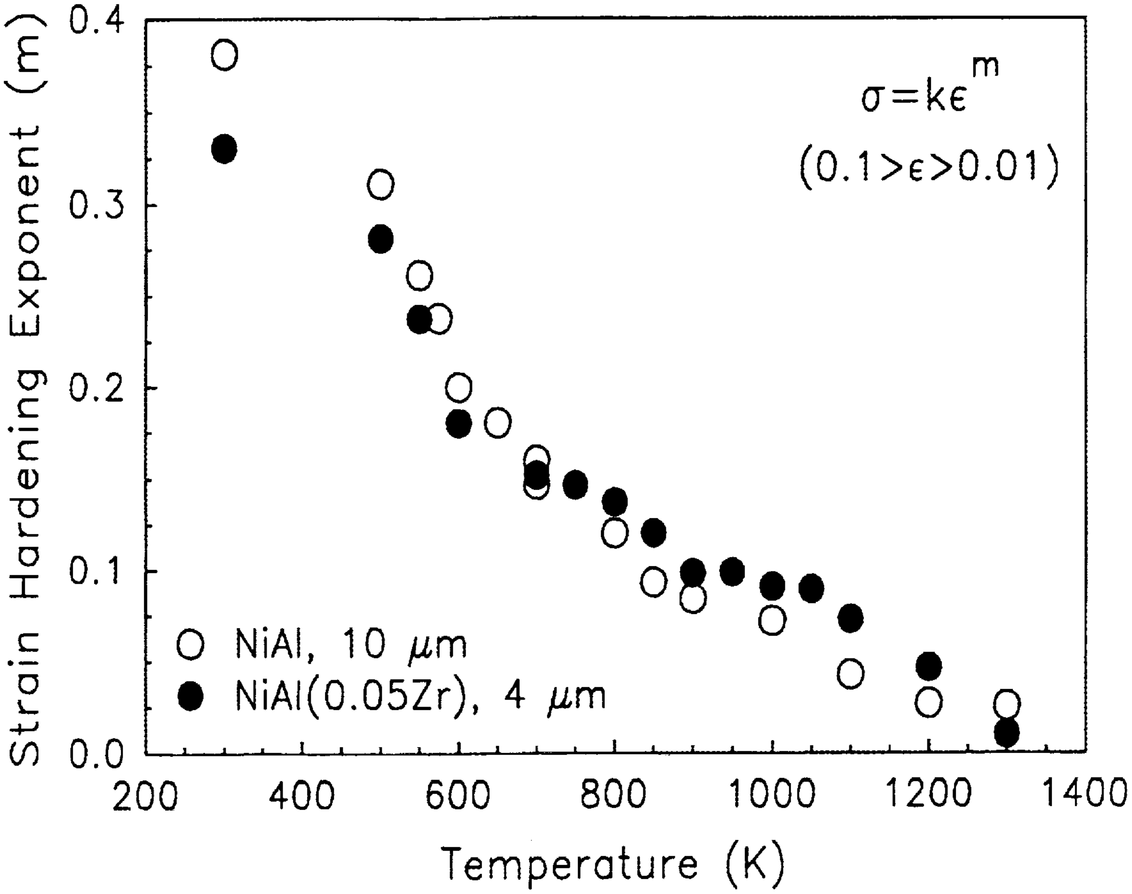

Fig. 5.7. Strain hardening exponent, m, for fine grained NiAl and NiAl(Zr) alloys as a function of temperature determined in compression at a strain rate of $1.4x10^{-4}$ s^{-1}.

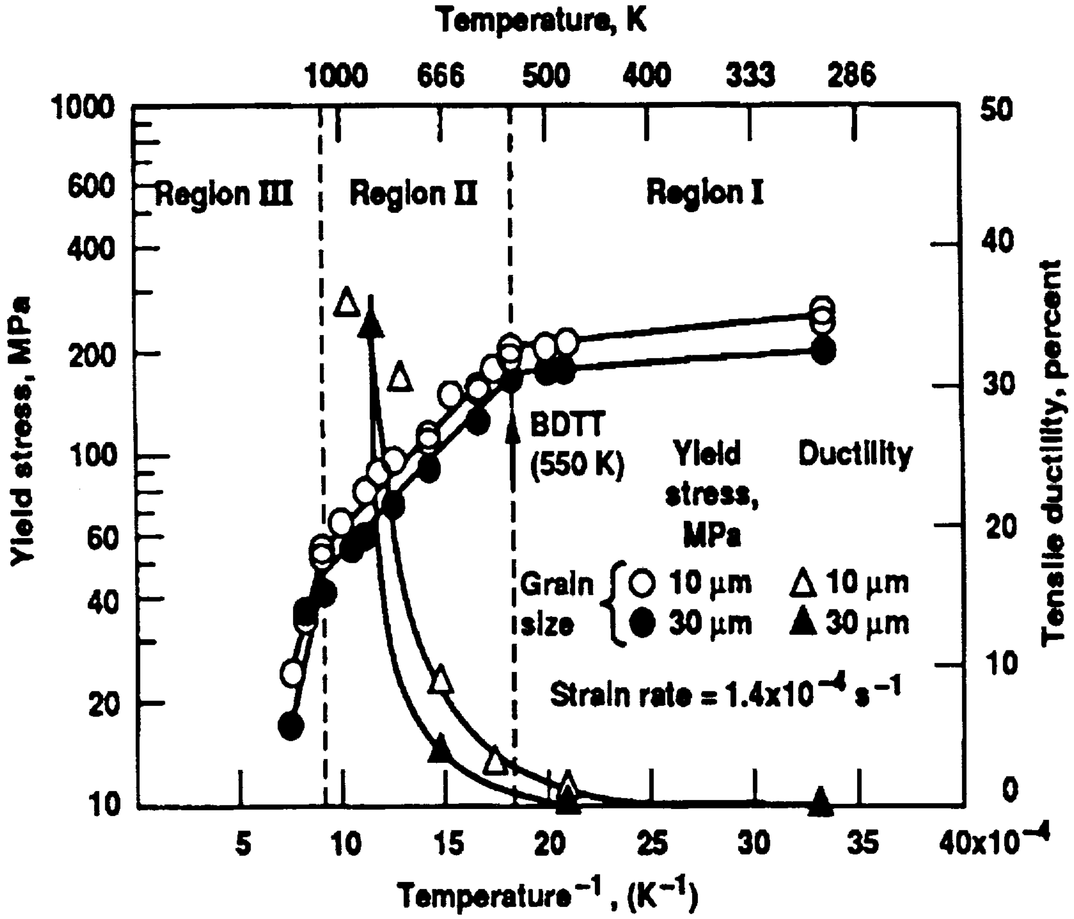

Fig. 5.8. Arrhenius representation of the yield stress for polycrystalline NiAl P541 and tensile ductility as a function of inverse temperature. The BDTT corresponds to a change in activation energy for plastic flow beginning at Region II.

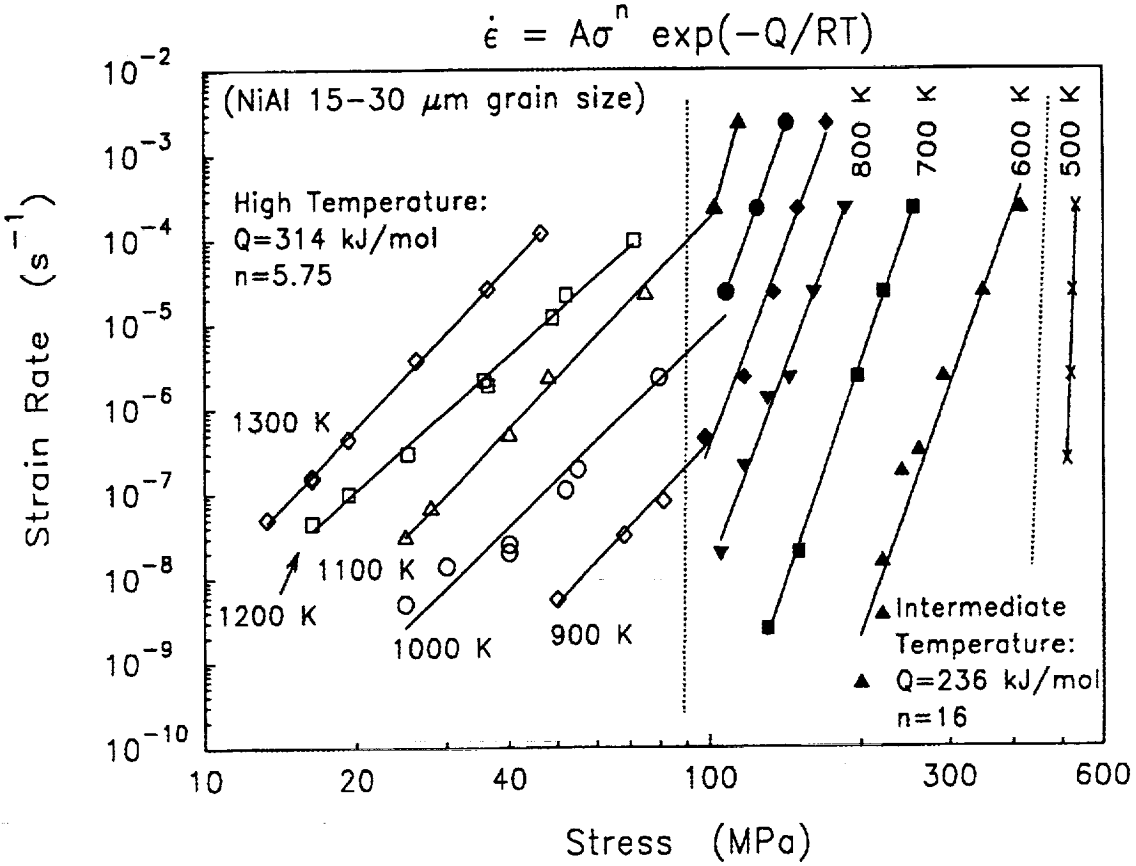

Fig. 5.9. The steady state flow stress for NiAl P541 as a function of strain rate and temperature. The low temperature deformation regime is represented by "x", the intermediate temperature deformation regime corresponds to the filled symbols and the high temperature deformation regime corresponds to the open symbols.

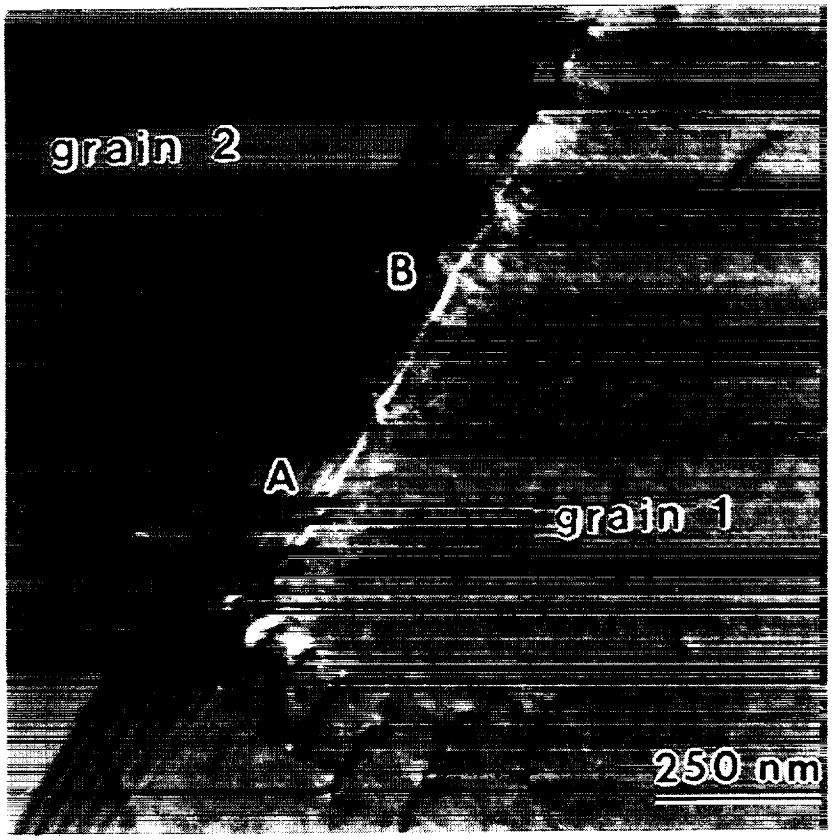

Fig. 5.10. Grain boundary trapping of dislocations from an intersecting slip band. Dislocations of type A originated from grain 1 and dislocations of type B originated from grain 2. All dislocations are <001> type.

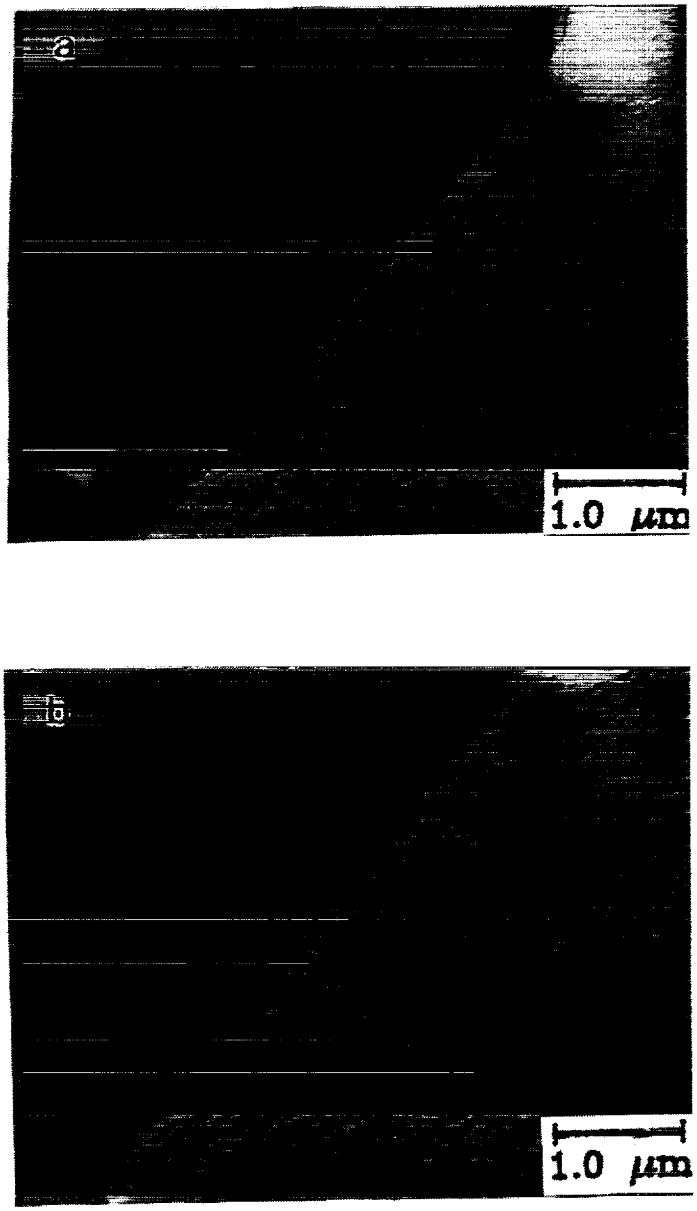

Fig. 5.11. Mobility of EGBD's in binary NiAl as determined from in situ annealing experiments. a) Grain boundary in NiAl (BDTT = 550 K) after annealing at 500 K for 120 s and b) same boundary after heating at 600 K for 120 s.

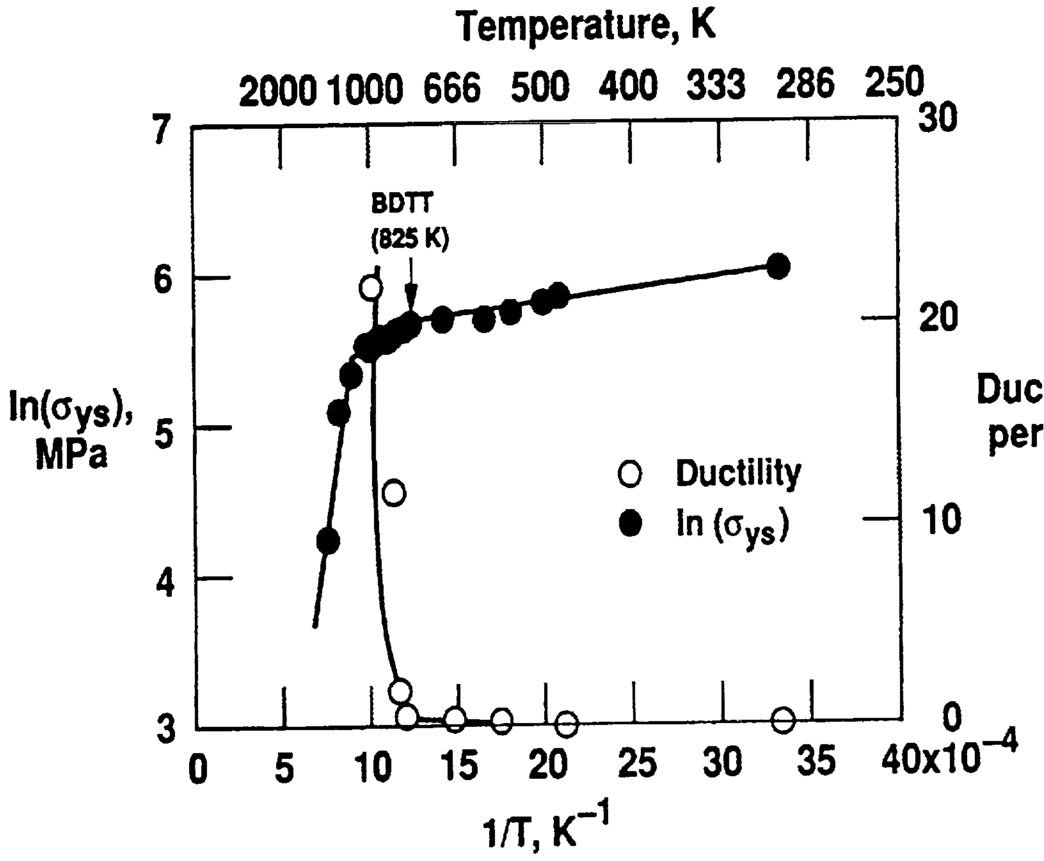

Fig. 5.12. Arrhenius representation of the yield stress for NiAl(0.05Zr) and the corresponding tensile ductility as a function of inverse temperature. The BDTT has been shifted to a higher temperature corresponding to the change in deformation from low to intermediate temperature behavior. Grain size 19 - 23 μm.

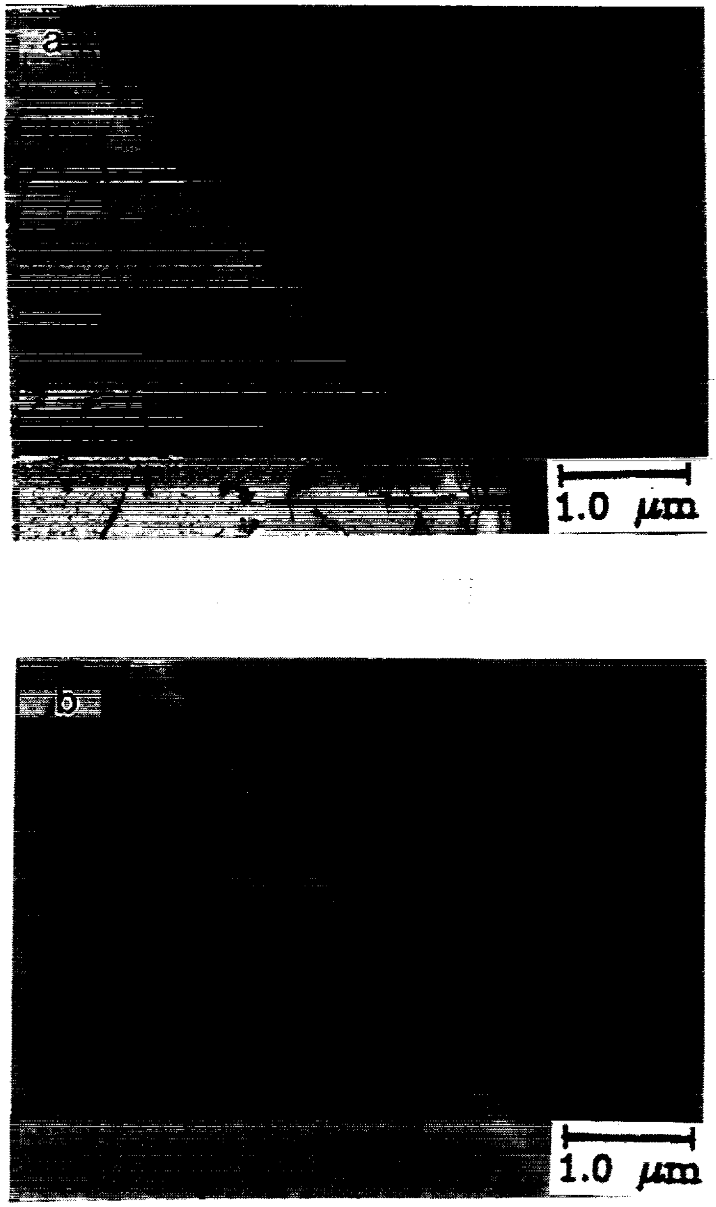

Fig. 5.13. Mobility of EGBD's in binary NiAl(0.05Zr) as determined from in situ annealing experiments. a) Grain boundary in NiAl(0.05Zr) (BDTT = 850 K) after annealing at 700 K for 120 s and b) same boundary after heating at 1000 K for 120 s.

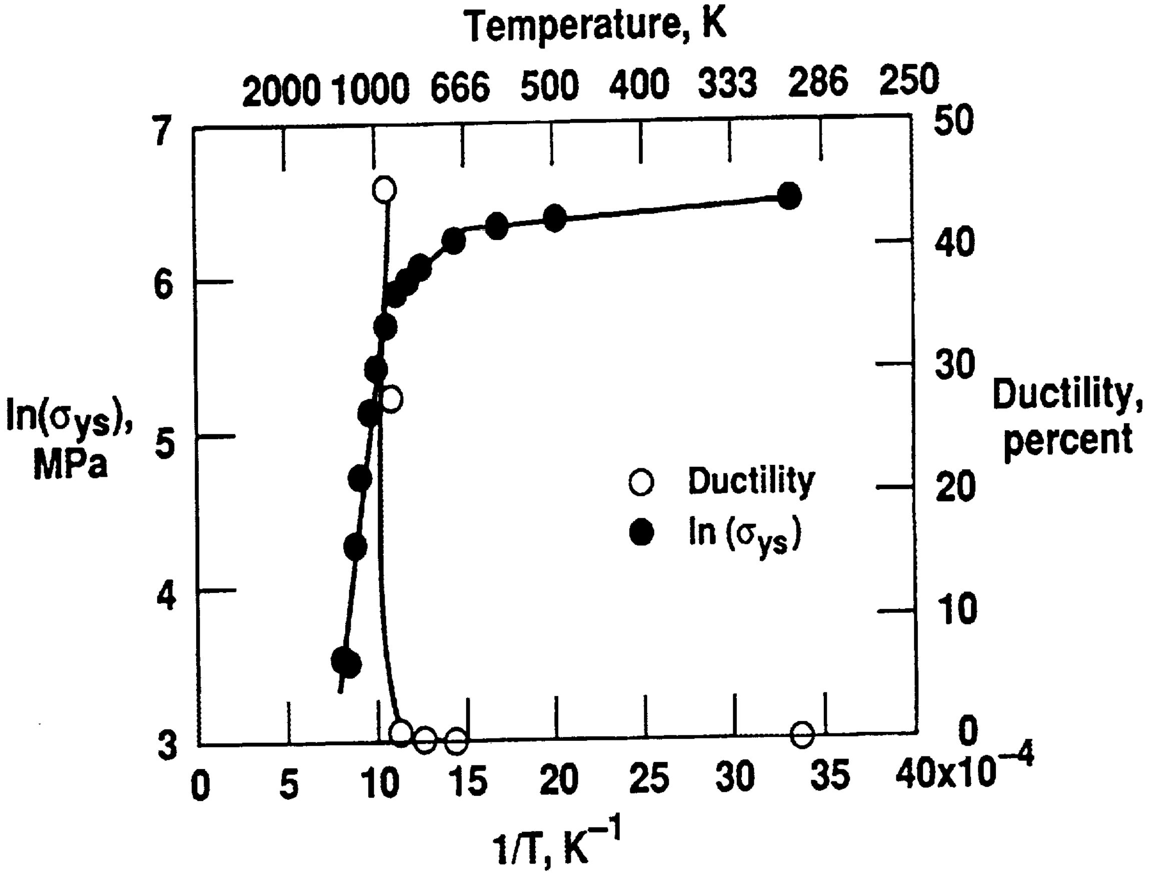

Fig. 5.14. Arrhenius representation of the yield stress for NiAl-3Re and the corresponding tensile ductility as a function of inverse temperature. The BDTT has been shifted to a higher temperature corresponding to the change in deformation from low to intermediate temperature behavior. Grain size 1 - 3 μm.

CHAPTER VI
THE EFFECT OF STRAIN RATE ON THE TENSILE PROPERTIES AND BRITTLE-TO-DUCTILE TRANSITION TEMPERATURE OF NiAl

6.1. Introduction

It was demonstrated in the previous chapter that the BDTT in NiAl occurred as a result of the operation of additional deformation mechanisms, specifically dislocation climb. However, dislocation climb is a thermally activated, rate dependent process. This raises an interesting and potentially troublesome problem. If the BDTT is the consequence of a rate dependent deformation process then the BDTT itself should be rate dependent. However, previous tensile testing of polycrystalline NiAl at intermediate temperatures has been conducted primarily over a very narrow range of strain rates, generally 10^{-4} to 10^{-3} s^{-1} (Rozner and Wasilewski 1966; Law and Blackburn 1987; Hahn and Vedula 1989; Mason et al. 1991; Schulson 1985). Over this range of strain rates, the BDTT for near stoichiometric, binary NiAl has been reported between 550 and approximately 700 K, consistent with the results obtained in the previous chapter.

The one anomaly to the typical BDTT range observed for binary NiAl was reported by Grala (1960) who determined the BDTT for cast NiAl to be almost 1000 K. However, tests by Grala were performed under constant loading rate conditions as opposed to an initially constant strain rate (constant crosshead velocity), as in the other studies mentioned above. The problem with a constant loading rate experiment is that with increasing test temperature, a sharp decrease in work hardening rate occurs, as was demonstrated in Fig. 5.7. Therefore, the effective strain rate on the NiAl samples tested by Grala would have been higher at elevated temperatures as the loading rate was held constant. The higher BDTT reported by Grala (1960) could then be a consequence of the faster strain rates that resulted during that study. Obviously, composition and microstructure (porosity) also could have played a role in the higher BDTT.

Consequently, the purpose of the experiments presented in this chapter was to ascertain the effect of strain rate on the BDTT of NiAl. This was accomplished by determining the tensile properties of binary NiAl as a function of temperature and strain rate at rates typically greater than those used in Chapter V or previously reported in the literature. In addition to providing a possible explanation for the high BDTT determined by Grala (1960), the effect of strain rate on the BDTT was established providing additional confirmation of a BDTT due to a rate dependent deformation mechanism. Finally, these experiments will serve as an initial indication of whether high loading rates or impact damage can be tolerated at temperatures that are normally thought to be above the BDTT for NiAl.

6.2. Materials and Experimental Procedures

A 38 mm diameter, vacuum-induction melted ingot of nominally stoichiometric NiAl was canned in mild steel. The ingot was extruded at 1400 K to an area reduction ratio of 16:1. Post-extrusion chemical analysis for this material is listed in Appendix A under alloy L2559. The Al and Ni percentages were determined by wet chemical techniques on triplicate samples and have an absolute error of ± 0.2 at.%. The chemical analysis indicated that within experimental accuracy the extrusion rod was stoichiometric in composition.

The microstructure of the as-extruded NiAl consisted of recrystallized and equiaxed grains with an average linear intercept grain size of 29 ± 3 μm. Round button-head tensile specimens were ground from the rod such that the gauge lengths were parallel to the extrusion direction. Typical gauge lengths were 30.5 mm and gauge diameters were 3.2 mm, see Fig. 4.5. Prior to testing, all samples were electropolished in a solution of 10% perchloric acid - 90% methanol. Tensile tests were performed to fracture in an

Instron screw-driven load frame at constant crosshead velocities corresponding to initial strain rates of 1.4×10^{-4} to 1.4×10^{-1} s^{-1} and at temperatures between 300 and 900 K. True stress-plastic strain data were calculated from the load-time plots by subtracting the elastic strain and assuming constant volume conditions. True plastic strain at failure was obtained from reduction-of-area measurements when necking was significant. Yield stress was determined by the 0.2% offset method. Post-test analyses of the tensile fracture surfaces were performed using a Cambridge 200 scanning electron microscope (SEM).

6. 3 Results

Figure 6.1 demonstrates the effect of test temperature on the tensile properties of the cast and extruded NiAl at an initial strain rate of 1.4×10^{-4} s^{-1}. The response of the cast and extruded NiAl alloy shown in Fig. 6.1 is essentially identical to the behavior of the powder extruded NiAl shown in Fig. 5.1. The cast and extruded material tested at room temperature at a rate of 1.4×10^{-4} s^{-1} exhibited an average tensile elongation of 0.7%. Tensile ductility remained constant up to a temperature of 525 K and then increased significantly with additional increases in temperature. From this data a BDTT of approximately 550 K was determined for the cast and extruded material at a strain rate of 1.4×10^{-4} s^{-1}. This temperature is consistent with the BDTT established in the previous chapter for powder extruded NiAl under similar test conditions.

The average room temperature yield strength of the cast and extruded NiAl was 212 MPa. From this level the yield stress gradually decreased with increasing test temperature (Fig. 6.1). The temperature dependence of the fracture strength had a similar form as tensile ductility versus temperature. The fracture strength decreased slightly with increasing test temperature up to 525 K and then increased dramatically above the BDTT. Recent work by Reuss and Vehoff (1990a,b) has shown that the fracture toughness for NiAl also increases with temperature in a manner similar to the fracture stress. A compilation of Reuss and Vehoff's data was presented in Fig. 5.2. The linear correlation between fracture toughness and tensile fracture strength for a constant flaw size would suggest this analogous temperature dependence.

The effect of strain rate on the tensile ductility of NiAl is illustrated in Fig. 6.2. This figure is a plot of tensile ductility (plastic strain to failure) versus temperature at strain rates of $1.4\text{x}10^{-4}$, $1.4\text{x}10^{-2}$ and $1.4\text{x}10^{-1}$ s^{-1}. The tensile ductility versus temperature relationship at the higher testing rates resembles the data at a strain rate of $1.4\text{x}10^{-4}$ s^{-1}, except that the ductility versus temperature curves are displaced to higher temperatures as the strain rate is increased. Consequently, the BDTT for NiAl is increased by about 200 K because of the three orders of magnitude increase in strain rate.

Changes in strain rate also affected the yield and fracture strengths of the as-extruded NiAl, however, the shapes of the yield and fracture strengths versus temperature curves did not change (Fig. 6.3). As with tensile ductility, the strength versus temperature relationships for NiAl shifted to higher temperatures as the strain rate was increased. The yield strength at all three strain rates slowly decreased as the temperature increased. Likewise, the fracture stresses remained constant or decreased slightly over a short temperature range and then increased dramatically at a temperature corresponding to the brittle-to-ductile transition for that testing rate, Fig. 6.3. Therefore, the effect of an increasing strain rate was to shift these strength versus temperature curves and the transition from brittle to ductile behavior to proportionally higher temperatures thereby increasing the BDTT for NiAl.

Besides changes in ductility and fracture strength at the brittle-to-ductile transition temperature, a significant change in fracture morphology was observed just above the BDTT. For example, at a strain rate of $1.4\text{x}10^{-4}$ s^{-1}, the fracture behavior of NiAl was predominantly intergranular for all temperatures below 550 K (Fig. 6.4a). In all cases, no obvious fracture initiation sites were observed. Above 550 K, the fracture morphology began to change to a combination of intergranular separation and transgranular cleavage with the percentage of transgranular fracture increasing with temperature. By 650 K, the fracture behavior was predominantly transgranular in nature (Fig. 6.4b). Again, no obvious initiation sites for failure were observed.

At the fastest testing rate of 1.4×10^{-1} s^{-1}, limited tensile ductility and predominantly intergranular failure were observed as high as 800 K (Fig. 6.4c). Above the BDTT at this strain rate, transgranular-cleavage fracture comprised a greater area of the fracture surface and by 850 K, the fracture morphology had changed to predominantly transgranular (Fig. 6.4d). Therefore, regardless of the strain rate, the fracture mechanism for NiAl changed from intergranular below the BDTT to transgranular just above the BDTT, as summarized in Fig. 6.3.

6.4 Discussion

6.4.1. Rate dependent deformation behavior of NiAl

The observed changes in tensile ductility and fracture behavior with increasing temperature indicate that additional deformation mechanisms in addition to glide of <100> type dislocations are responsible for accommodating strains at the grain boundaries. In the previous chapter it was determined that the additional deformation mechanism responsible for this behavior is localized climb of <100> dislocations in the vicinity of the grain boundaries. Deformation by a combination of climb and glide of <100> dislocations results in 5 independent deformation modes, thus, maintaining grain to grain compatibility during testing (Groves and Kelly 1969). With grain boundary compatibility maintained through a combination of glide and climb of <100> dislocations, a change in fracture behavior results and extensive polycrystalline tensile ductility becomes possible above the BDTT.

However, because the BDTT occurs as a result of dislocation climb processes, which by definition are rate dependent, the BDTT also should be rate dependent. This would be the case when the strain rate imposed upon the sample at a given temperature is greater than what can be accommodated by climb. In such instances, essentially all the strain in the material would be carried by dislocation glide processes and the material would again be deformation-system-limited. The material would then fail in a brittle manner due to grain boundary incompatibility just as it does at room temperature. The results of this study demonstrate that changes in deformation rate do influence the tensile properties of polycrystalline NiAl in a manner consistent with this explanation. The similar shape but translated position of the ductility versus temperature curves with increasing strain rate indicates that a rate-dependent deformation mechanism is responsible for the brittle-to-ductile transition.

Figure 6.5 is a map of strain rate versus temperature defining the conditions for which the cast and extruded NiAl is ductile or brittle. The figure was generated by plotting strain rate versus the corresponding BDTT. Above the line, NiAl exhibits low ductility and fails in a predominantly intergranular fashion because climb processes are not able to contribute to the overall deformation of the alloy. The area below and to the right of the line contains the conditions of strain rate and temperature for which NiAl will exhibit significant tensile ductility because localized climb is able to accommodate strains across the grain boundaries.

A linear extrapolation of the binary NiAl data in Fig. 6.5 to higher loading rates would indicate that at impact loading rates of 10^5 s^{-1} , the BDTT would be approximately 1200 K. Realistically, there would be a limit at which climb processes could not keep up with the deformation rate no matter what the temperature. This may be a crucial issue for certain high temperature applications since it has been assumed that impact damage would not be a problem at certain operating temperatures because NiAl would be above its BDTT. In actuality, the BDTT in NiAl is a relative temperature dependent on composition, as demonstrated in Chapter V, and for a given composition, the BDTT is dependent on strain rate (Fig. 6.5).

While extrapolation of the data in Fig. 6.5 to higher strain rates should be performed with caution, extrapolation to lower strain rates is not valid. There is a limit where even short circuit diffusion processes no longer become significant. For NiAl this lower limit is about 500 K. As demonstrated during the *in-situ* TEM studies of EGBD mobility discussed in Chapter V, climb assisted by short circuit diffusion paths does not seem to be substantial at temperatures of 500 K and below. Room temperature tensile test results were also consistent with this conclusion. Tensile tests were performed at strain rates between 1.4×10^{-1} to as low as 1.4×10^{-7} s^{-1}; ductility was independent of strain rate over this range of strain rates at room temperature. Therefore, the BDTT in NiAl cannot be expected to occur at temperatures much below 550 K.

Data for another NiAl alloy (Schulson 1985) are also plotted in Fig. 6.5, demonstrating that alloy composition can shift the position of the intermetallic in strain rate-temperature space. Solute additions can affect the onset of climb by forming solute atmospheres around the dislocations and effectively pinning them. Thus, additional energy in the form of higher temperatures would be necessary to overcome this pinning effect. This was already found to be the case for NiAl(Zr) alloys and is suspected to be case in NiAl(Re) alloys as discussed in Chapter V. A similar situation could exist in off-stoichiometric alloys. Point defects, point defect agglomerates (Lasalmonie, Lequeux and Costa 1979) or some other change in grain boundary composition could act analogously by pinning dislocations and directly influencing the BDTT.

This argument is supported by the data of Schulson (1985), which is plotted in Fig. 6.5 for a Ni-49Al alloy of similar grain size as the stoichiometric NiAl alloy presented in this chapter. The ductile region for this non-stoichiometric alloy is shifted to higher temperatures in agreement with the above analysis. It is interesting to note that the slope of the strain rate versus BDTT relationship for the nonstoichiometric alloy is similar to that of the stoichiometric NiAl alloy even though it is shifted to higher temperatures. This implies that changes in strain rate have the same magnitude of affect on the BDTT for NiAl alloys as for the binary stoichiometric material.

6.4.2 Activation energy for deformation at the BDTT

The BDTT for NiAl increases with increasing strain rate because the additional deformation mechanisms responsible for the brittle-to-ductile transition are rate dependent. Consequently, it should be possible to calculate the activation energy for deformation at the BDTT by fitting the data presented in Fig. 6.5 to an Arrhenius equation of the form:

$$\dot{\varepsilon} = A\, e^{-Q/RT}$$

where $\dot{\varepsilon}$ is the strain rate, Q is the apparent activation energy for deformation at the BDTT, T is the brittle-to-ductile transition temperature, R is the gas constant, and A is a pre-exponential constant. From regression analysis of the log ε versus 1/BDTT data, Q was found to be 118 ± 16 kJ/mol. This would represent the activation energy for deformation at the onset of the BDTT. In the previous chapter, the activation energy for deformation throughout the entire regime where glide plus localized climb occurred was estimated at 236 kJ/mol. These two activation energies are consistent values. The value determined in this chapter represents a lower bound and is the activation energy for deformation at the very onset of the BDTT, while the value determined from the previous chapter is based on steady state deformation behavior above the BDTT but below the power law creep regime.

The activation energy for high temperature deformation or creep of metallic materials generally corresponds to the activation energy for self diffusion at temperatures above approximately 0.5 T_m. For NiAl, the activation energy for lattice diffusion is on the order of 300 kJ/mol (Hancock and McDonnell 1971), while the activation energy for creep is generally reported between 280 - 350 kJ/mol (Whittenberger 1987, 1988; Yang and Dodd 1973; Rudy and Sauthoff 1985; Vandervoort, Mukherjee and Dorn 1966). Thus, the behavior of NiAl at elevated temperatures is consistent with a dislocation creep mechanism. From values of the stress exponent and other considerations that were discussed in section 2.5, it is acknowledged that this dislocation creep mechanism is controlled by dislocation climb as opposed to viscous glide.

The apparent activation energies calculated above and from Chapter V for deformation at the BDTT are considerably less than 300 kJ/mol. This is because the deformation phenomenon responsible for the BDTT in NiAl occurs at temperatures well below 0.5 T_m. Below 0.5 T_m, the activation energy for deformation corresponds to the activation energy for short-circuit diffusion processes, e.g., grain boundary or dislocation-pipe diffusion (Hancock, Dillamore and Smallman 1972; Smallman 1985). The activation energy for diffusion along short-circuit paths is usually 1/3 to 2/3 of the activation energy for bulk diffusion (Brophy, Rose and Wulff 1967; Shewmon 1983). Therefore, the observed activation energies of approximately 118 - 236 kJ/mol determined for the deformation processes responsible for the onset of ductile behavior in NiAl correspond to a deformation mechanism for which dislocation climb is still the most likely rate limiting step. In this low temperature regime, however, dislocation climb is controlled by short-circuit diffusion processes instead of lattice diffusion. Hence, climb controlled by short-circuit diffusion would be limited to regions such as grain boundaries, but this is exactly where additional deformation mechanisms are necessary for relieving compatibility stresses. Typical dislocation glide processes would still dominate the deformation behavior of the grain interiors. This explanation is consistent with the conclusions formed in Chapter V.

Similarly, dislocation climb processes driven by short circuit diffusion along dislocation cores could be used to explain the brittle-to-ductile transition in [001] oriented single crystals. In [001] crystals, strain rate has the same effect on the BDTT as in polycrystalline NiAl, increasing the BDTT by about 65 K for every one order of magnitude increase in strain rate (Lahrman, Field and Darolia 1991). The temperature range over which the BDTT occurs for hard crystals corresponds to the change in deformation from <111> slip to deformation controlled by <100> and <110> dislocations.

Because the resolved shear stress for glide of <100> dislocations would be small and the <110> dislocations have a decomposed core structure and can only move by non-conservative processes (Mills et al. 1993), a significant amount of strain in these crystals would have to be accommodated by thermally activated deformation processes.

Soft single-crystal NiAl orientations also exhibit limited tensile ductility at room temperature and undergo a dramatic increase in ductility at intermediate temperatures. But in contrast to polycrystalline NiAl and hard orientation single crystals, soft orientation single crystals only exhibit about a 25 K increase in BDTT for a one order of magnitude increase in strain rate (Lahrman, Field and Darolia 1991). The problems associated with grain boundaries in polycrystalline NiAl are obviously not a consideration in single crystals. However, the onset of thermally activated deformation processes may still play an important role in the relaxation of stress concentrations that occur at surface notches or internal defects such as inclusions, pores or shrinkage cavities. Dislocation glide alone, generally on a single slip system, would not be sufficient to accommodate the complex stress state near these types of defects in single crystals. Therefore, single crystals (Takasugi, Kishino and Hanada 1993), like polycrystalline NiAl undergo a dramatic change in tensile ductility at intermediate temperatures where thermally activated deformation processes become active.

6.5. Summary and Conclusions

1. The brittle-to-ductile transition temperature (BDTT) for polycrystalline NiAl is dependent on strain rate, with a three orders of magnitude increase in strain rate resulting in approximately a 200 K increase in transition temperature.
2. Regardless of the strain rate, at temperatures just above the BDTT the fracture strength increased significantly and the fracture morphology changed from mostly intergranular to predominantly transgranular.

3. The rate dependence of the BDTT suggests that the mechanism for the brittle-to-ductile transition in NiAl is associated with the onset of a thermally activated rate dependent deformation process. Furthermore, the apparent activation energy calculated for the onset of the BDTT as a function of strain rate suggests that this activity is dependent on the operation of a short-circuit diffusion process. These results support the argument that the mechanism for the brittle-to-ductile transition in NiAl is associated with the onset of localized dislocation climb processes in the vicinity of the grain boundaries as described in Chapter V.

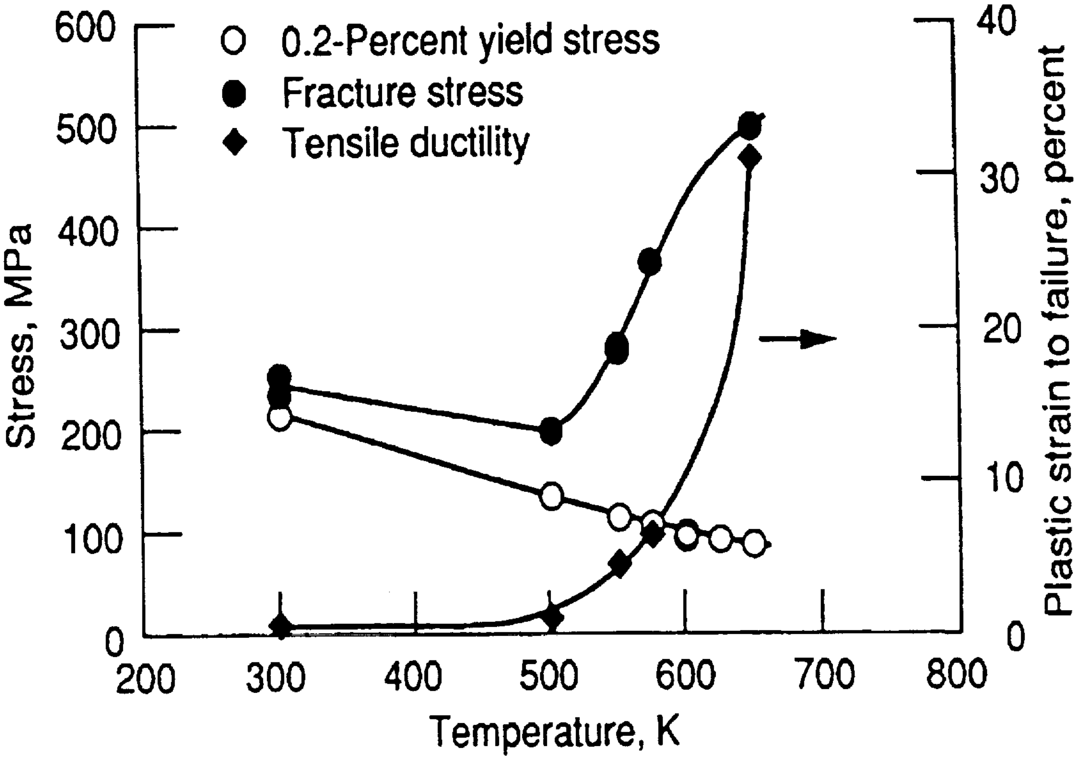

Fig. 6.1. Effect of test temperature on the tensile strength and ductility of cast and extruded NiAl at an initial strain rate of $1.4 \times 10^{-4}\ s^{-1}$.

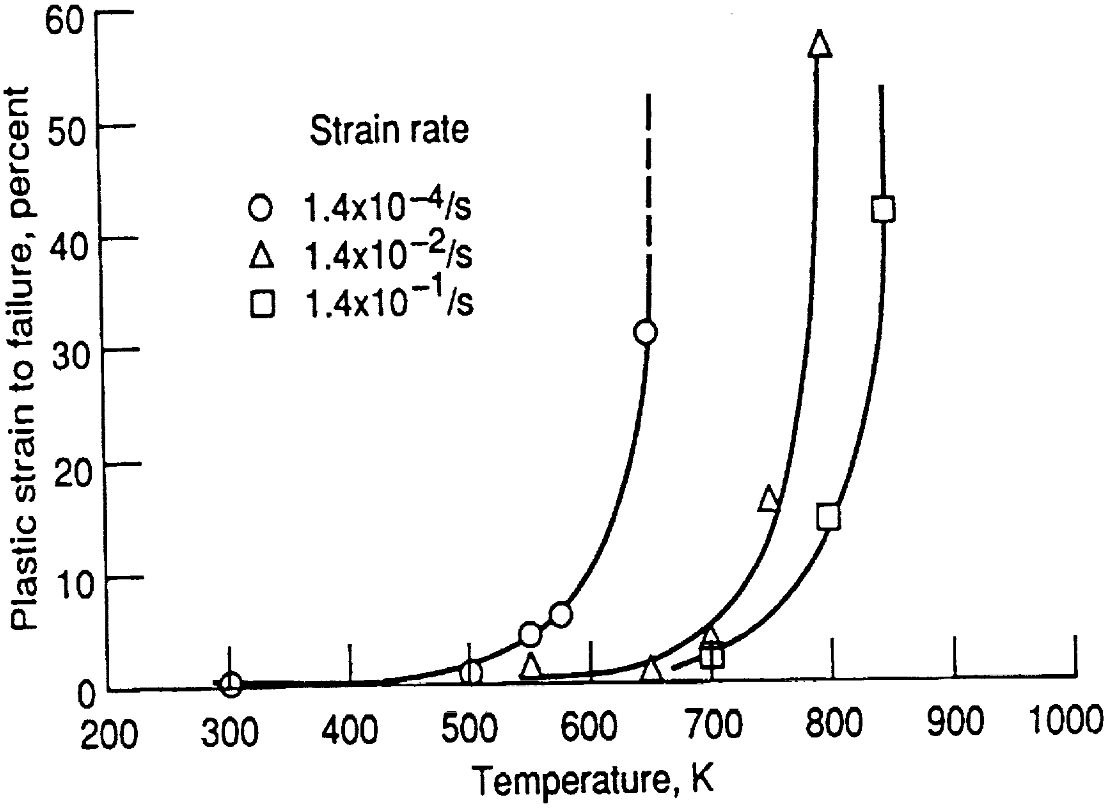

Fig. 6.2. Effect of strain rate on the tensile ductility of cast and extruded NiAl.

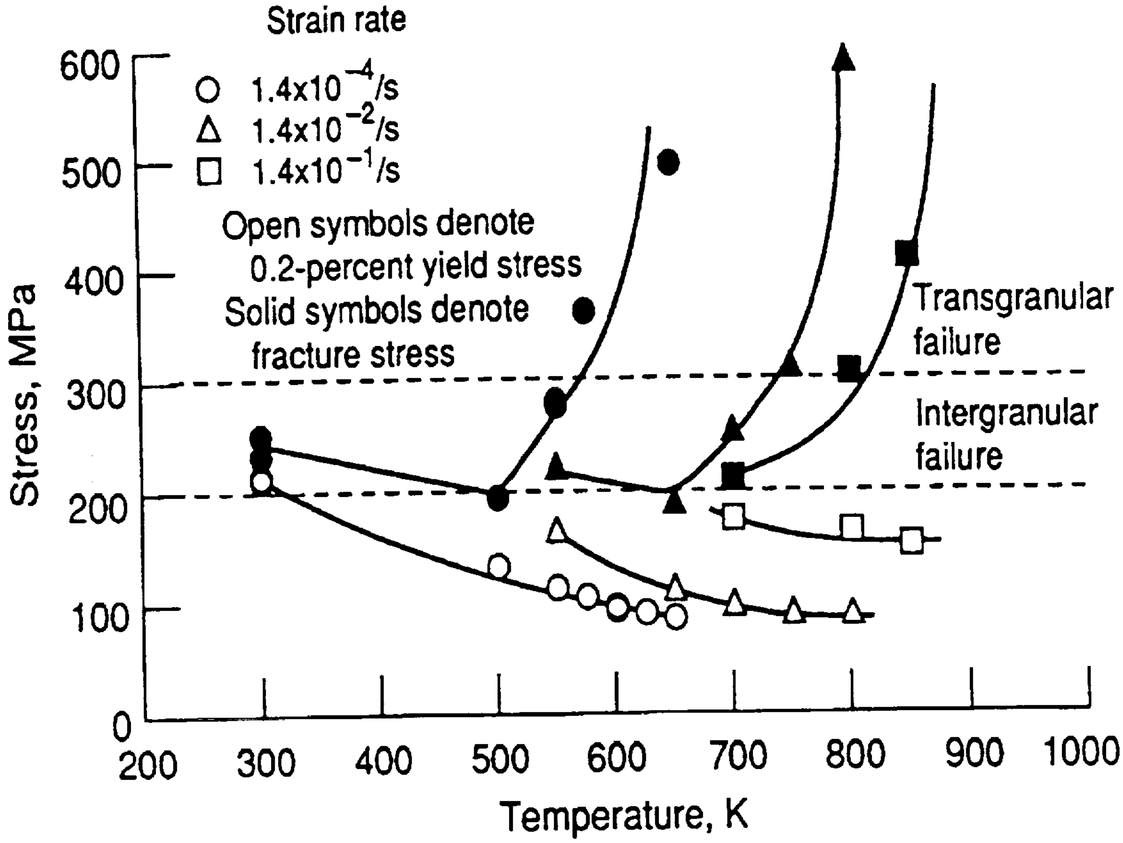

Fig. 6.3. Effect of strain rate on the tensile yield strength and fracture strength of cast and extruded NiAl. Open symbols denote 0.2% yield stress values and solid symbols represent fracture stress values.

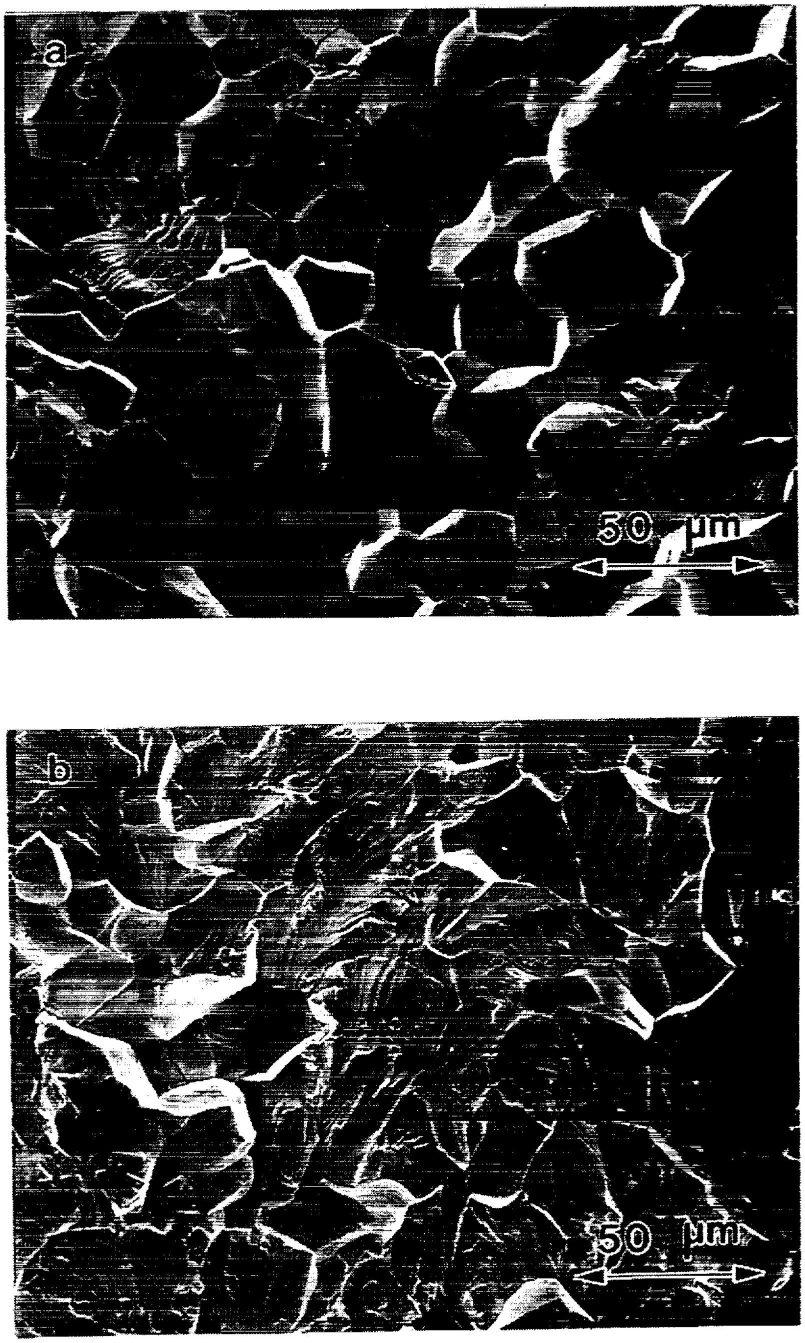

Fig. 6.4. Tensile fracture surfaces of NiAl tested at: a) 550 K and an initial strain rate of $1.4x10^{-4}$ s^{-1}, b) 650 K and an initial strain rate of $1.4x10^{-4}$ s^{-1}, c) 800 K and an initial strain rate of $1.4x10^{-1}$ s^{-1} and d) 850 K and an initial strain rate of $1.4x10^{-1}$ s^{-1}.

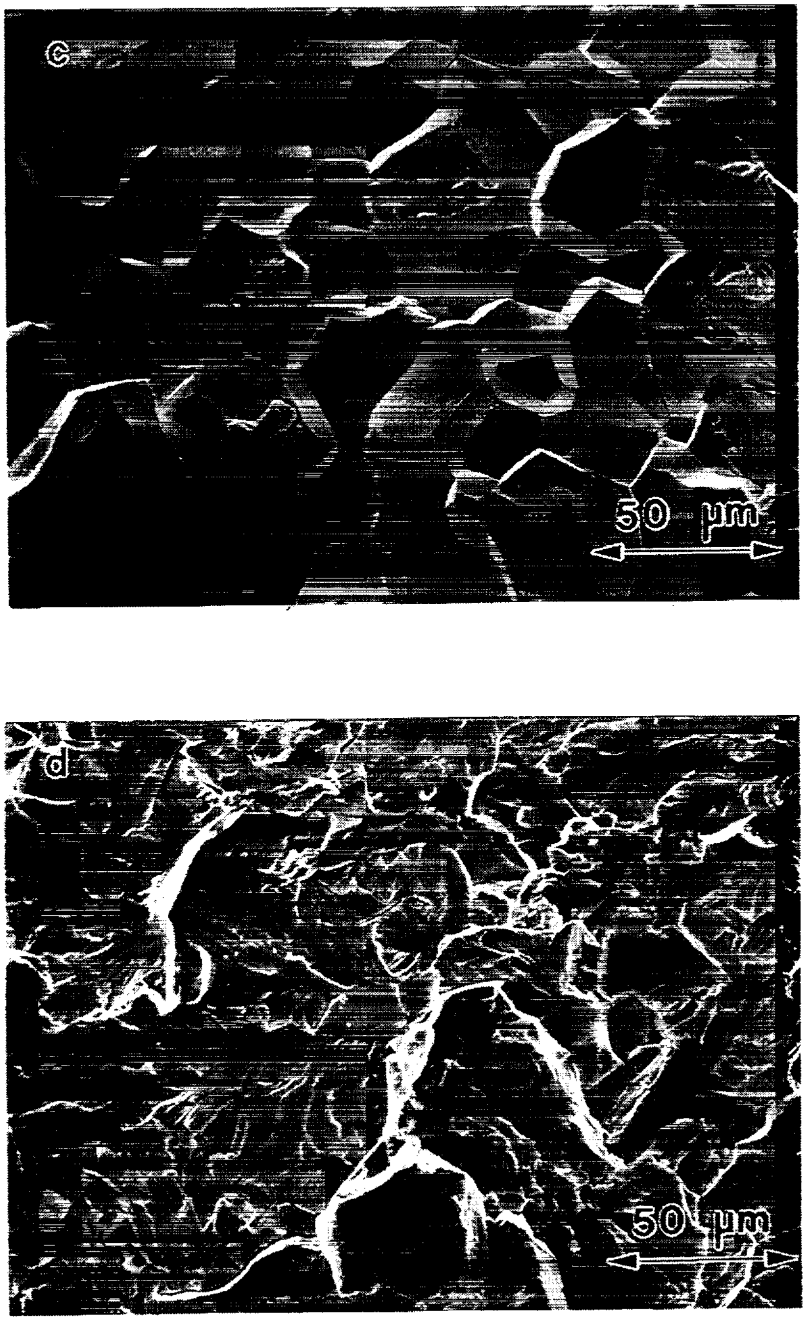

Fig. 6.4. cont. Tensile fracture surfaces of NiAl tested at: a) 550 K and an initial strain rate of $1.4\mathrm{x}10^{-4}\ s^{-1}$, b) 650 K and an initial strain rate of $1.4\mathrm{x}10^{-4}\ s^{-1}$, c) 800 K and an initial strain rate of $1.4\mathrm{x}10^{-1}\ s^{-1}$ and d) 850 K and an initial strain rate of $1.4\mathrm{x}10^{-1}\ s^{-1}$.

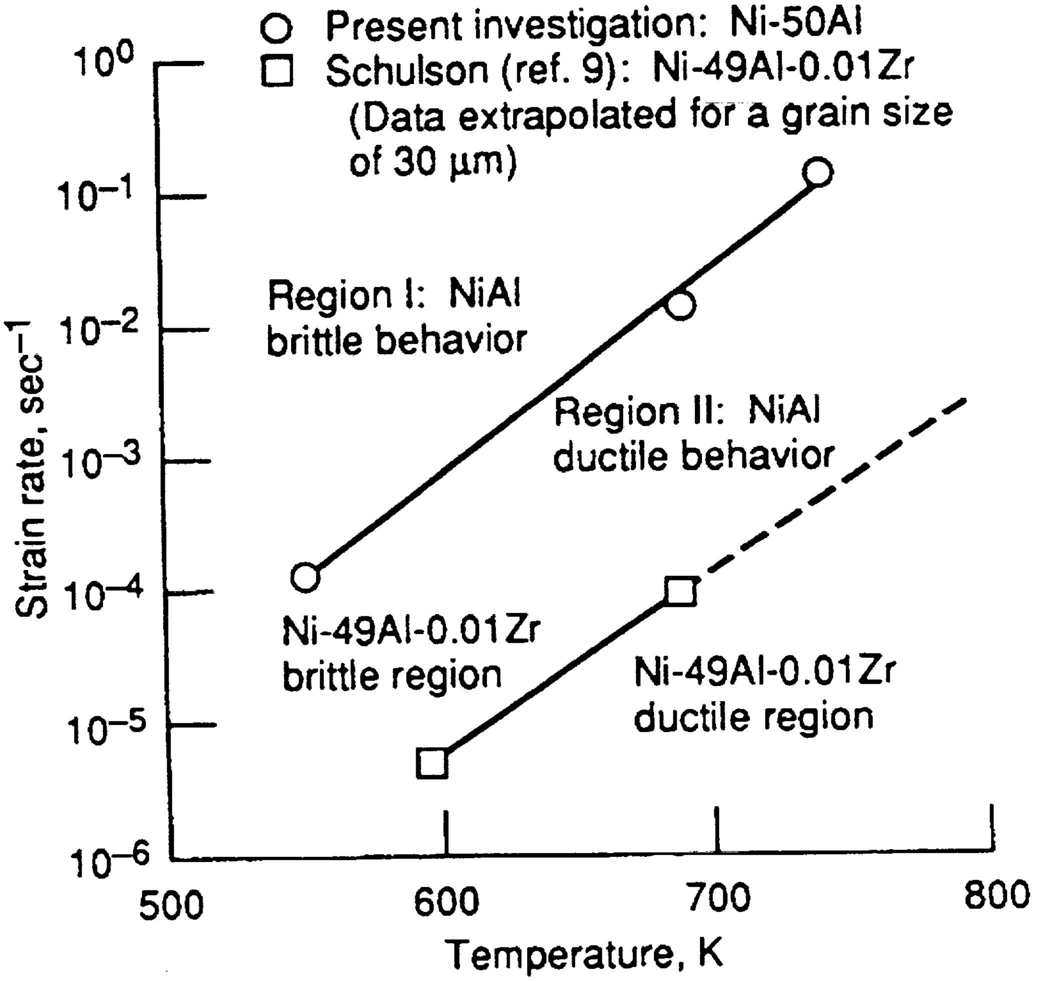

Fig. 6.5. Strain rate versus temperature map indicating the strain rate-temperature conditions for which NiAl and Ni-49Al-0.01Zr [9] are ductile and brittle. The plotted points are strain rate versus the BDTT (defined as the minimum temperature for which ≥ 5% tensile ductility occurs).

CHAPTER VII

EFFECTS OF DILUTE TERNARY ALLOYING ADDITIONS AND SUBSTITUTION SCHEMES ON THE TENSILE PROPERTIES AND BDTT OF POLYCRYSTALLINE NiAl

7.1. Introduction

Recent emphasis in the development of NiAl alloys has focused on either improving the creep resistance of the material or addressing the problem of low temperature ductility and toughness. In the case of creep resistance, significant progress has been achieved in both polycrystalline (Whittenberger, Arzt and Lutton 1990a,b) and single crystal alloys (Darolia 1991) through conventional metallurgical techniques. On a relative strength basis, several NiAl alloys have been developed that can compete quite effectively with Ni-base superalloys (Whittenberger 1993; Darolia 1993; Nathal 1992). On the other hand, much less success has been attained in solving the problems associated with poor low temperature ductility and toughness.

A lack of progress in resolving the ductility and toughness issues in NiAl was the primary motivation for this investigation. The approach I have taken was to determine the underlying flow and fracture mechanisms in NiAl in hopes of eventually manipulating these processes in a manner that would improve the low temperature properties. Up to this point, emphasis has been on identifying and analyzing the flow and fracture mechanisms in binary polycrystalline NiAl. The remaining chapters will focus on preliminary results of alloying studies that were initiated in order to understand the impact of ternary additions and impurities on mechanical properties. The results are meant as a guide to future alloy development efforts, as outlined in Chapter IX.

There are several methodologies that have generally been pursued in order to improve the room temperature properties of polycrystalline NiAl. The first approach involved the careful control of stoichiometry and thermomechanical processing to create a clean, moderately fine grain size material. Such binary NiAl alloys, which are generally made from cast and then extruded ingots, have tensile ductilities on the order of 1 to 3 percent (Hahn and Vedula 1989; George and Liu 1990; Nagpal and Baker 1990b). But, as demonstrated in Chapter IV, polycrystalline binary NiAl can never be expected to exhibit tensile ductilities greater than a few percent because of grain compatibility problems. The second approach was the use of macroalloying additions. These additions can be used to generate a ductile second phase (Noebe, Misra and Gibala 1991) or added in an attempt to alter the slip behavior of the alloy by lowering the ordering energy (Law and Blackburn 1987; Cotton, Noebe and Kaufman 1993b). Ductile phase reinforcement has been discussed in detail in Chapter III and alloying to alter slip processes will be reviewed in Chapter IX.

Another approach that has been investigated as a possible solution to the ductility problem in NiAl was the use of microalloying additions. This approach has been extremely successful in the development of Ni_3Al alloys. In polycrystalline NiAl alloys, the prime microalloying additions investigated have been B (Law and Blackburn 1987; George and Liu 1990) and Zr (discussed in Chapter V). Unfortunately, both elements tend to decrease the room temperature tensile ductility of polycrystalline NiAl and increase the BDTT. On the other hand, microalloying additions of Fe and Ga were shown to have a beneficial effect on the tensile ductility of single crystal NiAl (Darolia 1991; Darolia, Lahrman and Field 1992). An increase in the room temperature tensile elongation of <110> oriented NiAl single crystals from 1 to nearly 6% occurred when these elements were added in amounts of 0.1 - 0.25 at.%.

Consequently, the purpose of this chapter is to report on the effect of microalloying additions of Fe and Ga on the tensile properties and BDTT of polycrystalline NiAl and to compare the observed behavior to polycrystalline NiAl containing an alloying addition such as Zr that tends to embrittle the material. A related issue that was raised during this investigation was the effect of alloy substitution scheme on properties. A series of dilute NiAl(Ga) alloys were studied to determine the effect of ternary substitution schemes on the mechanical behavior of NiAl. The results are discussed in terms of grain boundary composition and its subsequent effect on mechanical properties.

7.2. Materials and Experimental Procedures

Microalloyed NiAl was produced by vacuum induction melting ingots of stoichiometric NiAl and NiAl containing 0.1 at.% Fe or Ga substituted for Al (Ni-49.9Al-0.1Fe and Ni-49.9Al-0.1Ga). The ingots were sealed in mild steel extrusion cans and extruded at 1200 K to an area reduction ratio of 16:1. For the Zr-containing alloy, -60/+100 mesh prealloyed powder of nominal composition Ni-49.95Al-0.1Zr was obtained from Homogeneous Metals, Inc.(Heat P1187), placed in a mild steel extrusion can, evacuated, sealed, and was extruded at 1500 K to an area reduction ratio of 16:1. Because of the significantly higher strength of Zr-doped alloys under fast strain rate conditions (Whittenberger and Noebe 1993), a higher processing temperature was necessary to successfully extrude this material and a prealloyed powder precursor was used instead of a cast ingot. It should be noted that this is not the same Zr-doped alloy studied in Chapter V. The alloy examined in Chapter V, P896, contained 0.05 at.% Zr, while this alloy contains twice the level of Zr. Post-extrusion chemical analyses of all four alloys by inductively coupled plasma atomic emission spectroscopy indicated that all alloys were within experimental accuracy of their intended compositions.

A series of additional Ga doped alloys with different substitution schemes were also produced in a manner similar to that described above for the Ni-49.9Al-0.1Ga alloy. Vacuum induction melted ingots with Ga substituted for Al (Ni-49Al-1Ga, Ni-45Al-5Ga) and an ingot with Ga substituted for Ni (Ni-50Al-1Ga) were sealed in mild steel extrusion cans and extruded at 1200 K to an area reduction ratio of 16:1.

Round button-head tensile specimens were ground from the extruded rods such that the gage length of the sample was parallel to the extrusion direction. Sample dimensions were 30.5 mm and 3.2 mm for the tensile gage lengths and gage diameters, respectively, (see Fig. 4.5). Prior to testing, all samples were electropolished in a 10% perchloric acid-90% methanol solution cooled to 208 K. Tensile tests were performed to failure in a universal screw-driven load frame at a constant crosshead velocity corresponding to an initial strain rate of $1.4x10^{-4}$ s^{-1}. Tests were run in an air atmosphere between 300 and 1100 K by heating the samples in a resistance furnace with temperature control and temperature gradients along the tensile gage section held within ± 2 K. True stress-plastic strain data were calculated from the load-time plots by subtracting the elastic strain and machine compliance and assuming constant volume conditions and uniform deformation. True stress at failure was obtained by accounting for the reduction-of-area when necking was significant. Yield stress was determined by the 0.2% offset method. Post-test analyses of the tensile surfaces were performed using a Cambridge 200 scanning electron microscope (SEM). The percentage of intergranular fracture was determined from fractographs of each sample taken from at least four different locations on the fracture surface.

7.3. Results and Discussion

7.3.1. Effect of microalloying additions on room temperature properties

The microstructure of the as-extruded microalloyed materials consisted of recrystallized, equiaxed grains with average linear intercept grain sizes ranging from 18-20 μm for the NiAl, Ni-49.9Al-0.1Fe, and Ni-49.9Al-0.1Ga and 4 μm for the Zr-doped NiAl (Table 7.1). Multiple samples (3 - 6) of each alloy were tested at room temperature and the average tensile properties are reported in Table 7.1. The room temperature tensile tests for each particular alloy composition were very reproducible as evident from the very small standard deviations reported with the tensile properties. The binary NiAl alloy exhibited the largest tensile elongation (1.4%) before fracture, followed by the Fe- and Ga-doped alloys with tensile ductilities of nearly 1%. In contrast, the Zr-doped alloy did not exhibit any tensile ductility below 700 K.

The yield strength of the binary NiAl was only slightly lower than that for the NiAl(0.1Fe) and NiAl(0.1Ga) alloys. From the yield strength data in Table 7.1, the hardening rates (dσ/dc) for Fe and Ga in NiAl were determined to be 230 and 250 MPa/at.%, respectively. These values for the hardening rates of Fe and Ga are comparable to hardening rates observed for other elements of similar atomic size in NiAl (Noebe, Bowman and Nathal 1993). The hardening rate for Zr in NiAl was on the order of 5900 MPa/at.%, though some of this strengthening can be attributed to grain boundary effects (Zeller, Noebe and Locci 1990). The fracture stresses of the cast and extruded NiAl, NiAl(0.1Fe) and NiAl(0.1Ga) alloys were all similar but were only one third of that observed for the Zr-doped NiAl.

Representative room temperature true stress-true plastic strain curves for the NiAl, NiAl(0.1Fe) and NiAl(0.1Ga) alloys are shown in Fig. 7.1. The binary alloy exhibited an initial region of high work hardening rate followed by a slight yield point and small Luders strain or region of zero work hardening that finally led to normal work hardening behavior. Similar tensile stress-strain curves have been previously observed for binary NiAl (Hahn and Vedula 1989). On the other hand, the doped alloys exhibited slightly higher initial yield stresses followed almost immediately by normal work hardening behavior. For binary NiAl and the Fe and Ga modified alloys the work hardening rates were the same after 0.3% strain, indicating that the alloying additions had no effect on the work hardening rate after the yield point. It is also evident that because the Fe and Ga-doped alloys failed at essentially the same stress as the binary NiAl, but had higher yield strengths, a slightly lower tensile ductility resulted. The Zr-doped NiAl did not exhibit any measurable tensile plasticity before failure at room temperature and therefore, was not included in Fig. 7.1. However, compression stress-strain data for the NiAl(0.1Zr) and the NiAl(0.05Zr) alloy (Fig. 5.7) indicate that Zr also has little effect on the work hardening behavior of NiAl.

The results indicate that neither Fe nor Ga additions had any positive effect on the room temperature tensile ductility of polycrystalline NiAl. This was in contrast to the beneficial effect observed by Darolia (1991) for NiAl single crystals doped with Fe or Ga. In the case of single crystal NiAl, the mechanism for enhanced ductility has not been identified, though a change in slip behavior has been ruled out (Darolia, Field and Lahrman 1992). Therefore, a significant increase in the tensile ductility of polycrystalline NiAl containing microalloying additions would not be expected. During plastic deformation, "Griffith-like" defects are generated at the grain boundaries in NiAl and NiAl alloys because of the incompatible strains that occur due to an insufficient number of independent slip systems. These defects, which are on the same scale as the grain size, then propagate catastrophically once a critical stress intensity is achieved (Chapter IV).

Since the binary NiAl, NiAl(0.1Fe) and NiAl(0.1Ga) materials have essentially the same grain size, the maximum defect size should also be the same in each alloy. Once a critical stress intensity was reached during deformation of these alloys, a grain boundary microcrack would then propagate through the samples. No critical defects such as machining flaws or inclusions were observed on any of the fracture surfaces, which supports the contention that fracture initiates at the grain boundaries. Since all three alloys failed at nearly the same fracture stress at room temperature, (Table 7.1), and assuming that the critical defect size was proportional to the grain size, the use of a Griffith type fracture toughness equation would indicate that the small additions of Fe and Ga did not alter the fracture toughness of the NiAl. Therefore, no beneficial effect could be attributed to the Ga or Fe additions.

In the case of the Zr-doped NiAl, the yield strength determined in compression was considerably higher than the tensile yield strength of the other three alloys. Also, the yield strength of the NiAl(Zr) alloy was very close to its tensile fracture stress (Table 7.1). This would suggest that the onset of yielding was responsible for initiating fracture in the Zr-doped material. But, due to the much higher applied stress, the first grain boundary defects formed are subjected to a much higher stress intensity and fracture occurs immediately without any significant macroscopic tensile ductility. These concepts were discussed in detail in section 4.3.2.

The percentage of room temperature intergranular fracture observed for all four alloys was proportional to the tensile ductility of the material, Table 7.1, implying that the formation of grain boundary defects and the ease of continued intergranular fracture increase with plastic strain. This is consistent with previous discussions and the observations of intergranular cracking in compression samples presented in Chapter IV. Both observations are also in agreement with the results of Margevicius (1992) for binary NiAl alloys tested under increasing levels of hydrostatic pressure, where the percentage of intergranular fracture was found to increase proportionally with tensile elongation.

Table 7.1. Average Room Temperature Tensile Properties for Microalloyed NiAl

Alloy	Grain Size (μm)	0.2% Yield Stress (MPa)	Fracture Stress (MPa)	Tensile Elongation (%)	Intergranular Fracture (%)
NiAl	18	180 ± 9	257 ± 7	1.4 ± 0.1	65
NiAl(0.1Fe)	18	203 ± 4	251 ± 4	0.8 ± 0.2	46
NiAl(0.1Ga)	20	205 ± 3	266 ± 7	0.9 ± 0.2	48
NiAl(0.1Zr)	4	772 ± 29*	758 ± 30	0	28

* yield stress determined in compression.

7.3.2. Effect of microalloying additions on the BDTT

The temperature dependent tensile properties of binary NiAl and the three microalloyed materials are summarized in Fig. 7.2. In all cases, the mechanical behavior of the doped alloys mirrored the behavior of the binary NiAl, though the strengthening effect due to the solute was much greater for the Zr-doped material. For all materials, the yield strength decreased with increasing temperature. The binary NiAl, NiAl(0.1Fe) and NiAl(0.1Ga) exhibited similar yield strengths as a function of temperature, while the Zr-doped material was significantly stronger at all temperatures. Even at 1100 K, the Zr-doped NiAl exhibited a higher yield strength than the other three alloys at room temperature.

The manner in which the fracture strength and tensile ductility depended on temperature was also similar for all four aluminides, though the absolute values were different. The fracture strength decreased slightly with temperature until the BDTT was reached and then increased significantly with additional increases in temperature. As a result, the tensile ductility for each alloy was initially constant with temperature before sharply increasing at the BDTT. For example, an increase in temperature of less than 75 K near the BDTT of all the alloys produced a change in tensile elongation from 1-2% to greater than 50-80% in these materials. The microalloying additions of 0.1 at.% Fe and Ga possibly resulted in a slight increase in the BDTT compared to binary NiAl, though the binary NiAl, NiAl(0.1Fe) and NiAl(0.1Ga) alloys all exhibited BDTT's between 550 and 625 K. Zirconium, on the other hand, had a very dramatic effect on the BDTT. As demonstrated in Chapter V, 0.05 at.% Zr increased the BDTT of NiAl to 850 - 875 K, while increasing the Zr content to 0.1 at.% shifted the BDTT further to nearly 1050 K, Fig. 7.2.

The temperature dependence of the yield stress, fracture stress and tensile elongation for the binary NiAl and microalloyed materials in Fig. 7.2 is consistent with the behavior described previously in Chapters V and VI. It is evident from the very dramatic change in mechanical behavior at the BDTT of these alloys that other deformation mechanisms, in addition to glide of <001> type dislocations, must be present to accommodate strains at the grain boundaries. It was already demonstrated that localized climb of <001> dislocations in the vicinity of the grain boundaries is responsible for the change in mechanical behavior at the BDTT.

Zirconium, which is a very large atom relative to Ni or Al, segregates to the grain boundaries in NiAl (Zeller, Noebe and Locci 1990). It was also determined in that study that the amount of Zr at the grain boundaries increased proportionally to the amount of Zr present in the bulk alloy. For a NiAl(0.1Zr) alloy, up to 8 at.% Zr was present at one surface of the grain boundary. Consequently, Zr with its high hardening rate should be very effective at pinning dislocations at the grain boundaries and preventing their motion until much higher temperatures are reached. At some elevated temperature there would be sufficient thermal energy so that the dislocations could break free of the Zr atoms without much difficulty, resulting in a sharp BDTT at a temperature much greater than that for binary NiAl. This behavior was demonstrated in the in-situ annealing experiments presented in Chapter V.

In a similar argument, because Ni, Fe, Ga and Al are comparable in size they would easily occupy substitutional atom sites. Both Fe and Ga also have a large solubility in NiAl. As a result, these elements would not be expected to strongly segregate to the grain boundaries. Therefore, at very small levels they should have less of an effect on the BDTT, consistent with the results in Fig 7.2. However, Matsugi, Wenman and Stoloff (1992) have demonstrated that at higher levels, Fe does appear to have a rather significant effect on the BDTT. A possible explanation for this result will be presented in the following section.

7.3.3. Effect of substitution scheme on tensile properties of dilute ternary NiAl alloys

Matsugi, Wenman and Stoloff (1992) have investigated the effect of Fe additions on the BDTT of NiAl. In their research, a Ni-50Al-0.3Fe alloy was studied, which had a BDTT of roughly 750 K. Therefore, Fe does effect the BDTT of NiAl, though not as significantly as Zr or Re. In the alloy studied by Matsugi, Wenman and Stoloff (1992), Fe was substituted for Ni because it was assumed that Fe would prefer the Ni-sublattice, minimizing the number of constitutional defects in the alloy. However, Fe actually occupies Al-sublattice sites in dilute NiAl-Fe alloys (Duncan et al. 1994). Instead of a stoichiometric alloy, their material was essentially 0.3 at.% Al-rich (49.7Ni/50.3Al+ Fe). In contrast, the Fe- and Ga -doped alloys studied in this chapter were produced by substituting the microalloying addition for Al with relatively little impact on the BDTT. Consequently, alloy substitution scheme, replacing Ni versus Al with a particular alloying addition, may have an effect on the BDTT. A series of ternary NiAl(Ga) alloys were produced to further analyze this hypothesis. But first, some additional comments about ternary alloy site occupancy in NiAl are necessary.

Experimental evidence confirms that Cr (Field, Lahrman and Darolia 1991c; Cotton, Noebe and Kaufman 1993a), Fe (Duncan et al. 1994) and V (Munroe and Baker 1992) all substitute on the Al-sublattice in NiAl. In fact, based on thermodynamic considerations (Kao et al. 1994), all elements, X, that have a lower heat of formation as Al-X compounds than the heat of formation of NiAl will occupy Al-sublattice positions in dilute alloys. In other words, all elements except Pd, Pt, Rh and possibly Co are expected to occupy the Al-sublattice. This is consistent with the limited available experimental data mentioned previously.

Based on this argument, when Ga is added to NiAl for Ni as in the Ni-50Al-1Ga alloy, the material becomes Al-rich. When Ga is substituted for Al in the Ni-49.9Al-

0.1Ga, Ni-49Al-1Ga, and Ni-45Al-5Ga alloys, the materials remain 'stoichiometric' in composition with a minimum number of constitutional defects. The effect of these substitution schemes on tensile properties is demonstrated in Fig. 7.3. When Ga is substituted for Al in the NiAl alloy the BDTT is not significantly affected. The BDTT of Ni-49Al-1Ga is about 600 K, essentially the same as that for the Ni-49.9Al-0.1Ga alloy. Furthermore, the BDTT for both of these NiAl(Ga) alloys are not that different from binary NiAl, which at best has a BDTT of 550 K. Even at higher levels of Ga, such as Ni-45Al-5Ga, the BDTT is still only between 625 and 650 K. In stark contrast to this behavior, the Ni-50Al-1Ga alloy has a BDTT of just over 800 K. Therefore, the BDTT of ternary NiAl(Ga) alloys is 150 - 200 K higher for those alloys where Ga was substituted for Ni compared to alloys where Ga was added for Al. It should be noted that the BDTT for the Ni-50Al-1Ga alloy was consistent with the BDTT reported by Matsugi, Wenman and Stoloff (1992) for the Fe-doped alloy, where Fe was also substituted for Ni.

Figure 7.3 also contains the yield stress and fracture stress data for the NiAl(Ga) alloys as a function of temperature. As demonstrated repeatedly throughout this report, the BDTT corresponds to a significant increase in both fracture stress and tensile ductility for the alloys while yield stress exhibits only a moderate decrease with increasing temperature. It is interesting to note that the Ni-50Al-1Ga alloy in Fig. 7.2 behaves similarly to the NiAl(0.1Zr) alloy in Fig. 7.3. This would imply that the mechanism, resulting in the increase in BDTT of both alloys, may be analogous.

The effect of alloy substitution scheme on the BDTT is not just unique to NiAl-Ga and maybe NiAl-Fe alloys but is a more general phenomenon. For example, Fig. 7.4 demonstrates a similar effect in NiAl(Cu) alloys. The BDTT for ternary alloys containing Cu, which was added equally for Ni and Al, is 200 K higher than for alloys with the same Cu level but substituted exclusively for Al (Noebe 1993). It should be noted that in this unpublished study, alloys produced with Cu substituted exclusively for Ni were so brittle that it was not possible to machine test samples. Consequently, alloy substitution scheme has a very profound effect on the ductility of ternary NiAl alloys.

The major point made by Figs. 7.3 and 7.4 is that when an alloying addition is highly soluble in NiAl, the substitution scheme and not the amount of the alloying addition has the most pronounced effect on the BDTT. Alloys that have an overall Al-rich composition have much higher BDTT's than binary NiAl or ternary alloys whose overall composition would be close to 'stoichiometric'. Therefore, one can speculate that non-stoichiometric alloys, especially those that are Al-rich, exhibit a grain boundary structure or segregation of solute to the grain boundaries that interferes with localized climb of dislocations in the vicinity of the grain boundaries, thus, affecting or increasing the BDTT. This would parallel the behavior of NiAl(Zr) alloys described in Chapter V.

Based on the data and observations available, this is just a hypothesis. However, the entire premise of stoichiometry controlling grain boundary chemistry and in the end, controlling the BDTT of NiAl is an intriguing idea and could have profound ramifications in the design of future alloying schemes. Consequently, the relationship between alloy composition, grain boundary chemistry, and BDTT is one topic that deserves further investigation.

7.4. Summary and Conclusions

1. While beneficial to the room temperature ductility of single crystal NiAl, 0.1 at.% Fe and Ga additions did not improve the room temperature ductility of polycrystalline NiAl and for the most part, have little impact on the tensile properties of NiAl. In contrast, microalloying additions of 0.1 at.% Zr adversely influence the tensile ductility of NiAl and increase the BDTT to nearly twice that for binary NiAl.
2. Regardless of the alloying addition, the dependence of tensile properties on temperature was similar: a) yield strengths gradually decreased with temperature, b) fracture stresses moderately decreased with temperature until the BDTT, and then

increased significantly, and c) tensile elongations remained essentially constant and low until the BDTT was reached and then increased dramatically.

3. For microalloying additions to have any real impact on the tensile ductility of polycrystalline NiAl, they will either have to alter the slip behavior of the alloy so that five independent slip systems are active, or the additions must result in a significant increase in fracture toughness.

4. The overall stoichiometry of binary and ternary NiAl alloys apparently influences the grain boundary composition in a manner that inhibits localized climb processes, subsequently affecting the BDTT.

5. All the observations in this chapter concerning the tensile behavior of ternary NiAl alloys are consistent with the description of NiAl flow and fracture behavior presented in previous chapters.

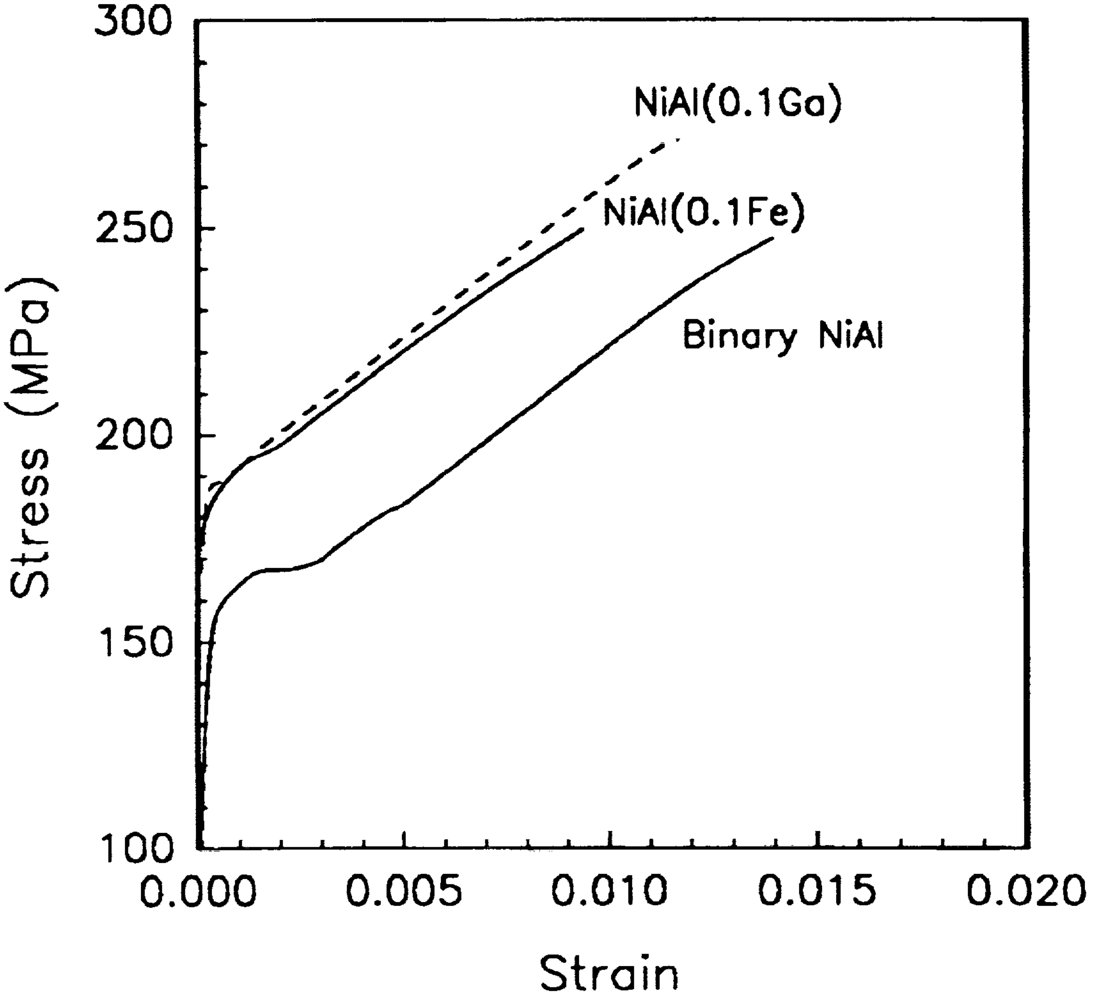

Fig. 7.1. Room temperature tensile stress-strain response for NiAl, NiAl(0.1Ga), and NiAl(0.1Fe). Samples were tested at a strain rate of 1.4×10^{-4} s^{-1}.

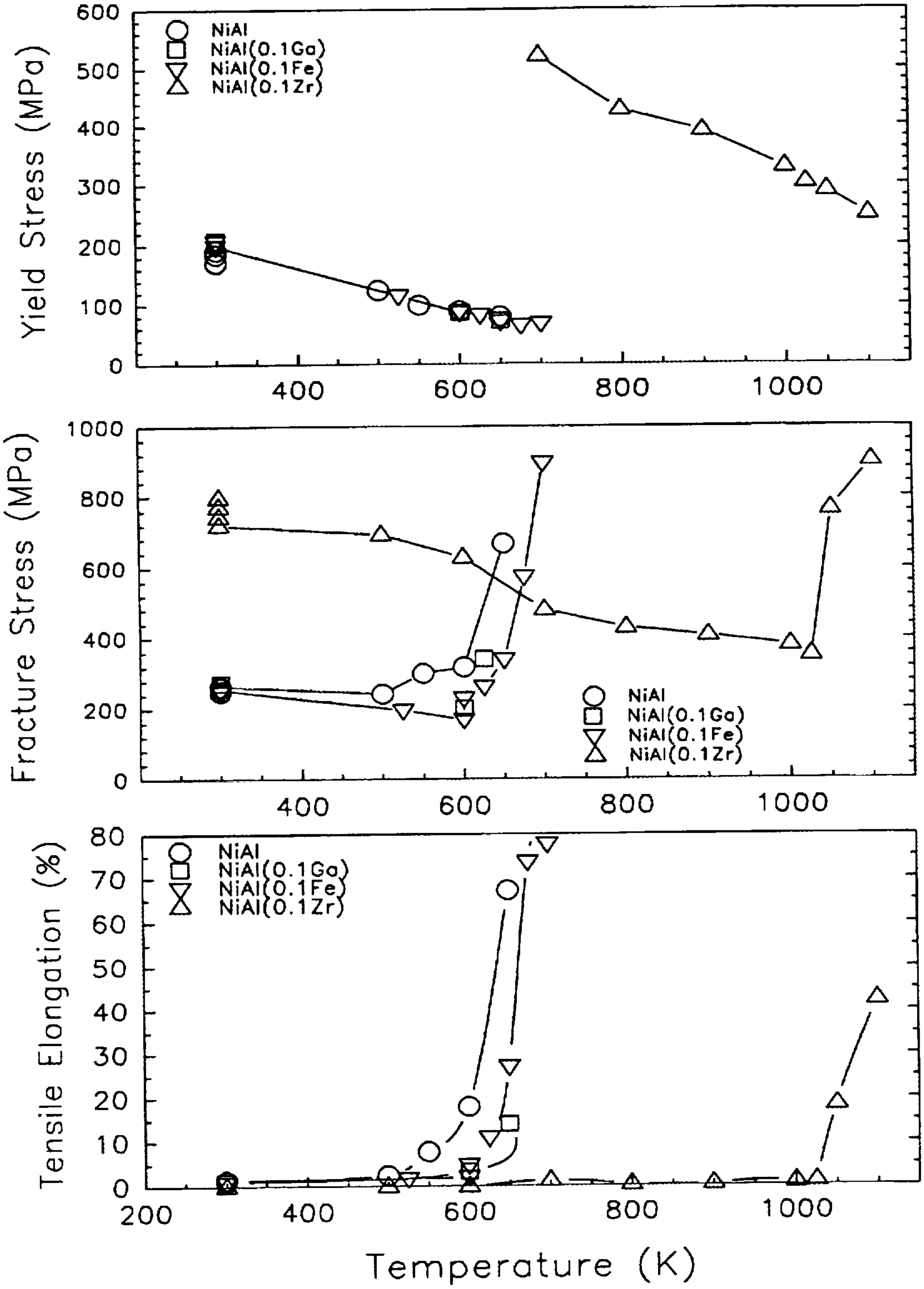

Fig. 7.2. The effect of temperature on the tensile properties (0.2% offset yield stress, fracture stress and tensile elongation) of binary NiAl and microalloyed NiAl containing 0.1 at.% Ga, Fe, or Zr. All tests were run at a strain rate of $1.4x10^{-4}$ s^{-1}.

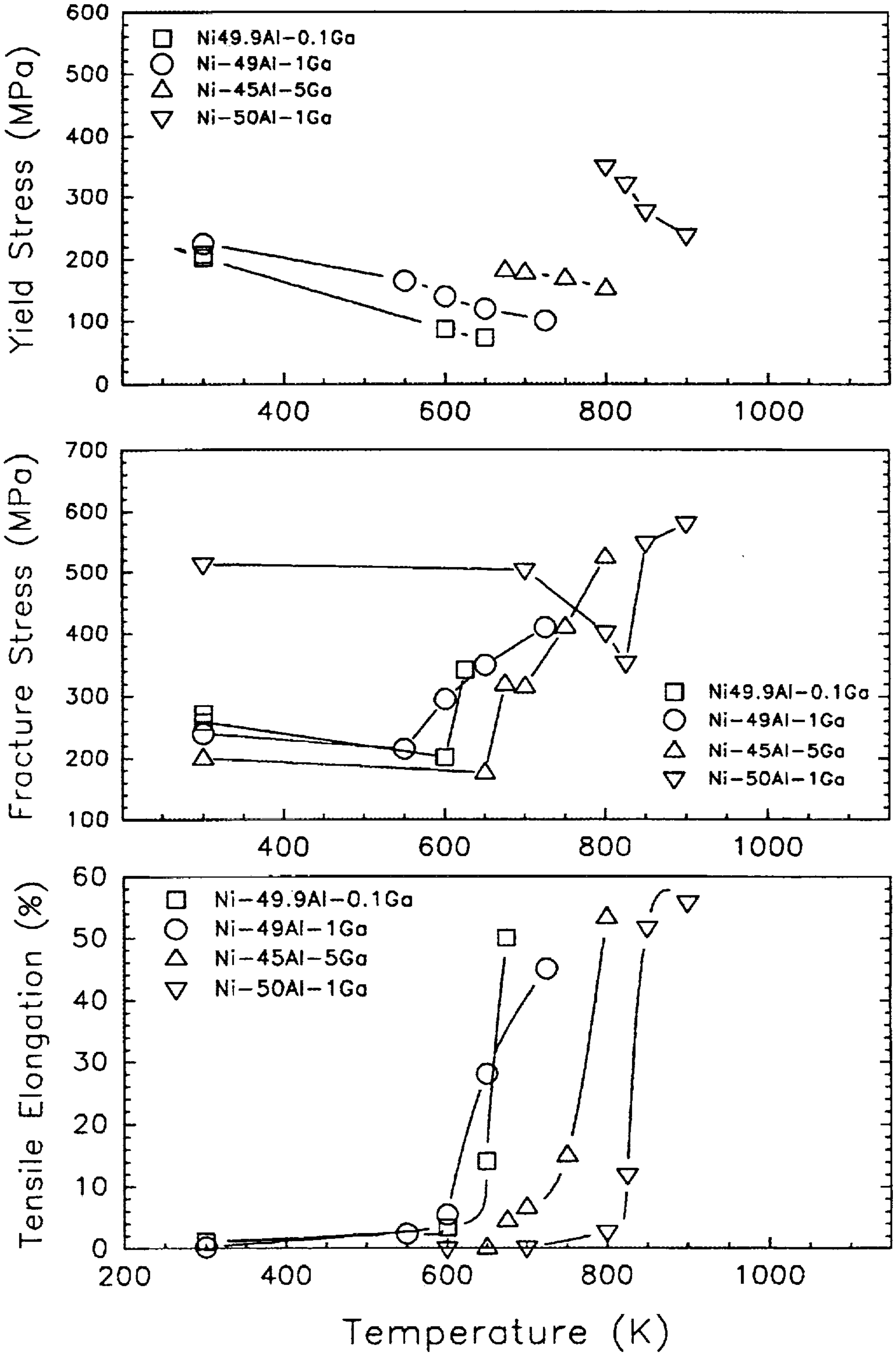

Fig. 7.3. The effect of substitution scheme on the tensile properties (0.2% offset yield stress, fracture stress and tensile elongation) of ternary NiAl(Ga) alloys. All tests were run at a strain rate of $1.4x10^{-4}$ s^{-1}.

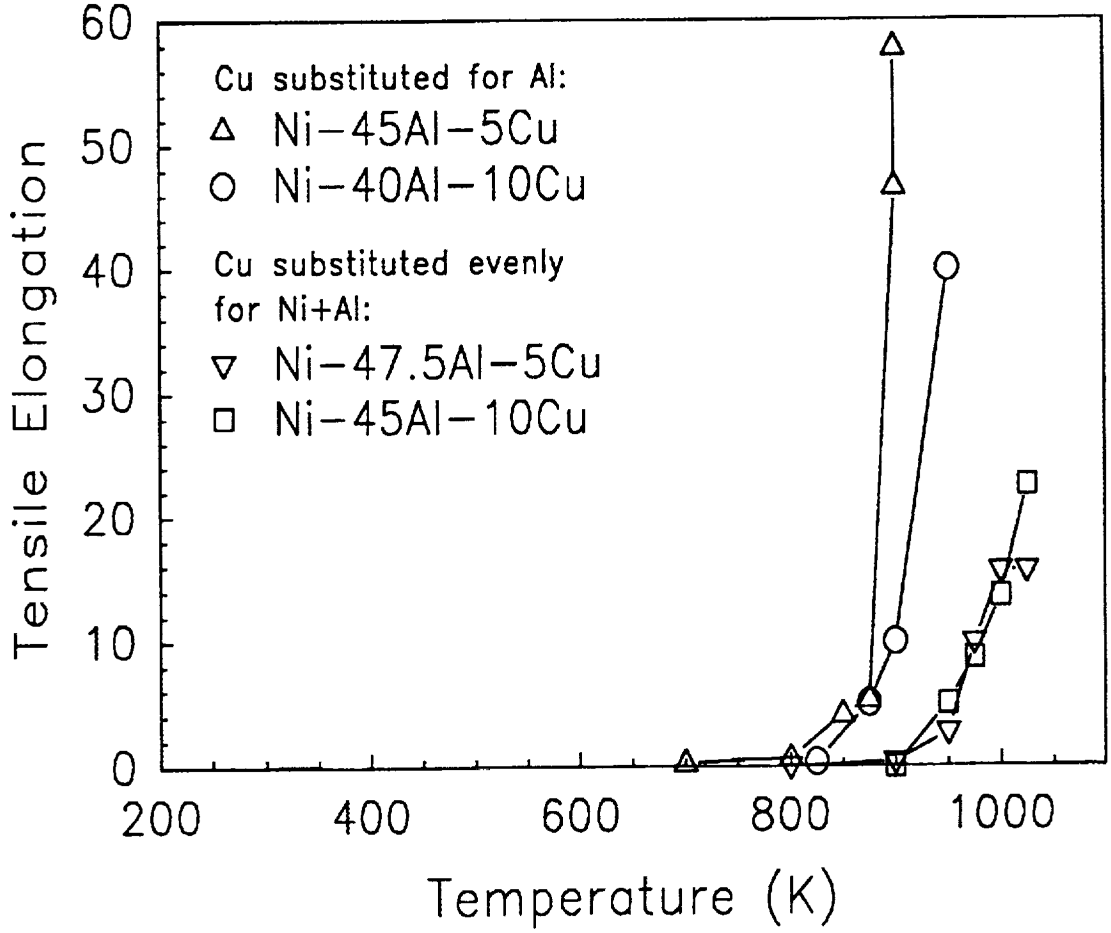

Fig. 7.4. The effect of alloy substitution scheme on the BDTT of ternary NiAl(Cu) alloys tested at a strain rate of $1.4x10^{-4}\ s^{-1}$.

CHAPTER VIII
EFFECT OF INTERSTITIAL ELEMENTS ON THE MECHANICAL BEHAVIOR OF NiAl

8.1. Introduction

Poor tensile ductility and fracture toughness below the brittle-to-ductile transition temperature are the primary factors limiting the acceptance of NiAl as a high temperature structural material (Bowman and Noebe 1992). Consequently, much of the current research has been directed towards understanding the relationship between various metallurgical parameters (such as processing conditions, heat treatment, alloying additions and stoichiometry) on low temperature mechanical properties. However, one area that has been neglected by many investigators is interstitial impurity effects.

In single crystal NiAl, the yield strength is essentially proportional to the total interstitial content of the alloy (Weaver, Kaufman and Noebe 1993). However, the yield strength of single crystals was even more sensitive to substitutional alloying additions and thermal vacancies, which can mask any strength differences due to interstitial elements (Weaver, Kaufman and Noebe 1993). Therefore, while interstitial elements may have an impact on strength the effect is not very pronounced at the levels normally present in commercial purity materials. Interstitial levels also have only a marginal influence on the deformation mechanisms in NiAl as determined by differences in the activation volumes and stress exponents for conventional purity and high purity materials (Kitano, Pollock and Noebe 1994). Furthermore, various annealing and prestrain treatments performed in an effort to introduce strain aging effects in conventional purity NiAl resulted in absolutely no difference in these activation parameters (Kitano and Pollock 1993).

Still, it has been suggested (Hack et al. 1993) that interstitial impurities may have a detrimental impact on the low temperature fracture behavior of NiAl, especially considering the influence that such elements have on bcc metals, i.e. strain aging embrittlement of mild steels (Leslie 1981). Existence of a similar embrittlement phenomenon in NiAl has been suggested by Hack, Brzeski and Darolia (1992) and Brzeski et al. (1993) for NiAl single crystals containing 330-660 atomic parts per million (appm) total of C, O, and N, though the specific element(s) responsible for the embrittlement were not identified. George and Liu (1990) have shown that an intentional carbon addition of approximately 1000 appm reduces the room temperature tensile elongation of cast plus extruded polycrystalline NiAl from just over 2 percent to essentially zero. In this case, however, the loss in tensile ductility can be attributed simply to solution hardening effects, where C is responsible for increasing the yield strength of the alloy above the cleavage strength.

Nevertheless, the relationship between interstitial impurities and fracture behavior in NiAl is not clear. Work by Margevicius and Lewandowski (1991,1993) has demonstrated that the yield point commonly observed in polycrystalline NiAl can be eliminated by prestraining the material by hydrostatic pressurization prior to testing. The elimination of the yield point was attributed to an increase in the mobile dislocation density. However, the yield point could be recovered in the prestrained NiAl by aging the material at a temperature of 673 K (Margevicius et al. 1993). The flow behavior of polycrystalline NiAl due to prestrain and various thermal treatments as described by Margevicius and Lewandowski (1991,1993) and Margevicius et al. (1993) is a classic example of strain aging behavior due to the pinning of dislocations by obstacles such as interstitial impurities. Yet, in contrast to the fracture toughness results reported by Hack, Brzeski and Darolia (1992), the tensile ductilities of the polycrystalline NiAl samples tested by Margevicius et al. (1993) were independent of any combination of prestrain and/or thermal treatments.

Therefore, it is probably safe to conclude that interstitial elements have a definitive influence on the flow behavior of NiAl but the relationship between interstitial elements and fracture behavior is still unclear. Moreover, there has been no work done to identify those interstitial elements responsible for the various observations of strain aging behavior and embrittlement recorded in the literature. Consequently, the purpose of this chapter is to begin to sort out the effects of individual impurities on the mechanical behavior of NiAl by examining the consequences of nitrogen doping on the microstructure and tensile properties of NiAl.

8.2. Materials and Experimental Procedures

A nitrogen-doped NiAl alloy (Heat P1810) was produced by Homogeneous Metals, Inc., of Troy, NY, using a conventional vacuum atomization process (Fig. 4.1) with the exception that nitrogen gas was used instead of argon during powder production. During the vacuum atomization process, the molten metal is supersaturated with gas under high pressure. When the pressurized metal is suddenly exposed to a lower pressure (partial vacuum), the gas expands causing the molten liquid to atomize (Wentzell 1974). Usually an inert gas such as argon is used to pressurize the molten metal but in order to increase the nitrogen content in the subsequent NiAl powder material, nitrogen gas was used to charge the melt and was also used as a cover gas in the atomization chamber.

The resulting stoichiometric, -100/+325 mesh prealloyed NiAl(N) powder was placed in a mild steel extrusion can, which was evacuated and subsequently extruded at 1200 K to an area reduction ratio of 16:1. Round button-head tensile specimens were ground from the extruded rod so that the gage length of the sample was parallel to the extrusion direction. Sample dimensions were 30.5 mm and 3.2 mm for the tensile gage lengths and gage diameters, respectively. Prior to testing, all samples were electropolished in a 10% perchloric acid-90% methanol solution that was cooled to 208 K. Tensile tests were performed to failure in a universal screw-driven load frame at a constant crosshead velocity corresponding to an initial strain rate of $1.4\times10^{-4}\ s^{-1}$. Tests were performed in air between 300 and 700 K by heating the samples in a 3-zone resistance furnace. The temperature gradient along the tensile gage section was held within ± 2 K at all temperatures. True stress-plastic strain data were calculated from the load-time plots by accounting for the elastic strain and machine compliance and assuming constant volume conditions and uniform deformation. Yield stress values were determined by the 0.2% offset method.

Microstructural characterization of the as-extruded material and selected tensile samples was performed in a Phillips 400T transmission electron microscope (TEM) operating at 120 kV. Specimens for TEM observation were prepared by electrochemical polishing of thin slices cut from the as-extruded rod or gage sections of tested tensile specimens. Samples were prepared in a twin-jet Tenupol-3 polisher using a solution of 70% ethanol, 14% distilled water, 10% butylcellosolve, and 6% perchloric acid, cooled to 263 K. An applied potential of 20-25 V with a corresponding current of 10-15 mA produced electron transparent foils.

Table 8.1
Interstitial Content of N-Doped NiAl and Typical Polycrystalline NiAl Alloys
(atomic percent analysis)

Material	Carbon	Oxygen	Nitrogen
PM-NiAl(N)			
P1810	0.0057	0.0347	0.0904
PM-NiAl			
P541	0.0110	0.0170	0.0009
P1418	0.0143	0.0227	0.0006
CE-NiAl			
L2692	0.0114	0.0074	0.0006

8.3. Results

8.3.1. Microstructural characterization

Interstitial analysis of the as-extruded, nitrogen-doped material, designated PM-NiAl(N), is shown in Table 8.1. For comparison purposes, Table 8.1 also contains interstitial contents for two different binary NiAl alloys produced by the same powder metallurgy route as described in the experimental section except that argon gas was used instead of nitrogen gas during powder production. These binary powder metallurgy alloys are designated as PM-NiAl and can be further identified by the respective heat number, either P541 or P1418. Binary NiAl alloy P541 was the main material investigated in Chapters IV and V. Table 8.1 also contains the interstitial analysis of a typical cast plus extruded NiAl alloy L2692. This is the same binary CE-NiAl alloy that was presented in Chapter VII. Complete compositional analyses of all these alloys including Ni and Al concentrations are also listed in Appendix A.

The oxygen content in the PM-NiAl(N) was higher than the other three materials while the carbon level was less than half of that measured in the binary NiAl alloys. However, the main difference in interstitial level for these materials was the nitrogen content. The nitrogen level in the doped alloy was at least two orders of magnitude greater than in the conventional binary polycrystalline alloys listed in Table 8.1.

The as-extruded microstructure of the nitrogen-doped alloy consisted of fine (2-6 μm) equiaxed grains that contained a "recovered" structure composed of dislocation networks and subgrain boundaries, Fig. 8.1a. Semi-continuous stringers of very fine nanometer size precipitates were observed primarily along some of the grain boundaries as indicated by the arrows in Fig. 8.1b. Because not all the boundaries contained these stringers, they probably represent prior particle boundaries from the original powder particles. Energy dispersive spectroscopic analysis of the stringers indicated that the particles were rich in Al and N but also contained O. Individual particles that made up the stringers were too fine to analyze by selected area diffraction (SAD) but are most likely precipitates of AlN and Al_2O_3 (Aikin et al. 1994; Wheeler and Noebe 1994). Occasionally, larger precipitates, several hundred nanometers in size, were observed within individual grains. These precipitates were faceted or hexagonal in shape and are marked "A" in Fig. 8.1b. Analysis of microdiffraction patterns taken of these particles indicated that they were AlN precipitates (Noebe and Garg 1994). Therefore, the majority of the nitrogen in the doped alloy was not in solution but was instead present in the form of fine precipitates.

8.3.2. Tensile properties

Typical room temperature tensile true stress-true plastic strain curves for the PM-NiAl(N) alloy, the two binary NiAl alloys produced by conventional powder processing, and CE-NiAl are shown in Fig.8.2. All alloys represented in Fig. 8.2 were produced by extrusion at nominally 1200 K to an area reduction ratio of 16:1 and were tested at room temperature in the as-extruded condition. The binary PM-NiAl alloys represent samples from two different heats of powder and display roughly the same behavior. The three binary NiAl alloys exhibited discontinuous yield behavior. Both PM-NiAl alloys displayed a pronounced yield point and Luders strain while the CE-NiAl alloy exhibited a slight yield point and small Luders strain or region of low work hardening rate. Similar tensile stress-strain curves have been reported previously for binary NiAl alloys (Rozner and Wasilewski 1966; Hahn and Vedula 1989; Margevicius et al. 1993).

In contrast, the nitrogen-doped alloy exhibited a continuous and smooth yield behavior with no sign of a yield point or any discontinuous flow behavior. The PM-NiAl(N) alloy was also tested after receiving a thermal treatment (1100 K/2 hrs/FC) that maximizes the yield point and Luders strain in conventional NiAl alloys. Even after this thermal treatment, the PM-NiAl(N) alloy did not exhibit any indication of a yield point or Luders strain. The yield strength of the PM-NiAl(N) alloy was between that of the binary PM-NiAl and CE-NiAl. The higher yield strength of the two PM-NiAl alloys could possibly be attributed to a difference in stoichiometry since both alloys deviate from the absolute stoichiometric composition by several tenths of a percent (see Appendix A). However, the PM-NiAl(N) and CE-NiAl were stoichiometric and similar in composition within experimental accuracy (±0.2at.%). The room temperature tensile elongation of the nitrogen-doped alloy ranged from about 1.5 to 3% and was greater on average than any of the NiAl alloys previously studied at NASA LeRC.

The dislocation structure in a tensile sample of PM-NiAl(N) deformed to about 2% plastic strain at room temperature is shown in Fig. 8.3. Even after this relatively small strain, the dislocations began to organize into a cell structure. This type of dislocation structure has been observed in previous studies of near stoichiometric NiAl alloys after only a few percent plastic strain (Bowman et al. 1992; Nagpal and Baker 1992) and is indicative of very easy cross-slip within the NiAl grains.

The temperature dependent tensile properties (0.2% offset yield stress, fracture stress and tensile elongation) for the PM-NiAl(N) alloy are summarized in Fig. 8.4. The temperature dependent tensile behavior of the nitrogen-doped alloy was very similar to the cast plus extruded NiAl alloys, reported in Chapters VI and VII, and the powder processed NiAl presented in Chapter V. The yield strength decreased slightly with increasing temperature, while the fracture strength and tensile elongation increased very dramatically just above room temperature. The brittle-to-ductile transition temperature (BDTT) for this material was between 525 and 550 K, which seems to be the lower limit for NiAl alloys. Consequently, there is no indication that nitrogen has any embrittling effect on NiAl that would impact room temperature behavior or the BDTT.

8.4. Discussion

It is apparent from this study that the solubility of nitrogen and oxygen in NiAl is low, as evident from the presence of nitride and oxide precipitates. Furthermore, Auger analysis of as-extruded and solution annealed samples indicated that there was absolutely no tendency for segregation of nitrogen or other interstitial elements to the grain boundaries (Wheeler and Noebe 1993). The tensile test results indicate that the interstitial elements O and N, at levels in excess of their solubility limit, have absolutely no detrimental influence on the properties of NiAl. In fact, the room temperature tensile ductility is as good, and the BDTT is as low, as those reported for any polycrystalline NiAl alloys. The presence of nitrogen also did not affect the slip behavior of NiAl. Cross-slip was just as prominent in the doped alloy as in binary NiAl.

Even though the doped alloy has a total interstitial content of approximately 1300 appm compared to 300-400 appm for conventional purity materials, there was no indication of a yield point phenomenon in this material that would be indicative of dislocation-interstitial interactions. While the N-doped NiAl had a much higher total interstitial level compared to the other alloys studied, it did have a much lower carbon level. This suggests that carbon is primarily responsible for the strain aging effects observed in NiAl such as the discontinuous yield behavior shown in Fig. 8.2. Finally, the yield stress was significantly lower for the PM-NiAl(N) alloy than for similarly produced binary PM-NiAl alloys. Part of this strength difference could be attributed to variations in stoichiometry between the various PM alloys. But part of this difference in strength may be attributed to the lower C content in the NiAl(N) alloy. All three PM-alloys had yield stresses substantially higher than that for the cast plus extruded NiAl. The reason for the high yield stress for powder metallurgy processed materials and the effect of very minor deviations from stoichiometry on the mechanical properties of NiAl are presently under further investigation.

In a study by George and Liu (1990), the same amount of carbon was added to NiAl as nitrogen was added to NiAl in this investigation. However, carbon was attributed with embrittling NiAl (George and Liu 1990). In α-Fe, both nitrogen and carbon tend to have similar effects on properties resulting in various strain aging phenomena (Leslie 1981). Therefore, it was surprising that nitrogen was not detrimental to the mechanical properties of NiAl. This probably can be explained by the low solubility of nitrogen in

NiAl due to the automatic gettering of elements like N and O by Al. It is also likely that the lower level of carbon in the nitrogen-doped alloy compared to conventional NiAl alloys may be responsible for the good mechanical properties exhibited by the N-doped material.

In qualitative agreement with the good tensile ductility exhibited by the PM-NiAl(N), the alloy also possessed superior fracture toughness. In a companion study by Bieler, Noebe and Hebsur (1994) it was determined that the PM-NiAl(N) material had a fracture toughness of almost 8 ± 1 MPa $m^{1/2}$, independent of grain size. In contrast, binary NiAl, including the cast plus extruded and PM alloys studied in this investigation have fracture toughness values on the order of 5 MPa $m^{1/2}$ (Hebsur and Noebe 1993). This represents a 35% increase in fracture toughness for the nitrogen-doped material. It is not my contention that the nitrogen is responsible for this improvement in low temperature properties. On the contrary, it is probably the lower C content in this alloy that is the underlying cause of this behavior.

It appears that nitrogen and oxygen are innocuous to NiAl and have no detrimental impact on mechanical behavior. If anything, these elements are beneficial since the fine oxide and nitride precipitates help refine the grain size and also offer a substantial benefit in terms of elevated temperature creep strength (Whittenberger and Noebe 1993). For example the NiAl(N) alloy has a 200 K creep strength advantage over binary PM-NiAl alloys.

Conversely, carbon is most likely responsible for the strain aging effects observed in both polycrystalline and single crystal NiAl. To what extent carbon is harmful to properties is still an open issue. However, it is now apparent that a lower carbon level would seem to result in a higher tensile ductility and fracture toughness for both single crystal (Brzeski et al. 1993) and polycrystalline NiAl. Nevertheless, additional work needs to be performed on the NiAl(C) system in a rational and systematic fashion using alloys with controlled interstitial levels. Such a program is in progress at NASA LeRC. Further efforts in studying the effects of carbon on the NiAl system are in progress at The University of Florida, Oak Ridge National Laboratory, The University of Tennessee and General Electric Aircraft Engines. Therefore, additional results on the effect of interstitial elements, particularly C, should be forthcoming to the literature from a number of sources over the next several years.

8.5. Summary and Conclusions

1. The solubility of nitrogen in NiAl is well below 900 appm.
2. Nitrogen has no adverse impact on the tensile properties of NiAl. The nitrogen containing material exhibited above average yield strength, tensile strength, and tensile elongation compared to other NiAl alloys investigated during this study. The brittle-to-ductile transition temperature for the PM-NiAl(N) alloy was between 525 and 550 K, one of the lowest BDTT's reported.
3. The temperature dependence of the tensile properties for the nitrogen-doped alloy was similar to that of binary NiAl. The yield strength decreased mildly with temperature while the fracture stress and tensile ductility were constant and then increased dramatically at the BDTT.
4. While nitrogen and oxygen do not appear to be a concern for mechanical properties, carbon should be considered a detrimental impurity in NiAl. However, additional research needs to be performed on NiAl(C) alloys to understand the relationship between flow and fracture behavior and C level.

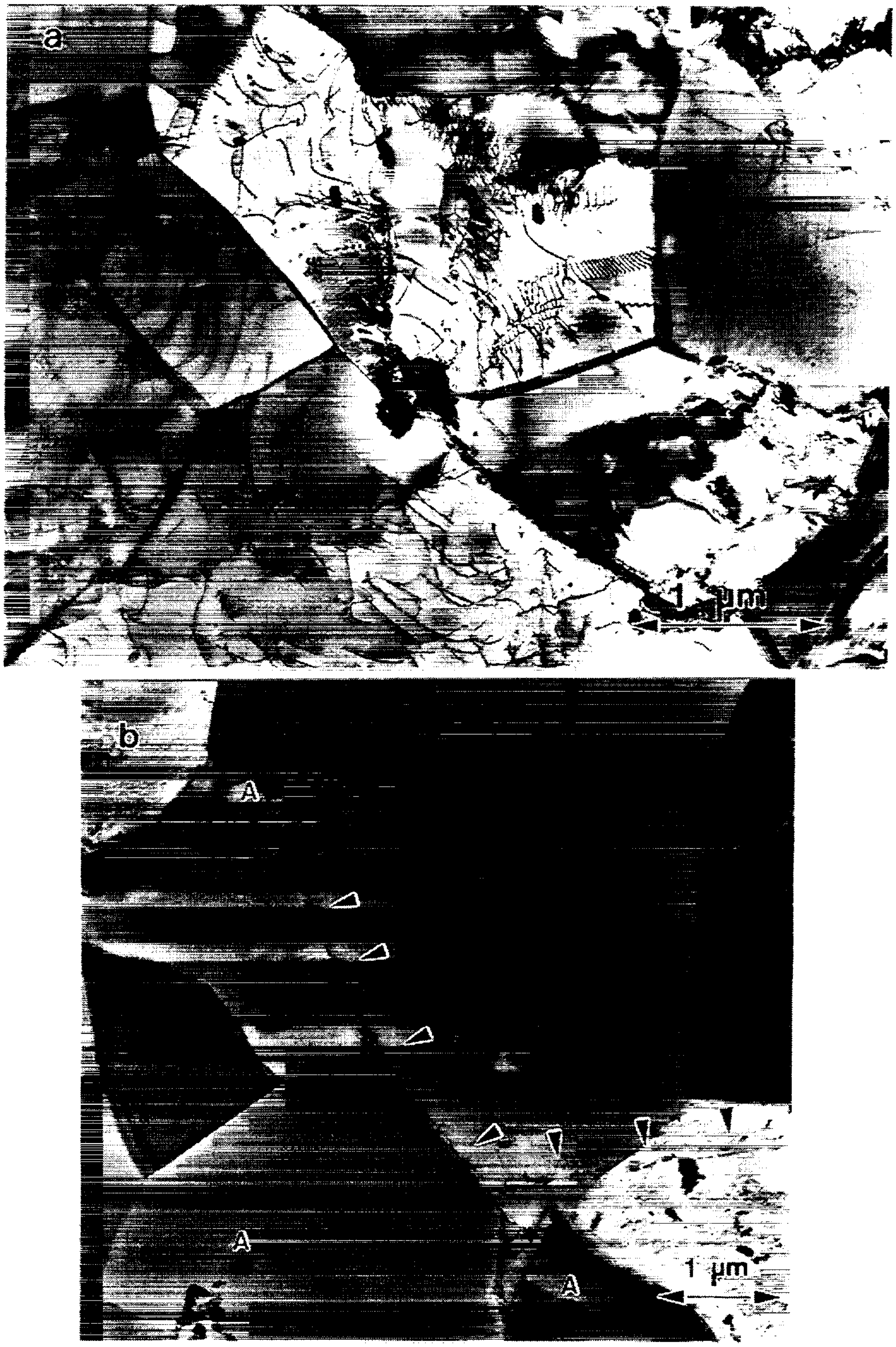

Fig. 8.1. Microstructure of as-extruded PM-NiAl(N): a) equiaxed grains containing dislocation networks and subgrain boundaries and b) AlN precipitates (marked "A") and prior particle boundaries (indicated by the arrows).

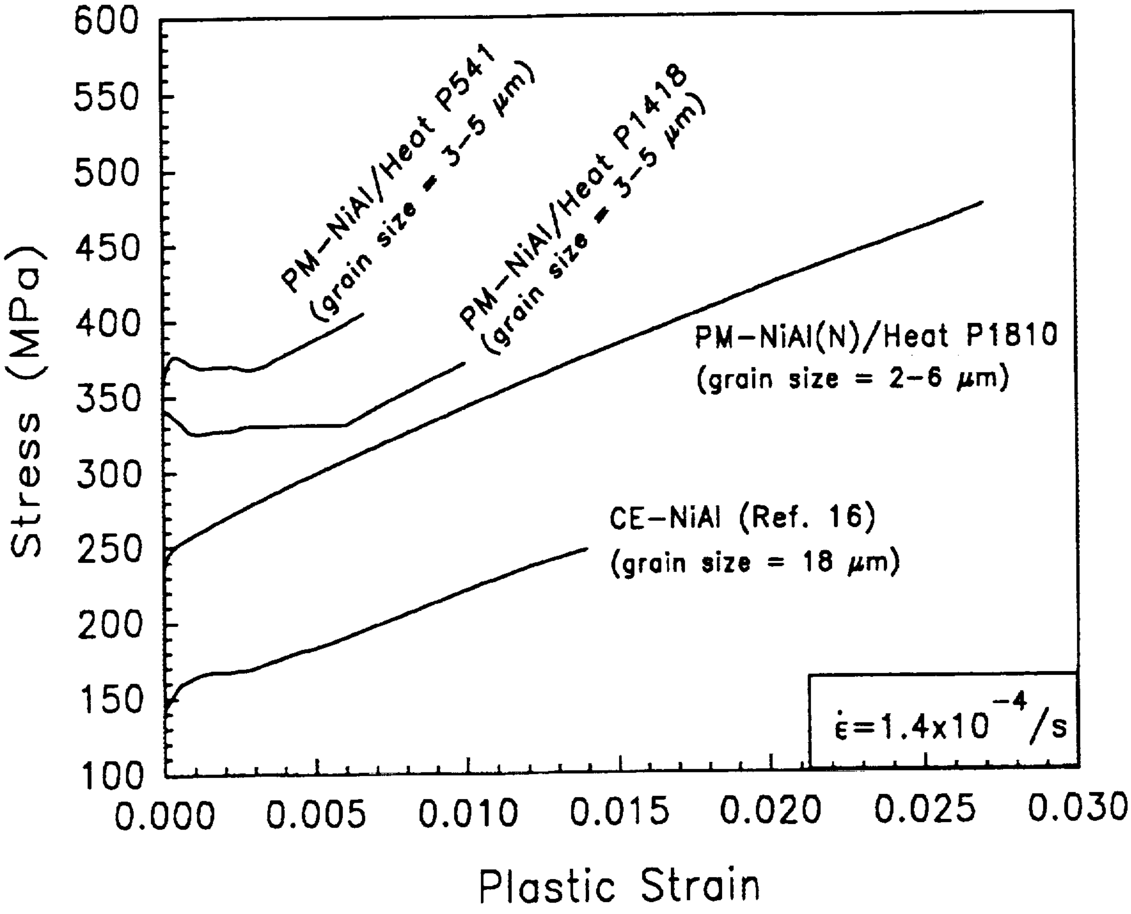

Fig. 8.2. Room temperature tensile stress-strain response for as-extruded NiAl alloys and PM-NiAl(N). Interstitial levels for all alloys are reported in Table I.

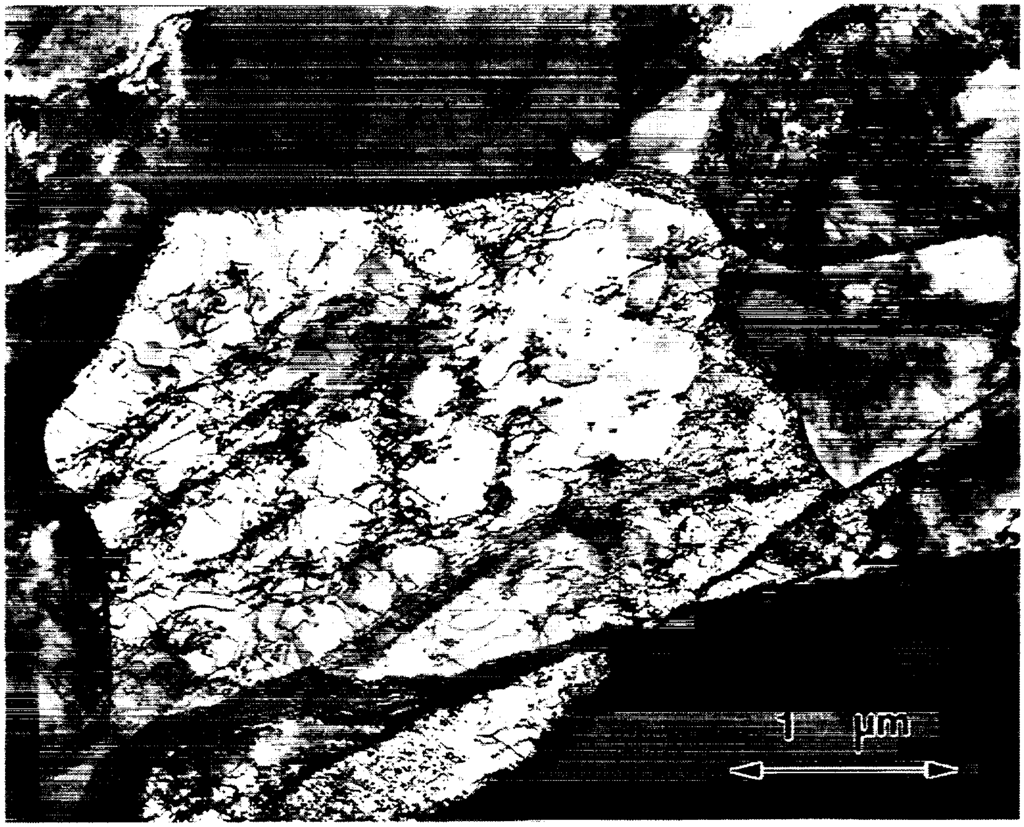

Fig. 8.3. Dislocation morphology in the PM-NiAl(N) alloy deformed in tension at room temperature to approximately 2% plastic strain.

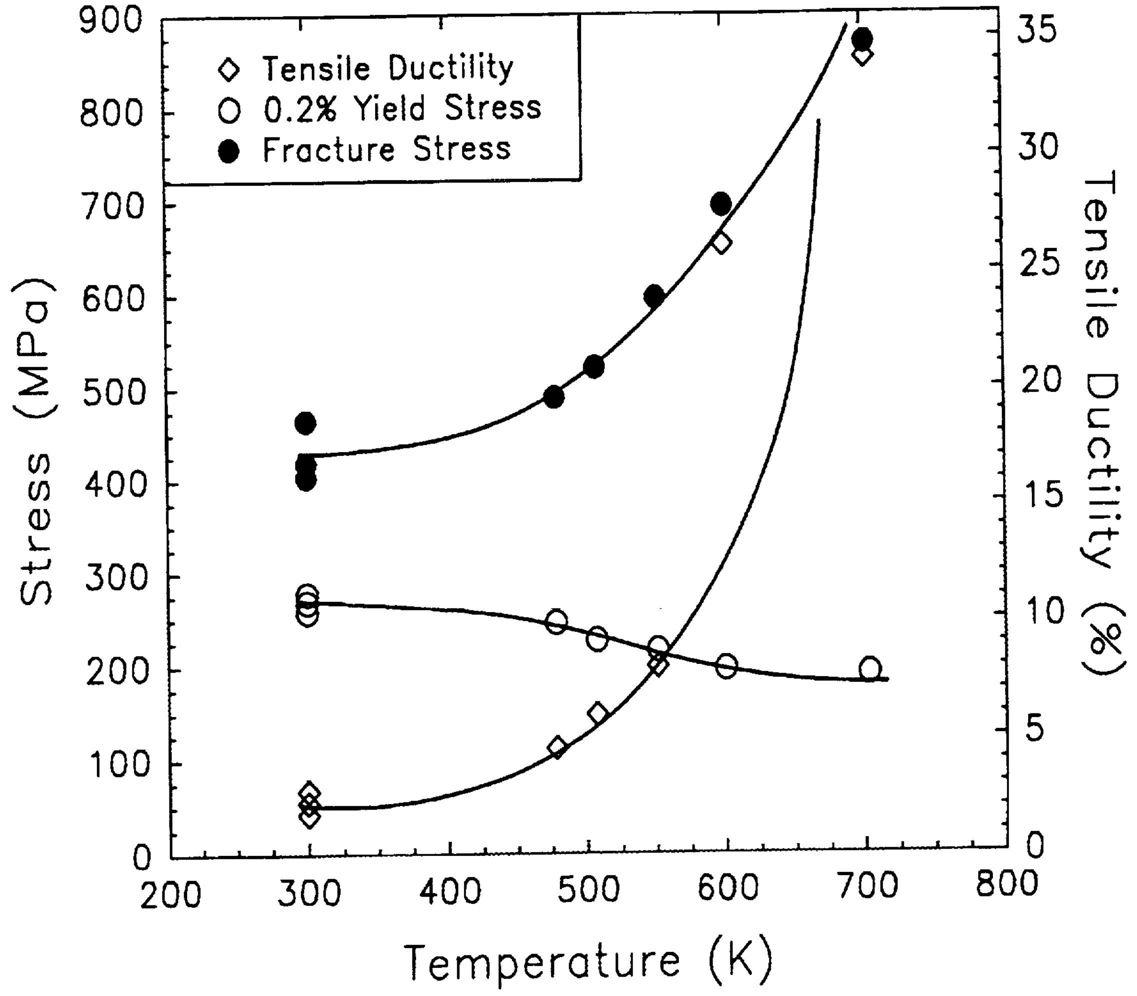

Fig. 8.4. Temperature dependence of the tensile properties (0.2% offset yield stress, fracture stress and tensile elongation) for nitrogen-doped NiAl tested at a strain rate of 1.4x10^{-4} s^{-1}.

CHAPTER IX
PROSPECTS FOR FUTURE ALLOY DEVELOPMENT

9.1 Flow and Fracture Behavior of Polycrystalline NiAl

Through this investigation and companion studies a more accurate and comprehensive understanding of the flow and fracture behavior of polycrystalline NiAl near the BDTT has been developed. Below the BDTT NiAl behaves in a brittle manner. Brittle intergranular fracture in binary, near stoichiometric NiAl is a consequence of incompatible deformation at the grain boundaries due to the operation of only three independent slip systems. Intergranular fracture is not a consequence of 'weak' grain boundaries nor should the grain boundaries in NiAl be considered inherently weak. In the absence of plastic deformation, as exhibited by ternary or off-stoichiometric alloys, fracture occurs by cleavage originating at internal or surface defects.

Nevertheless, binary near-stoichiometric NiAl can exhibit significant macroscopic plasticity when tested in compression and up to a few percent tensile elongation at room temperature. These observations are not a contradiction of the Von Mises criterion, since on a microscopic scale, fracture occurs at the grain boundaries due to the generation of incompatible strains. Because NiAl is bound by the Von Mises criterion, it does not have the potential for exhibiting significant tensile ductility below its BDTT. Furthermore, grain size refinement alone will not solve this predicament since it does not address the root problem for the poor ductility.

At intermediate temperatures the mechanical behavior of NiAl changes dramatically. While the yield stress is only mildly affected by temperature, fracture stress, fracture toughness and tensile elongation are essentially independent of temperature for a few hundred degrees above room temperature and then increase significantly over a very small temperature range. This dramatic change in mechanical behavior is known as the BDTT. Polycrystalline NiAl undergoes this brittle-to-ductile transition at a temperature of about 550 K, although certain alloying additions can shift the BDTT to temperatures above 1000 K. The transition in mechanical behavior at the BDTT was found to correspond to a change in deformation mechanism as revealed in an Arrhenius representation of the yield stress. With *in-situ* TEM analysis it was determined that the change in deformation mechanism resulting in the BDTT was due to the onset of localized dislocation climb processes in the vicinity of the grain boundaries, providing additional deformation modes that allow the Von Mises criterion to be fulfilled. Fulfillment of the Von Mises criterion was corroborated by the absence of intergranular microcrack formation in samples deformed just above the BDTT. The localized climb processes responsible for the BDTT operate at much lower temperatures than bulk climb processes, which are not dominant until temperatures greater than about 1000 K. Thus, explaining the low BDTT for binary NiAl.

Alloying additions such as Zr that tend to segregate to the grain boundaries and retard these localized climb processes will cause an increase the BDTT. It should also be noted that these alloying additions do not have to be present in very large concentrations to have a dramatic impact on the BDTT as long as they strongly segregate to the grain boundaries. Also, the overall stoichiometry of binary or ternary NiAl alloys has a significant effect on the BDTT, implying a strong relationship between bulk composition and grain boundary structure and/or composition. Non-stoichiometric alloys, especially those that are Al-rich have much higher BDTT's than near stoichiometric compounds.

However, the BDTT should be viewed as a relative temperature. As already mentioned, it is dependent on composition. For a specific alloy composition, the BDTT is strain rate dependent for rates greater than about 10^{-4} s^{-1}. This is a natural consequence since the BDTT is due to a rate dependent deformation mechanism in the form of dislocation climb. This fact should be of concern , irrespective of use temperature, when considering NiAl for applications where impact loading could occur.

9.2. Potential Alloying Schemes

With the additional information now available concerning the flow and fracture behavior of NiAl, the question arises as to how this information can be used to design a better material. Because the BDTT for polycrystalline NiAl is due to thermally activated deformation processes that do not occur at temperatures much below 550 K, it is unreasonable to expect a BDTT below room temperature. (Unless you raise room temperature). To shift the BDTT to much lower temperatures, an alloying scheme would have to be developed that resulted in the operation of alternative or additional slip modes. This approach will be discussed in section 9.2.2. One of the few other viable alternatives is to take this research full circle and re-investigate the option of designing two-phase alloys as was originally discussed in Chapter III. Through extrinsic toughening mechanisms and slip transfer processes that seem to be uniquely successful in NiAl-based alloys, it may be possible to design a well rounded engineering material. Consequently, a second look at the processing and design of two-phase alloys based on NiAl will be discussed in section 9.2.3.

Finally, incremental improvements in low temperature properties may be possible through general compositional control, microalloying or macroalloying additions. This approach is summarized in section 9.3.1. No momentous breakthroughs, equivalent to the ductilization of Ni_3Al by B, are anticipated through this general approach. Yet, it still may be possible to generate incremental improvements in properties. For example, the NiAl(N) alloy discussed in Chapter VIII had good tensile ductility and a 35% improvement in fracture toughness relative to other polycrystalline NiAl alloys. While this improvement in properties was probably due more to a lower C content rather than to the presence of N, this does represent the kind of improvements in properties that may be achievable.

9.2.1. Possible macroalloying and microalloying additions.

In general, alloying additions and their effect on the microstructure of NiAl can be summarized by their position in the periodic table (Noebe Misra and Gibala 1991; Cotton, Noebe and Kaufman 1993d) as demonstrated in Fig. 9.1. Because NiAl is isostructural with a number of other intermetallic compounds and has a wide phase field, the solubility of Mn, Cu and groups VIII and IIIA elements is generally quite large. This family of elements offers a considerable alloying potential that is mainly unexplored at this time. The problem is that there is no scientific rationale for studying many of these elements other than for some serendipitous effect.

The refractory metal group VIB elements plus V and Re exhibit very little solubility in NiAl and form no ternary intermetallic phases, with the exception of V in Ni-rich alloys. Instead, these elements form pseudobinary eutectic systems with stoichiometric NiAl and therefore, have the potential to both strengthen NiAl at high temperatures and act as a ductile reinforcing agent at low temperatures (Johnson et al. 1992,1993). Groups IIIB, IVB and VB elements also have very limited solubility in NiAl and form at least one ternary ordered intermetallic compound with Ni and Al. The most common of these intermetallics are the Heusler phases, Ni_2AlX, and the Laves phases, NiAlX. These are ordered phases that are significantly more brittle than NiAl and would, therefore, preclude the development of a ductile phase toughened material. However, NiAl/Heusler and NiAl/Laves alloys are being actively investigated because of their superior creep resistance. In fact, the most creep resistant NiAl based alloys produced to date are single crystal NiAl/Heusler compounds. (Darolia 1993)

While many elements have limited solubility in NiAl, microalloying schemes are possible with any of the elements in the periodic table. But to date, microalloying studies have been fairly limited. Microalloying additions of Fe, Ga and Mo at the 0.1-0.2 at.%

level result in a consistent increase in the room temperature tensile ductility of soft orientation single crystal NiAl (Darolia, Lahrman, Field 1992). The mechanism for this increase in ductility has not been determined, though, a change in slip vector or even an obvious modification in dislocation morphology has been ruled out (Darolia, Lahrman and Field 1992). A similar alloying approach with these elements has been attempted on polycrystalline NiAl without success, as discussed in Chapter VII. The major limitation in improving the tensile properties of polycrystalline NiAl through microalloying additions is that the additions are so small, a change in slip behavior to a slip system that results in five independent deformation modes is not expected. Therefore, the grain boundary compatibility problem, which is a limiting factor in the low temperature ductility of polycrystalline NiAl, is not resolved. Conversely, many microalloying additions have been found to have a very dramatic but deleterious effect on the mechanical properties of polycrystalline NiAl, as demonstrated for Zr additions.

In the case of single crystalline NiAl, microalloying additions are probably acting as gettering agents for carbon. The influence of the alloying addition is not in altering the behavior of NiAl, but in gettering a detrimental impurity in the intermetallic, permitting NiAl to display its inherent properties. The similarity in the room temperature tensile properties of high purity, low interstitial NiAl and microalloyed single crystals supports this idea since both materials exhibit 4 - 5% tensile elongations, compared to 1% or less for commercially pure NiAl (Johnson, et al. 1992; Lahrman, Field and Darolia 1993a).

Based on the present knowledge of NiAl, the following considerations should be taken into account when developing a general alloying scheme for NiAl:

1. Process the material in a manner that minimizes the carbon content. This may provide an increase in fracture toughness.

2. In addition, it may be necessary to getter the C by using ternary alloying additions such as Fe. This is probably the real benefit behind the microalloying effect observed in single crystal NiAl. While this approach does not seem to make any difference in polycrystalline

alloys, it does not appear to jeopardize properties (see Chapter VII). Furthermore, it may be necessary to use a post-processing heat treatment to optimize the gettering effect in polycrystalline alloys. This possibility has not been examined to date.

3. Take into account the site occupancy of all the alloying additions and design the overall alloy composition so that it is as close to stoichiometric as possible. Otherwise an unnecessary increase in the BDTT may result.
4. Pray for serendipity.

9.2.2 Alloying to impart a change in slip character

Another strategy for improving the ductility and toughness of polycrystalline NiAl is the addition of ternary macroalloying elements in an effort to alter or modify slip processes (Law and Blackburn 1987; Cotton, Noebe and Kaufman 1993b). The general approach has been the identification of elements which should lower the ordering energy of NiAl, thus making <111> slip easier. Cr, Mn and V are reasonable choices for promoting <111> slip in NiAl based on calculations resulting from interatomic potential models (Hong and Freeman 1991). These models have demonstrated that up to 70% reductions in APB energy are possible when Cr, Mn, or V additions are substituted for Ni or Al at levels of at least 17 at.%. In reality, such large alloying additions are not possible. The solubility of Cr in NiAl is approximately 1 - 2 at.% on either sublattice (Cotton, Noebe and Kaufman 1993c). The solubility of V in NiAl is on the order of 5 at.% percent when substituted for Al and essentially zero when substituted for Ni (Cotton, Kaufman and Noebe 1991), which according to calculations, would be the preferred substitution method for lowering the APB energy.

In spite of the low solubility of Cr in NiAl, but in apparent agreement with the concept presented above, <111> slip has been reported in polycrystalline NiAl alloyed with approximately 5% Cr or Mn (Law and Blackburn 1987). Although the operation of <111> slip satisfies the requirement for generalized polycrystalline plasticity, no tensile ductility was reported in these materials at low temperatures. A change in fracture mode from intergranular to transgranular cleavage was also observed. However, as discussed in Chapter IV a change in fracture mode would be expected since the yield strength of the alloy was greatly affected by the alloying additions.

Nevertheless, this result prompted more detailed work on NiAl(Cr) alloys by Cotton et al. (1993a-c). Analysis of over 2000 dislocation segments in deformed NiAl(Cr) alloys covering 16 different ternary alloy compositions, failed to identify any significant <111> dislocation activity. To eliminate any chance that processing or impurity effects could influence slip behavior, a piece of the original casting studied by Law and Blackburn was also examined. Again, no evidence of <111> dislocations was observed in the as-cast or deformed material. Therefore, in spite of the contention by Law and Blackburn (1987), Cr additions to NiAl do not promote <111> slip.

Fe would be another obvious alloying addition for slip alteration since B2 FeAl alloys deform by <111> dislocations (Crimp and Vedula 1991). However, single phase β-Ni-Fe-Al alloys like binary NiAl exhibit only 0 to 2.5% tensile ductility at room temperature (Guha, Munroe and Baker 1991; Russell et al. 1991; Raj, Locci and Noebe 1992). As in the case of NiAl, the observed slip vector in these Ni-Fe-Al alloys was <100> so that the ternary alloys were still slip system limited. The slip behavior of a complete series of polycrystalline (Ni,Fe)-40Al alloys has been examined by Patrick et al. (1991). Their final conclusion was that at room temperature <100> slip is dominant in alloys containing up to 40 at.% Fe. Despite the lack of tensile ductility, ternary Ni-Fe-Al alloys may exhibit very high toughness levels, approaching 25 MPa $m^{1/2}$ in fine-grained material (Kostrubanic et al. 1991).

Other studies that are usually referenced to support the operation of <111> slip in NiAl due to Cr or V additions were performed on [001] oriented single crystals (Field, Lahrman and Darolia 1991c; Miracle, Russell and Law 1989). Since <111> is already the preferred slip vector in this crystal orientation, no conclusion about the influence of alloying on slip mode can be drawn from these studies. Therefore, alloying of NiAl with the intention of altering the operative slip vector has been unsuccessful to date. Not only is the slip system left unchanged, but the BDTT of NiAl macroalloyed with Cr (Cotton, Noebe and Kaufman 1993b) and Fe (Raj, Locci and Noebe 1992) is significantly increased compared to the BDTT of binary NiAl. However, very little effort has been expended on NiAl(Mn) alloys. Due to the much greater solubility of Mn in NiAl compared to either Cr or V (Chakrabarti 1977), more extensive investigation of Mn on the slip behavior of NiAl is warranted.

9.2.3 Ductile phase reinforced and multi-phase alloys

No breakthroughs have occurred resulting in significant improvements in either tensile ductility or fracture toughness of single phase NiAl alloys. Sound approaches, such as alloying for slip modification have been attempted and have failed. Therefore, other than look for applications that can accommodate the present level of ductility and toughness in NiAl alloys, multi-phase alloy design is about the only reasonable approach left for consideration. Instead of trying to alter the inherent properties of the intermetallic, this alternative approach to enhancing the ductility and toughness of NiAl is based modifying the microstructure of the material. The mechanical behavior of NiAl could be altered through operation of extrinsic toughening mechanisms. A significant improvement in properties can also occur through slip transfer processes, as demonstrated in Chapter III, which is an intrinsic toughening mechanism. An example of an intermetallic system that has been successfully toughened by such an approach is Ti_3Al through the use of two-phase Ti-24Al-11Nb or similar alloys (Chan 1990b). Unfortunately, a successful counterpart to this system has not been identified for NiAl, though work is continuing in this area.

Furthermore, property goals have been relaxed. NiAl alloys would probably be acceptable with little or no tensile ductility if the fracture toughness could be increased to at least 20 MPa $m^{1/2}$, assuming no significant degradation of other properties and the ability to meet a yet undefined creep strength. Therefore, future research will tend to emphasize toughness testing and alloying for improved fracture resistance. Alloy design based on multi-phase structures is the most promising method for achieving this goal with a NiAl/refractory metal alloy being the most likely system to succeed in the short term.

Through optimization of processing and alloying conditions, NiAl/α alloys can exhibit fairly reasonable fracture toughness values. For example, when a NiAl-9Mo eutectic is arc melted it has a fracture toughness of approximately 9 MPa $m^{1/2}$ (Subramanian et al. 1990). But after directional solidification the eutectic composite consists of ~11 vol.% of 1 μm diameter rods in a single crystal NiAl matrix and has a fracture toughness of 15 MPa $m^{1/2}$ due to crack bridging and ductile rupture of the Mo ligaments (Darolia et al. 1992). However, increasing the Mo content beyond the eutectic composition does not result in any additional toughening (Johnson et al. 1992). Directionally solidified eutectics containing other refractory metal phases demonstrate similar or higher levels of toughness. Directionally solidified NiAl-Cr and NiAl-Cr(Mo) eutectics have fracture toughness values of approximately 18 - 24 MPa $m^{1/2}$ compared to only 5 -6 MPa $m^{1/2}$ for as-cast NiAl-Cr eutectics (Darolia et al. 1992; Johnson et al. 1994). It has even been suggested (Sauthoff 1993) that extruded NiAl-10Cr alloys, when given the proper heat treatment, can exhibit fracture toughness values on the order of 20 MPa $m^{1/2}$.

Encouraging results have also been generated by Johnson et al. (1993,1994) in the development of multiphase NiAl-based alloys that exhibit a good combination of creep strength and fracture toughness. These NiAl-based alloys contain a refractory metal phase for improved fracture resistance and/or an intermetallic Laves phase for additional creep strength. The properties of these two- and three-phase alloys are summarized in Fig. 9.2. This figure also demonstrates the difficulty in balancing toughness and creep resistance in the same alloy. There are several very creep resistant alloys that have low toughness and a few very tough alloys that have poor creep strength and no environmental resistance. But there are also a few alloys that have a fairly good combination of properties. These are present in the upper right corner of the figure.

Figure 9.3 is the same plot as Fig. 9.2 except with the incorporation of an average Ni-base superalloy. Even though all the NiAl-based data in the plot are from one research group (Johnson et al. 1992,1993,1994), no other NiAl-based alloys significantly exceed the window of properties defined in the figure for the NiAl-based eutectics. From Fig. 9.2, it is clear that NiAl alloys still have a long way to go to match the balance of properties obtained with conventional superalloys. However, there are countless quaternary and higher order NiAl alloy systems to be investigated that are similar to the few shown in Figs. 9.2 and 9.3 but may posses even better properties. Therefore, multiphase alloy design is still about the only reasonable approach in the development of structural NiAl alloys.

9.3. Concluding Remarks

Our knowledge of the behavior of NiAl has come a long way since the first exploratory studies of the late 1950's and early 1960's. Most of this progress has emerged in only the last few years and along with this investigation have contributed to the overall understanding of this intermetallic system. Still, many very fundamental questions remain to be answered. These include the type of structural defects formed in ternary and higher order alloys, a description of how deviations from stoichiometry and ternary additions effect grain boundary structure and chemistry, and finally the relationship between these structural changes and properties. A fundamental understanding of the cleavage behavior of NiAl and a better understanding of the intrinsic behavior of pure "NiAl" and the effect that interstitial elements have on properties is also lacking. Of all these issues, the only one that is receiving attention at the moment is the effect of interstitial carbon on mechanical behavior. Consequently, the bulk of the defect structure and grain boundary structure versus property relationships in the NiAl system are not being addressed in any systematic fashion. This report lays the groundwork in these areas by giving investigators a place to begin new research efforts to prove or disprove the hypotheses proposed in the later chapters.

Even more critical than the lack of fundamental knowledge about NiAl alloys is the ever remaining issue of poor tensile ductility and fracture toughness. Hopefully, under these tight economic conditions there will actually be time to develop this intermetallic into a structural alloy. If instead, economic pressures force the cancellation of the single crystal NiAl development efforts at General Electric, there will be a ripple effect throughout the entire intermetallics community. Such news would hasten the redirection of NiAl research at national labs such as NASA LeRC and Oak Ridge, which would in turn cause a significant curtailment in research at the university level. This creates a major dilemma. In this period of short term research goals, there is diminishing interest in NiAl. A breakthrough or some major improvement in low temperature properties is necessary to continue to generate interest in this material (particularly from major funding organizations). But without more fundamental research on this material a breakthrough is less likely. Some degree of patience is necessary and justified. For instance, Ni-based superalloys and Al-Li alloys for aerospace applications were developed over a period of several decades and at a much greater intensity level than what NiAl is presently experiencing.

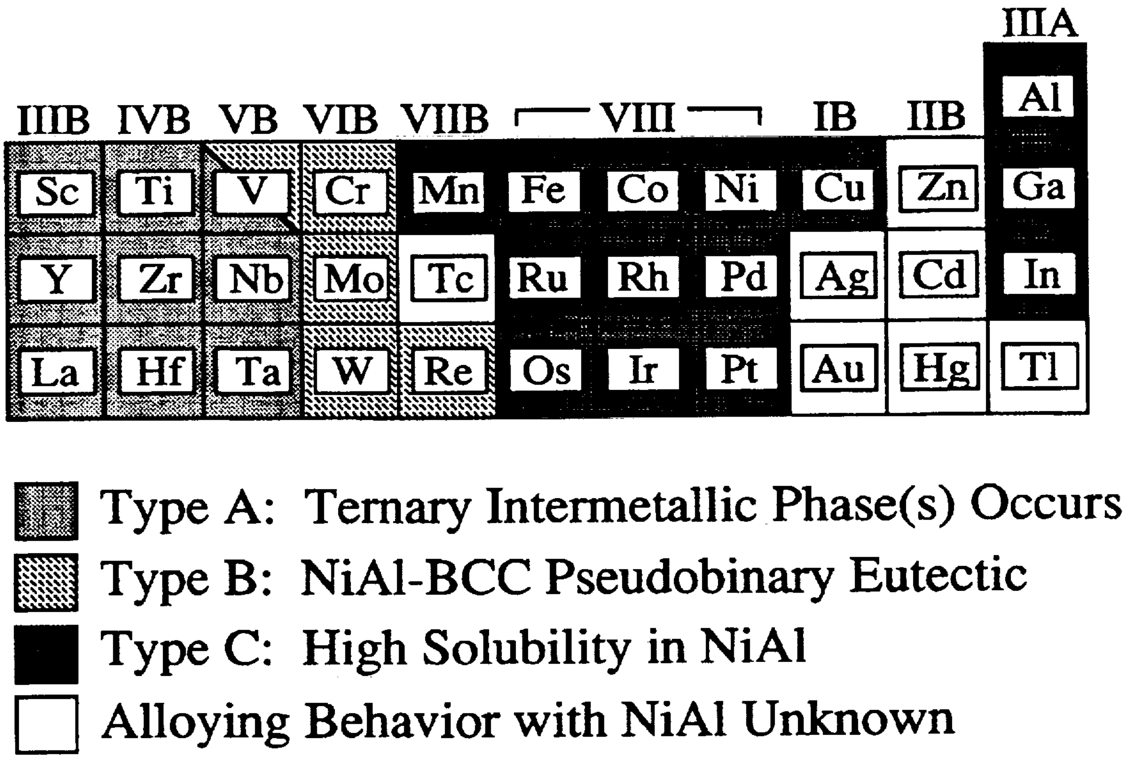
IIIA
IIIB IVB VB VIB VIIB VIII IB IIB
Al
Sc Ti V Cr Mn Fe Co Ni Cu Zn Ga
Y Zr Nb Mo Tc Ru Rh Pd Ag Cd In
La Hf Ta W Re Os Ir Pt Au Hg Tl
Type A: Ternary Intermetallic Phase(s) Occurs
Type B: NiAl-BCC Pseudobinary Eutectic
Type C: High Solubility in NiAl
Alloying Behavior with NiAl Unknown

Fig. 9.1. Portion of the Periodic Table of Elements illustrating the general effect of ternary alloying additions on the microstructure of NiAl. (After Cotton, Noebe and Kaufman. 1993d.)

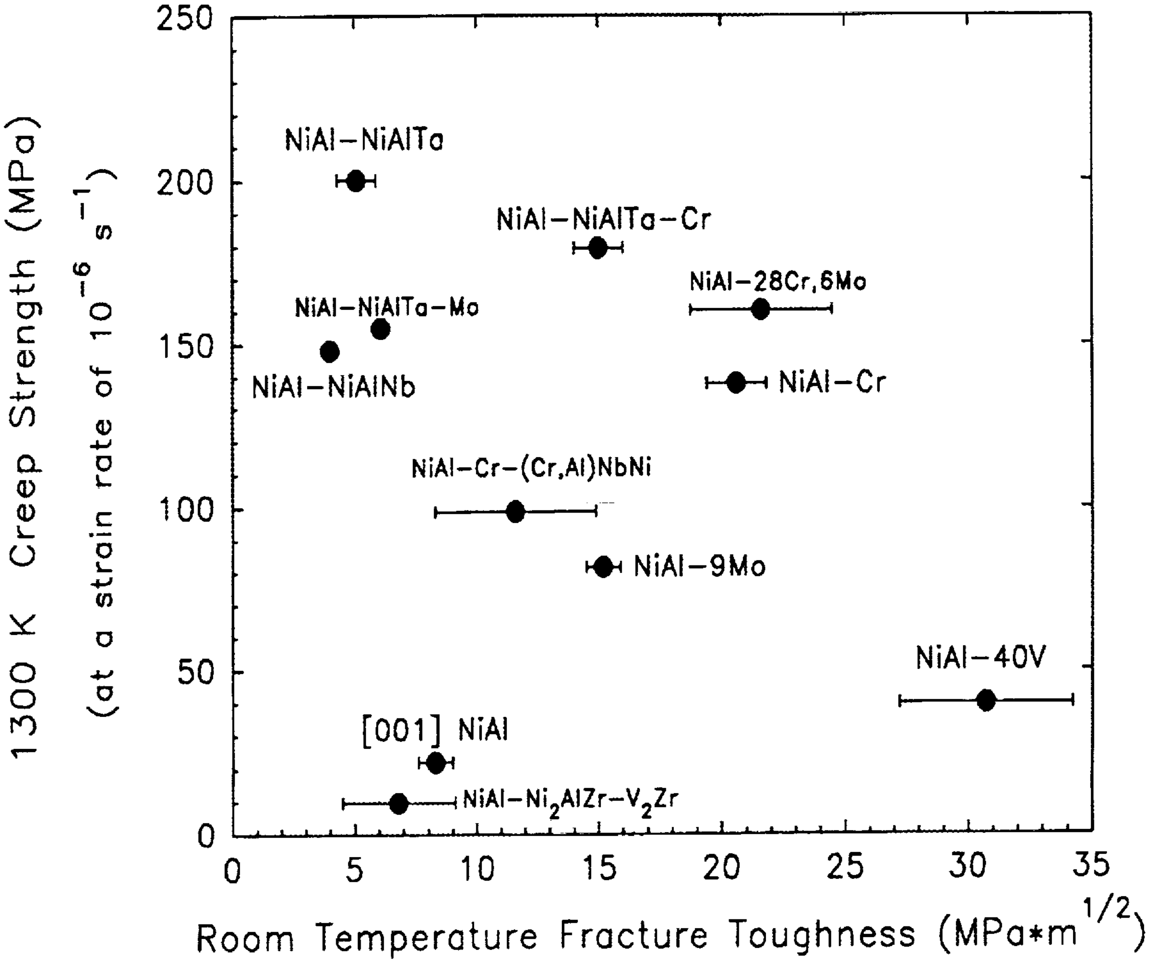

Fig. 9.2. Relative performance of NiAl-based eutectics compared on a creep strength versus room temperature fracture toughness basis. (After Johnson et al 1992, 1993, 1994).

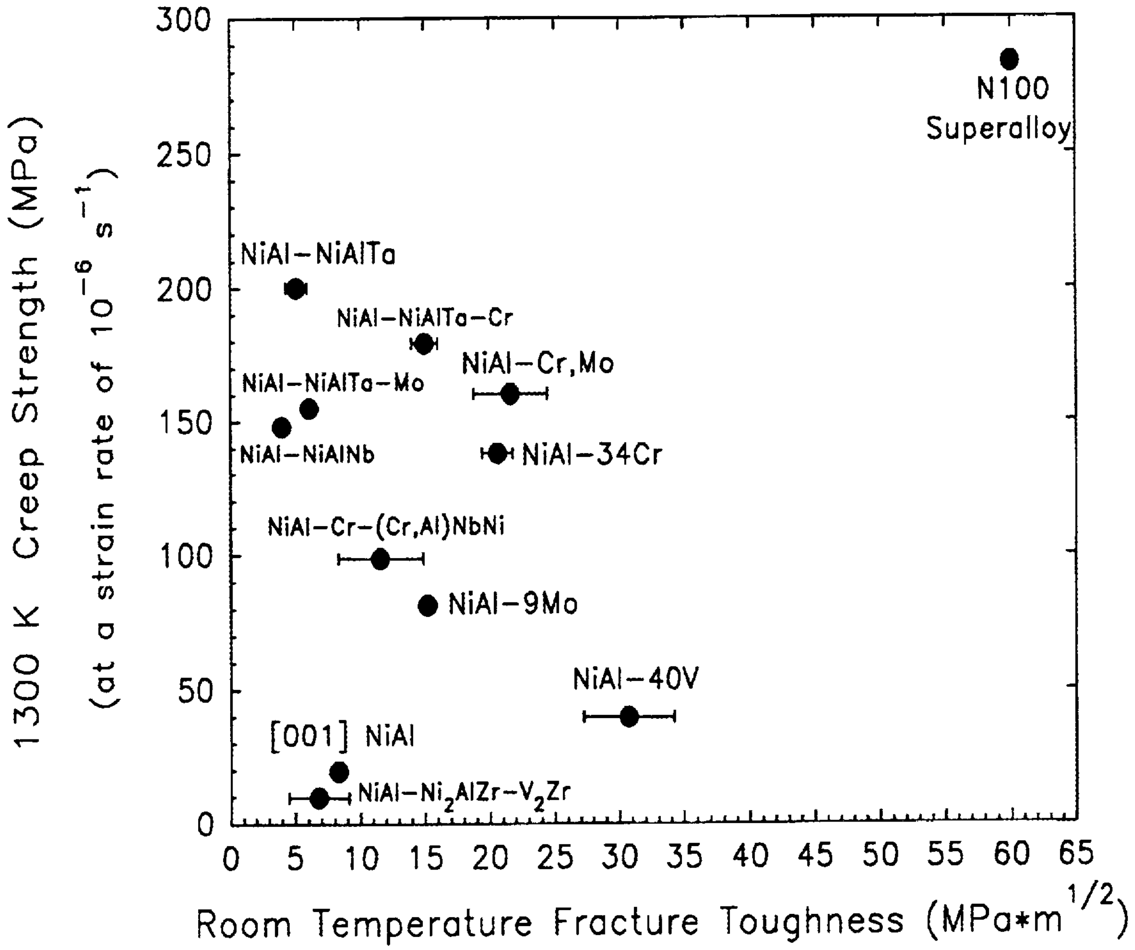

Fig. 9.3. Relative performance of NiAl-based eutectics compared to a typical Ni-base superalloy indicating how much progress is still needed to compete with conventional materials.

REFERENCES

Antolovich, S.D. and Fahr, D 1972. An Experimental Investigation of the Fracture Characteristics of Trip Alloys. *Eng. Fract. Mech.* **4**:133-144.

Aikin, B.J.M., Dickerson, R.M., Jayne, D.T., Farmer, S. and Whittenberger, J.D. 1994. Formation of Aluminum Nitride During Cryomilling of NiAl. *Scripta Metall. Mater.* **30**:119-122.

Aoki, K. and Izumi, O. 1979. Improvement in Room Temperature Ductility of the L12 Type Intermetallic Compound Ni_3Al by Boron Addition. *J. Jpn. Inst. Met.* **43**:1190-1196.

Ashby, M.F. 1970. The Deformation of Plastically Non-homogeneous Materials. *Philos. Mag.* **21**:399-424.

Ashby, M.F. 1972. A First Report on Deformation-Mechanism Maps. *Acta Metall.* **20**:887-897.

Ashby, M.F., Gandhi, C and Taplin, D.M.R. 1979. Fracture-Mechanism Maps and Their Construction for F.C.C. Metals and Alloys. *Acta Metall.* **27**:699-729.

Aswath, P.B. and Suresh, S. 1989. Fatigue Crack Growth Behavior of a Titanium Aluminide Intermetallic. *Mater. Sci. Eng. A* **114**:L5-L10.

Baker, I. and Nagpal, P. 1990. Properties of B2 Compounds. In High Temperature Aluminides and Intermetallics, ed. S.H. Whang et al., pp. 425-452. Warrendale, PA.: The Minerals, Metals and Materials Society.

Baker, I., Nagpal, P., Liu, F. and Munroe, P.R. 1991. The Effect of Grain Size on the Yield Strength of FeAl and NiAl Alloys. *Acta Metall. Mater.* **39**:1637-1644.

Baker, I. and Schulson, E.M. 1984. The Structure of Extruded NiAl. *Metall. Trans. A* **15**:1129-1136

Ball, A. and Smallman, R.E. 1966a. The Deformation Properties and Electron Microscopy Studies of the Intermetallic Compound NiAl. *Acta Metall.* **14**:1349-1355.

Ball, A. and Smallman, R.E. 1966b. The Operative Slip System and General Plasticity of NiAl-II. *Acta Metall.* 14:1517-1526.

Bannister, M.K., Spearing, S.M., Lofvander, J.P.A. and De Graef, M. 1992. Fatigue of Extruded Steel/NiAl Composites. In Intermetallic Matrix Composites II, ed. D.B. Miracle et al., pp. 177-182, Pittsburgh, PA: Mat. Res. Soc. Symp. Proc. Vol. 273.

Barker, D.R. 1982. The Strength and Ductility of Polycrystalline NiAl. M.E. Thesis, Dartmouth College, Hanover, N.H., 1982.

Barrett, C.A. 1988. Effect of 0.1 at.% Zirconium on the Cyclic Oxidation Behavior of β-NiAl. *Oxid. Met.* **30**:361-390.

Benhaddane, K. and Beauchamp, P. 1986. Core Structure of the a<100><001> Edge Dislocation in a B2 ordered Alloy. *Phys. Status Solidi (A)* **98**:195-202.

Berkowitz, A.E., Jaumot, F.E. and Nix, F.C. 1954. Diffusion of Co^{60} in Some Ni-Al Alloys Containing Excess Vacancies. *Phys. Rev.* **95**:1185-1189.

Bevk, J., Dodd, R.A. and Strutt, P.R. 1973. The Orientation Dependence of Deformation Mode and Structure in Stoichiometric NiAl Single Crystals Deformed by High Temperature Steady-State Creep. *Metall. Trans.* **4**:159-166.

Bieler, T.R., Noebe, R.D., Whittenberger, J.D. and Luton, M.J. 1992. Extrusion Textures in NiAl and Reaction Milled NiAl/AlN Composites. In Intermetallic Matrix Composites II, ed. D.B. Miracle et al., pp. 165-170, Pittsburgh, PA: Mat. Res. Soc. Symp. Proc. Vol. 273.

Bieler, T.R., Noebe, R.D., Hebsur, M. and Saminathan, R. 1994. The Effects of Extrusion Parameters on Recrystallization Kinetics, Texture and Corresponding Fracture Toughness of NiAl. to be published in Advances in Hot Deformation Textures and Microstructures, ed K.J. Bowman et al., Warrendale, PA.: The Minerals, Metals and Materials Society.

Blackburn, M.J. and Smith, M.P. 1989. Improved Toughness Alloys Based On Titanium Aluminides. WRDC-TR-89-4095. (Avail. NTIS, AD-A218149.)

Bond, G.M., Robertson, I.M. and Birnbaum, H.K. 1987. Effect of Boron on the Mechanism of Strain Transfer Across Grain Boundaries in Ni_3Al. *J. Mater. Res.* **2**:436-440.

Bowman, K.J., Noebe, R.D., Jenny, J.R. and Kim, S.T. 1993. Texture in Hot-Worked B2-Structure Aluminides. *Mater. Sci. Eng.* **A160**:201-208.

Bowman, R.R. 1992. Influence of Interfacial Characteristics on the Mechanical Properties of Continuous Fiber Reinforced NiAl Composites. In Intermetallic Matrix Composites II, ed. D.B. Miracle et al., pp. 145-155, Pittsburgh, PA: Mat. Res. Soc. Symp. Proc. Vol. 273.

Bowman, R.R., Misra, A., Locci, I. 1993. Unresolved Technical Barriers to the Development of a Structurally Viable Al_2O_3/NiAl Composite. In HITEMP Review-1993: Advanced High Temperature Engine Materials Technology Program, NASA CP-19117, pp. 57-1 to 57-12.

Bowman, R.R. and Noebe, R.D. 1992. Development of NiAl and NiAl-Based Composites For Structural Applications: A Status Report. In Superalloys 1992, ed. S.D. Antolovich et al., pp. 341-350, Warrendale, PA: The Minerals, Metals & Materials Society.

Bowman, R.R., Noebe, R.D., and Darolia, R. 1989. Mechanical Properties and Deformation Mechanisms of NiAl. In HITEMP Review-1989: Advanced High Temperature Engine Materials Technology Program, NASA CP-10039, pp. 47-1 to 47-15.

Bowman, R.R., Noebe, R.D., Raj, S.V., and Locci, I.E. 1992. Correlation of Deformation Mechanisms with the Tensile and Compressive Behavior of NiAl and NiAl(Zr) Intermetallic Alloys. *Metall. Trans. A* **23A**:1493-1508.

Bradley, A.J. and Taylor, A. 1937. An X-ray Analysis of the Nickel-Aluminum System. *Proc. R. Soc. (London)* **A159**:56-72.

Bremer, F.J., Beyss, M., Karthaus, Hellwig, A., Schober, T., Welter, J.-M. and Wenzl, J. 1988. Experimental Analysis of the Ni-Al Phase Diagram. *J. Crystal Growth* **87**:185-192.

Brzeski, J.M., Hack, J.E., Darolia, R. and Field, R.D. 1993. Strain Aging Embrittlement of the Ordered Intermetallic Compound NiAl. *Mater. Sci. Eng.* **A170**:11-18.

Brophy, H., Rose, R.M. and Wulff, J. 1967. Thermodynamics of Structure. John Wiley & Sons, Inc., pp. 80-83.

Budberg, P.B. 1958. The Alloys of the Ternary System Nickel-Aluminum-Tungsten. *J. Inorg. Chem. USSR* **3**:694-698.

Camus, P.P., Baker, I., Horton, J.A. and Miller, M.K. 1988. Grain Boundary Chemistry of NiAl. *J. de Physique* **49-C6**:329-332.

Castro, G.R., Isern, H., Schneider, U., Stocker, M. and Wandelt, K. 1991. Two-Dimensional Phase Transition of Adsorbed Xenon on NiAl(110) and Al(110). *J. Vac. Sci. Technol. A* **9**:1676-1679.

Chaki, T.K. 1991. Mechanism of Boron-Induced Strengthening of Grain Boundaries in Ni_3Al. *Philos. Mag. Lett.* **63**:123-126.

Chakrabarti, D.J. 1977. Phase Stability in Ternary Systems of Transition Elements with Aluminum. *Metall. Trans. B* **8B**:121-123.

Chakravorty, S and Wayman, C.M. 1976. The Thermoelastic Martensitic Transformation in β' Ni-Al Alloys: Parts I and II. *Metall. Trans. A* **7A**:555-582.

Chambers, S.A. and Loebs, V.A. 1990. Schottky Barrier Height and Thermal Stability of the NiAl/n-Ge/GaAs(001) Interface. *J. Vac. Sci. Technol.* **8**:2074-2078.

Chan, K.S. 1990a. Theoretical Analysis of Grain Size Effects on Tensile Ductility. *Scripta Metall. Mater.* **24**:1725-1730.

Chan, K.S. 1990b. Fracture and Toughening Mechanisms in an Alpha-2 Titanium Aluminide Alloy. *Metall. Trans. A* **21A**:2687-2699.

Chang, K.-M., Darolia, R. and Lipsitt, H.A. 1992. Cleavage Fracture in B2 Aluminides. *Acta Metall. Mater.* **40**:2727-2737.

Chen, S.P., Voter, A.F., Albers, R.C., Boring, A.M. and Hay, P.J. 1989. Theoretical Studies of Ni3Al and NiAl with Impurities. In High Temperature Ordered Intermetallic Alloys III, ed. C.T. Liu et al., pp. 149-154, Pittsburgh, PA: Mat. Res. Soc. Symp. Proc. Vol. 133

Committee on Application Potential for Ductile Ordered Alloys 1984. Structural Uses for Ductile Ordered Alloys. National Materials Advisory Board Report #419, Washington, D.C., National Academy Press.

Cooper, M.J. 1963. An Investigation of the Ordering of the Phases CoAl and NiAl. *Philos. Mag.* **8**:805-810.

Copley, S.M. and Kear, B.H. 1967. A Dynamic Theory of Coherent Precipitation Hardening with Application to Nickel-Base Superalloys. *Metall. Soc. AIME Trans.* **239**:984-992.

Cotton, J.D., Kaufman, M.J. and Noebe, R.D. 1991. Constitution of Pseudobinary Hypoeutectic β-NiAl + α-V Alloys. *Scripta Metall. Mater.* **25**:1827-1832.

Cotton, J.D. and Margevicius, R.W., 1994. Study of the Brittle-To-Ductile Transition in NiAl by Texture Analysis. submitted to *Acta Metall. Mater.*

Cotton, J.D. and Noebe, R.D. 1994. Discussion of 'The Role of Microstructure on Strength and Ductility of Hot-Extruded Mechanically Alloyed NiAl'. Accepted *Metall. Trans. A.*

Cotton, J.D., Noebe, R.D. and Kaufman, M.J. 1993a. Chromium-Bearing NiAl Intermetallic Alloys: Part I. Microstructure and Mechanical Properties. *Intermetallics* **1**:3-20.

Cotton, J.D., Noebe, R.D. and Kaufman, M.J. 1993b. Chromium-Bearing NiAl Intermetallic Alloys: Part II. Slip Systems. *Intermetallics* **1**:117-126.

Cotton, J.D., Noebe, R.D. and Kaufman, M.J. 1993c. NiAl-Rich Portion of the NiAl-Cr Pseudobinary Eutectic System. *J. Phase Equil.* **14**:579-582.

Cotton, J.D., Noebe, R.D. and Kaufman, M.J. 1993d. Ternary Alloying Effects In Polycrystalline β-NiAl. In International Symposium on Structural Intermetallics, ed. R. Darolia et al., pp. 513-522, Warrendale, PA.: The Minerals, Metals and Materials Society.

Cottrell, A.H. 1958. Theory of Brittle Fracture in Steel and Similar Metals. *Trans. Metall. Soc. AIME* **212**:192-205.

Crimp, M.A., Tonn, S.C. and Zhang, Y. 1993. Dislocation Core Structures in B2 NiAl Alloys. *Mater. Sci. Eng.* **A170**:95-102.

Crimp, M.A. and Vedula, K. 1991. Room-temperature deformation of single-crystal B2 Fe-Al alloys: the effect of stoichiometry and cooling rate. *Philos. Mag. A* **63**:559-570.

Cullers, C.L. 1993. Deformation Mechanisms of NiAl Cyclicly Deformed Near the Brittle-to-Ductile Transition Temperature. NASA CR-191121.

Darolia, R. 1991. NiAl Alloys for High-Temperature Structural Applications. *J. Metals* **43**(3):44-49.

Darolia, R. 1993. Structural Applications of NiAl. In International Symposium on Structural Intermetallics, ed. R. Darolia et al., pp. 495-504, Warrendale, PA.: The Minerals, Metals and Materials Society.

Darolia, R., Chang, K.-M., and Hack, J.E. 1993. Observation of High Index {511} Type Fracture Planes and Their Influence on Toughness in NiAl Single-Crystals. *Intermetallics* **1**:65-78.

Darolia, R., Lahrman, D. and Field, R.D., 1992. The Effect of Iron, Gallium and Molybdenum on the Room Temperature Tensile Ductility of NiAl. *Scripta Metall. Mater.* **26**:1007-1012.

Darolia, R., Lahrman, D.F., Field, R.D., Dobbs, J.R., Chan, K.M., Goldman, E.H. and Konitzer, D.G. 1992. Overview of NiAl Alloys For High Temperature Applications. Ordered Intermetallics - Physical Metallurgy and Mechanical Behavior, ed. C.T. Liu et al., pp. 679-698, Dordrecht, The Netherlands: Kluwer Academic Publishers.

Darolia, R., Lahrman, D.F., Field, R.D. and Freeman, A.J. 1989. Alloy Modeling and Experimental Correlation For Ductility Enhancement in NiAl. In High Temperature Ordered Intermetallic Alloys III, ed. C.T. Liu et al., pp. 113-118, Pittsburgh, PA: Mat. Res. Soc. Symp. Proc. Vol. 133.

DeMarco, H.K. and Ardell, A.J. 1993. Mechanical Behavior of Monocrystalline NiAl Using A Miniaturized Disk-Bend Test. In High Temperature Ordered Intermetallic Alloys V, ed. I. Baker et al., pp. 641-646, Pittsburgh, PA: Mat. Res. Soc. Symp. Proc. Vol. 288.

Dollar, M., Dymek S., Hwang, S.J. and Nash P. 1992. The Occurrence of <110> Slip in NiAl. *Scripta Metall. Mater.* **26**:29-34.

Dollar, M., Dymek S., Hwang, S.J. and Nash P. 1993. The Role of Microstructure on Strength and Ductility of Hot-Extruded Mechanically Alloyed NiAl. *Metall. Trans. A* **24A**:1993-2000.

Doychak, J. 1992. Metal- and Intermetallic-Matrix Composites for Aerospace Propulsion and Power Systems. *J. Metals* **44**(6):46-51.

Doychak, J., Barrett, C.A. and Smialek, J.L. 1989. Oxidation Between 1000 °C and 1600 °C and Limiting Criteria for the Use of Zr-Doped Beta NiAl Alloys. In Corrosion and Particle Erosion at High Temperatures, eds. V. Srinivasa and K. Vedula, pp. 487-514, Warrendale, PA: The Minerals, Metals & Materials Society.

Duncan, A.J., Kaufman, M.J., Liu, C.T., and Miller, M.K. 1994. Site Occupation of Iron In Intermetallic NiAl. Submitted to *Appl. Surf. Sci.*

Dulmaine, B. 1989. Stability and Kinetics of Formation of Ni_5Al_3 in a Nickel Aluminide Alloy. Fall TMS meeting, Indianapolis, IN, Oct. 1989.

Edwards, 1993. Low-Cycle Fatigue Behavior of Polycrystalline NiAl at Room Temperature. M.S. Thesis, The University of Michigan, Ann Arbor, MI.

Edwards, K.M. and Gibala, R. 1993. Low-Cycle Fatigue Behavior of Polycrystalline NiAl at Room Temperature. In High Temperature Ordered Intermetallic Alloys V, ed. I. Baker et al., pp. 665-670, Pittsburgh, PA: Mat. Res. Soc. Symp. Proc. Vol. 288.

Elliot, C.K., Odette, G.R., Lucas, G.E., and Sheckerd, J.W. 1988. Toughening Mechanisms in Intermetallic Gamma-TiAl Alloys. In High Temperature/High Performance Composites, ed. F.D. Lemkey et al., pp. 95-101, Pittsburgh, PA: Mat. Res. Soc. Symp. Proc. Vol. 120.

Evans, A.G. 1990. Perspective on the Development of High Toughness Ceramics. *J. Am. Ceram. Soc.* **73**:187-206.

Evans, A.G., He, M.Y., and Hutchinson, J.W. 1989. Interface Debonding and Fiber Cracking in Brittle Matrix Composites. *J. Am. Ceram. Soc.* **72**:2300-2303.

Evans, A.G. and Marshall, D.B. 1989. The Mechanical Behavior of Ceramic Matrix Composites. *Acta Metall.* **37**:2567-2583.

Farkas, D. and Vailhe, C. 1993. Planar Fault Energies and Dislocation Core Spreading in B2 NiAl. *J. Mater. Res.* **8**:3050-3058.

Field, R.D., Lahrman, D.F. and Darolia, R. 1991a. Room Temperature Deformation in "Soft" Orientation NiAl Single Crystals. In High Temperature Ordered Intermetallic Alloys IV, ed. L. Johnson et al., pp. 255-260, Pittsburgh, PA: Mat. Res. Soc. Symp. Proc. Vol. 213.

Field, R.D., Lahrman, D.F. and Darolia, R. 1991b. Slip Systems in <001> Oriented NiAl Single Crystals. *Acta Metall. Mater.* **39**:2951-2959.

Field, R.D., Lahrman, D.F. and Darolia, R. 1991c. The Effect of Alloying on Slip Systems in <001> Oriented NiAl Single Crystals. *Acta Metall. Mater.* **39**:2961-2969.

Field, R.D., Lahrman, D.F. and Darolia, R. 1993. A Mechanistic Study of the Microalloying Effect In NiAl Base Alloys. In High Temperature Ordered Intermetallic Alloys V, ed. I. Baker et al., pp. 423-428, Pittsburgh, PA: Mat. Res. Soc. Symp. Proc. Vol. 288.

Fleischer, R.L., 1987. Number of Active Slip Systems in Polycrystalline Brass: Implications For Ductility In Other Structures. *Acta Metall.* **35**:2129-2136.

Fleischer, R.L., 1993. Solid Solution Strengthening of Intermetallic Compounds. In High Temperature Ordered Intermetallic Alloys V, ed. I. Baker et al., pp. 165-170, Pittsburgh, PA: Mat. Res. Soc. Symp. Proc. Vol. 288.

Fleischer, R.L. and Taub, A.I. 1989. Selecting High-Temperature Structural Intermetallic Compounds: The Materials Science Approach. *J. Metals* **41**(9):8-11.

Flinn, B.D., Ruhle, M., and Evans, A.G. 1989. Toughening in Composites of Al_2O_3 Reinforced With Al. *Acta Metall.* **37**:3001-3006.

Forbes, K.R., Glatzel, U., Darolia, R. and Nix, W.D. 1993. High Temperature Deformation of Single Crystals of NiAl. In High Temperature Ordered

Intermetallic Alloys V, ed. I. Baker et al., pp. 45-58, Pittsburgh, PA: Mat. Res. Soc. Symp. Proc. Vol. 288.

Franchy, R., Wuttig, M. and Ibach, H. 1987. The Adsorption of Sulfur, Carbon Monoxide and Oxygen on NiAl(111). *Surf. Sci.* **189-190**:438-447

Fraser, H.L., Smallman, R.E. and Loretto, M.H. 1973. The Plastic Deformation of NiAl Single Crystals Between 300 °K and 1050 °K: I. Experimental Evidence on the Role of Kinking and Uniform Deformation in Crystals Compressed Along <001>. *Philos. Mag.* **28**:651-665.

Gandhi, C. and Ashby, M.F. 1979. Fracture-Mechanism Maps for Materials which Cleave: F.C.C., B.C.C. and H.C.P. Metals and Ceramics. *Acta Metall.* **27**:1565-1602

George, E.P., 1991. Oak Ridge National Laboratory, Oak Ridge, TN. Unpublished data.

George, E.P. and Liu, C.T. 1990. Brittle Fracture and Grain Boundary Chemistry of Micro-alloyed NiAl. *J. Mater. Res.* **5**:754-762.

George, E.P., Liu, C.T. and Liao, J.J., 1991. Mechanical Properties, Fracture Behavior, and Grain-Boundary Chemistry of B-doped NiAl. in Alloy Phase Stability and Design, ed. G.M. Stocks et al., pp. 375-380, Pittsburgh, PA: Mat. Res. Soc. Symp. Proc. Vol. 186.

George, E.P., Liu, C.T. and Pope, D.P. 1992. Environmental Embrittlement: The Major Cause of Room-Temperature Brittleness in Polycrystalline Ni_3Al. *Scripta Metall. Mater.* **27**:365-370.

George, E.P., Liu, C.T. and Pope, D.P. 1993. Intrinsic Ductility and Environmental Embrittlement of Binary Ni_3Al. *Scripta Metall. Mater.* **28**:857-862.

Georgopoulos, P. and Cohen, J.B. 1977. The Defect Structure and Debye Waller Factors vs. Composition in β $Ni_{1\pm x}Al_{1\pm x}$. *Scripta Metall.* **11**:147-150.

Graham, R.B., 1984. The Effect of Temperature, Composition and Grain Size on the Mechanical Properties of NiAl. M.E. Thesis, Dartmouth College, Hanover, NH.

Grala, E.M. 1957. Investigation of the NiAl Phase of Nickel-Aluminum Alloys. NACA TN-3828.

Grala, E.M. 1960. Investigations of NiAl and Ni_3Al. In Mechanical Properties of Intermetallic Compounds, ed. J.H. Westbrook, pp. 358-402, New York: John Wiley & Sons, Inc.

Groves, G.W. and Kelly, A. 1963. Independent Slip Systems in Crystals. *Philos. Mag.* **8**:877-887.

Groves, G.W. and Kelly, A. 1969. Change of Shape Due to Dislocation Climb. *Philos. Mag.* **19**:977-986.

Guha, S., Munroe, P.R. and Baker I. 1991. Room Temperature Deformation Behavior of Multiphase Ni-20at.%Al-30at.%Fe and its Constituent Phases. *Mater. Sci. Eng.* **A131**:27-37.

Guseva, L.N. 1951. On the Nature of the β-phase in the System Ni-Al. *Dokaldy Akad. Nauk. S.S.S.R.* **77**:415-418.

Hack, J.E., Brzeski, J.M. and Darolia, R. 1992. Evidence of Inherent Ductility in Single Crystals of the Ordered Intermetallic Compound NiAl. *Scripta Metall. Mater.* **27**:1259-1263.

Hack, J.E., Brzeski, J.M., Darolia, R., and Field, R.D. 1993. Evidence of Inherent Ductility in Single Crystal NiAl. In High Temperature Ordered Intermetallic Alloys V, ed. I. Baker et al., pp. 679-684, Pittsburgh, PA: Mat. Res. Soc. Symp. Proc. Vol. 288.

Hahn, K.H. and Vedula, K. 1989. Room Temperature Tensile Ductility in Polycrystalline B2 NiAl. *Scripta Metall.* **23**:7-12.

Hancock, G.F., Dillamore, I.L., Smallman, R.E. 1972. The Creep of Dispersion-Strengthened Ni-Co Alloys. *Met. Sci. J.* **6**:152-156.

Hancock, G.F. and McDonnell, 1971. Diffusion in the Intermetallic Compound NiAl. *Phys. Status Solidi.* 4:143-150.

Harmouche, M.R. and Wolfenden, A. 1987. Temperature and Composition Dependence of Young's Modulus in Polycrystalline B2 Ni-Al. *J. Test. Eval.* **15**:101-104.

Hartfield-Wunsch, S. 1991. Monotonic and Cyclic Deformation of B2 Aluminides. Ph.D. Thesis, The University of Michigan, Ann Arbor, MI.

Hartfield-Wunsch, S. and Gibala, R. 1991. Cyclic Deformation of B2 Aluminides. In High Temperature Ordered Intermetallic Alloys IV, ed. L. Johnson, pp. 575-580, Pittsburgh, PA: Mat. Res. Soc. Symp. Proc. Vol. 213.

Hebsur, M. and Noebe, R.D. 1993. The effect of Processing Conditions and Alloying on the Fracture Toughness of NiAl. Unpublished data, NASA Lewis Research Center, Cleveland, Ohio.

Henig, E.-T. and Lukas, H.L. 1975. Kalorimetrische Bestimmung der Bildungsenthalpie und die Beschrzeibung der Fehlordnung der Geordneten β-Phase $(Ni,Cu)_{1-x}Al_x$. *Z. Metallk.* **66**:98-106.

Heredia, F.E. and Pope, D.P. 1988. Solid Solution Strengthening of Ni_3Al Single Crystals. In Superalloys 1988, ed. D.N. Duhl et al., pp. 315-324, Warrendale, PA: The Metallurgical Society.

Heredia, F.E. and Valencia, J.J. 1992. Fracture Toughness of NiAl *In-Situ* Eutectic Composites. In Intermetallic Matrix Composites II, ed. D.B. Miracle et al., pp. 197-204, Pittsburgh, PA: Mat. Res. Soc. Symp. Proc. Vol. 273.

Hing, P., Groves, G.W. 1972. The Strength and Fracture Toughness of Polycrystalline Magnesium Oxide Containing Metallic Particles and Fibers. *J. Mater. Sci.* 7:427-434.

Hocking, L.A., Strutt, P.R. and Dodd, R.A. 1971. Comparison of Steady-State Compression Creep Behavior in Stoichiometric CoAl and NiAl Single Crystals Between 850 and 1050 #C. *Inst. Met. J.* **99**:98-101.

Hong, T. and Freeman A.J. 1991. Effect of antiphase boundaries on the electronic structure and bonding character of intermetallic systems: NiAl. *Phys. Rev. B* **43**:6446-6458.

Huang, S.C., Field, R.D. and Krueger, D.D. 1990. Microscopy and Tensile Behavior of Melt Spun Ni-Al-Fe Alloys. *Metall. Trans. A* **21A**:959-970.

Hutchinson, J.W. 1964. Plastic Deformation of B.C.C. Polycrystals. *J. Mech. Phys. Solids* **12**:25-33.

Inoue, A., Masumoto, T., Tomioka, H. and Yano, N. 1985. Microstructure and Mechanical Properties of Ductile Intermetallic Compounds Produced by Melt Quenching. *Int. J. Rapid Solid.*, **1**:115-142.

Ishida, K., Kainuma, R., Ueno, N. and Nishizawa, T. 1991. Ductility Enhancement in NiAl(B2)-Base Alloys by Microstructural Control. *Metall. Trans. A* **22A**:441-446.

Jayaram, V. 1988. Comment on 'Number of Active Slip Systems in Polycrystalline Brass: Implications for Ductility in Other Structures'. *Scripta Metall.* **22**:741-742.

Johnson, D.R., Joslin, S.M., Oliver, B.F., Noebe, R.D. and Whittenberger, J.D. 1992. Intermetallic/Metallic Polyphase In-Situ Composites. In Intermetallic Matrix Composites II, ed. D.B. Miracle et al., pp. 87-92, Pittsburgh, PA: Mat. Res. Soc. Symp. Proc. Vol. 273.

Johnson, D.R., Joslin, S.M., Oliver, B.F, Noebe, R.D. and Whittenbereger, J.D. 1993. High Purity NiAl Single Crystals and Composites by Containerless Automated Processing. In First International Conference on Processing Materials for Properties, ed. H. Henein and T. Oki, pp. 865-870, Warrendale, PA.: The Minerals, Metals and Materials Society.

Johnson, D.R., X.F. Chen, Oliver, B.F, Noebe, R.D. and Whittenbereger, J.D. 1994. Processing and Mechanical Properties of In-Situ Composites from the NiAl-Cr and the NiAl-Cr,Mo Eutectic Systems. submitted to *Intermetallics.*

Johnson, D.R., X.F. Chen, Oliver, B.F, Noebe, R.D. and Whittenbereger, J.D. 1994. Directional Solidification and Mechanical Properties of NiAl-NiAlTa Alloys. submitted to *Intermetallics.*

Joo, G.C., Kalman, Z., Tsakalakos, T. and Chen, S.P. 1992. On the Growth of NiAl Intermetallics on III-V Semiconductors. *NanoStruct. Mater.* **1**:213-218.

Jung, I., Rudy, M., and Sauthoff, G. 1987. Creep in Ternary B2 Aluminides and Other Intermetallic Phases. In High Temperature Ordered Intermetallic Alloys II, ed. N.S. Stoloff et al., pp. 263-274, Pittsburgh, PA: Mat. Res. Soc. Symp. Proc. Vol. 81.

Kanne, W.R., Strutt, P.R. and Dodd, R.A. 1969. Nature of Slip Line Formation During Creep in Stoichiometric NiAl at Temperatures Between 475 and 775 C. *Trans. Metall. Soc. AIME* **245**:1259-1267.

Kao, C.R., Pike, L.M., Chen, S.-L. and Chang, Y.A. 1994. Site Preference of Substitutional Additions in Triple-Defect B2 Intermetallic Compounds. submitted to *Intermetallics*.

Kazmin, V.I., Mileiko, S.T. and Tvardovsky, V.V. 1990. Strength of Ceramic Matrix-Metal Fiber Composites. *Compos. Sci. Technol.* **38**:69-84.

Khadkikar, P.S., Locci, I.E., Vedula, K. and Michal, G.M. 1993. Transformation to Ni_5Al_3 in a 63.0 At. Pct. Ni-Al Alloy. *Metall. Trans. A* **24A**:83-94.

Khadkikar, P.S., Michal, G.M. and Vedula, K. 1990. Preferred Orientations in Extruded Nickel and Iron Aluminides. *Metall. Trans.* **21A**:279-288.

Khadkikar, P.S., Vedula, K. and Shabel, B.S. 1987. Two-Phase Nickel Aluminides. In High Temperature Ordered Intermetallic Alloys II, ed. N.S. Stoloff et al., pp. 157-164, Pittsburgh, PA: Mat. Res. Soc. Symp. Proc. Vol. 81.

Kim, J.T. 1990. On the Slip Behavior and Surface Film Effects In B2 Ordered NiAl Single Crystals. Ph.D. Thesis, University of Michigan, Ann Arbor, MI.

Kim, J.T. and Gibala, R. 1991. Slip Transition in [001] Oriented NiAl at High Temperatures. In High Temperature Ordered Intermetallic Alloys IV, ed. L. Johnson, pp. 261-266, Pittsburgh, PA: Mat. Res. Soc. Symp. Proc. Vol. 213.

Kim, J.T., Noebe, R.D. and Gibala, R. 1991. Observations of Dislocation Substructure in Surface Oxide Softened Single Crystals of NiAl. In Proceedings of International Symposium on Intermetallic Compounds - Structure and Mechanical Properties, ed. O. Izumi, pp. 591-595, Sendai, Japan: The Japan Institute of Metals.

Kitano, K and Pollock, T.M. 1993. The Kinetics of Low Temperature Deformation in NiAl Single Crystals. In Structural Intermetallics, ed. R. Darolia et al., pp. 591-600, Warrendale, PA.: The Minerals, Metals and Materials Society.

Kitano, K., Pollock, T.M., and Noebe, R.D. 1994. Impurities and Thermally Activated Deformation in NiAl Single Crystals. Submitted to *Scripta Metall. Mater.*

Kostrubanic, J., Koss, D.A., Locci, I.E. and Nathal, M. 1991. On Improving the Fracture Toughness of a NiAl-Based Alloy by Mechanical Alloying. In High Temperature Ordered Intermetallic Alloys IV, ed. L. Johnson et al., pp. 679-684, Pittsburgh, PA: Mat. Res. Soc. Symp. Proc. Vol. 213.

Kristic, V.D., Nicholson, P.S. and Hoagland, R.G. 1981. Toughening of Glasses by Metallic Particles. *J. Am. Ceram. Soc.* **64**:499-504.

Kruisman, J., Vitek, V. and DeHossan, J. Th M. 1988. Atomic Structure of Stoichiometric and Non-stoichiometric Grain Boundaries In A_3B Compounds with $L1_2$ Structure. *Acta Metall.* **36**:2729-2741.

Kumar, K.S., Mannan, S.K. and Viswanadham, R.K. 1992. Fracture Toughness of NiAl and NiAl-Based Composites. *Acta Metall. Mater.* **40**:1201-1222.

Lahrman, D.F., Field, R.D. and Darolia, R. 1991. The Effect of Strain Rate on the Mechanical Properties of Single Crystal NiAl. In High Temperature Ordered Intermetallic Alloys IV, ed. L. Johnson et al. pp. 603-607, Pittsburgh, PA: Mat. Res. Soc. Symp. Proc. Vol. 213.

Lahrman, D.F., Field, R.D. and Darolia, R. 1993a. Effect of Crystallographic Orientation on the Mechanical Properties of a NiAl+Fe Alloy. In High Temperature Ordered Intermetallic Alloys V, ed. I. Baker et al., pp. 679-684, Pittsburgh, PA: Mat. Res. Soc. Symp. Proc. Vol. 288.

Lahrman, D.F., Field, R.D. and Darolia, R. 1993b. Evaluation of Environmental Effects on the Room Temperature Tensile Properties of Single Crystal Stoichiometric NiAl and NiAl Alloys. *Scripta Metall. Mater.* **28**:709-714.

Lange, F.F. 1982a. Transformation Toughening: Part 1 - Size Effects Associated with the Thermodynamics in Constrained Transformations. *J. Mater. Sci.* **17**:225-234.

Lange, F.F. 1982b. Transformation Toughening: Part 4 - Fabrication, Fracture Toughness and Strength of Al_2O_3-ZrO_2 Composites. *J. Mater. Sci.* **17**:247-254.

Larsen, M., Misra, A., Hartfield-Wunsch, S., Noebe, R.D. and Gibala, R. 1990. Ductility Enhancement from Interface Dislocation Sources in a Directionally Solidified Beta ((Gamma+Gamma Prime') Ni-Fe-Al Composite Alloy). In Intermetallic Matrix Composites, ed. D.L. Anton et al., pp. 191-198, Pittsburgh, PA: Mat. Res. Soc. Symp. Proc. Vol. 194.

Lasalmonie, A., Lequeux, M.J., and Costa, P., 1979. The Clustering of Ni atoms in Ni-rich NiAl. In Strength of Metals and Alloys, vol. 2, pp. 1317-1321, eds. P. Haasen, V. Gerold and G. Kostorz, New York: Pergamon Press.

Law, C.C. and Blackburn, M.J. 1987. Rapidly Solidified Lightweight Durable Disk Material. Final Technical Report, AFWAL-TR-87-4102.

Lee, T.C. Robertson, I.M. and Birnbaum, H.K. 1989. Prediction of Slip Transfer Mechanisms Across Grain Boundaries. *Scripta. Metall.* **23**:799-803. (plus correction on page 1467).

Lee, T.C. Robertson, I.M. and Birnbaum, H.K. 1990a. TEM Insitu Deformation Study of the Interaction of Lattice Dislocations With Grain Boundaries in Metals. *Philos. Mag.* **62**:131-153.

Lee, T.C. Robertson, I.M. and Birnbaum, H.K. 1990b. An Insitu Transmission Electron Microscope Deformation Study of the Slip Transfer Mechanisms in Metals. *Metall. Trans. A* **21A**:2437-2447.

Lerch, B.A. and Noebe, R.D. 1993. Low Cycle Fatigue Behavior of Polycrystalline NiAl at 300 and 1000 K. NASA TM-105987.

Lerch, B.A. and Noebe, R.D. 1994. Unpublished research on fatigue of NiAl alloys. NASA Lewis Research Center, Cleveland, Ohio.

Leslie, W.C. 1981. The Physical Metallurgy of Steels. New York; McGraw-Hill Book Company.

Lewandowski, J.J., Dimiduk, D., Kerr, W. and Mendiratta, M.G. 1988. Microstructural Effects on Ductile Phase Toughening of Nb-Nb Silicide Composites. In High Temperature/High Performance Composites, ed. F.D. Lemkey et al., pp. 103-109, Pittsburgh, PA: Mat. Res. Soc. Symp. Proc. Vol. 120.

Lewandowski, J.J., Michal, G.M., Locci, I.E. and Rigney, J.D. 1990. Fracture Toughness and the Effects of Stress State on Fracture of Nickel Aluminides. In Alloy Phase Stability and Design, ed. G.M. Stocks et al., pp. 341-347, Pittsburgh, PA: Mat. Res. Soc. Symp. Proc. Vol. 186.

Liu, C.T. 1993a. Oak Ridge National Laboratory, Oak Ridge, TN. Personal communication.

Liu, C.T. 1993b. Recent Advances In Ordered Intermetallics. In High Temperature Ordered Intermetallic Alloys V, ed. I. Baker et al., pp. 3-19, Pittsburgh, PA: Mat. Res. Soc. Symp. Proc. Vol. 288.

Lloyd, C.H. and Loretto, M.H. 1970. Dislocations in Extruded β'-NiAl. *Phys. Status Solidi* **39**:163-170.

Lowell, C.E. 1993. Unpublished data. NASA Lewis Research Center, Cleveland Oh.

Lu, L., Kim, Y.S., Gokhale, A.B. and Abbaschian, R. 1990. Reactive Synthesis of $NbAl_3$ Matrix Composites. In Intermetallic Matrix Composites, ed. D.L. Anton et al., pp. 79-88, Pittsburgh, PA: Mat. Res. Soc. Symp. Proc. Vol. 194.

Lukasak, D.A. and Koss, D.A. 1990. The Flow and Fracture of Ti_3Al-Nb Alloy. *Metall. Trans. A*. **21A**: 135-143.

Lutze-Birk, A. and Jacobi, H. 1975. Diffusion of ^{114m}In in NiAl. *Scripta Metall.* **9**:761-765.

Maloy, S. and Gray, R. 1993. Personal communication. Los Alamos National Laboratory, Los Alamos, New Mexico.

Margevicius, R.W. 1992. Effects of Pressure on Flow and Fracture Behavior of NiAl. Ph.D. Thesis, Case Western Reserve University, Cleveland, Ohio.

Margevicius, R.W. and Cotton, J.D. 1994. Study of the Brittle-to-Ductile Transition in NiAl by Texture Analysis. submitted to *Acta. Metall. Mater.*

Margevicius, R.W. and Lewandowski, J.J. 1991. The Effects of Hydrostatic Pressure on the Mechanical Behavior of NiAl. *Scripta Metall. Mater.* **25**:2017-2022.

Margevicius, R.W. and Lewandowski, J.J. 1993. Pressure-Induced Dislocations and Subsequent Flow in NiAl. *Acta Metall. Mater.* **41**:485-496.

Margevicius, R.W., Lewandowski, J.J., Locci, I.E. and Noebe, R.D. 1993. Yield Point Behavior in NiAl. *Scripta Metall. Mater.* **29**:1309-1312.

Mason, D.P., Van Aken, D.C., Noebe, R.D., Locci, I.E. and King, K.L. 1991. Microstructure and Mechanical Properties of Near Eutectic β-NiAl Plus α-Re Alloys Produced by Rapid Solidification and Extrusion. In High Temperature

Ordered Intermetallic Alloys IV, ed. L. Johnson et al., pp. 1033-1038, Pittsburgh, PA: Mat. Res. Soc. Symp. Proc. Vol. 213.

Matsugi, K., Wenman, D.W., and Stoloff, N.S. 1992. Observation of the Brittle to Ductile Transition Temperature in the Iron Microalloyed Polycrystalline NiAl Intermetallic Compound. *Scripta Metall. Mater.* **27**:1633-1638.

McMeeking, R. and Evans, A.G. 1982. Mechanics of Transformation-Toughening in Brittle Materials. *J. Am. Ceram. Soc.* **65**:242-246.

Mills, M.J. and Miracle, D.B. 1993. The Structure of a<100> and a<110> Dislocation Cores in NiAl. *Acta Metall. Mater.* **41**:85-95.

Mills, M.J., Daw, M.S., Foiles, S.M. and Miracle, D.B. 1993. HRTEM Observation and EAM Calculation of Dislocation Cores in NiAl. In High Temperature Ordered Intermetallic Alloys V, ed. I. Baker et al., pp. 257-262, Pittsburgh, PA: Mat. Res. Soc. Symp. Proc. Vol. 288.

Miracle, D.B., 1990. The Deformation of Nickel Aluminide Bicrystals. Ph.D. Thesis, The Ohio State University, Columbus, Ohio.

Miracle, D.B., 1991. Deformation In NiAl Bicrystals. *Acta Metall. Mater.* **39**:1457-1468.

Miracle, D.B., 1993. The Physical and Mechanical Properties of NiAl. *Acta Metall. Mater.* **41**:*649-684.*

Miracle, D.B. and Darolia, R. 1993. Structural Applications of NiAl. In Intermetallic Compounds: Principles and Practice, ed. J.H. Westbrook and R.L. Fleischer, New York, NY.: John Wiley and Sons.

Miracle, D.B., Russell, S. and Law, C.C. 1989. Slip System Modification in NiAl. In High Temperature Ordered Intermetallic Alloys III, ed. C.T. Liu et al., pp. 225-230, Pittsburgh, PA: Mat. Res. Soc. Symp. Proc. Vol. 133.

Mises, R.V., 1928. Mechanics of Plastic Form Change of Crystals. *Z. Angew. Math. Mech.* **8**[3]:161-185.

Misra, A. 1994. Ph.D. Thesis. The University of Michigan, Ann Arbor, Michigan.

Misra, A., Noebe, R.D. and Gibala, R. 1992. On the Mechanisms of Ductility Enhancement In $\beta+\gamma'$-$Ni_{70}Al_{30}$ and $\beta+(\gamma+\gamma')$-$Ni_{50}Fe_{30}Al_{20}$ in-situ Composites. In Intermetallic Matrix Composites II, ed. D. Miracle et al., pp. 205-210, Pittsburgh, PA: Mat. Res. Soc. Symp. Proc. Vol. 273.

Misra, A., Noebe, R.D. and Gibala, R. 1993. The Role of Interfaces in the Room Temperature Mechanical Behavior of Directionally Solidified $\beta+\gamma'$-$Ni_{70}Al_{30}$ and $\beta+(\gamma+\gamma')$-$Ni_{50}Fe_{30}Al_{20}$ Alloys. In High Temperature Ordered Intermetallic Alloys V, ed. I. Baker et al., pp. 483-488, Pittsburgh, PA: Mat. Res. Soc. Symp. Proc. Vol. 288.

Mohamed, F.A. and Langdon, T.G. 1974. The Transition from Dislocation Climb to Viscous Glide in Creep of Solid Solution Alloys. *Acta Metall.* **22**:779-788.

Mises, R.V. 1928. Meckanik Der Plastischen Formenderung Von Kristallen (Mechanics of Plastic Form Change of Crystals). *Zeitschrift Fuer Angewandte Mathematik Und Mechanik*, **8**(3):161-185. (NASA TT-20718).

Moose, C.A., 1991. Interfacial Shear Studies of Sapphire Fiber-Reinforced Nickel Aluminide Matrix Composites. M.S. Thesis, Pennsylvania State University, University Park, PA.

Moskovic, R. 1977. Precipitation of Ni_3Al in a Nickel Rich NiAl. *J. Mater. Sci.* **12**:1895-1902.

Munroe, P.R. and Baker, I. 1992. Effect of Accelerating Voltage on Planar and Axial Channeling in Ordered Intermetallic Compounds. *J. Mater. Res.* 7:2119-2125.

Nagpal, P. and Baker, I. 1990a. Effect of Cooling Rate on Hardness of FeAl and NiAl. *Metall. Trans. A* **21A**:2281-2282.

Nagpal, P. and Baker, I. 1990b. The Effect of Grain Size on the Room-Temperature Ductility of NiAl. *Scripta Metall. Mater.* **24**:2381-2384.

Nagpal, P. and Baker, I. 1991. Room Temperature Fracture of FeAl and NiAl. *Mater. Character.* **27**:167-173.

Nagpal, P. and Baker, I. 1992. Dislocation Arrangements in Polycrystalline NiAl after Room Temperature Deformation. *J. Maters. Lett.* **11**:1209-1210.

Nagpal, P., Baker, I., Liu, F. and Munroe, P.R., 1991. Room Temperature Strength and Fracture of FeAl and NiAl. In High Temperature Ordered Intermetallic Alloys IV, ed. L. Johnson et al., pp. 533-538, Pittsburgh, PA: Mat. Res. Soc. Symp. Proc. Vol. 213.

Nardone, V.C. 1992. Fracture Behavior of Stainless Steel-Toughened NiAl Composite Plate. *Metall. Trans. A* **23A**:563-572.

Nardone, V.C. and Strife, J.R., 1991. NiAl-Based Microstructurally Toughened Composites. *Metall. Trans. A* **22A**:183-189.

Nathal, M.V. 1992. Creep Deformation of B2 Aluminides. In Ordered Intermetallics - Physical Metallurgy and Mechanical Behavior, ed. C.T. Liu et al., pp. 541-563, Dordrecht, The Netherlands: Kluwer Academic Publishers.

Nathal, M.V. and Ebert, L.J. 1985. Elevated Temperature Creep-Rupture Behavior of the Single Crystal Nickel-Base Superalloy NASAIR 100. *Metall. Trans. A* **16A**:427-439.

Nesbitt, J.A. and Barrett, C.C. 1993. Predicting the Oxidation-Limited Lifetime of β NiAl. In Structural Intermetallics, ed. R. Darolia et al., pp. 601-609, Warrendale, PA.: The Minerals, Metals and Materials Society.

Newkirk, J.W. and Sago, J.A. 1990. Ductile Phase Toughening of Cr3Si with Chromium. In Intermetallic Matrix Composites, ed. D.L. Anton et al., pp. 183-190, Pittsburgh, PA: Mat. Res. Soc. Symp. Proc. Vol. 194.

Nishiyama, Y., Miyashita, T., Isobe, S. and Noda T. 1990. Development of Titanium Aluminide Turbocharger Rotors. In High Temperature Aluminides and Intermetallics, ed. S.H. Whang et al., pp. 557-584. Warrendale, PA.: The Minerals, Metals and Materials Society.

Nix, W.D. and Ilschner, B. 1980. Mechanisms Controlling Creep of Single Phase Metals and Alloys. In Strength of Metals and Alloys: Proceedings of the Fifth International Conference, Vol. 3, ed. P. Hassen, V. Gerald and G. Kostorz, pp. 1503-1501, New York: Pergamon Press.

Noebe, R.D., 1987. Effect of Oxide Coatings on Deformation of NiAl Single Crystals. M.S. Thesis, Case Western Reserve University, Cleveland, Ohio.

Noebe, R.D. 1993. Unpublished research on the NiAl-Cu system. NASA Lewis Research Center, Cleveland, Ohio.

Noebe, R.D., Bowman, R.R., Locci, I.E., Raj, S.V., 1989. Effect of Zr Additions on the Microstructure and Mechanical Behavior of NiAl. In HITEMP Review-1989: Advanced High Temperature Engine Materials Technology Program, NASA CP-10039, pp. 48-1 to 48-15.

Noebe, R.D., Bowman, R.R., Kim, J.T., Larsen, M. and Gibala, R. 1990. The Potential for Ductility Enhancement from Surface and Interface Dislocation Sources in NiAl. In High Temperature Aluminides and Intermetallics, ed. S.H. Whang et al., pp. 271-300. Warrendale, PA.: The Minerals, Metals and Materials Society.

Noebe, R.D., Bowman, R.R. and Nathal, M.V. 1993. Review of the Physical and Mechanical Properties of the B2 Compound NiAl. *Inter. Mater. Rev.* **38**:193-232. (Also NASA TM-105598, April 1992.)

Noebe, R.D., Bowman, R.R. and Nathal, M.V. 1994. Physical and Mechanical Metallurgy of NiAl. Chapter 9 In Physical Metallurgy and Processing of Intermetallic Compounds, ed. N.S. Stoloff and V.K. Sikka, Van Nostrand Reinhold Pub., New York, NY.

Noebe, R.D. and Garg, A. 1994. Characterization of Nitrogen-Doped NiAl. *Scripta Metall. Mater.* **30**:815-820.

Noebe, R.D. and Gibala, R. 1986. Surface Oxide Softening of Single Crystal NiAl. *Scripta Metall.* **20**:1635-1639.

Noebe, R.D. and Lerch, B.A. 1992. Room Temperature Cyclic Deformation Behavior of Cast and Extruded NiAl. *Scripta Metall. Mater.* **27**:1161-1166.

Noebe, R.D., Misra, A. and Gibala, R. 1991. Plastic Flow and Fracture of B2 NiAl-Based Intermetallic Alloys Containing a Ductile Second Phase. *Iron Steel Inst. Jap. Int.* **31**:1172-1185.

Odette, G.R., Deve, H.E., Elliott, C.K., Hasegawa and Lucas, G.E. 1989. The Influence of Reaction Layer Structure and Properties on Ductile Phase Toughening in Titanium Aluminide-Niobium Composites. In Interfaces in Metal-Ceramic Composites, ed. R.Y. Lin et al., pp. 443-464, Warrendale, PA.: The Minerals, Metals and Materials Society.

Pank, D.R. 1988. The Effect of Alloying on the Microstructure and Mechanical Properties of Rapidly Solidified Ni-Al Alloys. M.S. Thesis, Pennsylvania State University.

Pank, D.R., Nathal, M.V. and Koss, D.A. 1990. Microstructure and Mechanical Properties of Multiphase NiAl-Based Alloys. *J. Mater. Res.* 5:942-949.

Parthasarathy, T.A., Rao, S.I. and Dimiduk, D.M. 1993. Molecular Statics Simulations of Core Structures and Motion of Dislocations in NiAl. *Philos. Mag. A* **67**:643-662.

Pascoe, R.T. and Newey, C.W.A. 1968a. Deformation Modes of the Intermediate Phase NiAl. *Phys. Status Solidi* **29**:357-366.

Pascoe, R.T. and Newey, C.W.A 1968b. The Mechanical Behavior of the Intermediate Phase NiAl. *Met. Sci. J.* **2**:138-143.

Pascoe, R.T. and Newey, C.W.A. 1971. Deformation Processes in the Intermediate Phase NiAl. *Met. Sci. J.* **5**:50-55.

Patrick, D.K., Chang, K.-M., Miracle, D.B. and Lipsitt, H.A. 1991. Burgers Vector Transition in Fe-Al-Ni Alloys. In High Temperature Ordered Intermetallic Alloys IV, ed. L. Johnson et al., pp. 267-272, Pittsburgh, PA: Mat. Res. Soc. Symp. Proc. Vol. 213.

Petton, G. and Farkas, D. 1991. Grain Boundary Structure Simulations In B2 Ordered NiAl. *Scripta Metall. Mater.* **25**:55-60.

Pope, D.P. 1990. Dislocation Mechanisms and Anomalous Flow in $L1_2$ Alloys. High Temperature Aluminides and Intermetallics, ed. S.H. Whang et al., pp. 51-61. Warrendale, PA.: The Minerals, Metals and Materials Society.

Raj, S.V. 1992. Fracture Behavior of a B2 Ni-30Al-20Fe-0.05Zr Intermetallic Alloy in the Temperature Range 300 to 1300 K. *Metall. Trans. A* **23A**:1691-1703.

Raj, S.V. and Farmer, S.C. 1993. Observation of a New Creep Regime in Polycrystalline Ni-50(at.%)Al Intermetallic Alloy. In High Temperature Ordered Intermetallic Alloys V, ed. I. Baker et al., pp. 647-652, Pittsburgh, PA: Mat. Res. Soc. Symp. Proc. Vol. 288.

Raj, S.V., Locci, I.E. and Noebe, R.D. 1992. Deformation Behavior of a Ni-30Al-20Fe-0.05Zr Intermetallic Alloy in the Temperature Range 300 to 1300 K. *Metall. Trans. A* **23A**:1705-1718.

Reuss, S. and Vehoff, H. 1990a. Temperature Dependence of the Fracture Toughness of Single Phase and Two Phase Intermetallics. *Scripta Metall. Mater.* **24**:1021-1026.

Reuss, S. and Vehoff, H. - As reported by G. Sauthoff 1990b. Mechanical Properties of Intermetallics at High Temperatures. In High Temperature Aluminides and Intermetallics, ed. S.H. Whang et al., pp. 344. Warrendale, PA.: The Minerals, Metals and Materials Society.

Reynaud, F. 1976. Mise en Evidence Par Diffraction Electronique de la Mise en Ordre des Atomes de Nickel en Exces par Rapport a la Stoechiometrie dans les Alliages β'-NiAl Riches en Nickel: Formation d'une Surstructure Ni_2Al. *J. Appl. Cryst.* **9**:263-268.

Rigney, J.D. and Lewandowski, J.J. 1992a. Fracture toughness of monolithic nickel aluminide intermetallics. *Maters. Sci. Eng.* **A149**:143-151.

Rigney, J.D. and Lewandowski, J.J. 1992b. Effects of reinforcement size and distribution on fracture toughness of composite nickel aluminide intermetallics. *Maters. Sci. Eng.* **A158**:31-45.

Robertson, I.M. and Wayman, C.M. 1984. Ni_5Al_3 and the Nickel-Aluminum Binary Phase Diagram. *Metallography* **17**:43-55.

Rozner, A.G. and Wasilewski, R.J. 1966. Tensile Properties of NiAl and NiTi. *J. Inst. Met.* **94**:169-175.

Rudy, M. and Sauthoff, G. 1985. Creep Behavior of the Ordered Intermetallic (Fe,Ni)Al Phase. In High Temperature Ordered Intermetallic Alloys, ed. C.C. Koch et al., pp. 327-333, Pittsburgh, PA: Mat. Res. Soc. Symp. Proc. Vol. 39.

Rusovic, N. and Warlimont, H. 1977. The Elastic Behavior of β_2-NiAl. *Phys. Stat. Sol. (A)* **44**:609-619.

Rusovic, N. and Warlimont, H. 1979. Young's Modulus of β_2-NiAl Alloys. *Phys. Stat. Sol. (A)* **53**:283-288.

Russell, K.C. and Edington, J.W. 1972. Precipitation Behavior and Mechanical Properties of a Nickel-36 at.% Aluminum Alloy. *Met Sci. J.* **6**:20-24.

Russell, S.M. and Law, C.C. 1990. Nickel Aluminide Materials Having Toughness and Ductility at Low Temperatures. U.S. Patent 4,961,905.

Russell, S.M., Law, C.C. and Blackburn, M.J. 1989. The Effect of Cobalt on Martensitic Toughening Parameters in NiAl. In High Temperature Ordered Intermetallic Alloys III, ed. C.T. Liu et al., pp. 627-632, Pittsburgh, PA: Mat. Res. Soc. Symp. Proc. Vol. 133.

Russell, S.M., Law, C.C., Blackburn, M.J., Clapp, P.C. and Pease, D.M. 1989. Lightweight Disk Alloy Development. PWA-FR-19577-8, Pratt & Whitney, West Palm Beach, FL.

Russell, S.M., Law, C.C., Blackburn, M.J., Clapp, P.C. and Pease, D.M. 1991. Lightweight Disk Alloy Development. PWA-FR-21413, Pratt & Whitney, West Palm Beach, FL.

Sands, T. 1988. Stability and Epitaxy of NiAl and Related Intermetallic Films on III-V Compound Semiconductors. *Appl. Phys. Lett.* **52**:197-199.

Sastry, S.M.L. and Lipsitt, H.A. 1977. Ordering Transformations and Mechanical Properties of Ti_3Al and Ti_3Al-Nb Alloys. *Metall. Trans. A* **8A**:1543-1552.

Sauthoff, G. 1990. Mechanical Properties of Intermetallics at High Temperatures. In High Temperature Aluminides and Intermetallics, ed. S.H. Whang et al., pp. 329-352. Warrendale, PA.: The Minerals, Metals and Materials Society.

Sauthoff, G. 1993. Personal communication.

Schneibel, J.H., Jenkins, M.G. and Maziasz, P.J. 1993. Crack Propagation in NiAl and FeAl. In High Temperature Ordered Intermetallic Alloys V, ed. I. Baker et al., pp. 549-554, Pittsburgh, PA: Mat. Res. Soc. Symp. Proc. Vol. 288.

Schramm, J. 1941. The Binary System Ni-NiAl. *Z. Metallk.* **33**:347-355.

Schulson, E.M. 1981. Comments on the Brittle to Ductile Transition of Long-Range Ordered Alloys. *Res. Mech. Lett.* **1**:111-114.

Schulson, E.M. 1982. The Strength and Ductility of Polycrystalline NiAl in Tension. In COSAM Program Overview, ed. J.R. Stephens, pp. 175-182, NASA TM-83006.

Schulson, E.M. 1985. The Effects of Grain Size on the Flow and Fracture of Long-Range Ordered Alloys. In High Temperature Ordered Intermetallic Alloys, ed. C.C. Koch et al., pp. 193-204, Pittsburgh, PA: Mat. Res. Soc. Symp. Proc. Vol. 39.

Schulson, E.M. and Barker, D.R. 1983. A Brittle to Ductile Transition in NiAl of a Critical Grain Size. *Scripta Metall.* **17**:519-522.

Seybolt, A.U. and Westbrook, J.H. 1964. Oxygen-Induced Grain Boundary Hardening in the Intermetallic Compounds AgMg, NiGa and NiAl. In Metals for the Space Age, Plansee Seminar Proc. 845-857.

Seybolt, A.U. , Westbrook, J.H. and Turnbull, D. 1964. Mechanisms for Grain Boundary and Free Surface Hardening by Oxygen-Vacancy Interactions. *Acta Metall.* **12**:1456-1457.

Shaw, D.M. 1983. Orientation Dependence of Creep Behavior of Single Crystal Gamma-Prime (Ni_3Al). *Scripta Metall.* **17**:997-1002.

Shen, Z., Wagoner, R.H. and Clark, W.A.T. 1988. Dislocation and Grain Boundary Interactions in Metals. *Acta Metall.* **36**:3231-3242.

Shewmon, P.G. 1983. Diffusion in Solids. McGraw-Hill, pp. 170-172.

Sigl, L.S., and Exner, H.E. 1987. Experimental Study of the Mechanics of Fracture in WC-Co Alloys. *Metall. Trans. A* **18A**:1299-1308.

Sigl, L.S., Mataga, P.A., Dalgleish, B.J., McMeeking, R.M., Evans, A.G., 1988. On the Toughness of Brittle Materials Reinforced With a Ductile Phase. *Acta Metall.* **36**:945-953.

Singleton, M.F., Murray, J.L. and Nash, P. 1986. NiAl. In Binary Alloy Phase Diagrams, ed. T.B. Massalski, pp. 140-143, Metals Park, Oh.: American Society for Metals.

Singleton, R.H., Wallace, A.V. and Miller, D.G. 1966. Nickel Aluminide Leading Edge For A Turbine Vane. In Summary of the Eleventh Refractory Composites Working Group Meeting, pp. 717-738. AFML-TR-66-179.

Smallman, R.E. 1985. Modern Physical Metallurgy, 4th Ed. pp. 448-451, Boston, MA.: Butterworth & Co.

Smialek, J.L. and Hehemann, R.F. 1973. Transformation Temperatures of Martensite in Beta-Phase Nickel Aluminide. *Metall. Trans.* **4**:1571-1575.

Stephens, J.R. 1988. High Temperature Metal Matrix Composites for Future Aerospace Systems. In AIAA'88: Proc. 24th Joint Propulsion Conf., pp. 1-10, AIAA-88-3059, Washington, D.C.: AIAA.

Stover, E.R. 1966. Effects of Alloying and Deformation Processing on the Mechanical Behavior of NiAl. WADC-TDR-60-184, Part VII, Vol. II. (Avail. NTIS, AD-810645)

Strutt, P.R., Dodd, R.A. and Rowe, G.M. 1970. Creep in Stoichiometric Beta-NiAl. In Strength of Metals and Alloys, Vol. III, pp. 1057-1061, Metals Park, OH.: ASM International.

Subramanian, P.R., Mendiratta, M.G., Miracle, D.B. and Dimiduk, D.M. 1990. Microstructures and Mechanical Properties of NiAl+Mo In-Situ Eutectic Composites. In Intermetallic Matrix Composites, ed. D.L. Anton et al., pp. 147-154, Pittsburgh, PA: Mat. Res. Soc. Symp. Proc. Vol. 194.

Swiatnicki, W.A., and Grabski, M.W. 1986. Effect of Carbon and Chromium on Grain Boundary Diffusional Properties In Austenitic Steels. *Acta Metall.* **34**:817-822.

Swiatnicki, W.A., and Grabski, M.W. 1989. Boron Influence on Grain Boundary Dislocations Mobility In Ni_3Al. *Acta Metall.* **37**:1307-1311.

Swiatnicki, W.A., Lojkowski, W., and Grabski, M.W. 1986. Investigation of Grain Boundary Diffusion In Polycrystals By Means of Extrinsic Grain Boundary Dislocations Spreading Rate. *Acta Metall.* **34**:599-605.

Takasugi, T., Kishino, J. and Hanada, S. 1993. Anomalous Elongation Behavior of Stoichiometric NiAl Single Crystals at Intermediate Temperatures. *Acta Metall. Mater.* **41**:1009-1020.

Takasugi, T., Wantanabe, S. and Hanada, S. 1992. The Temperature and Orientation Dependence of Tensile Deformation and Fracture in NiAl Single Crystals. *Maters. Sci. Eng.* **A149**:183-193.

Taylor, G.I. 1938. Plastic Strain in Metals. *Inst. Metals, J.* **62**:307-312.

Taylor, A. and Doyle, N.J. 1972. Further Studies on the Nickel-Aluminum System. I. The β-NiAl and δ-Ni_2Al_3 Phase Fields. *J. Appl. Cryst.* **5**:201-209.

Vandervoort, R.R., Mukherjee, A.K. and Dorn, J.E. 1966. Elevated-Temperature Deformation Mechanisms in β'-NiAl. *Trans. ASM* **59**:930-944.

Vedula, K., Hahn, K.H. and Boulogne, B. 1989. Room Temperature Tensile Ductility in Polycrystalline B2 NiAl. In High Temperature Ordered Intermetallic Alloys III, ed. C.T. Liu et al., pp. 299-304, Pittsburgh, PA: Mat. Res. Soc. Symp. Proc. Vol. 133.

Vedula, K. and Khadkikar, P.S. 1990. Effect of Stoichiometry on Low Temperature Mechanical Properties. In High Temperature Aluminides and Intermetallics, ed.

S.H. Whang et al., pp. 197-217. Warrendale, PA.: The Minerals, Metals and Materials Society.

Vehoff, H. 1993. Fracture and Toughness of Intermetallics. In High Temperature Ordered Intermetallic Alloys V, ed. I. Baker et al., pp. 71-82, Pittsburgh, PA: Mat. Res. Soc. Symp. Proc. Vol. 288.

Veyssiere, P. and Noebe, R.D. 1992. Weak-Beam Study of <111> Superlattice Dislocations in NiAl. *Philos. Mag.* **65**:1-13.

Vitek. V. and Chen, S.P. 1991. Modeling of Grain Boundary Structures and Properties in Intermetallic Compounds. *Scripta Metall. Mater.* **25**:1237-1242.

Wachtell, R.L. 1952. An investigation of various properties of NiAl. WADC Technical Report 52-291.

Walter, J.L. and Cline, H.E. 1970. The Effect of Solidification Rate on Structure and High Temperature Strength of the Eutectic NiAl-Cr. *Metall. Trans.* **1**:1221-1229.

Walston, W.S. and Darolia, R. 1993. Effect of Alloying on Physical Properties of NiAl. In High Temperature Ordered Intermetallic Alloys V, ed. I. Baker et al., pp. 237-242, Pittsburgh, PA: Mat. Res. Soc. Symp. Proc. Vol. 288.

Walston, W.S., Field, R.D., Dobbs, J.R., Lahrman, D.F. and Darolia, R. 1993. Microstructure and High Temperature Strength of NiAl Alloys. In Structural Intermetallics, ed. R. Darolia et al., pp. 523-532, Warrendale, PA.: The Minerals, Metals and Materials Society.

Wasilewski, R.J., 1966. Elastic Constants and Young's Modulus of NiAl. *Trans. Metall. Soc. AIME* **36**:455-457.

Wasilewski, R.J., Butler, S.R. and Hanlon, J.E. 1967. Plastic Deformation of Single-Crystal NiAl. *Trans. Metall. Soc. AIME* **239**:1357-1364.

Weaver, M.L., Kaufman, M.J. and Noebe, R.D. 1993. The Effects of Alloy Purity on the Mechanical Behavior of Soft Oriented NiAl Single Crystals. *Scripta Metall. Mater.* **29**:1113-1118.

Webber, J.G. and Van Aken, D.C. 1989. Studies of a Quasi-Binary Beta-NiAl and Alpha-Re Eutectic. *Scripta Metall.* **23**:193-196.

Wentzell, J.M. 1974. Metal Powder Production by Vacuum Atomization. *J. Vac. Sci. Technol.* **11**:1035-1041.

Westbrook, J.H. 1956. Temperature Dependence of Hardness of the Equi-Atomic Iron Group Aluminides. *J. Electrochem. Soc.* **103**:54-63.

Westbrook, J.H. and Wood, D.L. 1962. A Source of Grain-Boundary Embrittlement in Intermetallics. *J. Inst. Metals* **91**:174-182.

Wheeler, D. and Noebe, R.D. 1993. Auger analysis of various NiAl alloys. Unpublished research, NASA Lewis Research Center, Cleveland, Ohio.

Whittenberger, J.D. 1987. Effect of Composition and Grain Size on Slow Plastic Flow Properties of NiAl Between 1200 to 1400 K. *J. Mater. Sci.* **22**:394-402.

Whittenberger, J.D. 1988. The Influence of Grain Size and Composition on 1000 to 1400 K Slow Plastic Flow Properties of NiAl. *J. Mater. Sci.* **23**:235-240.

Whittenberger, J.D. 1993. Characteristics of an Elevated Temperature AlN Particulate Reinforced NiAl. In Structural Intermetallics, ed. R. Darolia et al., pp. 819-828, Warrendale, PA.: The Minerals, Metals and Materials Society.

Whittenberger, J.D., Arzt, E. and Luton, M.J. 1990a. Preliminary Investigation of a NiAl Composite Prepared by Cryomilling. *J. Mater. Res.* **5**:271-277.

Whittenberger, J.D., Arzt, E. and Luton, M.J. 1990b. 1300 K Compressive Properties of a Reaction Milled NiAl-AlN Composite. *J. Mater. Res.* **5**:2819-2827.

Whittenberger, J.D., Kumar, K.S. and Mannan, S.K. 1991. 1000 to 1300 K Slow Plastic Compression Properties of Al-Deficient NiAl. *J. Mater. Sci.* **26**:2015-2022.

Whittenberger, J.D. and Noebe, R. 1993. Creep behavior of NiAl alloys. Unpublished research, NASA Lewis Research Center, Cleveland, Ohio.

Whittenberger, J.D., Noebe, R.D., Cullers, C.L., Kumar, K.S. and Mannan, S.K., 1991. 1000 to 1200 K Time-Dependent Compressive Deformation of Single-Crystalline and Polycrystalline B2 Ni-40Al. *Metall. Trans. A* **22A**:1595-1607.

Whittenberger, J.D., Ray. R. and Jha, S.C. 1992. Influence of Grain Size on the Creep Behavior of HfC-Dispersed NiAl. *Mater. Sci. Eng.* **A151**:137-146.

Wolfenden, A., Raj, S.V., Kondlapudi, S.K.R. 1993. Strain Aging and Breakaway Strain Amplitude of Damping in NiAl and NiAlZr. submitted to *J. Mater. Res.*

Wood, D.L. et al. 1960-1966. Effect of Basic Physical Parameters on Engineering Properties of Intermetallic Compounds. WADD Technical Report 60-184, parts I-VII.

Wright, R.N., Knibloe, J.R. and Noebe, R.D. 1991. Consolidation of NiAl Powders Using Hot Isostatic Pressing. *Mater. Sci. Eng.* **A141**:79-83.

Wunderlich, W., Machon, L., and Sauthoff, G., 1992. Dislocation Analysis at Crack Tips at Phase Boundaries in an Intermetallic NiAl-NbNiAl Alloy. *Z. Metallkd.* **83**:679-684.

Xiao, L., Kim, Y.S., and Abbaschian, R. 1990. Ductile Phase Toughening of $MoSi_2$, Chemical Compatibility and Fracture Toughness. In Intermetallic Matrix Composites, ed. D.L. Anton et al., pp. 399-404, Pittsburgh, PA: Mat. Res. Soc. Symp. Proc. Vol. 194.

Yamaguchi, M. and Umakoshi, Y., 1975. The Core Structure of <001> Screw Dislocations in a Model CsCl Type Ordered Lattice. *Scripta Metall.* **9**:637-640.

Yaney, D.L. and Nix, W.D. 1988. Mechanisms of Elevated-Temperature Deformation in the B2 Aluminides NiAl and CoAl. *J. Mater. Sci.* **23**:3088-3098.

Yang, J.H. and Wayman, C.M. 1993. On the Ni_5Al_3 Phase and Related Phenomena in a NiAlFe Alloy. *Maters. Sci. Eng.* **A160**:241-249.

Yang, W.J. and Dodd, R.A. 1973. Steady-State Creep and Associated Microstructures in Stoichiometric and Non-Stoichiometric Polycrystalline NiAl. *Met. Sci. J.* 7:41-47.

Zeller, M.V., Noebe, R.D., and Locci, I.E. 1990. Grain Boundary Segregation Studies of NiAl and NiAl(Zr) Using Auger Electron Spectroscopy. In HITEMP Review-1990: Advanced High Temperature Engine Materials Technology Program, NASA CP-10051, pp. 21-1 to 21-17.

Appendix A

Detailed Description of Materials Studied
(Chemical Composition, Grain Size and Processing Parameters)

This appendix contains a summary of the major material systems studied during the course of this dissertation including the chemical composition, grain size, and processing parameters. Several notes of explanation are required. First, all chemical compositions are reported in atomic percent. When the composition for a particular heat of powder is given the metallic elements (Ni, Al, etc.) are equivalent for every extrusion run utilizing that particular heat of powder. The interstitial (O, C, N, S) levels of as-extruded powders are also very similar for each extrusion run as long as the powder was from the same heat and was the same particle size, therefore, an average value is reported. All powders were purchased from Homogeneous Metals Inc., Clayville, NY, and were produced by the vacuum atomization process. Cast and then extruded billets are identified by their respective extrusion numbers (L followed by a four digit number). The only real significance of this number other than for identification purposes is the fact that all extrusions are assigned a consecutive number as they are extruded.

The Ni and Al composition was usually determined by wet analytical chemistry (WC) methods (generally performed on triplicate samples) with an absolute accuracy of ± 0.2 atomic percent for Ni and Al in near stoichiometric alloys. This is presently the most accurate method for determining bulk composition. All other metallic elements such as Zr and on occasion Ni and Al were determined by flame atomic absorption/emission spectrophotometry (FAS), which has a relative accuracy of ± 5%.

Oxygen and nitrogen were determined in a LECO Oxygen/Nitrogen Determinator by a combustion technique. Carbon and sulfur were determined in a LECO Carbon/Sulfur Determinator also by a flame combustion technique. Both techniques have a relative accuracy of approximately ± 10% for the small interstitial levels encountered in the NiAl alloys that were analyzed.

Powder Extruded NiAl (Heat P541)

Material	Extrusion Conditions Temp. (K)	Extrusion Conditions Ext. Ratio	Grain Size (μm)
Vacuum Atomized Powder (Heat P541)	1150-1400	16:1	5 - 40

Chemical Composition (atomic percent)

Ni	Al	O	C	S	N
49.4 (WC)	50.6 (WC)	0.017	0.011	<0.001	<0.001

Mechanical Properties Reported in Chapter(s): IV & V

Comments: Major material system used to evaluate the baseline behavior of binary NiAl. Testing included room temperature fracture behavior, determination of yield strength as a function of temperature, grain size effects, BDTT determination, in-situ annealing experiments, and creep testing from 500 to 1200 K.

Powder Extruded Ni-36Al (Heat P895)

Material	Extrusion Conditions Temp. (K)	Extrusion Conditions Ext. Ratio	Grain Size (μm)
Vacuum Atomized Powder (Heat P895)	1200	16:1	8 - 10

Chemical Composition (atomic percent)

Ni	Al	Zr	O	C	S	N
63.83 (FAS)	36.08 (FAS)	0.05 (FAS)	0.016	0.019	<0.0014	<0.0017

Mechanical Properties Reported in Chapter(s): III

Comments: One of the two-phase material systems that was examined during studies of ductile phase toughening. In the as-extruded condition it contained 4 vol.% γ' and after annealing at 1000 K for 10 hours it contained 22 vol.% γ'.

Powder Extruded NiAl(0.05Zr) (Heat P896)

Material	Extrusion Conditions Temp. (K)	Extrusion Conditions Ext. Ratio	Grain Size (µm)
Vacuum Atomized Powder (Heat P896)	1200-1400	16:1	4 - 20

Chemical Composition (atomic percent)

Ni	Al	Zr	O	C	S	N
49.6 (WC)	50.3 (WC)	0.05 (FAS)	0.014	0.013	<0.001	<0.001

Mechanical Properties Reported in Chapter(s): V

Comments: Major material system that was used for determination of Zr effects on the mechanical properties of NiAl. Testing included measurement of yield strength as a function of temperature, grain size effects, BDTT determination, and in-situ annealing experiments.

Powder Extruded NiAl(0.1Zr) (Heat P1187)

Material	Extrusion Conditions Temp. (K)	Extrusion Conditions Ext. Ratio	Grain Size (µm)
Vacuum Atomized Powder (Heat P1187)	1500	16:1	4

Chemical Composition (atomic percent)

Ni	Al	Zr	O	C	S	N
49.6 (WC)	50.2 (WC)	0.093 (FAS)	0.025	0.014	<0.004	0.0018

Mechanical Properties Reported in Chapter(s): VII

Comments: Zr-doped alloy used during general studies of microalloying effects. Tensile properties were determined as a function of temperature.

Powder Extruded NiAl (Heat P1418)

Material	Extrusion Conditions Temp. (K)	Extrusion Conditions Ext. Ratio	Grain Size (μm)
Vacuum Atomized Powder (Heat P1418)	1200	16:1	10 -12

Chemical Composition (atomic percent)

Ni	Al	O	C	S	N
50.6 (WC)	49.3 (WC)	0.023	0.014	<0.001	<0.001

Mechanical Properties Reported in Chapter(s): VIII

Comments: Room temperature stress-strain behavior reported in Chapter VIII as another baseline data point for the behavior of binary powder extruded NiAl.

Powder Extruded NiAl(N) (Heat P1810)

Material	Extrusion Conditions Temp. (K)	Extrusion Conditions Ext. Ratio	Grain Size (μm)
Vacuum Atomized Powder (Heat P1810)	1200	16:1	2 - 6

Chemical Composition (atomic percent)

Ni	Al	O	C	S	N
50.3 (WC)	49.7 (WC)	0.035	0.006	<0.001	0.090

Mechanical Properties Reported in Chapter(s): VIII

Comments: Major material system used to evaluate the effect of interstitial content, namely nitrogen, on mechanical properties. Microstructural characterization was performed and tensile properties were determined as a function of temperature.

CAST and Extruded NiAl (L2559)

Material	Extrusion Conditions Temp. (K)	Extrusion Conditions Ext. Ratio	Grain Size (μm)
Vacuum Induction Melted Ingot	1400	16:1	29 ± 3

Chemical Composition (atomic percent)

Ni	Al	O	C	S	N
49.92 (WC)	50.03 (WC)	0.009	0.031	<0.0005	<0.0009

Mechanical Properties Reported in Chapters: VI

Comments: Material used to study the effect of strain rate on the BDTT of NiAl.

Cast and Extruded NiAl (L2692)

Material	Extrusion Conditions Temp. (K)	Extrusion Conditions Ext. Ratio	Grain Size (μm)
Vacuum Induction Melted Ingot	1200	16:1	18 ± 2

Chemical Composition (atomic percent)

Ni	Al	O	C	S	N
50.2 (WC)	49.8 (WC)	0.010	0.025	0.002	<0.003

Mechanical Properties Reported in Chapter(s): VII & VIII

Comments: Baseline cast plus extruded NiAl alloy used in Chapters VII and VIII. Tensile properties were determined as a function of temperature.

Appendix B

Room Temperature Tensile Properties and Fracture Behavior of NiAl Alloys

(A Detailed Description of the Alloys Presented in Figure 4.12)

Symbol	Alloy Comp. (at.%)	Processing Route	Grain Size (μm)	Yield Strength (MPa)	Fracture Strength (MPa)	Fracture* Morphology
a	Ni-50.6Al (Heat P541)	Powder Extruded	10 - 11	394 ± 28[c]	416 ± 21	Mixed Mode
b	Ni-50.6Al (Heat P541)	Powder Extruded	33	274[c]	277	Mixed Mode
c	NiAl (L2559)	VIM Casting + Extruded	29 ± 3	211 - 213	232 - 252	Mostly Intergranular
d	NiAl (L2692)	VIM Casting + Extruded	18 ± 2	172 - 192	252 - 264	Mostly Intergranular
e	NiAl(0.004B) (L2522)	VIM Casting + Extruded	33 ± 4	227 - 229	260 - 279	Mixed Mode
f	NiAl(0.05Zr) (Heat P896)	Powder Extruded	4 - 5	620[c]	630	Transgranular
g	NiAl(0.05Zr) (Heat P896)	Powder Extruded	13 - 19	410 - 420[c]	400 - 420	Mostly Transgranular
h	NiAl(3Re) (L2666)	Extruded Melt Spun Ribbon	1 - 3	660 - 668[c]	497	Mostly Transgranular
i	NiAl(0.5W,0.1C) (L2617)	Extruded Melt Spun Ribbon	1 - 3	704 - 715[c]	635	Transgranular

Symbol	Alloy Comp. (at.%)	Processing Route	Grain Size (µm)	Yield Strength (MPa)	Fracture Strength (MPa)	Fracture* Morphology
j	NiAl(0.5W) (L2673)	Extruded Melt Spun Ribbon	8	457 - 465^c	460	Mixed Mode
k	NiAl(0.05Hf) (L2621)	Extruded Melt Spun Ribbon	9 - 11	380 - 390^c	415	Transgranular
l	Ni-50.6Al (Heat P541)	PowderExt. @ WPAFB	16	146 ± 15	212 ± 6	Mixed Mode
m	NiAl(1Cr) (L2661)	VIM Casting + Extruded	24 ± 3	430 - 444^c	266	Mostly Transgranular
n	Ni-48Al-2Cr (L2659)	VIM Casting + Extruded	20 ± 4	520 - 540^c	325 - 481	Transgranular
o	Ni-45Al-5Cr (L2613)	Powder Extruded	9 - 13	808 - 830^c	500 - 632	Transgranular
p	Ni-50.3Al (Hahn & Vedula 1989)	VIM Casting + Extruded	11 - 16	240	320	^Mixed Mode
q	NiAl (Nagpal & Baker 1991)	VIM Casting + Extruded	13 - 25	115	180 - 200	^Mostly Intergranular

Symbol	Alloy Comp. (at.%)	Processing Route	Grain Size (μm)	Yield Strength (MPa)	Fracture Strength (MPa)	Fracture* Morphology
r	NiAl (George & Liu 1990)	VIM Casting + Extruded	25 - 35	154	229	^Mostly Intergranular
s	NiAl(0.12B)+ (George & Liu 1990)	VIM Casting + Extruded	25 - 35	~694**	329	^Transgranular
t	NiAl(0.11C)+ (George & Liu 1990)	VIM Casting + Extruded	25 - 35	~710@	336	^Mostly Transgranular
u	NiAl(0.24Be)+ (George & Liu 1990)	VIM Casting + Extruded	25 - 35	178	307	^Mostly Intergranular

Notes on Appendix B
Room Temperature Tensile Properties and Fracture Behavior of NiAl Alloys

---

[*] The following scale was used in evaluating the fracture mode of NiAl alloys:

Description	% Intergranular Fracture
Transgranular	0 - 20
Mostly Transgranular	20 - 40
Mixed Mode	40 - 60
Mostly Intergranular	60 - 80
Intergranular	80 - 100

[c] yield stress determined in compression (no macro-yield behavior in tension).

[#] Based on qualitative description found in the reference
(percent intergranular fracture was not quantitatively measured)

^Based on quantitative measurement from published micrograph.

[+] Ternary additions appear to be different from that in the original reference because they were given in weight percent composition while the Tables list every component in atomic percent.

[**] Estimate based on data from George, Liu & Liao (1991).

[@] Estimate based on the strength difference between alloys i versus j in this Table.

REPORT DOCUMENTATION PAGE

Form Approved
OMB No. 0704-0188

Public reporting burden for this collection of information is estimated to average 1 hour per response, including the time for reviewing instructions, searching existing data sources, gathering and maintaining the data needed, and completing and reviewing the collection of information. Send comments regarding this burden estimate or any other aspect of this collection of information, including suggestions for reducing this burden, to Washington Headquarters Services, Directorate for Information Operations and Reports, 1215 Jefferson Davis Highway, Suite 1204, Arlington, VA 22202-4302, and to the Office of Management and Budget, Paperwork Reduction Project (0704-0188), Washington, DC 20503.

1. AGENCY USE ONLY (*Leave blank*)

2. REPORT DATE
April 1994

3. REPORT TYPE AND DATES COVERED
Technical Memorandum

4. TITLE AND SUBTITLE
The Effect of Various Metallurgical Parameters on the Flow and Fracture Behavior of Polycrystalline NiAl Near the Brittle-To-Ductile Transition

5. FUNDING NUMBERS
WU–505–63–52

6. AUTHOR(S)
Ronald D. Noebe

7. PERFORMING ORGANIZATION NAME(S) AND ADDRESS(ES)

National Aeronautics and Space Administration
Lewis Research Center
Cleveland, Ohio 44135–3191

8. PERFORMING ORGANIZATION REPORT NUMBER
E–8669

9. SPONSORING/MONITORING AGENCY NAME(S) AND ADDRESS(ES)

National Aeronautics and Space Administration
Washington, D.C. 20546–0001

10. SPONSORING/MONITORING AGENCY REPORT NUMBER
NASA TM–106534

11. SUPPLEMENTARY NOTES
Responsible person, Ronald D. Noebe, organization code 5180, (216) 433–2093.

12a. DISTRIBUTION/AVAILABILITY STATEMENT

Unclassified - Unlimited
Subject Category 26

12b. DISTRIBUTION CODE

13. ABSTRACT ***(Maximum 200 words)***

This report summarizes an investigation of the effect of various metallurgical parameters such as interfaces, alloying additions, test temperature and strain rate on the flow and fracture behavior of polycrystalline NiAl. From this study a more complete understanding of the deformation and fracture behavior of polycrystalline NiAl near the brittle-to-ductile transition temperature has been developed. A mechanism for the BDTT is proposed that is based on the operation of localized dislocation climb processes that operate within the vicinity of the grain boundaries and provide the additional deformation mechanisms necessary for grain-to-grain compatibility during plastic deformation. Finally, methods for improving the low temperature mechanical behavior of NiAl were considered and reviewed within the context of the present knowledge of NiAl-based materials and the operative deformation and fracture mechanisms determined in this study. Special emphasis was placed on the use of second phases for improving low temperature properties.

14. SUBJECT TERMS
Mechanical properties; Intermetallic NiAl; Brittle-to-Ductile transition; Fracture; Review

15. NUMBER OF PAGES
256

16. PRICE CODE
A12

17. SECURITY CLASSIFICATION OF REPORT
Unclassified

18. SECURITY CLASSIFICATION OF THIS PAGE
Unclassified

19. SECURITY CLASSIFICATION OF ABSTRACT
Unclassified

20. LIMITATION OF ABSTRACT

NSN 7540-01-280-5500

Standard Form 298 (Rev. 2-89)
Prescribed by ANSI Std. Z39-18
298-102